FÈUE WHE

More

In learning about systems containing large numbers of particles, the meaning of the *temperature* needs to be more carefully defined. It is closely related to another descriptor of such systems, the *entropy*. To help you understand both concepts better, we have included *Temperature and Entropy* on the home page: www.whfreeman.com/tiplermodernphysics5e. See also Equations 8-4 *a*, *b*, *c*, and *d* here.

Maxwell Distribution of Molecular Speeds

The Boltzmann distribution is a very fundamental relation from which many properties of classical systems, both gases and condensed matter, can be derived. Two of the most important are Maxwell's distribution of the speeds of molecules in a gas and the equipartition theorem. Considering the first of these, Maxwell derived the velocity and speed distributions of gases in 1859, some five years before Boltzmann derived Equation 8-1. As with the Boltzmann distribution, we will present the results here, illustrating their application with examples and including fuller descriptions and derivations in the Classical Concept Review. Maxwell obtained the velocity distribution, $F(v_x, v_y, v_z)$, which can also be used to obtain the speed distribution, by assuming that the components v_x, v_y, and v_z of the velocity were independent and that therefore the probability of a molecule having a certain v_x, v_y, v_z could be factored into the product of the separate probabilities of its having v_x, v_y, and v_z. He also assumed that the distribution could depend only on the speed; i.e., the velocity components could occur only in the combination $v_x^2 + v_y^2 + v_z^2$. He thus wrote for the distribution function for v_x

$$f(v_x) = Ce^{-mv_x^2/2kT} \qquad \textbf{8-5}$$

where $f(v_x)$ is the distribution function for v_x only; i.e., $f(v_x)dv_x$ is the fraction of the total number of molecules that have their x component of velocity between v_x and $v_x + dv_x$.[3] Similar expressions can be written for $f(v_y)$ and $f(v_z)$. The constant C is determined by the normalization condition. The complete normalized velocity distribution is

$$F(v_x, v_y, v_z) = f(v_x)f(v_y)f(v_z) = \left(\frac{m}{2\pi kT}\right)^{3/2} e^{-m(v_x^2+v_y^2+v_z^2)/2kT} \qquad \textbf{8-6}$$

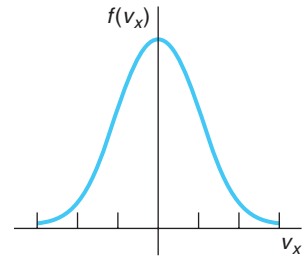

Figure 8-2 The distribution function $f(v_x)$ for the x component of velocity. This is a Gaussian curve symmetric about the origin.

The utility of distribution functions is that they make possible the calculation of average or expectation values of physical quantities; i.e., they allow us to make predictions regarding the physical properties of systems. For example, the observation from Figure 8-2 that the average value of v_x is zero can be verified by computing $\langle v_x \rangle$ as indicated by Equation 8-7.

$$\langle v_x \rangle = \int_{-\infty}^{+\infty} v_x f(v_x)\, dv_x = \int_{-\infty}^{+\infty} v_x \left(\frac{m}{2\pi kT}\right)^{1/2} e^{-mv_x^2/2kT}\, dv_x \qquad \textbf{8-7}$$

Writing $\lambda = m/2kT$, we have

$$\langle v_x \rangle = (\lambda/\pi) \int_{-\infty}^{+\infty} v_x e^{-\lambda v_x^2}\, dv_x$$

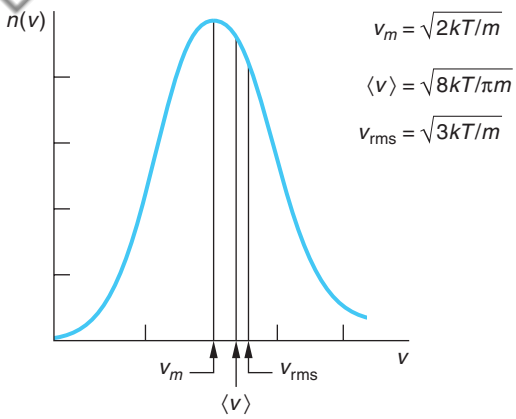

Figure 8-3 Maxwell speed distribution function $n(v)$. The most probable speed v_m, the average speed $\langle v \rangle$, and the rms speed v_{rms} are indicated.

From Table B1-1 we see that the value of the integral is zero, so $\langle v_x \rangle = 0$, as expected.

The probability distribution function for the speeds of the molecules in a classical ideal gas can be derived from the Boltzmann distribution. The result is the famous *Maxwell distribution of molecular speeds*:

$$n(v)\,dv = 4\pi N\left(\frac{m}{2\pi kT}\right)^{3/2} v^2 e^{-mv^2/2kT}\,dv \qquad \textbf{8-8}$$

The distribution of speeds is shown graphically in Figure 8-3. The most probable speed v_m, the average speed $\langle v \rangle$, and the rms speed v_{rms} are indicated in the figure. Although the velocity distribution function F (see Equation 8-6 and Figures 8-4 and 8-5) is a maximum at the origin (where $v_x = v_y = v_z = 0$), the speed distribution function $n(v)$ approaches zero as $v \to 0$ because the latter is proportional to the volume of the spherical shell $4\pi v^2\,dv$ (see Equation 8-8), which approaches zero. At very high speeds, the speed distribution function again approaches zero because of the exponential factor $e^{-mv^2/2kT}$.

The most probable speed v_m is that where $n(v)$ has its maximum value. It is left as an exercise (see Problem 8-9) to show that its value is

$$v_m = \left(\frac{2kT}{m}\right)^{1/2} \qquad \textbf{8-9}$$

The average speed $\langle v \rangle$ is obtained in general and for a specific situation in the next example.

One of the ways used to separate ^{235}U from the far more abundant ^{238}U isotope is to react the uranium metal with fluorine, forming UF_6, a gas. ^{235}UF diffuses through a membrane just a bit faster than ^{238}UF since both molecules have the same average kinetic energy. After several stages of diffusion, the concentration of ^{235}U is high enough for making nuclear reactor fuel (see Chapter 11).

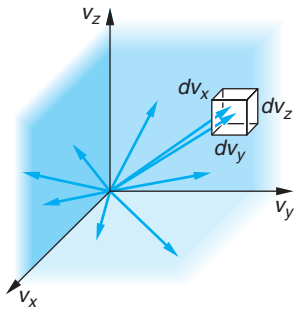

Figure 8-4 Velocity vectors in velocity space. The velocity distribution function gives the fraction of molecular velocities whose vectors end in a cell of volume $dv_x dv_y dv_z$.

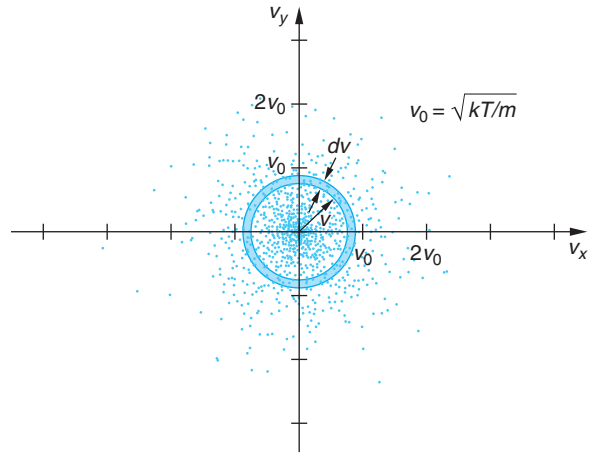

Figure 8-5 Two-dimensional representation of velocity distribution in velocity space. Each molecular velocity with components v_x, v_y, and v_z is represented by a point in velocity space. The velocity distribution function is the density of points in this space. The density is maximum at the origin. The speed distribution is found by multiplying the density times the volume of the spherical shell $4\pi v^2\,dv$. [*This computer-generated plot courtesy of Paul Doherty, The Exploratorium.*]

EXAMPLE 8-3 **Average Speed of N_2 Molecules** Obtain the average speed $\langle v \rangle$ of the Maxwell distribution and use it to compute the average speed of nitrogen molecules at 300 K. The mass of the N_2 molecule is 4.68×10^{-26} kg.

SOLUTION

1. The average speed $\langle v \rangle$ is found by multiplying the distribution of speeds (Equation 8-8) by v, integrating over all possible speeds, and dividing by the total number of molecules N:

$$\langle v \rangle = \frac{1}{N} \int_0^\infty v n(v)\, dv = \int_0^\infty A v^3 e^{-\lambda v^2}\, dv$$

where $\lambda = m/2kT$ and $A = 4\pi(m/2kT)^{3/2}$.

2. Writing this as

$$\langle v \rangle = A I_3$$

where

$$I_3 = \int_0^\infty v^3 e^{-\lambda v^2}\, dv$$

3. Using Table B1-1 for evaluating I_3, we have

$$\begin{aligned} \langle v \rangle &= A\lambda^{-2}/2 \\ &= \frac{4\pi}{2}\left(\frac{m}{2\pi kT}\right)^{3/2}\left(\frac{2kT}{m}\right)^2 \\ &= \left(\frac{8kT}{\pi m}\right)^{1/2} \end{aligned} \qquad \textbf{8-10}$$

4. The $\langle v \rangle$ found in step 3 can now be used to find the average speed of nitrogen molecules at $T = 300$ K. Substituting the mass of a nitrogen molecule into Equation 8-10 yields

$$\begin{aligned} \langle v \rangle &= \left[\frac{8 \times 1.38 \times 10^{-23} \times 300}{\pi \times 4.68 \times 10^{-26}}\right]^{1/2} \\ &= 475 \text{ m/s} \\ &= 1700 \text{ km/h} \end{aligned}$$

The average speed is about 8 percent less than $v_{rms} = (3kT/m)^{1/2}$, as indicated in Figure 8-3. The rms speed can be computed from the speed distribution following the same procedure as in Example 8-3 or, as we will see below, from the equipartition theorem. Figure 8-6, a plot of Equation 8-8 for H_2 and O_2 molecules at 300 K, illustrates the effect of mass on the speed distribution.

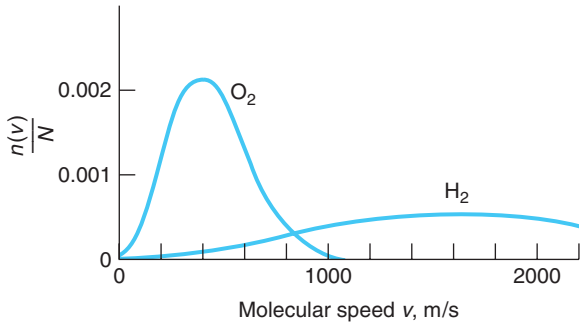

Figure 8-6 Graph of $n(v)/N$ versus v from Equation 8-8 for O_2 and H_2 molecules, both at $T = 300$ K.

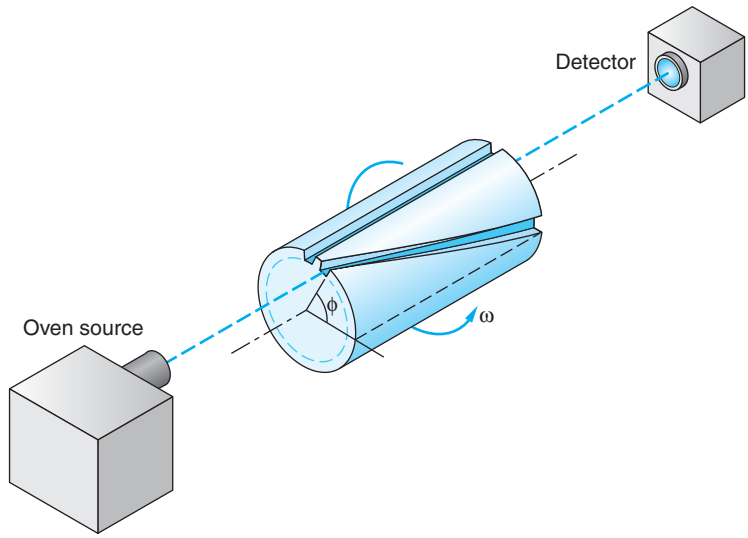

Figure 8-7 Schematic sketch of apparatus of Miller and Kusch for measuring the speed distribution of molecules. Only one of the 720 helical slits in the cylinder is shown. For a given angular velocity ω only molecules of a certain speed from the oven pass through the helical slits to the detector. The straight slit is used to align the apparatus. [*From R. C. Miller and P. Kusch, Physical Review,* **99**, *1314 (1955).*]

Evaporation is a cooling process, even at very low temperatures! The sample from which a BE condensate will form, confined at about 1 mK, is cooled further by allowing the atoms in the high-speed "tail" of the Maxwell distribution to "leak" from the sample, taking kinetic energy with them and thus reducing the temperature (see Section 8-3).

Maxwell's speed distribution has been precisely verified by many experiments, so there is little incentive to perform additional measurements. One of the more recent experiments, that of R. C. Miller and P. Kusch, illustrated in Figures 8-7 and 8-8, is applicable to the measurement of any sort of molecular speed distribution, and variations of it are used to measure the speeds in jet or nozzle molecular beams.

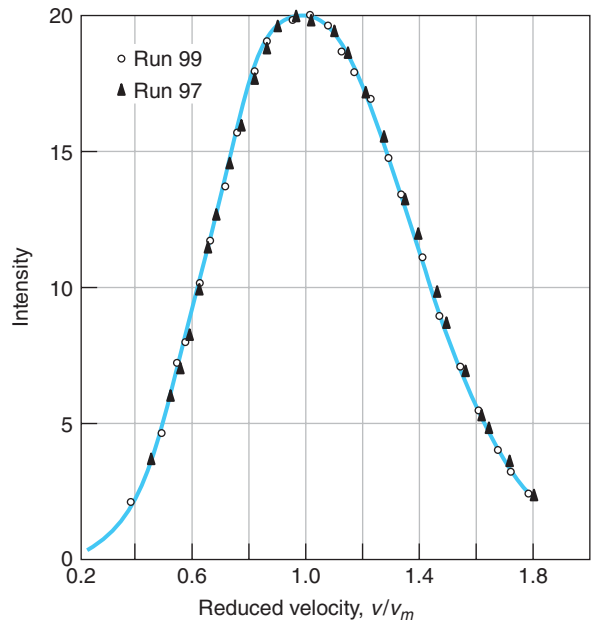

Figure 8-8 Data of Miller and Kusch showing the distribution of speed of thallium atoms from an oven at 870 K. The data have been corrected to give the distribution inside the oven since the faster molecules approach the exit slit more frequently and skew the external distribution slightly. The measured value for v_m at 870 K is 376 m/s. The solid curve is that predicted by the Maxwell speed distribution. [*From R. C. Miller and P. Kusch, Physical Review,* **99**, *1314 (1955).*]

Questions

1. How does v_{rms} for H_2 molecules compare with v_{rms} for O_2 molecules under standard conditions?

FEUE WHE

Maxwell Distribution of Kinetic Energy

Maxwell's distribution of molecular speeds also provides, as a bonus, the distribution of the molecular translational kinetic energy and the average kinetic energy of a molecule. These can also be determined from Equation 8-2. Since $E = \frac{1}{2}mv^2$, $v^2 = 2E/m$, and $dv = (2mE)^{1/2}\,dE$, $g(E)\,dE$ is

$$g(E)\,dE = 4\pi C(2E/m)(2mE)^{-1/2}\,dE \qquad \textbf{8-11}$$

Substituting the above into Equation 8-2, we have

$$n(E)\,dE = 4\pi A'(2/m^3)^{1/2}E^{1/2}e^{E/kT}\,dE \qquad \textbf{8-12}$$

Evaluating A' using the fact that $\int_0^\infty n(E)\,dE = N$, the total number of particles, allows us to write *Maxwell's distribution of kinetic energy* as

$$n(E)\,dE = \frac{2\pi N}{(\pi kT)^{3/2}}E^{1/2}e^{-E/kT}\,dE \qquad \textbf{8-13}$$

The kinetic energy distribution is sketched in Figure 8-9. The average kinetic energy is computed in the same manner as the average speed; i.e., the distribution is multiplied by E (the quantity being averaged), and the result is integrated[4] over all values of E (from $0 \rightarrow \infty$) and divided by the number of molecules N:

$$\langle E\rangle = \frac{1}{N}\int_0^\infty E\,n(E)\,dE = \frac{2\pi}{(\pi kT)^{3/2}}\int_0^\infty E^{3/2}e^{-E/kT}\,dE = \frac{3}{2}kT \qquad \textbf{8-14}$$

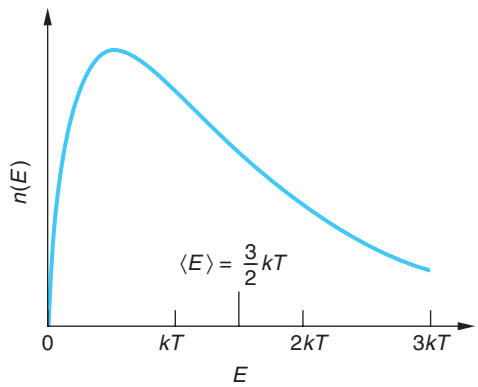

Figure 8-9 Maxwell distribution of kinetic energies for the molecules of an ideal gas. The average energy $\langle E\rangle = 3kT/2$ is shown.

EXAMPLE 8-4 **Escape of H_2 from Earth's Atmosphere** A rule of thumb used by astrophysicists is that a gas will escape from a planet's atmosphere in 10^8 years if the average speed of its molecules is one-sixth of the escape velocity. Compute the average speed from the average kinetic energy and show that the absence of hydrogen in Earth's atmosphere suggests that Earth must be older than 10^8 years (mass of H_2 molecules $= 3.34 \times 10^{-27}$ kg).

SOLUTION

The escape speed at the bottom of the atmosphere, i.e., Earth's surface, is 11.2 km/s, and one-sixth of that value is 1.86 km/s. If we assume $T = 300$ K, the average energy of a hydrogen molecule (or any other molecule since $\langle E \rangle$ is independent of mass) is

$$\langle E \rangle = \frac{3}{2}kT = \frac{3 \times 1.38 \times 10^{-23} \times 300}{2} = 6.21 \times 10^{-21}\ \text{J}$$

Thus,

$$\tfrac{1}{2}mv^2 = 6.21 \times 10^{-21}\ \text{J}$$

or, for hydrogen molecules,

$$v^2 = \frac{2 \times 6.21 \times 10^{-21}}{3.34 \times 10^{-27}} = 3.72 \times 10^6\ \text{m}^2/\text{s}^2$$

Therefore,

$$v = 1.93\ \text{km/s}$$

Remarks: *Since $v > (1/6)v_{esc} = 1.86$ km/s, the absence of hydrogen in the atmosphere suggests that the age of Earth is greater than 10^8 years.*

Questions

2. How does $\langle E_k \rangle$ for He molecules compare with $\langle E_k \rangle$ for Kr molecules under standard conditions?
3. H_2 molecules can escape so freely from Earth's gravitational field that H_2 is not found in Earth's atmosphere. (See Example 8-4.) Yet the average speed of H_2 molecules at ordinary atmospheric temperatures is much less than the escape speed. How, then, can all of the H_2 molecules escape?
4. Why wouldn't you expect all molecules in a gas to have the same speed?

Heat Capacities of Gases and Solids

The second important property of classical systems derivable from the Boltzmann distribution is one that applies to both gases and solids. Called the *equipartition theorem*, it states that

> In equilibrium, each degree of freedom contributes $\frac{1}{2}kT$ to the average energy per molecule.

A *degree of freedom* is a coordinate or a velocity component that appears squared in the expression for the total energy of a molecule. For example, the one-dimensional harmonic oscillator has two degrees of freedom, x and v_x; a monatomic gas molecule has three degrees of freedom, v_x, v_y, and v_z.

More

That each degree of freedom in a classical material should have the same average energy per molecule is not at all obvious. On the home page we have included *A Derivation of the Equipartition Theorem* for a special case, the harmonic oscillator, to illustrate how the more general result arises: www.whfreeman.com/tiplermodernphysics5e. See also Equations 8-15 through 8-23 here.

FEUE WHE

C_V for Gases

The power of the equipartition theorem is its ability to accurately predict the heat capacities of gases and solids, but therein is also found its most dramatic failures. As an example, consider a rigid-dumbbell model of a diatomic molecule (Figure 8-10*a*) that can translate in the x, y, and z directions and can rotate about axes x' and y' through the center of mass and perpendicular to the z' axis along the line joining the two atoms.[5] The total energy for this rigid-dumbbell model molecule is then

$$E = \tfrac{1}{2}mv_x^2 + \tfrac{1}{2}mv_y^2 + \tfrac{1}{2}mv_z^2 + \tfrac{1}{2}I_{x'}\omega_{x'}^2 + \tfrac{1}{2}I_{y'}\omega_{y'}^2$$

where $I_{x'}$ and $I_{y'}$ are the moments of inertia about the x' and y' axes. Since this molecule has 5 degrees of freedom, 3 translational and 2 rotational, the equipartition theorem predicts the average energy to be $(5/2)kT$ per molecule. The energy per mole U is then $(5/2)N_Akt = (5/2)RT$ and the molar heat capacity at constant volume $C_V = (\partial U/\partial T)_V$ is $(5/2)R$. The observation that C_V for both nitrogen and oxygen is about $(5/2)R$ enabled Rudolf Clausius to speculate (in about 1880) that these gases must be diatomic gases, which can rotate about two axes as well as translate. (See Table 8-1.)

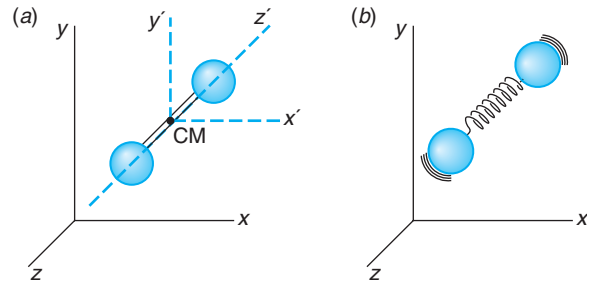

Figure 8-10 (*a*) Rigid-dumbbell model of a diatomic gas molecule that can translate along the x, y, or z axis and rotate about the x' or y' axis fixed to the center of mass. If the spheres are smooth or are points, rotation about the z' axis can be neglected. (*b*) Nonrigid-dumbbell model of a diatomic gas molecule that can translate, rotate, and vibrate.

Table 8-1 C_V for some gases at 15°C and 1 atm

Gas	C_V (cal/mol-deg)	C_V/R
Ar	2.98	1.50
He	2.98	1.50
CO	4.94	2.49
H_2	4.87	2.45
HCl	5.11	2.57
N_2	4.93	2.49
NO	5.00	2.51
O_2	5.04	2.54
Cl_2	5.93	2.98
CO_2	6.75	3.40
CS_2	9.77	4.92
H_2S	6.08	3.06
N_2O	6.81	3.42
SO_2	7.49	3.76
$R = 1.987$ cal/mol-deg		

From J. R. Partington and W. G. Shilling, *The Specific Heats of Gases* (London: Ernest Benn, Ltd., 1924).

If a diatomic molecule is not rigid, the atoms can also vibrate along the line joining them (Figure 8-10*b*). Then, in addition to the translational energy of the center of mass and rotational energy, there can be vibrational energy. The vibration, a simple harmonic motion, adds two more squared terms to the energy, one for the potential energy and one for kinetic energy. For a diatomic molecule that is translating, rotating, and vibrating, the equipartition theorem thus predicts a molar heat capacity of $(3 + 2 + 2)\frac{1}{2}R$, or $(7/2)R$. However, measured values of C_V for diatomic molecules (see Table 8-1) show no contribution from the vibrational degrees of freedom. The equipartition theorem provides no explanation for their absence.

Experimental values of C_V for several diatomic gases are included in Table 8-1. For all of these except Cl_2, the data are consistent with the equipartition theorem prediction, assuming a rigid, nonvibrating molecule. The value for Cl_2 is about halfway between that predicted for a rigid molecule and that predicted for a vibrating molecule. The situation for molecules with three or more atoms, several of which are also listed in Table 8-1, is more complicated and will not be examined in detail here.

The equipartition theorem in conjunction with the point-atom, rigid-dumbbell model was so successful in predicting the molar heat capacity for most diatomic molecules that it was difficult to understand why it did not do so for all of them. Why should some diatomic molecules vibrate and not others? Since the atoms are not points, the moment of inertia about the line joining the atoms, while small, is not zero, and there are three terms for rotational energy rather than two. Assuming no vibration, C_V should then be $(6/2)R$. This agrees with the measured value for Cl_2 but not for the other diatomic gases. Furthermore, monatomic molecules would have three terms for rotational energy if the atoms were not points, and C_V should also be $(6/2)R$ for these atoms rather than the $(3/2)R$ that is observed. Since the average energy is calculated by *counting* terms, it should not matter how small the atoms are as long as they are not merely points. In addition to these difficulties, it is found experimentally that the molar heat capacity depends on temperature, contrary to the predictions from the equipartition theorem. The most spectacular case is that of H_2, shown in Figure 8-11. It seems as if at very low temperatures, below about 60 K, H_2 behaves like a monatomic molecule and does not rotate. It seems to undergo a transition, and between about 250 K and 700 K it has $C_V = (5/2)R$, thus behaving like a rotating rigid

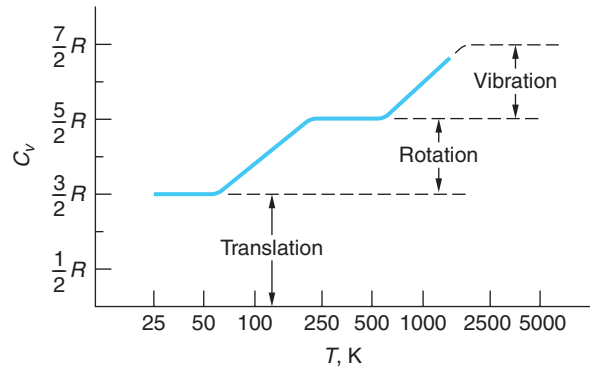

Figure 8-11 Temperature dependence of molar heat capacity of H_2. Between about 250 and 750 K, C_V is $(5/2)R$, as predicted by the rigid-dumbbell model. At low temperatures, C_V is only $(3/2)R$, as predicted for a nonrotating molecule. At high temperatures C_V seems to be approaching $(7/2)R$, as predicted for a dumbbell model that rotates and vibrates, but the molecule dissociates before this plateau is reached.

dumbbell. At very high temperatures H_2 begins to vibrate, but the molecule dissociates before C_V reaches $(7/2)R$. Other diatomic gases show similar behavior except that at low temperatures they liquefy before C_V reaches $(3/2)R$. The failure of the equipartition theorem to account for these observations occurs because classical mechanics itself fails when applied to atoms and molecules. As we will see, it must be replaced by quantum mechanics.

C_V for Solids

The equipartition theorem is also useful in understanding the heat capacity of solids. In 1819 P. Dulong and A. Petit pointed out that the molar heat capacity of most solids was very nearly equal to 6 cal/K-mol $\approx 3R$. This result was used by them to obtain unknown molecular weights from the experimentally determined heat capacities. The empirical *Dulong-Petit law* is easily derived from the equipartition theorem by assuming that the internal energy of a solid consists entirely of the vibrational energy of the molecules (see Figure 8-12). If the force constants in the x, y, and z directions are κ_1, κ_2, and κ_3, respectively, the vibrational energy of each molecule is

$$E = \tfrac{1}{2}mv_x^2 + \tfrac{1}{2}mv_y^2 + \tfrac{1}{2}mv_z^2 + \tfrac{1}{2}\kappa_1 x^2 + \tfrac{1}{2}\kappa_2 y^2 + \tfrac{1}{2}\kappa_3 z^2$$

Since there are six squared terms, the average energy per molecule is $6(\frac{1}{2}\,kT)$, and the total energy of 1 mole is $3N_A kT = 3RT$, giving $C_V = 3R$.

At high temperatures, all solids obey the Dulong-Petit law. For temperatures below some critical value, C_V drops appreciably below the value of $3R$ and approaches zero as T approaches zero. The critical temperature is a characteristic of the solid. It is lower for soft solids such as lead than for hard solids such as diamond. The temperature dependence of C_V for several solids is shown in Figure 8-13.

The fact that C_V for metals is not appreciably different from that for insulators is puzzling. The classical model of a metal is moderately successful in describing the conduction of electricity and heat. It assumes that approximately one electron per atom is free to move about the metal, colliding with the atoms much as the molecules do in a gas. According to the equipartition theorem, this "electron gas" should have an average kinetic energy of $(3/2)kT$ per electron; thus, the molar heat capacity should be about $(3/2)R$ greater for a conductor than for an insulator. Although the molar heat capacity for metals is slightly greater than $3R$ at very high temperatures, the difference is much less than the $(3/2)R$ predicted for the contribution of the electron gas.

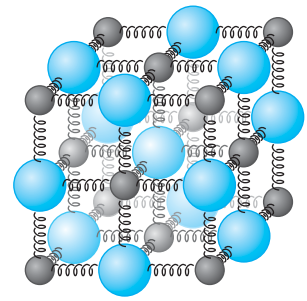

Figure 8-12 Simple model of a solid consisting of atoms connected to each other by springs. The internal energy of the solid then consists of kinetic and potential vibrational energy.

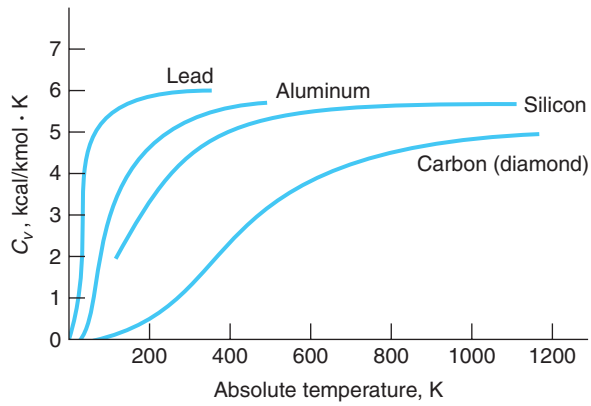

Figure 8-13 Temperature dependence of molar heat capacity of several solids. At high temperatures C_V is $3R$, as predicted by the equipartition theorem. However, at low temperatures C_V approaches zero. The critical temperature at which C_V becomes nearly $3R$ is different for different solids.

The Boltzmann distribution and statistical mechanics were enormously successful in predicting the observed thermal properties of physical systems; however, the failure of the theory to account correctly for the heat capacities of gases and solids was a serious problem for classical physics, constituting as it did a failure of classical mechanics itself. The search for an understanding of specific heats was instrumental in the discovery of energy quantization in the early years of the twentieth century. The following sections show how quantum mechanics provides a basis for the complete understanding of the experimental observations.

EXAMPLE 8-5 **Broadening of Spectral Lines** In Chapter 5 we saw that spectral lines emitted by atoms had a certain natural width due to the uncertainty principle. However, in luminous gases, such as sodium and mercury vapor lamps and the visible surface of the Sun, the atoms are moving with the Maxwell velocity distribution. The velocity distribution results in a Doppler effect that Rayleigh showed was proportional to the Boltzmann factor and led to a broadening Δ of spectral lines equal to

$$\Delta = 0.72 \times 10^{-6} \lambda \sqrt{T/M}$$

where λ is the wavelength of the line, T is the absolute temperature, and M is the molecular weight. From this, compute the velocity (Doppler) broadening of the hydrogen H_α line emitted by H atoms at the surface of the Sun, where $T = 5800$ K.

SOLUTION

The wavelength of the H_α line is 656.3 nm and the atomic weight of H is 1, so

$$\Delta = 0.72 \times 10^{-6} \times 656.3 \sqrt{5800/1} = 0.036 \text{ nm}$$

For comparison, the natural width of the H_α line is about 0.0005 nm. Note that the effect of the pressure of the gas in causing spectral line broadening via collisions is also an important factor and, in fact, at high pressures, is the dominant cause. Collisions reduce the level lifetime, hence broaden the energy width (uncertainty principle). This is the reason that the Sun's visible spectrum is a continuous one.

8-2 Quantum Statistics

Bose-Einstein and Fermi-Dirac Distributions

The classical systems that were the subject of Section 8-1 consisted of identical but distinguishable particles. They were treated like billiard balls: exactly the same as one another but with numbers painted on their sides. Indeed, that was the point of the first assumption on the first page of the kinetic theory review in the Classical Concept Review on the Web site. However, the wave nature of particles in quantum mechanics prevents identical particles from being distinguished from one another. The finite extent and the overlap of wave functions makes identical particles indistinguishable. Thus, if two identical particles 1 and 2 pass within a de Broglie wavelength of each other in some event, we cannot tell which of the emerging particles is 1 and which is 2—i.e., we cannot distinguish between the several possible depictions of the event in Figure 8-14. The treatment of classical particles that led to the Boltzmann distribution can be extended to systems containing large numbers of identical indistinguishable particles.

FEUE WHE

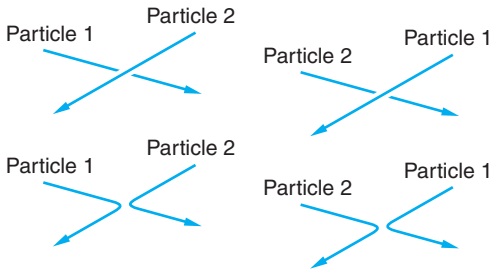

Figure 8-14 The wave nature of quantum-mechanical particles prevents us from determining which of the four possibilities shown actually occurred when the two identical, indistinguishable particles passed within a de Broglie wavelength of each other.

The first such theoretical treatment for particles with zero or integer spins—i.e., those that do not obey the exclusion principle, such as helium atoms (spin 0) and photons (spin 1), was done by Bose[6] in 1924, when he realized that the Boltzmann distribution did not adequately account for the behavior of photons. Bose's new statistical distribution for photons was generalized to massive particles by Einstein shortly thereafter. The resulting distribution function, called the *Bose-Einstein distribution* $f_{BE}(E)$, is given by

$$f_{BE}(E) = \frac{1}{e^{\alpha}e^{E/kT} - 1} \qquad \textbf{8-24}$$

where e^{α} is a system-dependent normalization constant. Particles whose statistical distributions are given by Equation 8-24 are called *bosons*.

Following the discovery of electron spin and Dirac's development of relativistic wave mechanics for spin-$\frac{1}{2}$ particles, Fermi[7] and Dirac[8] completed the statistical mechanics for quantum mechanical particles by deriving the probability distribution for large ensembles of identical indistinguishable particles that obey the exclusion principle. The result is called the *Fermi-Dirac distribution* $f_{FD}(E)$ and is given by

$$f_{FD}(E) = \frac{1}{e^{\alpha}e^{E/kT} + 1} \qquad \textbf{8-25}$$

where, again, e^{α} is a system-dependent normalization constant. Particles whose behavior is described by Equation 8-25 are called *fermions* or *Fermi-Dirac particles*.

Comparison of the Distribution Functions

We can write the Boltzmann distribution (Equation 8-1) in the form

$$f_B(E) = \frac{1}{e^{\alpha}e^{E/kT}} \qquad \textbf{8-26}$$

where the normalization constant A in Equation 8-1 is replaced by $e^{-\alpha}$. After doing so, one is immediately struck by the very close resemblance between the three distributions (Equations 8-24, 8-25, and 8-26), the Fermi-Dirac and Bose-Einstein probability functions differing from that of Boltzmann only by the ± 1 in the denominator. The question immediately arises as to the significance of this seemingly small difference. In particular, since integrals of the form $\int_0^{\infty} F(E)f_{BE}(E)\,dE$ and $\int_0^{\infty} F(E)f_{FD}(E)\,dE$ require the use of numerical methods for their solutions, it would be helpful to know if and under what conditions the Boltzmann distribution can be used for indistinguishable quantum-mechanical particles.

Enrico Fermi on a picnic in Michigan in July 1935. The bandage covers a cut on his forehead received when he accidentally hit himself with his racket while playing tennis.

Let us first examine the physical meaning of the difference between the distributions. Consider a system of two identical particles, 1 and 2, one of which is in state n and the other in state m. As we discussed in Section 7-6, there are two possible single-particle-product solutions to the Schrödinger equation. They are

$$\psi_{nm}(1, 2) = \psi_n(1)\psi_m(2) \qquad \textbf{8-27}a$$

$$\psi_{nm}(2, 1) = \psi_n(2)\psi_m(1) \qquad \textbf{8-27}b$$

where the numbers 1 and 2 represent the space coordinates of the two particles. If the two identical particles are distinguishable from each other, i.e., if they are classical particles, then we can tell the difference between the two states represented by Equations 8-27a and 8-27b. However, for indistinguishable particles we have seen that the solutions must be the symmetric or antisymmetric combinations given in Section 7-6:

$$\psi_S = \frac{1}{\sqrt{2}}[\psi_n(1)\psi_m(2) + \psi_n(2)\psi_m(1)] \qquad \textbf{8-28}a$$

$$\psi_A = \frac{1}{\sqrt{2}}[\psi_n(1)\psi_m(2) - \psi_n(2)\psi_m(1)] \qquad \textbf{8-28}b$$

The factor $1/\sqrt{2}$ is the normalization constant. As we have discussed earlier (see Section 7-6), the antisymmetric function ψ_A describes particles that obey the exclusion principle, i.e., fermions. The symmetric function ψ_S describes indistinguishable particles that do not obey the exclusion principle, i.e., bosons.

Writing $\psi_A \equiv \psi_{FD}$ and $\psi_S \equiv \psi_{BE}$ to keep us reminded of the probability distributions followed by the fermions and bosons, respectively, let us now consider the probability that, if we look for the two particles, we will find them *both* in the same state, say state n. For two distinguishable particles Equations 8-27a and 8-27b both become

$$\psi_{nn}(1, 2) = \psi_{nn}(2, 1) = \psi_n(1)\psi_n(2) = \psi_n(2)\psi_n(1) = \psi_B \qquad \textbf{8-29}$$

where we have written $\psi_{nn}(1, 2) \equiv \psi_B$ to remind us that distinguishable particles follow the Boltzmann distribution. Thus, the probability density of finding both distinguishable particles in state n is

$$\psi_B^*\psi_B = \psi_n^*(1)\psi_n^*(2)\psi_n(1)\psi_n(2) \qquad \textbf{8-30}$$

Turning to indistinguishable particles, the wave function for two bosons both occupying state n is, from Equation 8-28a,

$$\psi_{BE} = \frac{1}{\sqrt{2}}[\psi_n(1)\psi_n(2) + \psi_n(2)\psi_n(1)] = \frac{2}{\sqrt{2}}\psi_n(1)\psi_n(2) \qquad \textbf{8-31}$$

and the probability density of finding both bosons in state n is then

$$\psi_{BE}^*\psi_{BE} = 2\psi_n^*(1)\psi_n^*(2)\psi_n(1)\psi_n(2) = 2\psi_B^*\psi_B \qquad \textbf{8-32}$$

Thus, the probability that both bosons would be found by an experiment to be occupying the same state is *twice* as large as for a pair of classical particles. This surprising discovery can be generalized to large ensembles of bosons as follows:

> The presence of a boson in a particular quantum state *enhances* the probability that other identical bosons will be found in the same state.

It is as if the presence of the boson attracts other identical bosons. Thus, the -1 that appears in the denominator of Equation 8-24 results physically in an increased

FÈUE WHE

probability that multiple bosons will occupy a given state, compared with the probability for classical particles in the same circumstances. The laser is the most common example of this phenomenon (see Chapter 9). We will consider another result of this intriguing behavior in Section 8-3.

If the two indistinguishable particles are fermions, the wave function for both occupying the same state is, as we have previously discussed in Section 7-6,

$$\psi_{FD} = \frac{1}{\sqrt{2}}[\psi_n(1)\psi_n(2) - \psi_n(2)\psi_n(1)] = 0 \qquad \textbf{8-33}$$

And, of course, the probability density $\psi^*_{FD}\psi_{FD} = 0$, also. This result, too, can be generalized to large ensembles of fermions as follows:

> The presence of a fermion in a particular quantum state *prevents* any other identical fermions from occupying the same state.

It is as if identical fermions actually repel one another. The $+1$ in the denominator of Equation 8-25 is thus due to the exclusion principle. We will consider consequences of this peculiar property of fermions further in Chapter 10. Figure 8-15 compares the distributions of bosons and fermions.

With the physical discussion above in mind, now let's compare the three functions. Figure 8-16 shows a comparison of the three distributions for $\alpha = 0$ over the energy range from zero up to $5kT$. Notice that for any given energy the f_{BE} curve for bosons lies above that for f_B for classical particles, reflecting the enhanced probability pointed out by Equation 8-32. Similarly, the f_{FD} curve for fermions lies below those for both f_{BE} and f_B, a consequence of the exclusion of identical fermions from states that are already occupied. Notice that Equations 8-24 and 8-25 both approach the Boltzmann distribution when $e^{\alpha} \gg e^{E/kT}$. For this situation $f_{BE}(E) \approx f_B(E) \ll 1$ and $f_{FD}(E) \approx f_B(E) \ll 1$. Thus, $f_{BE}(E)$ and $f_{FD}(E)$ both approach the classical Boltzmann distribution when the probability that a particle occupies the state with energy E is much less than 1. The same is also clearly the case when, for a given α, $E \gg kT$, as Figure 8-16 illustrates.

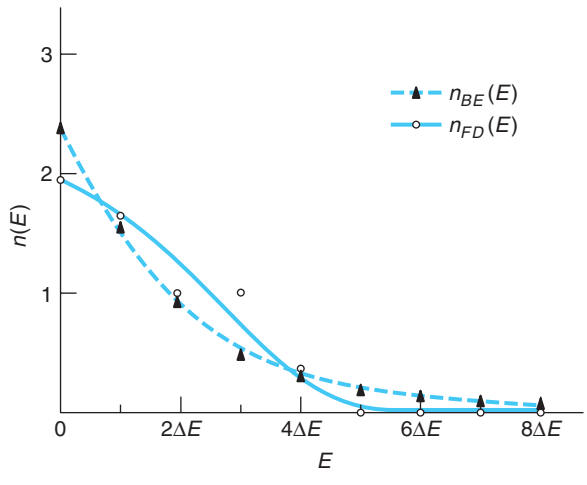

Figure 8-15 $n(E)$ versus E for a system of six identical, indistinguishable particles. $n_{BE}(E)$ is for particles with zero or integer spin (bosons). $n_{FD}(E)$ is for particles with $\frac{1}{2}$-integer spin (fermions). Compare with Figure 8-1.

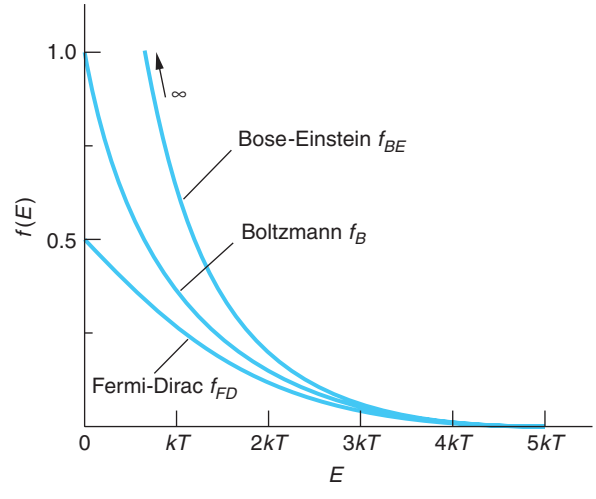

Figure 8-16 Graph of the distributions f_B, f_{BE}, and f_{FD} versus energy for the value $\alpha = 0$. f_{BE} always lies above f_B, which in turn is always above f_{FD}. All three distributions are approximately equal for energies larger than about 5 kT.

At the beginning of this section we noted that identical quantum particles were rendered indistinguishable from one another by the overlap of their de Broglie waves. This provides another means of determining for a given system when the Boltzmann distribution may be used that can be shown to be equivalent to the $f_B(E) \ll 1$ condition above but that is sometimes easier to apply. If the de Broglie wavelength λ is much smaller than the average separation $\langle d \rangle$ of the particles, then we can neglect the overlap of the de Broglie waves, in which case the particles can be treated as if they were distinguishable:

$$\lambda \ll \langle d \rangle \qquad \textbf{8-34}$$

where

$$\lambda = \frac{h}{p} = \frac{h}{\sqrt{2mE_k}} = \frac{h}{\sqrt{2m(3kT/2)}} = \frac{h}{\sqrt{3mkT}} \qquad \textbf{8-35}$$

The average separation of the particles is $\langle d \rangle = (V/N)^{1/3}$, where N/V is the number of particles per unit volume in the system. Thus, the condition stated by Equation 8-34 becomes

$$\frac{h}{\sqrt{3mkT}} \ll \left(\frac{V}{N}\right)^{1/3}$$

which when cubed and rearranged becomes

$$\left(\frac{N}{V}\right)\frac{h^3}{(3mkT)^{3/2}} \ll 1 \qquad \textbf{8-36}$$

Equation 8-36 gives the condition under which the Boltzmann distribution can be used. Note that in general the condition requires low particle densities and high temperatures for particles of a given mass. The next example illustrates the application of the condition.

EXAMPLE 8-6 Statistical Distribution of He in the Atmosphere He atoms have spin 0 and hence are bosons. He makes up 5.24×10^{-6} of the molecules in the atmosphere. (*a*) Can the Boltzmann distribution be used to predict the thermal properties of atmospheric helium at $T = 273$ K? (*b*) Can it be used for liquid helium at $T = 4.2$ K?

SOLUTION

(*a*) N_A atoms of air occupy 2.24×10^{-2} m^3 at standard conditions. The number of He atoms per unit volume is then

$$\frac{N_A}{V} = \frac{6.02 \times 10^{23} \times 5.24 \times 10^{-6}}{2.24 \times 10^{-2}\ \text{m}^3} = 1.41 \times 10^{20}\ \text{molecules He/m}^3$$

The left side of Equation 8-36 is then

$$\frac{(1.41 \times 10^{20})(6.63 \times 10^{-34})^3}{(3 \times 1.66 \times 10^{-27} \times 4 \times 1.38 \times 10^{-23} \times 273)^{3/2}} = 6.3 \times 10^{-11} \ll 1$$

The behavior of the helium in the atmosphere can therefore be described by the Boltzmann distribution.

FÈUE WHE

(*b*) The density of liquid helium at its boiling point $T = 4.2$ K is 0.124 g/cm^3. The particle density N/V is then

$$\frac{N}{V} = \frac{N_A \text{ molecules}}{4 \text{ g}} \times (0.124 \text{ g/cm}^3) \times (10^2 \text{ cm/m})^3 = 1.87 \times 10^{28} \text{ He atoms/m}^3$$

The left side of Equation 8-36 is then

$$\frac{(1.87 \times 10^{28})(6.63 \times 10^{-34})^3}{(3 \times 1.66 \times 10^{-27} \times 4 \times 1.38 \times 10^{-23} \times 4.2)^{3/2}} = 4.39$$

which is *not* $\ll 1$. Therefore, the Boltzmann distribution does not adequately describe the behavior of liquid helium, so the Bose-Einstein distribution must be used.

Using the Distribution: Finding $n(E)$

In order to find the actual number of particles $n(E)$ with energy E, each of the three distribution functions given by Equations 8-24, 8-25, and 8-26 must be multiplied by the density of states, as indicated by Equation 8-2.

$$n_B(E) = g_B(E) f_B(E) \qquad \textbf{8-37}a$$

$$n_{BE}(E) = g_{BE}(E) f_{BE}(E) \qquad \textbf{8-37}b$$

$$n_{FD}(E) = g_{FD}(E) f_{FD}(E) \qquad \textbf{8-37}c$$

Finding $g(E)$ enables the constant e^{α} to be determined for particular systems from the normalization condition that we have used several times, namely, the total number of particles $N = \int_0^\infty n(E)\, dE$.

Density of States

As an example of determining $g(E)$, consider an equilibrium system of N classical particles confined in a cubical volume of side L. Treating the cube as a three-dimensional infinite square well, in Chapter 7 we found the energy of a particle in such a well to be

$$E_{n_1 n_2 n_3} = \frac{\hbar^2 \pi^2}{2mL^2}(n_1^2 + n_2^2 + n_3^2) \qquad \textbf{7-4}$$

which we will for the convenience of our present discussion write as

$$E_n = E_0(n_x^2 + n_y^2 + n_z^2) \qquad \textbf{8-38}$$

where x, y, and z replace 1, 2, and 3 and $E_0 = \hbar^2\pi^2/2mL^2$. The three quantum numbers n_x, n_y, and n_z specify the particular quantum state of the system. Recalling that $g(E)$ is the number of states with energy between E and $(E + dE)$, our task is to find an expression for the total number of states from zero energy up to E, then differentiate that result to find the number within the shell dE. This is made quite straightforward by (1) observing that Equation 8-38 is the equation of a sphere of radius $R = (E/E_0)^{1/2}$ in $n_x\, n_y\, n_z$ "space" and (2) recalling that the quantum numbers must be integers, each combination of which represents a particular energy and corresponds to a point in the "space." (See Figure 8-17.) Since the quantum numbers must all be positive, the "space" is confined to that octant of the sphere, as Figure 8-17 shows.

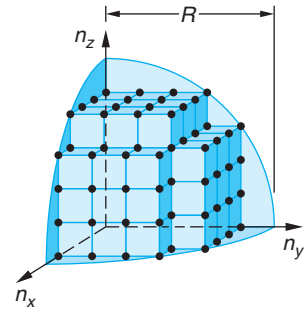

Figure 8-17 A representation of the allowed quantum states for a system of particles confined in a three-dimensional infinite square well. The radius $R \propto E^{1/2}$.

The number of states N within radius R (equal to the number of different combinations of the quantum numbers) in the volume is given by

$$N = \left(\frac{1}{8}\right)\left(\frac{4\pi R^3}{3}\right) = \frac{\pi}{6}\left(\frac{E}{E_0}\right)^{3/2} \qquad \textbf{8-39}$$

The density of states in $n_x\, n_y\, n_z$ "space" is

$$g(E) = \frac{dN}{dE} = \frac{\pi}{4}E_0^{-3/2}E^{1/2} = \frac{(2m)^{3/2}L^3}{4\pi^2\hbar^3}E^{1/2} \qquad \textbf{8-40}$$

or

$$g(E) = \frac{(2m)^{3/2}V}{4\pi^2\hbar^3}E^{1/2} = \frac{2\pi(2m)^{3/2}V}{h^3}E^{1/2} \qquad \textbf{8-41}$$

where the volume $V = L^3$. If the particles were electrons, then each state could accommodate two (one with spin up and one with spin down) and the density of states $g_e(E)$ would be twice that given by Equation 8-41, or

$$g_e(E) = \frac{4\pi(2m_e)^{3/2}V}{h^3}E^{1/2} \qquad \textbf{8-42}$$

We can compute the constant e^{α} in the Boltzmann distribution for these two cases from the normalization condition

$$N = \int_0^\infty n_B(E)\,dE = \int_0^\infty g_B(E)f_B(E)\,dE = \int_0^\infty g_B(E)e^{-\alpha}e^{-E/kT}\,dE \qquad \textbf{8-43}$$

If the distinguishable particles are electrons, $g_B(E) = g_e(E)$ and we have that

$$N = e^{-\alpha}\frac{4\pi(2m_e)^{3/2}V}{h^3}\int_0^\infty E^{1/2}e^{-E/kT}\,dE$$

which, when evaluated, yields

$$N = \frac{2(2\pi m_e kT)^{3/2}V}{h^3}e^{-\alpha}$$

or

$$e^{-\alpha} = \frac{Nh^3}{2(2\pi m_e kT)^{3/2}V} \quad \text{or} \quad e^{\alpha} = \frac{2(2\pi m_e kT)^{3/2}V}{Nh^3} \qquad \textbf{8-44}$$

For particles that do not obey the exclusion principle, the 2 multiplying the parentheses in Equation 8-44 is not present. Note that $e^{-\alpha}$ depends upon the number density of particles N/V. Note too that $e^{-\alpha}$ is essentially the quantity on the left side of Equation 8-36, which was obtained from de Broglie's relation for classical particles. Thus, the test for when the Boltzmann distribution may be used given by Equation 8-36 is equivalent to the condition that $e^{-\alpha} \ll 1$.

FÈUE WHE

Questions

5. How can identical particles also be distinguishable classically?
6. What are the physical conditions under which the Boltzmann distribution holds for a system of particles?
7. Do the opposite spins of two electrons in the same state make them distinguishable from each other?
8. How would you characterize a boson? A fermion?

8-3 The Bose-Einstein Condensation

We saw in Section 8-2 that, for ordinary gases, the Bose-Einstein distribution differs very little from the classical Boltzmann distribution, basically because there are many quantum states per particle due to the low density of gases and the large mass of the particles. However, for liquid helium, there is approximately one particle per quantum state at very low temperatures, and the classical distribution is invalid, as was illustrated in Example 8-6. The somewhat daring idea that liquid helium can be treated as an ideal gas obeying the Bose-Einstein distribution was suggested in 1938 by F. London in an attempt to understand the amazing properties of helium at low temperatures. When liquid helium is cooled, several remarkable changes take place in its properties at a temperature of 2.17 K. In 1924, H. Kamerlingh Onnes and J. Boks measured the density of liquid helium as a function of temperature and discovered a cusp in the curve at that temperature, as illustrated in Figure 8-18. In 1928, W. H. Keesom and M. Wolfke suggested that this discontinuity in the slope of the curve was an indication of a phase transition. They used the terms "helium I" for the liquid above 2.17 K, called the *lambda point* (see Figure 8-19), and "helium II" for the liquid below that temperature. In London's theory, called the two-fluid model, helium II is imagined to consist of two parts, a normal fluid with properties similar to helium I and a superfluid (i.e., a fluid with viscosity ≈ 0) with quite different properties. The density of liquid helium II is the sum of the densities of the normal fluid and the superfluid:

$$\rho = \rho_s + \rho_n \qquad \textbf{8-45}$$

As the temperature is lowered from the lambda point, the fraction consisting of the superfluid increases and that of the normal fluid decreases until, at absolute zero, only the superfluid remains. The superfluid corresponds to the helium atoms being in the lowest possible quantum state, the ground state. These atoms are not excited to higher states, so the superfluid cannot contribute to viscosity. When the viscosity of helium II is measured by the rotating disk method (a standard technique for measuring the viscosity of liquids), only the normal-fluid component exerts a viscous force on the disk. As the

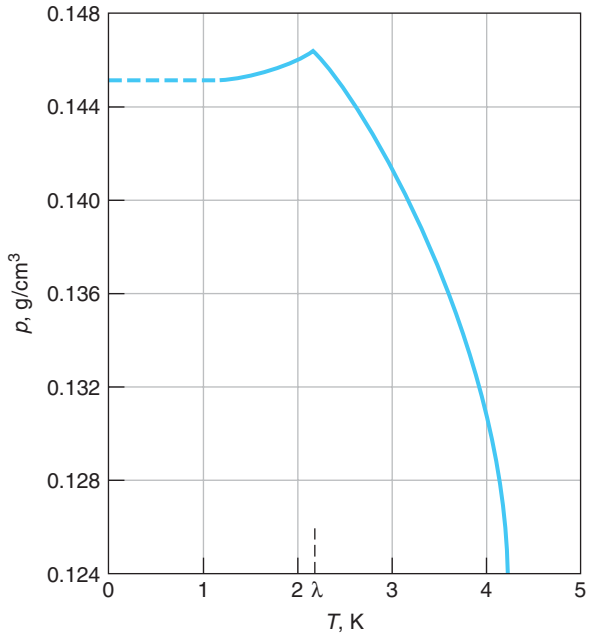

Figure 8-18 Plot of density of liquid helium versus temperature, by Kamerlingh Onnes and Boks. Note the discontinuity at 2.17 K. [*From F. London, Superfluids (New York: Dover Publications, Inc., 1964). Reprinted by permission of the publisher.*]

temperature is lowered, the fraction of helium in the normal component decreases from 100 percent at the lambda point to 0 percent at $T = 0$ K; thus, the viscosity decreases rapidly with temperature in agreement with experiment.

It is not at all obvious that liquid helium should behave like an ideal gas, because the atoms do exert forces on each other. However, these are weak van der Waals forces (to be discussed in Chapter 9), and the fairly low density of liquid helium (0.145 g/cm^3 near the lambda point) indicates that the atoms are relatively far apart. The ideal gas model is therefore a reasonable first approximation. It is used mainly because it is relatively simple and because it yields qualitative insight into the behavior of this interesting fluid.

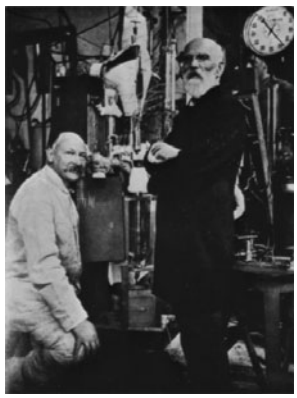

H. Kamerlingh Onnes and J. D. Van der Waals by the helium liquefier in the Kamerlingh Onnes Laboratory in Leiden in 1911. [*Courtesy of the Kamerlingh Onnes Laboratory.*]

EXPLORING
Liquid Helium

In a classic experiment conducted in 1908, H. Kamerlingh Onnes[9] succeeded in liquefying helium, condensing the last element that had steadfastly remained in gaseous form and culminating a determined effort that had consumed nearly a quarter of a century of his life. Even then, he nearly missed seeing it. After several hours of cooling, the temperature of the helium sample, being measured by a constant-volume helium gas thermometer, refused to fall any further. The liquid hydrogen being used to precool the system was gone, and it appeared that the experiment had failed when one of the several interested visitors gathered in Kamerlingh Onnes's lab suggested that perhaps the temperature was steady because the thermometer was immersed in boiling liquid that was so completely transparent as to be very hard to see. At the visitor's suggestion, a light was shined from below onto the glass sample vessel and the gas-liquid interface became clearly visible! Condensation to the very low-density, transparent liquid had occurred at 4.2 K.

The liquid helium must have been boiling vigorously. Soon afterward Kamerlingh Onnes was able to reduce the temperature further, passing below 2.17 K, at which point the vigorous boiling abruptly ceased. He must have observed the sudden cessation of the violent boiling, yet he made no mention of it then or in the reports of any of his many later experiments. Indeed, it was another quarter century before any mention of this behavior would appear in the literature,[10] even though many investigators must have surely seen it. The abrupt halt in boiling at 2.17 K signaled a phase transition in which helium changed from a normal fluid to a *superfluid*, that is, bulk matter that flows essentially without resistance (viscosity ≈ 0). Of all the elements, only the two naturally occurring isotopes of helium exhibit this property. The transition to the superfluid phase in ^{4}He occurs at 2.17 K. In ^{3}He, which accounts for only 1.3×10^{-4} percent of natural helium, the transition occurs at about 2 mK. This transition should not be interpreted as due in some way to a peculiarity in the structure of helium. Liquid phases of other bosons do not become superfluids because all other such systems solidify at temperatures well above the critical temperature for Bose-Einstein condensation. Only helium remains liquid under its vapor pressure at temperatures approaching absolute zero.[11] The fundamental reason that it does not solidify is that the interaction potential energy (see Section 9-3) between helium molecules is quite weak. Since helium atoms have small mass, their zero-point motion (i.e., their motion in the lowest-allowed energy level—see Section 5-6) is large, in fact, so large that its kinetic energy exceeds the interaction potential energy, thus melting the solid at low pressure. It is the superfluid phase of ^{4}He that we will be referring to throughout the remainder of this section. It turns out that ^{3}He becomes a superfluid for a different reason. (*Hint:* ^{4}He has spin 0, hence is a boson; ^{3}He has spin $\frac{1}{2}$ and is thus a fermion.)

Liquid helium, because of its extremely low boiling temperature, is the standard coolant for superconducting magnets throughout the world. Medical diagnostic MRI systems use such magnets. The large particle accelerators at, e.g., CERN and Fermilab use hundreds of them (see Chapter 11).

FEUE WHE

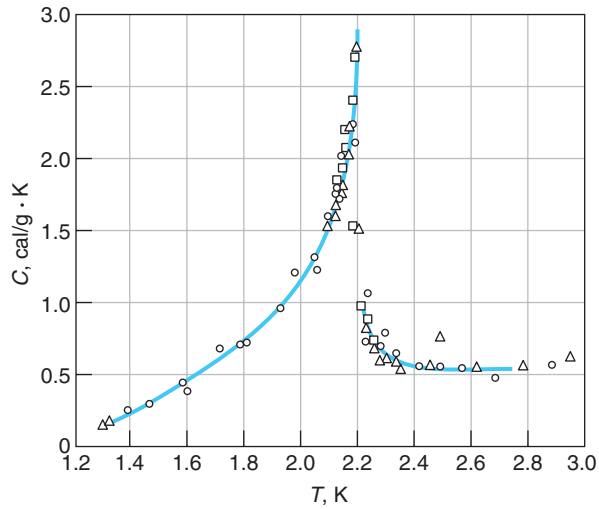

Figure 8-19 Specific heat of liquid helium versus temperature. Because of the resemblance of this curve to the Greek letter λ, the transition point is called the lambda point. [*From F. London, Superfluids (New York: Dover Publications, Inc., 1964). Reprinted by permission of the publisher.*]

Experimental Characteristics of Superfluid ^{4}He

In 1932 W. Keesom and K. Clusius measured the specific heat as a function of temperature and made a dramatic discovery of an enormous discontinuity, obtaining the curve shown in Figure 8-19. Because of the similarity of this curve to the Greek letter λ, the transition temperature 2.17 K is called the *lambda point*. Figure 8-20 shows this same curve measured with much greater resolution. Just above the lambda point, He boils vigorously as it evaporates. The bubbling immediately ceases at the lambda point, although evaporation continues. This effect is due to the sudden large increase in the thermal conductivity at the lambda point. In normal liquid helium, like other liquids, the development of local hot spots causes local vaporization, resulting in the formation of bubbles. Below the lambda point the thermal conductivity becomes so large, dissipating heat so rapidly, that local hot spots cannot form. Measurements of thermal conductivity show that helium II conducts heat better than helium I by a factor of more than a million; in fact, helium II is a better heat conductor than any metal, exceeding that of copper at room temperature by a factor of 2000. This conduction process is different from ordinary heat conduction, for the rate of conduction is not proportional to the temperature difference. Bubble formation ceases (even though evaporation continues) because all parts of the fluid are at exactly the same temperature.

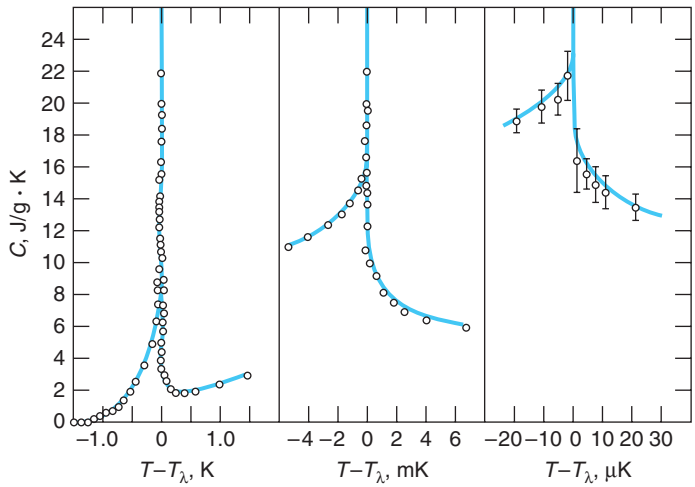

Figure 8-20 The lambda point with high resolution. The specific heat curve maintains its shape as the scale is expanded. [*From M. J. Buckingham and W. M. Fairbank, "The Nature of the λ-Transition," Progress in Low Temperature Physics, edited by C. J. Gorter, Vol. III, (Amsterdam: North-Holland Publishing Company, 1961).*]

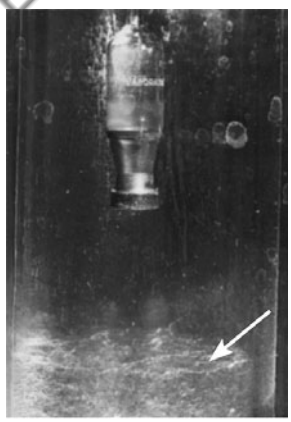

(*a*)

(*b*)

Figure 8-21 (*a*) Liquid helium being cooled by evaporation just above the lambda point boils vigorously. (*b*) Below the lambda point the boiling ceases and the superfluid runs out through the fine pores in the bottom of the vessel suspended above the helium bath. [*Courtesy of Clarendon Laboratory. From K. Mendelssohn, The Quest for Absolute Zero: The Meaning of Low Temperature Physics, World University Library (New York: McGraw-Hill Book Company, 1966).*]

This lambda-point transition is clearly visible on the surface of the liquid shown in Figures 8-21*a* and *b*, which also illustrates the phenomenon largely responsible for applying the name *superfluid* to helium II. The small container of liquid helium suspended above the surface has a bottom made of tightly packed, ultrafine powder (fine emery powder or jeweler's rouge). The microscopic channels through the powder are too small for the ordinary liquid to pass through, but when the temperature drops below the lambda point, the superfluid flows through essentially unimpeded, the viscosity suddenly dropping at that point by a factor of about one million.[12]

Figures 8-22*a* and *b* illustrate the *creeping film* effect. A container containing liquid helium has a thin film (several atomic layers thick) of helium vapor coating the walls, just as is the case with any other enclosed liquid. However, if the level of liquid helium in the container is raised above the general level in the reservoir, such as the cup in the photo of Figure 8-22*a*, the superfluid film on the walls creeps up the inner walls, over the top, and down the outside and returns to the reservoir until both surfaces are level or the cup is empty! In the *thermomechanical effect*, which involves two containers of liquid helium II connected by a superleak, if heat is added to one side, e.g., by a small heater as illustrated in Figure 8-23*a*, the superfluid on the other side migrates *toward* the heated side, where the level of liquid (still superfluid) rises. If the system is suitably arranged, as in Figure 8-23*b*, the rising liquid can jet out a fine capillary in the so-called *fountain effect*.[13]

Superfluid ^{3}He

Physicists thought for a long time that ^{3}He could not form a superfluid since its nucleus consists of two protons and a neutron. It thus has $\frac{1}{2}$-integer spin and obeys Fermi-Dirac statistics, which prohibits such particles from sharing the same energy state. However, early in the 1970s D. M. Lee, D. D. Osheroff, and R. C. Richardson showed that when cooled to 2.7 mK, the spins of *pairs* of ^{3}He atoms can align parallel, creating, in effect, a boson of spin 1 and allowing the liquid to condense to a superfluid state. Two additional superfluid states were subsequently discovered, a spin-0 state (antiparallel spins) at 1.8 mK and a second spin-1 state that is created when an external magnetic field aligns the spins of the ^{3}He pairs. The three scientists received the 1996 Nobel Prize for their discovery.

(*a*)

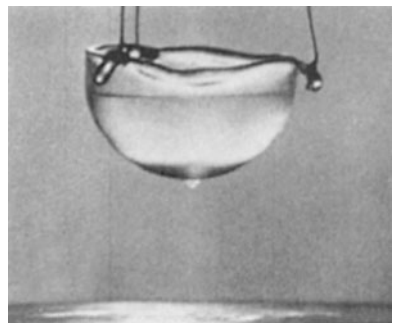

(*b*)

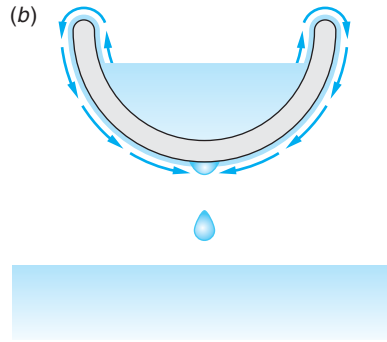

Figure 8-22 (*a*) The creeping film. The liquid helium in the dish is at a temperature of about 1.6 K. A thin film creeps up the sides of the dish, over the edge, and down the outside to form the drop shown, which then falls into the reservoir below. [*Courtesy of A. Leitner, Rensselaer Polytechnic Institute.*] (*b*) Diagram of creeping film. If the dish is lowered until partially submerged in the reservoir, the superfluid creeps out until the levels in the dish and reservoir are the same. If the level in the cup is initially lower than that of the reservoir, superfluid creeps into the dish.

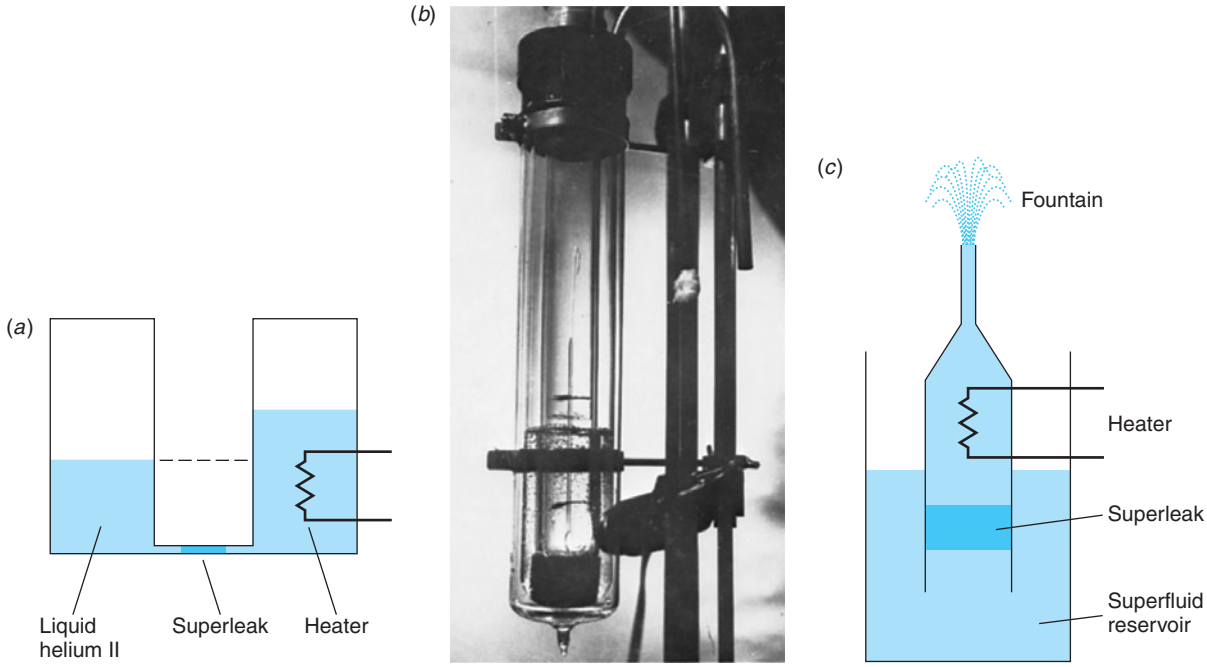

Figure 8-23 (*a*) Diagram of the thermomechanical effect. The level of the fluid rises in the container where the heat is being added. (*b*) A bulb containing liquid helium is in a cold bath of liquid helium II at 1.6 K. When light containing infrared radiation is focused on the bulb, liquid helium rises above the ambient level. The height of the level depends on the narrowness of the tube. If the tube is packed with powder and the top drawn out into a fine capillary, the superfluid spurts out in a jet as shown, hence the name "fountain effect." (*c*) Diagram showing the components in the photograph in (*b*). [*Photo courtesy of Helix Technology Corporation.*]

In the Bose-Einstein distribution the number of particles in the energy range dE is given by $n(E)dE$, where we have from Equation 8-37*b*

$$n(E) = \frac{g(E)}{e^{\alpha}e^{E/kT} - 1} \qquad \textbf{8-46}$$

where $g(E)$ is given by Equation 8-41. The constant α, which is determined by normalization, cannot be negative, for if it were, $n(E)$ would be negative for low values of E. This situation would make no sense physically since, if α were negative for small energies (i.e., $|\alpha| > E/kT$), then $f_{BE}(E)$ would be negative. But $f_{BE}(E)$ is the number of particles in the state with energy E, and a negative value would be meaningless. The normalization condition is

$$N = \int_0^{\infty} n(E)\,dE = \frac{2\pi V}{h^3}(2m)^{3/2}\int_0^{\infty}\frac{E^{1/2}\,dE}{e^{\alpha}e^{E/kT} - 1} = \frac{2\pi V}{h^3}(2mkT)^{3/2}\int_0^{\infty}\frac{x^{1/2}\,dx}{e^{\alpha+x} - 1} \qquad \textbf{8-47}$$

where $x = E/kT$ and the integral in this equation is a function of α.

The usual justification for using a continuous energy distribution to describe a quantum system with discrete energies is that the energy levels are numerous and closely spaced. In this case, as we have already seen, for a gas of N particles in a macroscopic box of volume V (the container), this condition holds, as you can demonstrate for yourself by computing the spacing using Equation 7-4 for a three-dimensional box.

FEUE WHE

However, in replacing the discrete distribution of energy states by a continuous distribution, we ignore the ground state. This is apparent from Equation 8-41, where we see that $g(E) \propto E^{1/2}$ therefore, if $E = 0$, $g(E) = 0$ also. This has little effect for a gas consisting of Fermi-Dirac particles since there can be only two particles in any single state, and ignoring two particles out of 10^{22} causes no difficulty. In a Bose-Einstein gas, however, there can be any number of particles in a single state. If we ignore the ground state, as we have up to now, the normalization condition expressed by Equation 8-47 cannot be satisfied below some minimum critical temperature T_c corresponding to the minimum possible value of α, $\alpha = 0$. This implies that at very low temperatures there are a significant number of particles in the ground state.

The critical temperature T_c can be found by evaluating Equation 8-47 numerically. The integral has a maximum value of 2.315 when α has its minimum value of 0. This results in a maximum value for N/V given by

$$\frac{N}{V} \leq \frac{2\pi}{h^3}(2mkT)^{3/2}(2.315)$$

Since N/V is determined by the density of liquid helium, this implies a value for the critical temperature, given by

$$T \geq \frac{h^2}{2mk}\left[\frac{N}{2\pi(2.315)V}\right]^{2/3} = T_c \qquad \textbf{8-48}$$

Inserting the known constants and the density of helium, we find for the critical temperature

$$T_c = 3.1 \text{ K} \qquad \textbf{8-49}$$

For temperatures below 3.1 K the normalization Equation 8-47 cannot be satisfied for any value of α. Evidently at these temperatures there are a significant number of particles in the ground state, which we have not included.

We can specifically include the ground state by replacing Equation 8-47 with

$$N = N_0 + \frac{2\pi V}{h^3}(2mkT)^{3/2}\int_0^\infty \frac{x^{1/2}\,dx}{e^{\alpha+x} - 1} \qquad \textbf{8-50}$$

where N_0 is the number in the ground state. If we choose $E_0 = 0$ for the energy of the ground state, this number is

$$N_0 = \frac{g_0}{e^\alpha e^{E_0/kT} - 1} = \frac{1}{e^\alpha - 1} \qquad \textbf{8-51}$$

where g_0, the density of states or statistical weight, is 1 for a single state. We see that N_0 becomes large as α becomes small. With the inclusion of N_0, which depends on α, the normalization condition (Equation 8-50) can be met and α can be computed numerically for any temperature and density. For temperatures below the critical temperature T_c we see from Equation 8-51 that $e^\alpha = 1 + 1/N_0$. Expanding e^α for small α yields $e^\alpha = 1 + \alpha + \ldots$, and we thus conclude that α is of the order of N_0^{-1} and that the fraction of molecules in the ground state is given approximately by

$$\frac{N_0}{N} \approx 1 - \left(\frac{T}{T_c}\right)^{3/2} \qquad \textbf{8-52}$$

FÈUE WHE

In the London two-fluid model the N_0 atoms that we added in Equation 8-50 have condensed to the ground state. These particles in the ground state constitute the superfluid. The remaining $(N - N_0)$ atoms are the normal fluid. That fraction of the fluid that is superfluid for $T \leq T_c$ is shown in Figure 8-24.

The value $T_c = 3.1$ K is not very different from the observed lambda-point temperature $T = 2.17$ K, especially considering that our calculation is based on the assumption that the liquid helium is an ideal gas. The process of atoms dropping into the ground state as the temperature is lowered below T_c is called *Bose-Einstein condensation*. Such an occurrence was predicted by Einstein in 1924, before there was any evidence that such a process could occur in nature.

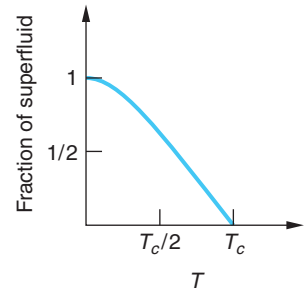

Figure 8-24 Graph of the fraction of superfluid in a sample of liquid helium as a function of temperature.

The Bose-Einstein Condensate

Like all atoms, the constituents of ^{4}He (protons, neutrons, and electrons) are fermions; however, they are assembled in such a way that the total spin of the ground state is integer (zero), so that the ^{4}He *atom* is a boson. Indeed, a review of the periodic table shows that, although atoms can be either fermions or bosons, the ground-state spins are mostly integer, so in their lowest energy state most atoms are bosons. This fact is of no great consequence in determining the properties of a gas in a macroscopic container because the spacing between the quantized energies is extremely small, so the probability that any particular level is occupied by an atom is also small. For example, the spacing between adjacent levels in a cubical box with a volume of 1 cm^3 containing sodium gas is about 10^{-20} eV (see Equation 8-38), so even at relatively low temperatures the atoms in a sample of a few billion would be widely spread among the allowed levels, as in Figure 8-25*a*. In addition, the average distance between atoms in the box would be about $(10^{-6}\ \text{m}^3/10^9\ \text{atoms})^{1/3} = 10^{-5}$ m, or tens of thousands of atomic diameters, so the interactions between the atoms are minuscule.

If our goal is to form a Bose-Einstein condensate (BEC) from the widely separated atomic bosons of the gas sample in the box, the obvious approach is that used to condense any gas; that is, the sample is cooled and the density is increased until the gas liquefies. However, this approach presents us with a formidable problem: as the gas liquefies, the atoms get very close together, the density approximating that of the solid. The atoms now interact strongly, mainly via their outer electrons, and thus all begin to act like fermions! (This is essentially what happens in liquid helium II, where even at very low temperatures the fraction of the atoms in the ground state [superfluid phase] is only about 10 percent or so.)

This problem was solved by C. E. Wieman and E. Cornell in 1995, more than 70 years after Einstein's prediction. They did it by forming the BEC directly from a supersaturated vapor, cooling the sample but never allowing it to reach ordinary thermal equilibrium.[14] This was done with standard cooling methods and a very neat "trick." First, a sample of rubidium vapor at room temperature was illuminated by the beams from six small diode

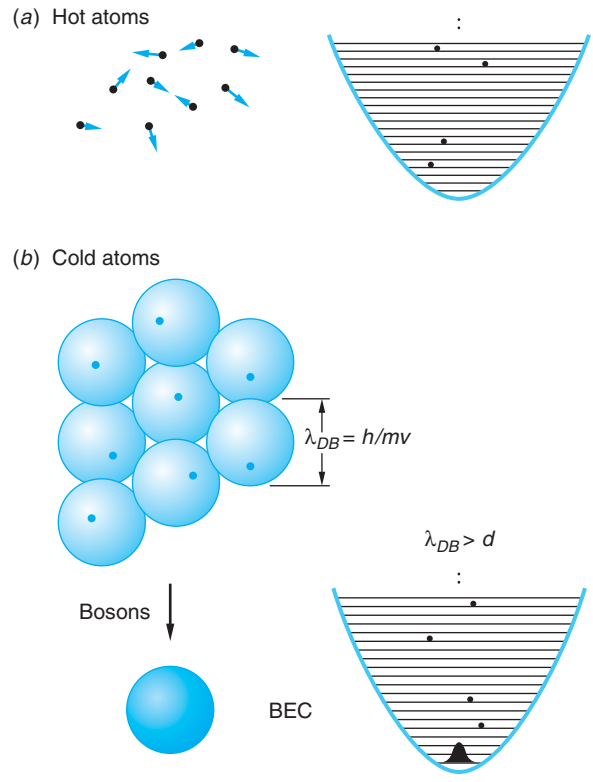

Figure 8-25 (*a*) The atoms in a sample of dilute gas in any macroscopic container are distributed over a very large number of levels, making the probability of any one level being occupied quite small. (*b*) Cooled to the point where the de Broglie wavelength becomes larger than the interatomic spacing, atoms fall into the ground state, all occupying the same region of space.

lasers of appropriate frequency. Collisions of the laser photons with atoms in the low-speed tail of the Maxwell distribution (see Figure 8-3) slowed those atoms, and within a second or two a sample of about 10^7 atoms collected in the volume defined by the intersecting laser beams, about 1.5 cm in diameter. The temperature of this laser-cooled sample was about 1 mK. Then a special magnetic trap (i.e., a magnetic field shaped so as to confine the atoms) was used to "squeeze" the cooled sample, whose atomic spins ($= 2\hbar$) had been polarized in the $m = 2$ direction. (Polarizing the spins was the "trick" referred to above. Equilibrium is reached in the spin-polarized vapor very rapidly, long before the true thermal equilibrium state—the solid—can form, thus maintaining the sample as a supersaturated vapor.) The warmer atoms on the high-speed tail of the Maxwell distribution of the trapped atoms are allowed to escape through a "leak" in the magnetic trap, taking with them a substantial amount of the kinetic energy and evaporatively cooling the remaining few thousand atoms to less than 100 nK, just as water molecules evaporating from the surface of a cup of hot coffee cool that which remains in the cup. These remaining cold atoms fall into the ground state of the confining potential and have, within the experimental uncertainties, reached absolute zero. They are the condensate. The BEC is illustrated in Figure 8-25*b*. The condensate, if left undisturbed in the dark, lives for 15 to 20 seconds, its destruction eventually resulting from collisions with impurity atoms in the vacuum that are also colliding with the hot (room temperature) walls of the experimental cell. The peak in Figure 8-26 is a *macroscopic quantum wave function* of the condensate.

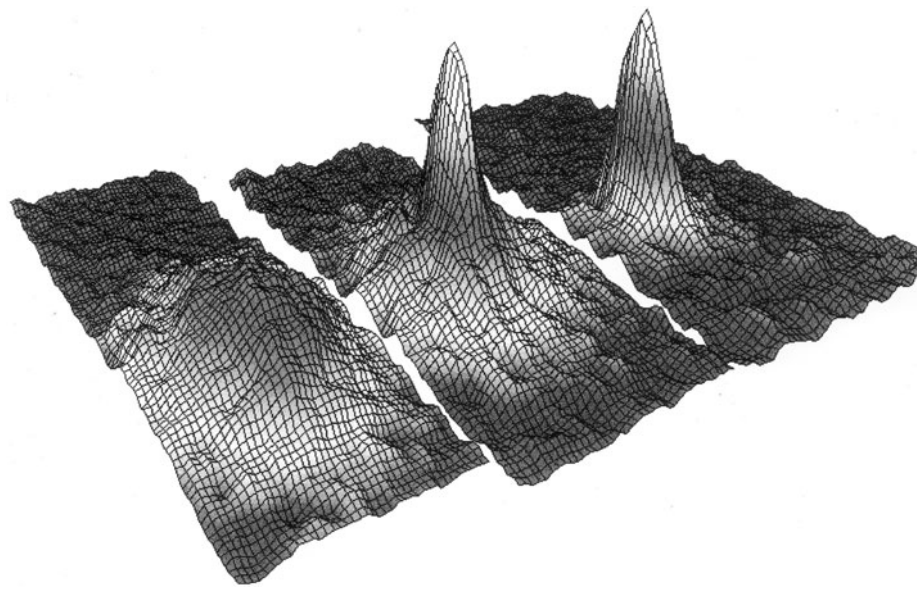

Figure 8-26 Two-dimensional velocity distributions of the trapped cloud for three experimental runs with different amounts of cooling. The axes are the x and z velocities, and the third axis is the number density of atoms per unit velocity-space volume. This density is extracted from the measured optical thickness of the shadow. The distribution on the left shows a gentle hill and corresponds to a temperature of about 200 nK. The middle picture is about 100 nK and shows the central condensate spire on the top of the noncondensed background hill. In the picture on the right, only condensed atoms are visible, indicating that the sample is at absolute zero, to within experimental uncertainty. The gray bands around the peaks are an artifact left over from the conversion of false-color contour lines into the present black and white. [*From C. E. Wieman, American Journal of Physics* ***64*** *(7), 853 (1996).*]

FÈUE WHE

Since the discovery by Wieman and Cornell, several other physicists have produced Bose-Einstein condensates. One of the largest produced (by W. Ketterle and co-workers) contained 9×10^7 sodium atoms, was about a millimeter long, and lived for half a minute. Its direct photograph is shown in Figure 8-27. As of this writing, the largest condensates are made of hydrogen and contain about 10^9 atoms.

Does this discovery have any potential use? The answer is, probably many that we can't even imagine yet, but here is one possibility. The BEC can form the basis of an *atomic laser*. This was demonstrated in late 1996, also by Ketterle and his colleagues, and is illustrated in Figure 8-28. The condensate is coherent matter, just as the laser beam is coherent light. It could place atoms on substrates with extraordinary precision, conceivably replacing microlithography in the production of microcircuitry. Here is another potential use for the BEC: It could form the basis for atomic interferometers, making possible measurements far more precise than those made with visible lasers since the de Broglie wavelengths are much shorter than those of light. Ketterle, Cornell, and Wieman shared the 2001 Nobel Prize in Physics for their work.

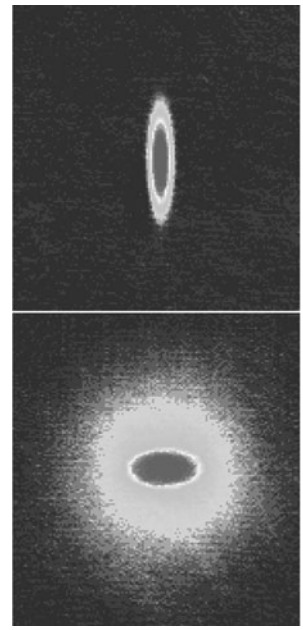

Figure 8-27 Successive images show shadow of a millimeter-long cloud of atoms containing Bose-Einstein condensate as it expands from its initial cigar shape (top). [*From D. S. Durfee, Science* ***272****, 1587 (1996).*]

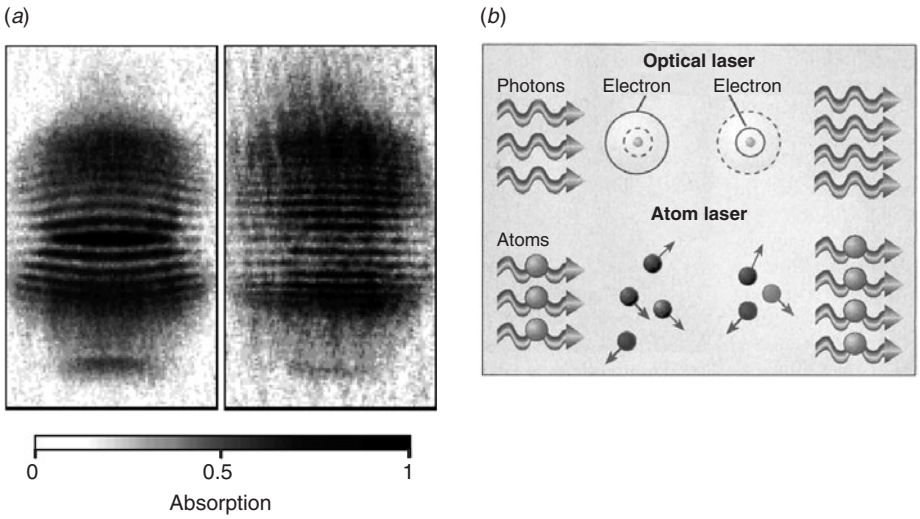

Figure 8-28 (*a*) When the two identical condensates of sodium atoms, each containing about 5×10^6 atoms, were allowed to expand freely and overlapped, phase contrast imagery revealed interference fringes, the "signature" of coherent waves—the first atomic laser. (*b*) Optical lasers amplify light by stimulating atoms to emit photons. Atom lasers amplify by stimulating more atoms to join the "beam." [(*a*) *From D. S. Durfee, Science* ***275****, 639 (1997).* (*b*) *From Science* ***279****, 986 (1998). Courtesy of L. Carroll.*]

Questions

9. Explain how the escaping "hot" rubidium atoms cool those remaining in the sample.
10. What is Bose-Einstein condensation?
11. Would you expect a gas or liquid of ^{3}He atoms to be much different from one of ^{4}He atoms? Why or why not?

8-4 The Photon Gas: An Application of Bose-Einstein Statistics

Photon Gas

Planck's empirical expression for the energy spectrum of the blackbody radiation in a cavity (Equation 3-18) can now be derived by treating the photons in the cavity as a gas consisting of bosons. The distribution is then given by

$$f_{BE}(E) = \frac{1}{e^{\alpha}e^{E/kT} - 1} \qquad \textbf{8-24}$$

As we saw in Section 8-2 and in particular in the discussion of Equation 8-44, the value of α is determined by the total number of particles that the system contains. However, in the case of photons contained in a cavity, which we are discussing, that seems to present a problem since the total number of photons is not constant. Photons are continually being created (emitted by the oscillators in the cavity walls) and destroyed (absorbed by the oscillators). Even so, this does indeed specify the value of α: it tells us that Equation 8-24 *for photons* cannot be a function of e^{α}; i.e.,

$$f_{\text{ph}}(E) = \frac{1}{e^{E/kT} - 1} \qquad \textbf{8-53}$$

The fact that the total number of photons is not constant makes it necessary that $\alpha = 0$ so that $e^{\alpha} = 1$. We will see in a moment that this must be true.

The number of photons with energy E is found by substituting Equation 8-53 into Equation 8-37*b*, which yields

$$n_{\text{ph}}(E) = g_{\text{ph}}(E)f_{\text{ph}}(E)$$

or

$$n_{\text{ph}}(E) = \frac{g_{\text{ph}}(E)}{e^{E/kT} - 1} \qquad \textbf{8-54}$$

The density of states $g_{\text{ph}}(E)$ is derived in the same manner as it was for massive particles in Section 8-2. The result, which we first encountered as $n(\lambda) = 8\pi\lambda^{-4}$ in our discussion of Planck's derivation of the blackbody spectrum, is given in terms of the photon frequency f as

$$g_{\text{ph}}(E)\,dE = \frac{8\pi V f^2\,df}{c^3} = \frac{8\pi V E^2\,dE}{c^3h^3} \qquad \textbf{8-55}$$

where V is the volume of the cavity. The energy density $u(E)dE$ in the energy interval between E and $E + dE$ is then given by

$$u(E)\,dE = \frac{Eg_{\text{ph}}(E)f_{\text{ph}}(E)\,dE}{V} = \frac{8\pi E^3\,dE}{c^3h^3(e^{E/kT} - 1)} \qquad \textbf{8-56}$$

or, in terms of the photon frequency f, using $E = hf$ for the conversion, we have

$$u(f)\,df = \frac{8\pi f^2}{c^3}\frac{hf\,df}{e^{hf/kT} - 1} \qquad \textbf{8-57}$$

FEUE WHE

Equation 8-57 is identical to Equation 3-18 when the latter is converted from wavelength λ to frequency f as the variable using $c = f\lambda$. We saw in Chapter 3 that Equation 3-18 is in precise agreement with experimental observations. This agreement serves as justification for the Bose-Einstein distribution function for photons given by Equation 8-53, which resulted from our argument that $\alpha = 0$ for photons. Notice that Planck's derivation presented in Chapter 3, in which the radiation in the blackbody cavity was treated as a set of distinguishable standing electromagnetic waves to which he (correctly) applied the Boltzmann distribution, agrees exactly with the derivation presented here, in which the radiation is treated as indistinguishable particles to which the Bose-Einstein distribution must be applied. This is an example of the wave-particle duality of photons.

EXAMPLE 8-7 Photon Density of the Universe The high temperature of the early universe implied a thermal (i.e., blackbody) electromagnetic radiation field which has, over aeons, cooled to the present 2.7 K. This cosmic background radiation was discovered in 1965. (See Chapter 13.) Compute the number of these photons per unit volume in the universe.

SOLUTION

1. The number of photons with energy E is given by Equation 8-54:
$$n_{ph}(E) = \frac{g_{ph}(E)}{e^{E/kT} - 1}$$

2. The total number per unit volume N/V is then given by
$$\frac{N}{V} = \frac{1}{V}\int_0^\infty n_{ph}(E)\,dE = \frac{1}{V}\int_0^\infty \frac{g_{ph}(E)\,dE}{e^{E/kT} - 1}$$

3. Substituting the density of states $g_{ph}(E)$ from Equation 8-55 yields
$$\frac{N}{V} = \int_0^\infty \frac{8\pi E^2\,dE}{(ch)^3(e^{E/kT} - 1)} = \frac{8\pi(kT)^3}{(ch)^3}\int_0^\infty \frac{(E/kT)^2(dE/kT)}{e^{E/kT} - 1}$$

4. Letting $x = E/kT$, this can be written
$$\frac{N}{V} = 8\pi\left(\frac{kT}{ch}\right)^3\int_0^\infty \frac{x^2\,dx}{e^x - 1}$$

5. Evaluating the integral from standard tables:
$$\int_0^\infty \frac{x^2\,dx}{e^x - 1} \approx 2.40$$

6. Substituting values into the expression for N/V in step 4 yields
$$\frac{N}{V} = 8\pi\left(\frac{1.38 \times 10^{-23}\ \text{J/K} \times 2.7\ \text{K}}{3.00 \times 10^8\ \text{m/s} \times 6.63 \times 10^{-34}\ \text{J}\cdot\text{s}}\right)^3 (2.40)$$
$$= 3.97 \times 10^8\ \text{photons/m}^3$$

Quantization of the Energy States of Matter

We pointed out earlier that the molar heat capacity C_V for solids falls appreciably below the classical Dulong-Petit value of $3R$ when the temperature falls below some critical value. In 1908 Einstein showed that the failure of the equipartition theorem in predicting the specific heats of solids at low temperatures could be understood if it were assumed that the atoms of the solid could have only certain discrete energy values. Einstein's calculation is closely related to Planck's calculation of the average energy of a harmonic oscillator, assuming the oscillator can take on only a discrete set of energies. The calculation itself presents no real problem, as we have seen in Chapter 3. Einstein's most important contribution in this area was the extension of the idea of quantization to any oscillating system, including matter. We will see in this subsection how the idea of quantized energy states for matter also explains the puzzling behavior of the heat capacities of diatomic gases that was pointed out in Section 8-1. In particular, we will be able to understand why the H_2 molecule seems to have only 3 degrees of freedom (corresponding to translation) at low temperatures, 5 degrees of freedom at intermediate temperatures (corresponding to translation and rotation), and 7 degrees of freedom at high temperature (corresponding to translation, rotation, and vibration).

Consider 1 mole of a solid consisting of N_A molecules, each free to vibrate in three dimensions about a fixed center. For simplicity, Einstein assumed that all the molecules oscillate at the same frequency f in each direction. The problem is then equivalent to $3N_A$ distinguishable one-dimensional oscillators, each with frequency f. The classical distribution function for the energy of a set of one-dimensional oscillators is the Boltzmann distribution, given by Equation 8-1. Following Planck, Einstein assumed that the energy of each oscillator could take on only the values given by

$$E_n = nhf \tag{8-58}$$

where $n = 0,1,2,\ldots$, rather than have an average value of kT as predicted by the equipartition theorem. He then used the Boltzmann distribution[15] to compute the average energy $\langle E \rangle$ for the distinguishable oscillators, just as we have done previously, from

$$\langle E \rangle = \int_0^\infty E n_B(E)\, dE \tag{8-59}$$

obtaining

$$\langle E \rangle = \frac{hf}{e^{hf/kT} - 1} \tag{8-60}$$

which is, of course, the same as Equation 3-17. We can expand the exponential, using $e^x \approx 1 + x + (x^2/2!) + \ldots$ for $x \ll 1$, where $x = hf/kT$ (see Appendix B2). At high temperatures the quantity $hf/kT \ll 1$ and then, keeping only the first two terms of the expansion,

$$e^{hf/kT} - 1 \approx \left(1 + \frac{hf}{kT} + \ldots\right) - 1 \approx \frac{hf}{kT}$$

and $\langle E \rangle$ approaches kT, in agreement with the equipartition theorem from classical statistics (see Equation 8-14).

FEUE WHE

The total energy for $3N_A$ oscillators is now

$$U = 3N_A\langle E\rangle = \frac{3N_A hf}{e^{hf/kT} - 1} \qquad \textbf{8-61}$$

and the heat capacity is

$$C_V = \frac{dU}{dT} = 3N_A k\left(\frac{hf}{kT}\right)^2 \frac{e^{hf/kT}}{(e^{hf/kT} - 1)^2} \qquad \textbf{8-62}$$

It is left as an exercise (see Problem 8-29) to show directly from Equation 8-62 that $C_v \to 0$ as $T \to 0$ and $C_v \to 3N_A k = 3R$ as $T \to \infty$.

By comparing the Einstein calculation of the average energy per molecule, Equation 8-60, with the classical one, we can gain some insight into the problem of when the classical theory will work and when it will fail. Let us define the critical temperature,

$$T_E = \frac{hf}{k} \qquad \textbf{8-63}$$

called the *Einstein temperature*. The energy distribution in terms of this temperature is

$$f_B(E_n) = Ae^{-E_n/kT} = Ae^{-nhf/kT} = Ae^{-nT_E/T}$$

For temperatures T much higher than T_E, small changes in n have little effect on the exponential in the distribution; that is $f_B(E_n) \approx f_B(E_{n+1})$. Then E can be treated as a continuous variable. However, for temperatures much lower than T_E, even the smallest possible change in n, $\Delta n = 1$, results in a significant change in $e^{-nT_E/T}$, and we would expect that the discontinuity of possible energy values becomes significant. Since hard solids have stronger binding forces than soft ones, their frequencies of molecular oscillation and therefore their Einstein temperatures are higher. For lead and gold, T_E is of the order of 50 to 100 K; ordinary temperatures of around 300 K are "high" for these metals, and they obey the classical Dulong-Petit law at these temperatures. For diamond, T_E is well over 1000 K; in this case 300 K is a "low" temperature, and C_v is much less than the Dulong-Petit value of $3R$ at this temperature.

The agreement between Equation 8-62 and experimental measurements justifies Einstein's approach to understanding the molar heat capacity of solids. Figure 8-29 shows a comparison of this equation with experiments. The curve fits the experimental points well except at very low temperatures, where the data fall slightly above the curve.

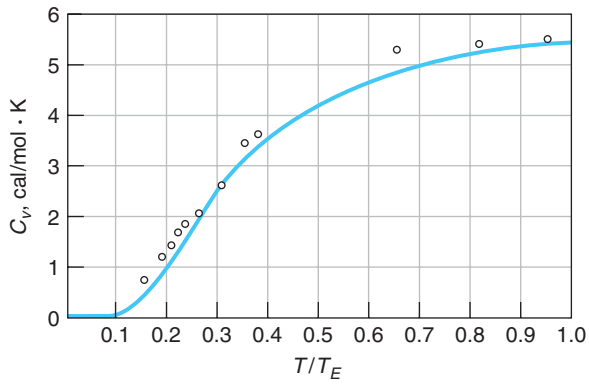

Figure 8-29 Molar heat capacity of diamond versus reduced temperature T/T_E. The solid curve is that predicted by Einstein. [*From Einstein's original paper, Annalen der Physik* ***22*** *(4), 180 (1907).*]

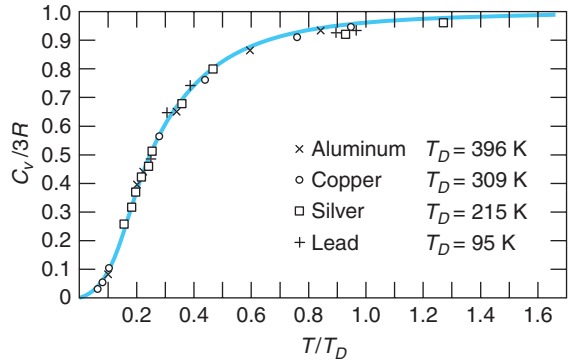

Figure 8-30 Molar heat capacity of several solids versus reduced temperature T/T_D, where T_D is the Debye temperature, defined as $T_D = hf_D/k$. The solid curve is that predicted by Debye. The data are taken from Debye's original paper. $C_v/3R = 1$ is the Dulong-Petit value. [*From Annalen der Physik* ***39*** *(4), 789 (1912), as adapted by David MacDonald, Introductory Statistical Mechanics for Physicists (New York: John Wiley & Sons, Inc., 1963); by permission.*]

The lack of detailed agreement of the curve with the data at low T is due to the oversimplification of the model. A refinement of this model was made by P. Debye, who gave up the assumption that all molecules vibrate at the same frequency. He allowed for the possibility that the motion of one molecule could be affected by that of the others and treated the solid as a system of coupled oscillators. The effect was to allow a range of vibrational frequencies from $f = 0$ up to a maximum f_D, called the *Debye frequency*, used to define the *Debye temperature* $T_D = hf_D/k$. This contrasts with the infinite range of oscillation modes in the blackbody cavity. Debye's argument was that the number of vibrational modes or frequencies cannot exceed the number of degrees of freedom of the atoms that make up the solid. Calculations with the Debye model are somewhat more involved and will not be considered here. The improvement of the Debye model over the Einstein model is shown by Figure 8-30. Note that *all* solids fall on the same curve.

Understanding Specific Heats of Gases

Let us now see if we can understand the specific heats of diatomic gases on the basis of discrete, or quantized, energies. In Section 8-1 we wrote the energy of a diatomic molecule as the sum of translational, rotational, and vibrational energies. If f is the frequency of vibration and the vibrational energy is quantized by $E_{\text{vib}} = nhf$, as we assumed for solids, we know from the previous calculation (see Equation 8-62) that for low temperatures, the average energy of vibration approaches zero and vibration will not contribute to C_V. We can define a critical temperature for vibration of a diatomic gas molecule by

$$T_v = \frac{hf}{k} \qquad \textbf{8-64}$$

where f is the frequency of vibration. Apparently $T_v > 15°$ C for all the diatomic gases listed in Table 8-1 except for Cl_2. From Figure 8-11 we can see that T_v is of the order of 1000 to 5000 K for H_2.

FEUE WHE

The rotational energy of a diatomic molecule is

$$E_R = \tfrac{1}{2} I\omega^2$$

where I is the moment of inertia and ω is the angular velocity of rotation. It is not obvious how the rotational energy is quantized or even if it is; however, let us make use of a result from Section 7-2, where we learned that the angular momentum is quantized. If L is the angular momentum of a diatomic molecule, $L = I\omega$, and we can write the energy as

$$E_R = \frac{L^2}{2I}$$

Equation 7-22 tells us that $L^2 = \ell(\ell + 1)\hbar^2$, where $\ell = 0,1,2,\ldots$. Thus, the rotational energy becomes

$$E_R = \ell(\ell + 1)\frac{h^2}{8\pi^2 I} \qquad \textbf{8-65}$$

The energy distribution function will contain the factor

$$e^{-E_R/kT} = e^{-\ell(\ell+1)h^2/8\pi^2 IkT}$$

and we can define a critical temperature for rotation similar to that for vibration as

$$T_R = \frac{E_R}{k} = \frac{h^2}{8\pi^2 Ik} \qquad \textbf{8-66}$$

If this procedure is correct, we expect that for temperatures $T \gg T_R$, i.e., $E_R \gg kT$, the equipartition theorem will hold for rotation and the average energy of rotation will approach $(\frac{1}{2})kT$ for each axis of rotation, while for low temperatures, $T \ll T_R$, the average energy of rotation will approach 0. Let us examine T_R for some cases of interest:

1. H_2. For rotation about the x or y axis as in Figure 8-10*a*, taking the z axis as the line joining the atoms, the moments of inertia I_x and I_y through the center of mass are

   $$I_x = I_y = \tfrac{1}{2}MR^2$$

   The separation of the atoms is about $R \approx 0.08$ nm. The mass of the H atom is about $M \approx 940 \times 10^6\ \text{eV}/c^2$. We first calculate kT_R:

   $$kT_R = \frac{h^2}{8\pi^2 I} = \frac{(hc)^2}{4\pi^2 Mc^2 R^2} = \frac{(1.24 \times 10^3\ \text{eV}\cdot\text{nm})^2}{4\pi^2(940 \times 10^6\ \text{eV})(0.08\ \text{nm})^2} \approx 6.4 \times 10^{-3}\ \text{eV}$$

   Using $k \approx 2.6 \times 10^{-2}\ \text{eV}/300\ \text{K}$, we obtain

   $$T_R = \frac{6.4 \times 10^{-3}}{2.6 \times 10^{-2}} 300\ \text{K} \approx 74\ \text{K}$$

   As can be seen from Figure 8-11, this is indeed the temperature region below which the rotational energy does not contribute to the heat capacity.

2. O_2. Since the mass of the oxygen atom is 16 times that of the hydrogen atom and the separation is roughly the same, the critical temperature for rotation will be $T_R \approx (74/16) \approx 4.6$ K. For all temperatures at which O_2 exists as a gas, $T \gg T_R$.

3. A monatomic gas, or rotation of diatomic gas about the z axis. We will take the H atom for calculation. The moment of inertia of the atom is mainly due to the electron since the radius of the nucleus is extremely small (about 10^{-15} m). The distance from the nucleus to the electron is about the same as the separation of atoms in the H_2 molecule. Since the mass of the electron is about 2000 times smaller than that of the atom, we have

$$I_H \approx \frac{1}{2000} I_{H_2}$$

and

$$T_R \approx 2000 \times 74 \text{ K} \approx 1.5 \times 10^5 \text{ K}$$

This is much higher than the dissociation temperature for any diatomic gas. Thus, $\langle E_R \rangle \approx 0$ for monatomic gases and for rotation of diatomic gases about the line joining the atoms for all attainable temperatures.

We see that energy quantization explains, at least qualitatively, the temperature dependence of the specific heats of gases and solids.

EXAMPLE 8-8 **Average Vibrational Energy** What is the average energy of vibration of the molecules in a solid if the temperature is (*a*) $T = hf/2k$, (*b*) $T = 4hf/k$?

SOLUTION

(*a*) This is lower than the critical temperature for vibration hf/k given by Equation 8-64, so we expect a result considerably lower than the high temperature limit of kT given by the equipartition theorem. From Equation 8-60 we have

$$\langle E \rangle = \frac{hf}{e^{hf/kT} - 1} = \frac{2kT}{e^2 - 1} = 0.31\, kT$$

(*b*) This temperature is four times the critical temperature, so we expect a result near the high temperature limit of kT. Using $hf/kT = 1/4$ in Equation 8-60, we have

$$\langle E \rangle = \frac{0.25kT}{e^{0.25} - 1} = 0.880\, kT$$

EXAMPLE 8-9 **Number of Oscillators** At the "low" and "high" temperatures of Example 8-8, find the ratio of the number of oscillators with energy $E_1 = hf$ to the number with $E_0 = 0$.

SOLUTION

At any temperature T, the Boltzmann distribution for the fraction of oscillators with energy $E_n = nhf$ is $f_B(E_n) = Ae^{-E_n/kT} = Ae^{-nhf/kT}$. For $n = 0$, this gives $f_0 = Ae^0 = A$. The ratio f_n/f_0 is then $f_n/f_0 = e^{-nhf/kT}$.

(*a*) For $n = 1$ and $kT = \frac{1}{2}hf$, we have $f_1/f_0 = e^{-hf/kT} = e^{-2} = 0.135$. Most of the oscillators are in the lowest energy state $E_0 = 0$.

(*b*) For the higher temperature $kT = 4hf$, we get $f_1/f_0 = e^{-hf/kT} = e^{-0.25} = 0.779$. At the higher temperature the states are more nearly equally populated and the average energy is larger.

FEUE WHE

EXAMPLE 8-10 Debye Frequency Note from Figure 8-30 that the Debye temperature of silver is 215 K. Compute the Debye frequency for silver and predict the Debye temperature for gold. Silver and gold have identical crystal structures and similar physical properties.

SOLUTION

1. From the definition of the Debye temperature T_D, the Debye frequency f_D for silver can be computed:

$$T_D = \frac{hf_D}{k}$$

or

$$f_D = \frac{kT_D}{h} = \frac{1.38 \times 10^{-23}\ \text{J/K} \times 215\ \text{K}}{6.63 \times 10^{-34}\ \text{J} \cdot \text{s}} = 4.48 \times 10^{12}\ \text{Hz}$$

2. We would expect the interatomic forces of silver and gold to be roughly the same, hence their vibrational frequencies to be in inverse ratio to the square root of their atomic masses:

$$\frac{f_D(\text{Ag})}{f_D(\text{Au})} = \sqrt{\frac{M(\text{Au})}{M(\text{Ag})}} = \frac{kT_D(\text{Ag})/h}{kT_D(\text{Au})/h} = \frac{T_D(\text{Ag})}{T_D(\text{Au})}$$

3. Solving this for $T_D(\text{Au})$ yields

$$T_D(\text{Au}) = T_D(\text{Ag})\sqrt{\frac{M(\text{Au})}{M(\text{Ag})}} = 215\sqrt{\frac{108}{197}}$$

$$= 159\ \text{K}$$

Remarks: This estimate is in reasonable agreement with the measured value of 164 K.

8-5 Properties of a Fermion Gas

The fact that metals conduct electricity so well led to the conclusion that they must contain electrons free to move about through a lattice of more or less fixed positive metal ions. Indeed, this conclusion had led to the development of a free-electron theory to explain the properties of metals within three years after the electron's discovery by Thomson and long before wave mechanics was even a glimmer in Schrödinger's eye. The free-electron theory of metals was quite successful in explaining a number of metallic properties, as we will discuss further in Chapter 10; however, it also suffered a few dramatic failures. For example, in a conductor at temperature T the lattice ions have average energy $3kT$ consisting, as we have seen, of $3kT/2$ of kinetic energy and $3kT/2$ of potential energy, leading to a molar heat capacity $C_V = 3R$ (rule of Dulong-Petit). Interactions (i.e., collisions) between the free electrons and lattice ions would be expected to provide the electrons with an average translational kinetic energy of $3kT/2$ at thermal equilibrium, resulting in a total internal energy U for metals of $3kT + 3kT/2 = 9kT/2$. Thus, metals should have $C_V = 4.5R$. In fact, they do not. The heat capacity of conductors is essentially the same as that of other solids, except for a slight temperature-dependent increase that is much smaller than $3R/2$. The problems with the classical free-electron theory are due mainly to the fact that electrons are indistinguishable particles that obey the exclusion principle, and as a

consequence they have the Fermi-Dirac distribution of energies rather than the Boltzmann distribution. In this section we will investigate the general characteristics of systems made up of fermions. In Chapter 10 we will see how the absence of a significant electron contribution to the heat capacity of conductors is explained.

In the Fermi-Dirac distribution given by

$$f_{FD}(E) = \frac{1}{e^{\alpha}e^{E/kT} + 1} \qquad \textbf{8-25}$$

it is convenient to write α as

$$\alpha = \frac{-E_F}{kT} \qquad \textbf{8-67}$$

where E_F is called the *Fermi energy*. Doing so allows Equation 8-25 to be written as

$$f_{FD}(E) = \frac{1}{e^{(E-E_F)/kT} + 1} \qquad \textbf{8-68}$$

The Fermi energy is an important quantity in systems of fermions, such as the electron gas in metals (discussed in Chapter 10) and the neutron gas in a neutron star. Notice in particular that for $E = E_F$ the quantity $e^{(E-E_F)/kT} = 1$ for all values of the temperature greater than zero and hence $f_{FD}(E_F) = \frac{1}{2}$. If we consider a system of fermions at $T = 0$ K, we find that

For $E < E_F$:

$$f_{FD}(E) = \frac{1}{e^{(E-E_F)/kT} + 1} = 1$$

and

For $E > E_F$:

$$f_{FD}(E) = \frac{1}{e^{\infty} + 1} = 0$$

In other words, at absolute zero all energy states from the ground state up to the Fermi energy are occupied and all energy states above the Fermi energy are empty. This is in sharp contrast with a system of bosons, such as the rubidium BE condensate, where all particles condense to the ground state at $T = 0$ K. This situation is illustrated in Figure 8-31*a*. If the system contains N fermions, we can find its Fermi energy by filling the energy states in increasing order starting with the ground state.

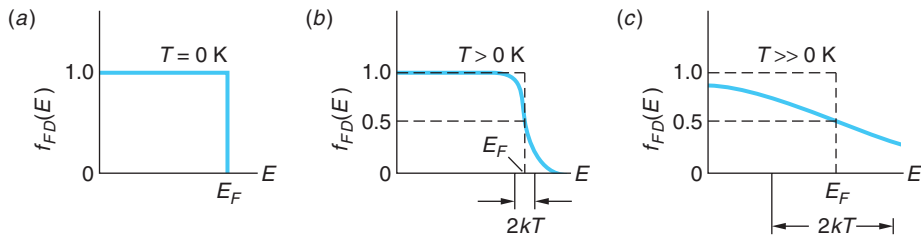

Figure 8-31 Fermi-Dirac distribution function $f_{FD}(E)$ for three different temperatures. (*a*) At $T = 0$ K, all levels above E_F are unoccupied. (*b*) For $T > 0$ K with $kT < E_F$, some particles near the Fermi energy can move to levels within about kT above E_F. (*c*) For high temperatures where $kT > E_F$, even particles in the lower energy states may move to higher levels so that $f_{FD}(0) < 1$.

FÈUE WHE

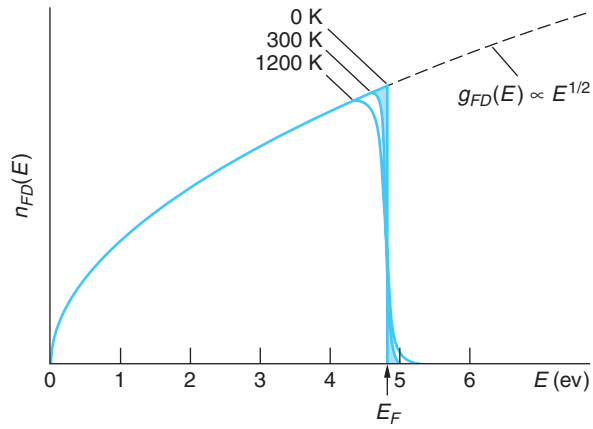

Figure 8-32 The distribution of fermion energies at three different temperatures for a material whose Fermi energy is 4.8 eV. Curves are plots of Equation 8-69 for the indicated values of temperature. (See text for explanation of shaded area.)

The energy state occupied by the Nth particle will be the Fermi energy. We can find the total energy of the system simply by adding up the energies of all N particles and their average energy by dividing that total by N. Each of these calculations will be done for electrons in Section 10-3.

If the temperature of the system is increased to some temperature $T > 0$ K but with kT remaining smaller than E_F, fermions within about kT of the Fermi energy could now move to previously unoccupied levels lying within about kT above the Fermi energy in response to collisions with the lattice ions. However, fermions occupying levels much lower than kT below E_F would not be able to move since the additional kT of energy that they might acquire in a collision would not be enough to move them past levels occupied by other fermions in order to reach the unoccupied levels near or above E_F. Figure 8-31*b* illustrates this situation. At temperatures so high that $kT > E_F$, fermions in even the very low-lying energy states will be able to move to higher states. Only then can $f_{FD}(0)$ drop below 1, as shown in Figure 8-31*c*. This latter situation also corresponds to the lowest curve in Figure 8-16.

The number $n_{FD}(E)$ of fermions with energy E is given by Equation 8-37*c*. The density of states was computed for fermions in Section 8-3 and is given by Equation 8-42, so we have for fermions that

$$n_{FD}(E) = \frac{\pi}{2}\left(\frac{8m}{h^2}\right)^{3/2} \frac{VE^{1/2}}{e^{(E-E_F)/kT} + 1} \qquad \textbf{8-69}$$

Figure 8-32 is a graph of Equation 8-69 for three different temperatures. The $T = 0$ K curve is the result of multiplying $f_{FD}(E)$ in Figure 8-31*a* by the $g_{FD}(E)$ function, which increases as $E^{1/2}$. The curves for $T = 300$ K and $T = 1200$ K result from multiplying $g_{FD}(E)$ by appropriate versions of Figure 8-31*b*. The shaded areas for $T > 0$ K represent those electrons near the Fermi energy, a very small number, that are able to move into the empty states above E_F at each temperature.

Quantum Degenerate Fermion Gas

Since fermions have half-integer spins, the Pauli exclusion principle prohibits two identical fermions from occupying the same quantum state. Thus, a system of half-integer-spin atoms cannot all occupy the ground state to form a fermion version of the Bose-Einstein condensate as is possible for integer-spin bosons. The fermion analog of

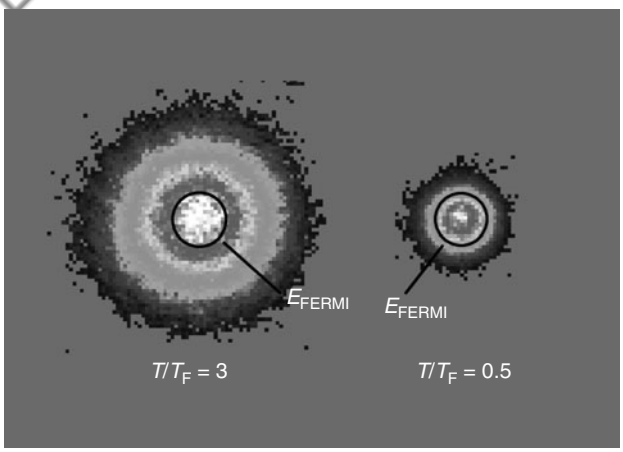

Figure 8-33 Quantum degenerate state of a Fermi gas. The images show that more of the atoms of the ultracold gas lie below the Fermi energy (black circles) than above it in the right sample than in the left one. The colder cloud on the right contains 0.78 million ^{40}K atoms at $T = 0.29\ \mu K$. The cloud on the left contains 2.5 million atoms at $T = 2.4\ \mu K$.

the BEC occurs when the atoms fill all of the energy states from the ground state up to the Fermi energy. The transition to this quantum degenerate state for a gas of fermions is a gradual one, quite unlike the sudden phase transition to the BEC. This makes it harder to detect, in addition to which the exclusion principle makes evaporative cooling that is so important in producing the BEC much less effective as the temperature of the fermion gas decreases. In 1999 these problems were solved by Deborah Jin and Brian DeMarco, four years after the first BEC was produced. They loaded a magnetic trap with ^{40}K (total atomic spin = 9/2), dividing the atoms between two magnetic substates to solve the evaporative cooling problem. One of several ways used to detect the quantum degenerate state of the ^{40}K atoms was to determine the total energy (from the momentum distribution) of the approximately 8×10^5 atoms in the sample (Figure 8-33). Classically, the total energy $(3/2)N_A kT \rightarrow 0$ as $T \rightarrow 0$. Quantum mechanically, however, the total energy should be higher than expected classically as T decreases and remain finite as $T \rightarrow 0$. This is exactly what Jin and DeMarco observed. High on the list of new things their discovery may make possible is the study of Cooper pairs (see Section 10-8) as they condense into a superconductor.

More recently, scientists have been successful in forming Bose-Einstein condensates from paired fermions using ^{6}Li and ^{40}K. The very loosely bonded ^{6}Li-^{6}Li and ^{40}K-^{40}K are bosons and dropped into their respective ground states when the temperature reached about 50×10^{-9} K.

Questions

12. Why does the exclusion principle make evaporative cooling less effective as T decreases for fermions in a single-spin state?
13. Why does the total energy of the fermion gas not approach zero as T $\rightarrow$ 0?

Summary

TOPIC	RELEVANT EQUATIONS AND REMARKS	
1. Boltzmann distribution	$f_B(E) = Ae^{-E/kT}$	**8-1**
	where the distribution $f_B(E)$ is the probability that the state with energy E will be occupied.	
Boltzmann's constant	$k = 1.381 \times 10^{-23}$ J/K $= 8.617 \times 10^{-5}$ eV/K	

FEUE WHE

TOPIC	RELEVANT EQUATIONS AND REMARKS	
Maxwell distribution of molecular speeds	$n(v)\,dv = 4\pi N\left(\frac{m}{2\pi kT}\right)^{3/2} v^2 e^{-mv^2/2kT}\,dv$	8-8
Equipartition theorem	In equilibrium, each degree of freedom contributes $\frac{1}{2}kT$ to the average energy per molecule.	
Average kinetic energy	$\langle E\rangle = \frac{3}{2}kT$	8-14
	where $\langle E\rangle$ is the average *translational* kinetic energy per molecule.	
Dulong-Petit law	$C_V = 3R$	
2. Quantum statistics		
Bose-Einstein distribution	$f_{BE}(E) = \frac{1}{e^{\alpha}e^{E/kT} - 1}$	8-24
Fermi-Dirac distribution	$f_{FD}(E) = \frac{1}{e^{\alpha}e^{E/kT} + 1}$	8-25
	In all three distributions f_B, f_{BE}, and f_{FD}, e^{α} is a normalization constant that depends on the particle density. The FD distribution applies to particles with $\frac{1}{2}$ -integral spin, the BE distribution to particles with zero or integral spin. At high energies both f_{BE} and f_{FD} approach f_B.	
	The Boltzmann distribution will be a good approximation of either f_{BE} or f_{FD} if $e^{\alpha} \ll 1$.	
3. Applications		
Liquid helium	^{4}He becomes a superfluid at 2.17 K, called the lambda point. ^{3}He, the only other naturally occurring isotope that has this property, becomes superfluid at about 2 mK.	
Bose-Einstein condensate	Bosons undergo a phase transition, condensing to the lowest quantum state.	
Degenerate Fermi gas	Fermions condensed to states from the ground state to the Fermi energy.	

General References

The following general references are written at a level appropriate for the readers of this book.

Blatt, F. J., *Modern Physics*, McGraw-Hill, New York, 1992.

Brehm, J. J., and W. J. Mullin, *Introduction to the Structure of Matter*, Wiley, New York, 1989.

Eisberg, R., and R. Resnick, *Quantum Physics of Atoms, Molecules, Solids, Nuclei, and Particles*, 2d ed., Wiley, New York, 1985. An excellent but somewhat more advanced discussion of quantum statistics can be found in Chapter 11 of this book.

Ford, K. W., *The Quantum World*, Harvard University Press, Cambridge, MA, 2005.

Kittel, C., and H. Kroemer, *Thermal Physics*, W. H. Freeman and Co., New York, 1995.

Leitner, A., *Liquid Helium II: The Superfluid*, Michigan State University, East Lansing, 1963. This 39-minute film is an excellent introduction to the subject of liquid helium II.

London, F., *Superfluids*, Vol. II:*Macroscopic Theory of Superfluid Helium*, 2d rev. ed., Dover, New York, 1954.

Mandel, F., *Statistical Physics*, Wiley, New York, 1988.

Mendelssohn, K., *The Quest for Absolute Zero: The Meaning of Low Temperature Physics*, World University Library, McGraw-Hill, New York, 1966.

Notes

1. The statistical approach may also be used as an approximation in systems where the number of particles is not particularly large. For example, in Chapter 11 we will discuss briefly a statistical model of the atomic nucleus, a system containing only of the order of 100 particles.

2. Ludwig E. Boltzmann (1844–1906), Austrian physicist. His pioneering statistical interpretation of the second law of thermodynamics earned for him recognition as the founder of statistical mechanics. He explained theoretically the experimental observations of Stefan, whom he served as an assistant while in college, that the quantity of radiation increased with the fourth power of the temperature. He eventually succeeded Josef Stefan in the chair of physics at Vienna. A strong proponent of the atomic theory of matter, his suicide was apparently motivated in part by opposition to his views by others.

3. To avoid having to repeat this rather long phrase frequently, which will occur for E as well as v, we will hereafter use the expression "the number in dv_x at v_x" or simply "the number in dv_x."

4. Or refer to a table of integrals.

5. Historically, rotation about the z' axis of the dumbbell was ruled out by assuming either that the atoms are points and the moment of inertia about this axis is therefore zero (not true) or that the atoms are hard smooth spheres, in which case rotation about this axis cannot be changed by collisions and therefore does not participate in the exchange of energy (also not true). Either of these assumptions also rules out the possibility of rotation of a monatomic molecule.

6. Satyendra Nath Bose (1894–1974), Indian physicist. Following publication of his paper on the statistics of indistinguishable particles, which was translated into German for publication by Einstein himself, Bose spent two years in Europe, then returned to India to devote himself to teaching. Lacking a Ph.D., he was denied a professorship until a one-sentence postcard from Einstein was received at Dacca University in his support.

7. Enrico Fermi (1901–1954), Italian-American physicist. An exceedingly prolific scientist and intrepid amateur tennis player whose work encompassed solid-state, nuclear, and particle physics, he is perhaps best known as the "father" of the nuclear reactor. He was awarded the Nobel Prize in Physics in 1938 for his work in nuclear physics.

8. Paul A. M. Dirac (1902–1984), English physicist. His development of relativistic wave mechanics for spin-$\frac{1}{2}$ particles led to his prediction in 1930 of the existence of the positron. Its discovery by Anderson two years later resulted in Dirac's being awarded (along with Schrödinger) the 1933 Nobel Prize in Physics. From 1932 until his retirement he occupied the Lucasian Chair of Mathematics at Cambridge University, which had been held 250 years earlier by Newton and is currently held by Stephen Hawking.

9. Heike Kamerlingh Onnes (1853–1926), Dutch physicist. His success in liquefying helium enabled him to investigate the properties of other materials at liquid helium temperatures. This in turn led to his discovery of superconductivity in 1911. His work on the behavior of materials at low temperatures earned him the Nobel Prize in Physics in 1913.

10. J. C. McLennan, H. D. Smith, and J. O. Wilhelm, *Philosophical Magazine*, **14,** 161 (1932).

11. At very low temperatures liquid ^{4}He does solidify at a pressure of about 25 atm, liquid ^{3}He at about 30 atm.

12. Narrow channels that permit only the superfluid to pass are, of course, called *superleaks*.

13. These and many other properties are elegantly displayed in the film *Liquid Helium II: The Superfluid*, available from the Instructional Media Center, Michigan State University, East Lansing, Michigan 48824.

14. In the thermodynamic equilibrium state their sample, rubidium, is a solid metal at room temperature.

15. Einstein used the Boltzmann distribution in its discrete form $f_B(E) = \sum_{n=0}^{\infty} Ae^{-E_n/kT}$.

Problems

Level I

Section 8-1. Classical Statistics: A Review

8-1. (*a*) Calculate v_{rms} for H_2 at $T = 300$ K. (*b*) Calculate the temperature T for which v_{rms} for H_2 equals the escape speed of 11.2 km/s.

8-2. (*a*) The ionization energy for hydrogen atoms is 13.6 eV. At what temperature is the average kinetic energy of translation equal to 13.6 eV? (*b*) What is the average kinetic energy of translation of hydrogen atoms at $T = 10^7$ K, a typical temperature in the interior of the Sun?

8-3. The molar mass of oxygen gas (O_2) is about 32 g/mol and that of hydrogen gas (H_2) about 2 g/mol. Compute (*a*) the rms speed of O_2 and (*b*) the rms speed of H_2 when the temperature is 0°C.

8-4. Show that the SI units of $(3RT/M)^{1/2}$ are m/s.

8-5. (*a*) Find the total kinetic energy of translation of 1 mole of N_2 molecules at $T = 273$ K. (*b*) Would your answer be the same, greater, or less for 1 mole of He atoms at the same temperature? Justify your answer.

8-6. Use the Maxwell distribution of molecular speeds to calculate $\langle v^2 \rangle$ for the molecules of a gas.

8-7. Neutrons in a nuclear reactor have a Maxwell speed distribution when they are in thermal equilibrium. Find $\langle v \rangle$ and v_m for neutrons in thermal equilibrium at 300 K. Show that $n(v)$ (Equation 8-8) has its maximum value at $v = v_m = (2kT/m)^{1/2}$.

8-8. A container holds 128 identical molecules whose speeds are distributed as follows:

No. of molecules	4	12	20	24	20	16	12	8	6	4
Speed range (m/s)	0.0–1.0	1.0–2.0	2.0–3.0	3.0–4.0	4.0–5.0	5.0–6.0	6.0–7.0	7.0–8.0	8.0–9.0	9.0–10.0

Graph these data and indicate on the graph v_m, $\langle v \rangle$, and v_{rms}.

8-9. Show that the most probable speed v_m of the Maxwell distribution of speeds is given by Equation 8-9.

8-10. Compute the total translational kinetic energy of one liter of oxygen held at a pressure of one atmosphere and a temperature of 20°C.

8-11. From the absorption spectrum it is determined that about one out of 10^6 hydrogen atoms in a certain star is in the first excited state, 10.2 eV above the ground state (other excited states can be neglected). What is the temperature of the star? (Take the ratio of statistical weights to be 4, as in Example 8-2.)

8-12. The first excited rotational energy state of the H_2 molecule ($g_2 = 3$) is about 4×10^{-3} eV above the lowest energy state ($g_1 = 1$). What is the ratio of the numbers of molecules in these two states at room temperature (300 K)?

8-13. A monatomic gas is confined to move in two dimensions so that the energy of an atom is $E_k = \frac{1}{2}mv_x^2 + \frac{1}{2}mv_y^2$. What are C_V, C_P, and γ for this gas? (C_P, the heat capacity at constant pressure, is equal to $C_V + nR$ and $\gamma = C_P/C_V$.)

8-14. Use the Dulong-Petit law that $C_V = 3R$ for solids to calculate the specific heat $c_V = C_V/M$ in cal/g for (*a*) aluminum, $M = 27.0$ g/mol, (*b*) copper, $M = 63.5$ g/mol, and (*c*) lead, $M = 207$ g/mol, and compare your results with the values given in a handbook. (Include the reference in your answer.)

8-15. Calculate the most probable kinetic energy E_m from the Maxwell distribution of kinetic energies (Equation 8-13).

8-16. (*a*) Show that the speed distribution function can be written $n(v) = 4\pi^{-1/2}(v/v_m)^2 v_m^{-1} e^{-(v/v_m)^2}$, where v_m is the most probable speed. Consider 1 mole of molecules and approximate dv by $\Delta v = 0.01\ v_m$. Find the number of molecules with speeds in dv at (*b*) $v = 0$, (*c*) $v = v_m$, (*d*) $v = 2\ v_m$, and (*e*) $v = 8\ v_m$.

8-17. Consider a sample containing hydrogen atoms at 300 K. (*a*) Compute the number of atoms in the first ($n = 2$) and second ($n = 3$) excited states compared to those in the ground state ($n = 1$). Include the effects of degeneracy in your calculations. (*b*) At what temperature would one percent of the atoms be in the $n = 2$ state? (*c*) At the temperature found in (*b*), what fraction of the atoms will be in the $n = 3$ state?

8-18. Consider a sample of noninteracting lithium atoms (Li, $Z = 3$) with the third (outer) electron in the $3p$ state in a uniform 4.0 T magnetic field. (*a*) Determine the fraction of the atom in the $m_\ell = +1, 0$, and -1 states at 300 K. (*b*) In the $3p \rightarrow 2s$ transition, what will be the relative intensities of the three lines of the Zeeman effect?

Section 8-2 Quantum Statistics

8-19. Find the number density N/V for electrons such that (*a*) $e^{-\alpha} = 1$ and (*b*) $e^{-\alpha} = 10^{-6}$.

8-20. (*a*) Compute $e^{-\alpha}\sqrt{b^2 - 4ac}$ from Equation 8-44 for O_2 gas at standard conditions. (*b*) At what temperature is $e^{-\alpha} = 1$ for O_2?

8-21. Given three containers all at the same temperature, one filled with a gas of classical molecules, one with a fermion gas, and one with a boson gas, which will have the highest pressure? Which will have the lowest pressure? Support your answer.

8-22. (*a*) For $T = 5800$ K, at what energy will the Bose-Einstein distribution function $f_{BE}(E)$ equal 1 (for $\alpha = 0$)? (*b*) Still with $\alpha = 0$, to what value must the temperature change if $f_{BE}(E) = 0.5$ for the energy in part (*a*)?

8-23. A container at 300 K contains H_2 gas at a pressure of one atmosphere. At this temperature H_2 obeys the Boltzmann distribution. To what temperature must the H_2 gas be cooled before quantum effects become important and the use of the Boltzmann distribution is no longer appropriate? (*Hint:* Equate the de Broglie wavelength at the average energy to the average spacing between molecules, using the ideal gas law to compute the density.)

Section 8-3 The Bose-Einstein Condensation

8-24. Compute N_0/N from Equation 8-52 for (*a*) $T = 3T_c/4$, (*b*) $T = \frac{1}{2}T_c$, (*c*) $T = T_c/4$, and (*d*) $T = T_c/8$.

8-25. Show that $N_0 \approx 1/\alpha$ for small values of α as asserted in the paragraph above Equation 8-52.

8-26. Like ^{4}He, the most common form of neon, ^{20}Ne, is a rare gas and the ^{20}Ne atoms have zero spin and hence are bosons. But unlike helium, neon does not become superfluid at low temperatures. Show that this is to be expected by computing neon's critical temperature and comparing it with the element's freezing point of 24.5 K.

Section 8-4 The Photon Gas: An Application of Bose-Einstein Statistics

8-27. If the Sun were to become cooler (without changing its radius), the energy density at the surface would decrease according to Equation 8-56. Suppose the Sun's temperature were to decrease by 5 percent. Compute the fractional change in the rate at which solar energy arrives at Earth. (Assume that the Sun's surface is in equilibrium and radiates as a blackbody.)

8-28. Find the average energy of an oscillator at (*a*) $T = 10hf/k$, (*b*) $T = hf/k$, and (*c*) $T = 0.1hf/k$ and compare your results with those from the equipartition theorem.

8-29. (*a*) Show that the rule of Dulong-Petit follows directly from Einstein's specific heat formula (Equation 8-62) as $T \rightarrow \infty$. (*b*) Show that $C_V \rightarrow 0$ as $T \rightarrow 0$.

8-30. Using Figure 8-13, compute the (approximate) frequency of atomic oscillations in silicon and in aluminum at 200 K.

8-31. Use Equation 8-62 to calculate the value of C_V for a solid at the Einstein temperature $T_E = hf/k$.

Section 8-5 Properties of a Fermion Gas

8-32. Use Equation 8-69 to plot an accurate graph of $n_{FD}(E)/V$ for electrons whose Fermi energy is 4.8 eV from $E = 4.5$ eV to $E = 5.1$ eV at $T = 300$ K. Determine from the graph the number of electrons per unit volume just below the Fermi energy that can move to states just above the Fermi energy.

8-33. Consider a gas of electrons (fermions) and a gas of photons (bosons). Which has more states available at $T = 1$ K? Explain why.

Level II

8-34. The molar heat capacity data given in Table 8-2 are taken from *AIP Handbook*, 2d ed. (McGraw-Hill, New York, 1963). Plot the data for these solids all on one graph and sketch in the curves C_V versus T. Estimate the Einstein temperature for each of the solids using the result of Problem 8-31.

8-35. Recalling that the Fermi-Dirac distribution function applies to all fermions, including protons and neutrons, each of which have spin $\frac{1}{2}$, consider a nucleus of ^{22}Ne consisting of 10 protons and 12 neutrons. Protons are distinguishable from neutrons, so two of each particle (spin up, spin down) can be put into each energy state. Assuming that the radius of the ^{22}Ne nucleus is 3.1×10^{-15} m, estimate the Fermi energy and the average energy of the nucleus in ^{22}Ne. Express your results in MeV. Do the results seem reasonable?

Table 8-2 Heat capacities in cal/mole • K for Au, diamond, Al, and Be

T, K	Au	Diamond	Al	Be
20	0.77	0.00	0.05	0.003
50	3.41	0.005	0.91	0.04
70	4.39	0.016	1.85	0.12
100	5.12	0.059	3.12	0.43
150	5.62	0.24	4.43	1.36
200	5.84	0.56	5.16	2.41
250	5.96	0.99	5.56	3.30
300	6.07	1.46	5.82	3.93
400	6.18	2.45	6.13	4.77
500	6.28	3.24	6.42	5.26
600	6.40	3.85	6.72	5.59
800	6.65	4.66	7.31	6.07
1000	6.90	5.16	7.00	6.51

8-36. What is the ground-state energy of 10 noninteracting bosons in a one-dimensional box of length L?

8-37. Make a plot of $f_{FD}(E)$ versus E for (*a*) $T = 0.1T_F$, and (*b*) $T = 0.5T_F$, where $T_F = E_F/k$.

8-38. Compute the fraction of helium atoms in the superfluid state at (*a*) $T = T_c/2$ and (*b*) $T = T_c/4$.

8-39. The depth of the potential well for free electrons in a metal can be accurately determined by observing that the photoelectric work function is the energy necessary to remove an electron at the top of the occupied states from the metal; an electron in such a state has the Fermi energy. Assuming each atom provides one free electron to the gas, compute the depth of the well for the free electrons in gold. The work function for gold is 4.8 eV.

8-40. An early method testing Maxwell's theoretical prediction for the distribution of molecular speeds is shown in Figure 8-34. In 1925 Otto Stern used a beam of Bi_2 molecules emitted from an oven at 850 K. The beam defined by slit S_1 was admitted into the interior of a rotating drum via slit S_2 in the drum wall. The identical bunches of molecules thus formed struck and

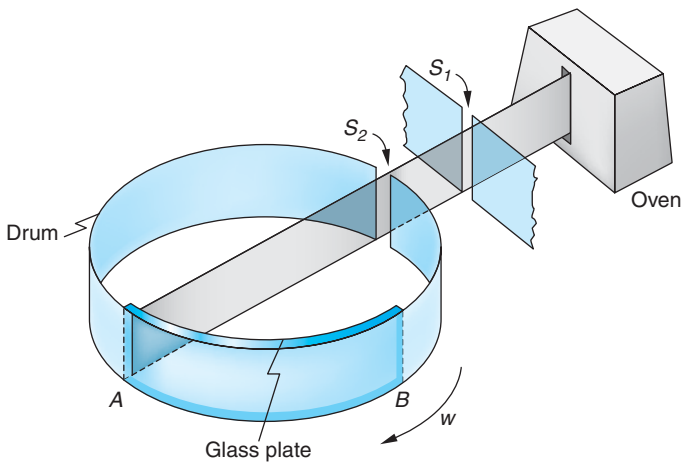

Figure 8-34

adhered to a curved glass plate fixed to the interior drum wall, the fastest molecules striking near A, which was opposite S_2, the slowest near B, and the others in between depending on their speeds. The density of the molecular deposits along the glass plate were measured with a densitometer. The density (proportional to the number of molecules) plotted against distance along the glass plate (dependent on v) made possible determination of the speed distribution. If the drum is 10 cm in diameter and is rotating at 6250 rpm, (*a*) find the distance from A where molecules traveling at v_m,$\langle v\rangle$, and v_{rms} will strike. (*b*) The plot in (*a*) must be corrected slightly in order to be compared with Maxwell's distribution equation. Why? (*c*) Would N_2 molecules work as well as Bi_2 molecules in this experiment? Why or why not?

8-41. The speed distribution of molecules in a container is the Maxwell distribution $f(v) \propto v^2 e^{-mv^2/2kT}$. The number with speed v that hit the wall in a given time is proportional to the speed v and to $f(v)$. Thus, if there is a very small hole in the wall (too small to have much effect on the distribution inside), the speed distribution of those that escape is $F(v) \propto vf(v) \propto v^3 e^{-mv^2/2kT}$. Show that the mean energy of those that escape is $2kT$.

Level III

8-42. This problem is related to the equipartition theorem. Consider a system in which the energy of a particle is given by $E = Au^2$, where A is a constant and u is any coordinate or momentum that can vary from $-\infty$ to $+\infty$. (*a*) Write the probability of the particle having u in the range du and calculate the normalization constant C in terms of A. (*b*) Calculate the average energy $\langle E\rangle = \langle Au^2\rangle$ and show that $\langle E\rangle = \frac{1}{2}kT$.

8-43. Calculate the average value of the magnitude of v_x from the Maxwell distribution.

8-44. Show that $f_{FD}(E) \rightarrow f_B(E)$ for $E \gg E_F$.

8-45. Carry out the integration indicated in Equation 8-43 to show that α is given by Equation 8-44.

8-46. Consider a system of N particles that has only two possible energy states, $E_1 = 0$ and $E_2 = \epsilon$. The distribution function is $f_i = Ce^{-E_i/kT}$. (*a*) What is C for this case? (*b*) Compute the average energy $\langle E\rangle$ and show that $\langle E\rangle \rightarrow 0$ as $T \rightarrow 0$ and $\langle E\rangle \rightarrow \epsilon/2$ as $T \rightarrow \infty$. (*c*) Show that the heat capacity is

$$C_V = Nk\left(\frac{\epsilon}{kT}\right)^2 \frac{e^{-\epsilon/kT}}{(1 + e^{-\epsilon/kT})^2}$$

(*d*) Sketch C_V versus T.

8-47. If the assumptions leading to the Bose-Einstein distribution are modified so that the number of particles is not assumed constant, the resulting distribution has $e^{\alpha} = 1$. This distribution can be applied to a "gas" of photons. Consider the photons to be in a cubic box of side L. The momentum components of a photon are quantized by the standing-wave conditions $k_x = n_1\pi/L$, $k_y = n_2\pi/L$, and $k_z = n_3\pi/L$, where $p = \hbar(k_x^2 + k_y^2 + k_z^2)^{1/2}$ is the magnitude of the momentum. (*a*) Show that the energy of a photon can be written $E = N(\hbar c\pi/L)$, where $N^2 = n_1^2 + n_2^2 + n_3^2$. (*b*) Assuming two photons per space state because of the two possible polarizations, show that the number of states between N and $N + dN$ is $\pi N^2\, dN$. (*c*) Find the density of states and show that the number of photons in the energy interval dE is

$$n(E)\, dE = \frac{8\pi(L/hc)^3 E^2\, dE}{e^{E/kT} - 1}$$

(*d*) The energy density in dE is given by $u(E)\, dE = En(E)\, dE/L^3$. Use this to obtain the Planck blackbody radiation formula for the energy density in $d\lambda$, where λ is the wavelength:

$$u(\lambda) = \frac{8\pi hc\lambda^{-5}}{e^{hc/\lambda kT} - 1}$$

PART 2

Applications of Quantum Mechanics and Relativity

Part 1 introduced the principles of the special and general relativity theories and illustrated how they led to profound alterations of our classical views of space and time. We then saw how the ideas and methods of quantum mechanics developed and how their application to atomic physics provides us with an understanding of atomic structure and spectra that is in excellent accord with our observations. In Part 2 we extend the applications of quantum theory and relativity to a wider variety of physical systems and phenomena that are, like atomic physics, of great interest to engineers, chemists, and physicists.

The topics we will discuss form the foundation of a broad range of theoretical and experimental research by physicists, chemists, and mathematicians and provide the basic understanding of the principles underlying many practical devices developed by engineers. They include molecular bonding and spectra (Chapter 9); the structure of solids and their thermal and electrical properties (Chapter 10); superconductors (Chapter 10); nuclear structure, radioactivity, and nuclear reactions (Chapter 11); and elementary particles, the quarks and leptons, that are the constituents of all visible matter (Chapter 12). Practical applications include the study of lasers (Chapter 9); semiconductors, semiconductor junctions, and transistors (Chapter 10), and radioactive dating and elemental analysis, nuclear fission and fusion, and reactors (Chapter 11). Many of these applications have revolutionized contemporary society. Part 2 concludes with a look outward into the cosmos from our solar system to the Big Bang, the realm of astrophysics and cosmology (Chapter 13), topics that stimulate the imagination of everyone. These chapters are independent of one another and can be studied in any order.

FÈUE WHE

This page intentionally left blank

CHAPTER 9

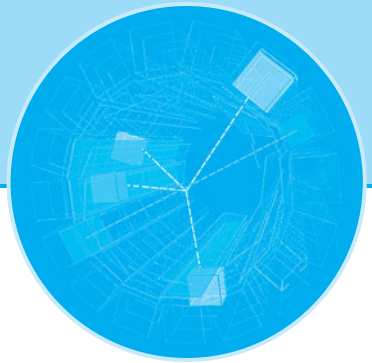

Molecular Structure and Spectra

In this chapter we will study the bonding of molecules—systems of two or more atoms. Properly, a molecule is the smallest constituent of a substance that retains its chemical properties. The study of the properties of molecules forms the basis for theoretical chemistry. The application of quantum mechanics to molecular physics has been spectacularly successful in explaining the structure of molecules and the complexity of their spectra and in answering such puzzling questions as why two H atoms join together to form a molecule but three H atoms do not. As in atomic physics, the detailed quantum-mechanical calculations are often difficult. When the difficulty would tend to obscure understanding of the physics, we will, as before, make our discussions semiquantitative or qualitative. In the final sections we will discuss the interaction of electromagnetic radiation with molecules, concluding with a discussion of the common general types of lasers.

There are essentially two extreme views we can take of a molecule. Consider, for example, H_2. We can think of it either as two H atoms somehow joined together or as a quantum-mechanical system of two protons and two electrons. The latter picture is more fruitful in this case because neither of the electrons in the H_2 molecule can be considered as belonging to either proton. Instead, the wave function for each electron is spread out in space about the whole molecule. For more complicated molecules, however, an intermediate picture is useful. Consider the N_2 molecule as an example. We need not consider the complicated problem of 2 nuclei and 14 electrons. The electron configuration of an N atom in the ground state is $1s^2 2s^2 2p^3$. Of the three electrons in the $2p$ state, two are in an $m_\ell = -1$ state with their spins paired (that is, with spins antiparallel so that the resultant spin for those two is zero). The third one is in an $m_\ell = 0$ level and its spin is, of course, unpaired. Only the electron with the unpaired spin is free to take part in the bonding of the N_2 molecule. We therefore can consider this molecule as two N^+ ions and two electrons that belong to the molecule as a whole. The molecular wave functions for these bonding electrons are called *molecular orbitals*. In many cases these molecular wave functions can be constructed from linear combinations of the atomic wave functions with which we are familiar.

Another type of bonding involves the transfer of one or more electrons between atoms, the bond resulting from Coulomb attraction between the ions, an example being NaCl. Again in this case, as in all four types of molecular bonding, it is the wave properties of the spin-$\frac{1}{2}$ electrons that are the key to understanding.

3819

9-1 The Ionic Bond

The two principal types of bonds that join two or more atoms together to form a molecule are called *ionic* and *covalent* bonds. Other types of bonds that are important in the bonding of liquids and solids are *dipole-dipole* bonds and *metallic* bonds. In many cases the bonding is a mixture of these mechanisms. We will discuss all of these in this chapter and the next, but it is important to recognize that all types of molecular bonding arise for the same fundamental reasons: the total energy of the stable bound molecule is lower than the total energy of the constituent atoms when they are widely separated, and there is a net attractive force between constituent atoms when their separation becomes larger than some equilibrium value. The bonding mechanisms are primarily due to electrostatic forces between the atoms or ions of the system together with the wave properties of electrons and the fact that they obey the exclusion principle. The complete description of molecular bonding is in most cases quite complex, involving as it does the mutual interactions of many electrons and nuclei; consequently, we will discuss each type using simplified models consisting of two or a few atoms, then illustrate qualitatively the extension of the results to more complex molecules.

The easiest type of bond to understand is the ionic bond, typically the strongest of the bonds and the one found in most salts. Consider KCl as an example. For the molecule to be stable, we must be able to show that $E(\text{KCl}) < E(\text{K}) + E(\text{Cl})$ when the K and Cl atoms are far apart and at rest. Let us define the energy of the system to be zero when the neutral atoms are widely separated. (See Figure 9-1.) The potassium atom has one 4*s* electron outside an argon core, $1s^2 2s^2 2p^6 3s^2 3p^6$. The ionization energy for K is low, as it is for all the alkali metals; for K only 4.34 eV is required to remove the outer electron from the atom. (See Table 9-1.) The removal of one electron from K leaves a positive ion with a spherically symmetric, closed-shell core. Chlorine, on the other hand, is only one electron short of having a closed argon core. The energy released by the acquisition of one electron is called the *electron affinity*, which in the case of Cl is 3.62 eV. Energy is released because the wave function of the "extra" electron penetrates the outer shell to a degree (see Figure 7-10*b*) and thus sees a net positive charge. The acquisition of one electron by chlorine results in a negative

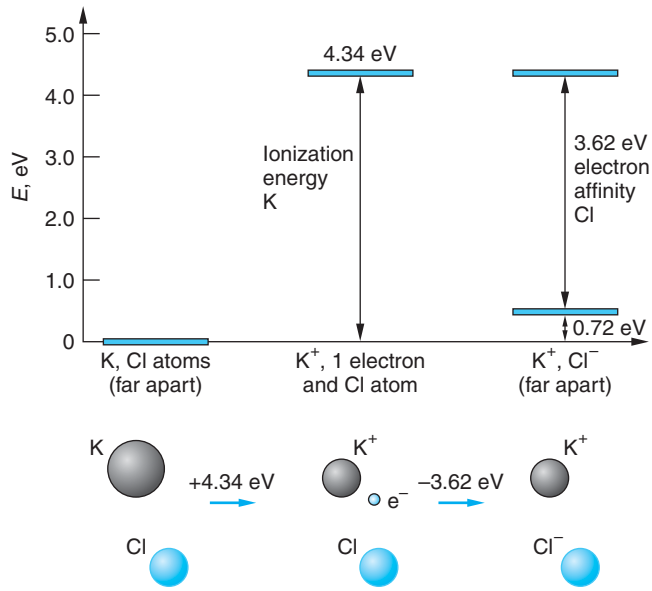

Figure 9-1 Net energy required to ionize a K and a Cl atom. An addition of 4.34 eV is required to remove the 4*s* electron from the neutral K atom, forming K^+ and a free electron. That electron (or some electron) can then occupy the vacancy in the 3*p* shell of the Cl atom forming a Cl^- ion. The electron is positively bound, with the release of 3.62 eV. Formation of the widely separated K^+ and Cl^- ions thus requires a net addition of 0.72 eV.

Table 9-1 Ionization energies of alkali metal atoms and electron affinities of halogen atoms

Alkali metal	Ionization energy (eV)	Halogen	Electron affinity (eV)
Li	5.39	F	3.40
Na	5.14	Cl	3.61
K	4.34	Br	3.36
Rb	4.18	I	3.06
Cs	3.89	At	2.8
Fr	4.07		

Source: Data from *Handbook of Chemistry and Physics,* 85th ed. (New York: Chemical Rubber Co., 2004).

ion with a spherically symmetric, closed-shell electron core. Thus, the formation of a K^+ ion and a Cl^- ion by the donation of one electron of K to Cl requires just $4.34-3.62 = 0.72$ eV. If this were the whole story, the KCl molecule would not form; however, the electrostatic potential energy of the two ions separated by a distance r is $-ke^2/r$. When the separation of the ions is less than about 2.8 nm, the negative potential energy of attraction is of greater magnitude than the energy needed to create the ions, and the ions move toward each other.

Since the electrostatic attraction increases as the ions get closer, it would seem that equilibrium could not exist. For very small separation of the ions, however, the wave function of the $3p$ electrons in the K^+ ion and the $3p$ electrons in the Cl^- ion begin to overlap. Since the $3p$ shells in each ion contain electrons with sets of quantum numbers identical to those in the other, a strong repulsion develops due to the exclusion principle. This "exclusion-principle repulsion" is primarily responsible for the repulsion of the atoms in all molecules (except H_2), no matter which type of bonding occurs. When the ions are very far apart, the wave function for a core electron of one ion does not overlap that of the other ion. We can distinguish the electrons by the ion to which they belong, and the electrons of one ion can have the same quantum numbers as in the other ion. However, when the ions are close, the wave functions of their core electrons begin to overlap, and some of the electrons must go into higher-energy quantum states because of the exclusion principle, thus increasing the total energy of the system. This is not a sudden process: the energy states of the electrons are gradually changed as the ions move closer together. The total potential energy U of the KCl system can be expressed in terms of the separation r of the ion centers as the sum of the electrostatic potential, the exclusion-principle repulsion, and net ionization energy.

$$U(r) = -\frac{ke^2}{r} + E_{ex} + E_{ion} \qquad \textbf{9-1}$$

where $E_{ion} = 0.72$ eV for K^+ and Cl^-, as was found above. The exclusion-principle repulsion E_{ex} can be written as

$$E_{ex} = \frac{A}{r^n} \qquad \textbf{9-2}$$

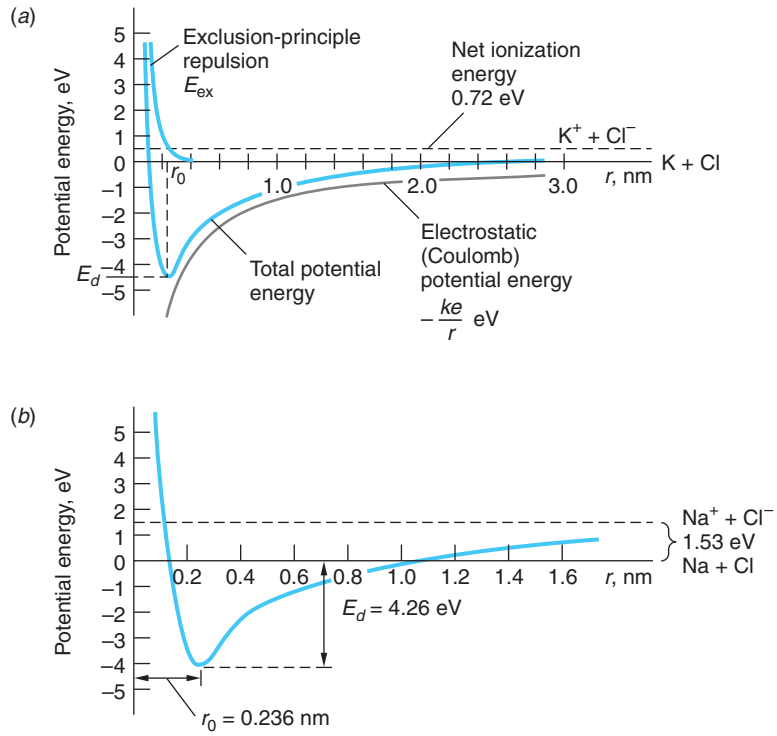

Figure 9-2 (*a*) Potential energy for K^+ and Cl^- ions as a function of separation distance *r*. The energy at infinite separation was chosen to be 0.72 eV, corresponding to the energy needed to form the ions from neutral atoms. The minimum energy for this curve is at the equilibrium separation $r_0 = 0.27$ nm for the ions in the molecule. (*b*) Potential energy for Na^+ and Cl^- ions as a function of *r*. Differences between the two similar molecules are due to the higher ionization potential and smaller core of Na.

where *A* and *n* are constants for each ionic molecule. Figure 9-2*a* is a sketch of the potential energy of the K^+ and Cl^- ions versus their separation. The energy is lowest at an equilibrium separation r_0 of about 0.27 nm. At smaller separations, the energy rises steeply as a result of the exclusion principle. The energy E_d required to separate the ions and form K and Cl *atoms*, called the *dissociation energy*, is about 4.40 eV. Figure 9-2*b* shows the total potential energy of another ionically bonded molecule, NaCl. Note the differences between the two total potential energy curves, which are due to the higher ionization potential and smaller closed-shell core of Na compared to K. Example 9-1 illustrates calculations used to construct curves like those in the diagram. Example 9-2 describes how the constants *A* and *n* in Equation 9-2 are found.

EXAMPLE 9-1 **Ionic Bonding in NaF** The ionization potential of sodium is 5.14 eV, the electron affinity of fluorine is 3.40 eV, and the equilibrium separation of sodium fluoride (NaF) is 0.193 nm. (*a*) How much energy is needed to form Na^+ and F^- ions from neutral sodium and fluorine atoms? (*b*) What is the electrostatic potential energy of the Na^+ and F^- ions at their equilibrium separation? (*c*) The dissociation energy of NaF is 4.99 eV. What is the energy due to repulsion of the ions at the equilibrium separation?

SOLUTION

(*a*) Since the energy needed to ionize sodium is 5.14 eV and the electron affinity of F is 3.40 eV, the energy needed to form Na^+ and F^- ions from neutral sodium and fluorine atoms is 5.14 eV − 3.40 eV = 1.74 eV = E_{ion}.

(*b*) The electrostatic potential energy of the Na^+ and F^- ions at their equilibrium separation (with $-ke^2/r = 0$ at infinite separation) is

FÈUE WHE

$$-\frac{ke^2}{r_0} = -\frac{(8.99 \times 10^9\ \text{N} \cdot \text{m}^2/C^2)(1.60 \times 10^{-19} C)^2}{1.93 \times 10^{-10}\ \text{m}}$$
$$= -1.19 \times 10^{-18}\ \text{J} = -7.45\ \text{eV}$$

(*c*) Choosing the total potential energy at infinity to be 1.74 eV (the net ionization energy needed to form Na^+ and F^- from the neutral atoms), the net electrostatic (Coulomb) potential U_C is

$$U_C = -\frac{ke^2}{r} + 1.74\ \text{eV}$$

At the equilibrium separation r_0, this energy is $U_C = -7.45\ \text{eV} + 1.74\ \text{eV} = -5.71\ \text{eV}$. Since the measured dissociation energy is 4.99 eV, the potential energy due to exclusion-principle repulsion E_{ex} of the Na^+ and F^- at equilibrium separation, from Equation 9-1, must be $5.71\ \text{eV} - 4.99\ \text{eV} = 0.72\ \text{eV}$.

EXAMPLE 9-2 Contribution from Exclusion-Principle Repulsion Find the values of A and n in Equation 9-2 for NaF.

SOLUTION

From Example 9-1 we have that the potential energy due to exclusion-principle repulsion at equilibrium separation of the ions is

$$E_{ex}(r_0) = \frac{A}{r_0^n} = \frac{A}{(0.193\ \text{nm})^n} = 0.72\ \text{eV}$$

At $r = r_0$ the net force on each ion must be zero because the potential energy has its minimum value at that point. This means that at $r = r_0$, the net Coulomb force F_C is equal in magnitude and opposite in sign to the exclusion-principle repulsive force, i.e.,

$$F_C = -\left(\frac{dU_C}{dr}\right)_{r=r_0} = \left(\frac{nA}{r^{n+1}}\right)_{r=r_0}$$

At $r = r_0$

$$F_C = \frac{U_C(r_0)}{r_0} = \frac{ke^2}{r_0^2} = 38.7\ \text{eV/nm}$$

Thus, we have that

$$\frac{nA}{r_0^{n+1}} = \frac{n}{r_0}\frac{A}{r_0^n} = \frac{n}{r_0}(0.72\ \text{eV}) = 38.7\ \text{eV/nm}$$

or

$$n = \frac{38.7\ \text{eV/nm}}{0.72\ \text{eV}} \times (0.193\ \text{nm}) = 10.4 \approx 10$$

and, therefore, $A = 5.4 \times 10^{-8}\ \text{eV} \cdot \text{nm}^{10}$. Finally, for NaF, E_{ex} is given by

$$E_{ex} = \frac{(5.4 \times 10^{-8}\ \text{eV} \cdot \text{nm}^{10})}{r^{10}}$$

FEUE WHE

It should be emphasized that our discussion of ionic bonding and, in particular, the graphs of potential energy in Figure 9-2 apply to the *ground states* of the molecules. The outer (valence) electrons of molecules may occupy excited states, just as they do in atoms. Since the electron wave functions of the excited states tend to extend farther from the ions than do those of the ground state, the potential energy curve is broader and shallower than for the ground state, resulting in a slightly weaker bond and a larger equilibrium separation of the ions. In our discussion we have ignored two additional contributions to the total energy of the molecule: (1) the zero-point energy (see Section 5-6), which decreases the magnitude of E_d, and (2) the van der Waals attraction, which increases the magnitude of E_d. Both are small and tend to partially offset each other. The latter, which arises from induced dipole moments, is the only form of bonding available for certain molecules and will be discussed later in this chapter.

The KCl equilibrium separation of 0.27 nm noted earlier is for gaseous diatomic KCl (which can be obtained by evaporation of solid KCl). Normally, KCl exists in a cubic crystal structure, with K^+ and Cl^- at alternate corners of a cube. The separation of the ions in a crystal is somewhat larger—about 0.32 nm. Because of the presence of neighboring ions of opposite charge, the Coulomb energy per ion pair is lower when the ions are in a crystal. This energy is usually expressed as $\alpha ke^2/r_0$, where r_0 is the equilibrium separation distance or *bond length* and α, called the *Madelung constant*, depends on the crystal structure, as will be discussed further in Chapter 10. For KCl, α is about 1.75. The values of E_d and r_0 listed in Table 9-2 are for several ionically bonded (gaseous) molecules.

Table 9-2 Dissociation energies E_d and equilibrium separations r_0 for several ionic molecules* in the gaseous state

Molecule	Dissociation energy (eV)	Equilibrium separation (nm)
NaCl	4.27	0.236
NaF	5.34	0.193
NaH	1.92	0.189
NaBr	3.81	0.250
LiCl	4.86	0.202
LiH	2.47	0.159
LiI	3.58	0.239
KCl	4.49	0.267
KBr	3.94	0.282
RbF	5.12	0.227
RbCl	4.43	0.279
CsI	3.50	0.332

*The two entries of molecules formed by an alkali atom and a hydrogen atom may seem odd, but hydrogen atoms, like those of a number of other elements, may form molecules as either positive or negative ions. The ionization energy of H is, of course, 13.6 eV; its electron affinity is 0.75 eV.

Source: Data from *Handbook of Chemistry and Physics,* 85th ed. (New York: Chemical Rubber Co., 2004).

FÈUE WHE

One final comment concerning ionic bonding: Few of the molecules in Table 9-2 are bonded exclusively by the ionic mechanism. As we will see in the next section, they may also be covalently bonded.

9-2 The Covalent Bond

A completely different mechanism is responsible for the bonding of such molecules as H_2, N_2, H_2O, and CO and also leads to bonding of many of the molecules in Table 9-2. If we calculate the energy needed to form the ions H^+ and H^- by the transfer of an electron from one atom to the other, we find the net ionization energy to be more than 12 eV. Adding this energy to the electrostatic energy (including the repulsion of the protons), we find that there is no separation distance for which the total energy is negative. The bond of H_2 thus cannot be ionic. The attraction of two hydrogen atoms is instead an entirely quantum-mechanical effect. The decrease in energy when two hydrogen atoms approach each other is due to the sharing of the two electrons by both atoms and is intimately connected with the symmetry properties of the electron wave functions. We can gain some insight into this phenomenon by first studying a simple one-dimensional quantum-mechanics problem—that of two finite square wells each of width L.

Consider first a single electron that is equally likely to be in either well. Since the wells are identical, symmetry requires that $|\Psi|^2$ be symmetric about the midpoint of the wells. Then Ψ must be either symmetric or antisymmetric about that point. These two possibilities for the ground state are shown in Figure 9-3. Previously, we did not distinguish between these two possibilities when superimposing (i.e., adding) wave functions because the energies $\pi^2\hbar^2/2mL^2$ and the probability densities Ψ^2 for both of these wave functions are the same when the wells are far apart. Figure 9-4 shows the symmetric and antisymmetric wave functions when the wells are very close together. Now the parts of the wave function describing the electron in one well or the other overlap, and the symmetric and antisymmetric resultant wave functions are quite different. Notice that for the symmetric wave functions the probability of the electron being found in the region between the wells is much larger than for the antisymmetric wave function. In the limiting case of no separation, the symmetric wave function Ψ_S approaches the ground-state wave function for a particle in a well

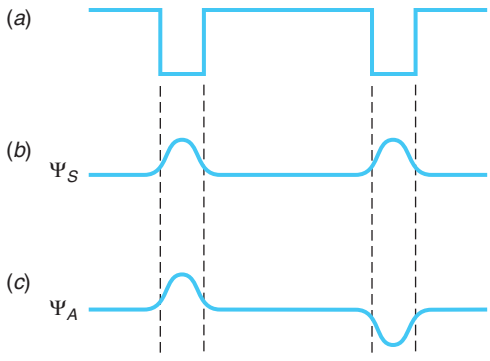

Figure 9-3 (*a*) Two square wells far apart. The electron wave function can be either (*b*) symmetric or (*c*) antisymmetric. The probability distributions and energies are the same for the two wave functions when the wells are far apart.

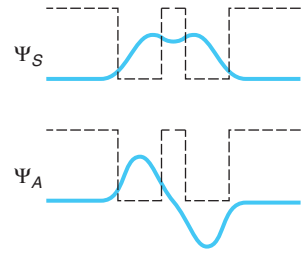

Figure 9-4 Symmetric and antisymmetric space wave functions for two square wells close together. The probability distributions and energies are not the same for the two wave functions in this case. The symmetric space wave function (and therefore the probability density) is larger between the wells than the antisymmetric space wave function.

of size $2L$ and the antisymmetric wave function Ψ_A approaches that for the first excited state in such a well; thus Ψ_S is a lower energy state than Ψ_A. This discussion has two important results:

1. The originally equal energies for Ψ_A and Ψ_S are split into two different energies as the wells become close.
2. The wave function for the symmetric state is large in the region between the wells, whereas that for the antisymmetric state is small.

Now consider adding a second electron to the two wells. The *total* wave function for the two electrons must be antisymmetric on exchange of the electrons since they obey the Pauli exclusion principle. Note that exchanging the electrons in the wells is the same as exchanging the wells; i.e., for a two-particle system, exchange symmetry is the same as space symmetry. The two electrons can therefore be in the space-symmetric state if the spins are antiparallel ($S = 0$) or in the space-antisymmetric state if their spins are parallel ($S = 1$).

H_2^+ Molecule

Now let us consider a real physical system with one electron, the hydrogen molecule ion H_2^+. For a one-dimensional model, the double potential well formed by the two protons is illustrated in Figure 9-5. The Hamiltonian (total energy) operator for this system is (see Equation 6-51 and Figure 9-5*b*)

$$H_{\text{op}} = \frac{p_{\text{op}}^2}{2m} + ke^2\left(-\frac{1}{r_1} - \frac{1}{r_2} + \frac{1}{r_0}\right)$$

In the ground state, the hydrogen atom wave function is proportional to e^{-r/a_0}. For our one-dimensional model, we will write this as $e^{-|x|/a_0}$. The symmetric and antisymmetric combinations for two values of the distance between the protons are shown in Figure 9-6. In general,

$$\Psi_S = \left(\frac{1}{\sqrt{2}}\right)(\Psi_{100}(r_1) + \Psi_{100}(r_2))$$

and

$$\Psi_A = \left(\frac{1}{\sqrt{2}}\right)(\Psi_{100}(r_1) - \Psi_{100}(r_2))$$

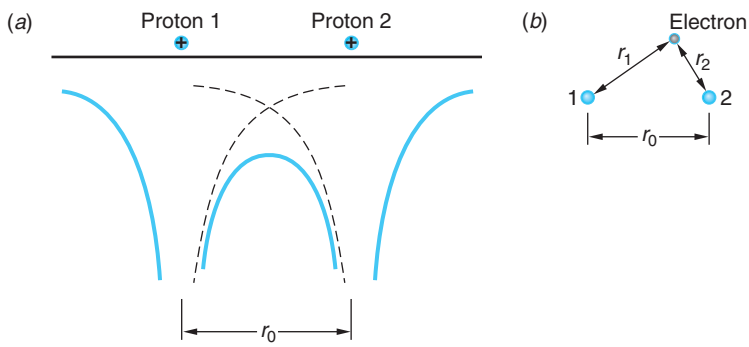

Figure 9-5 Coulomb potential for an electron resulting from two protons separated by a distance r_0. The solid line is the total potential for a one-dimensional model. The circled plus signs mark the locations of the protons.

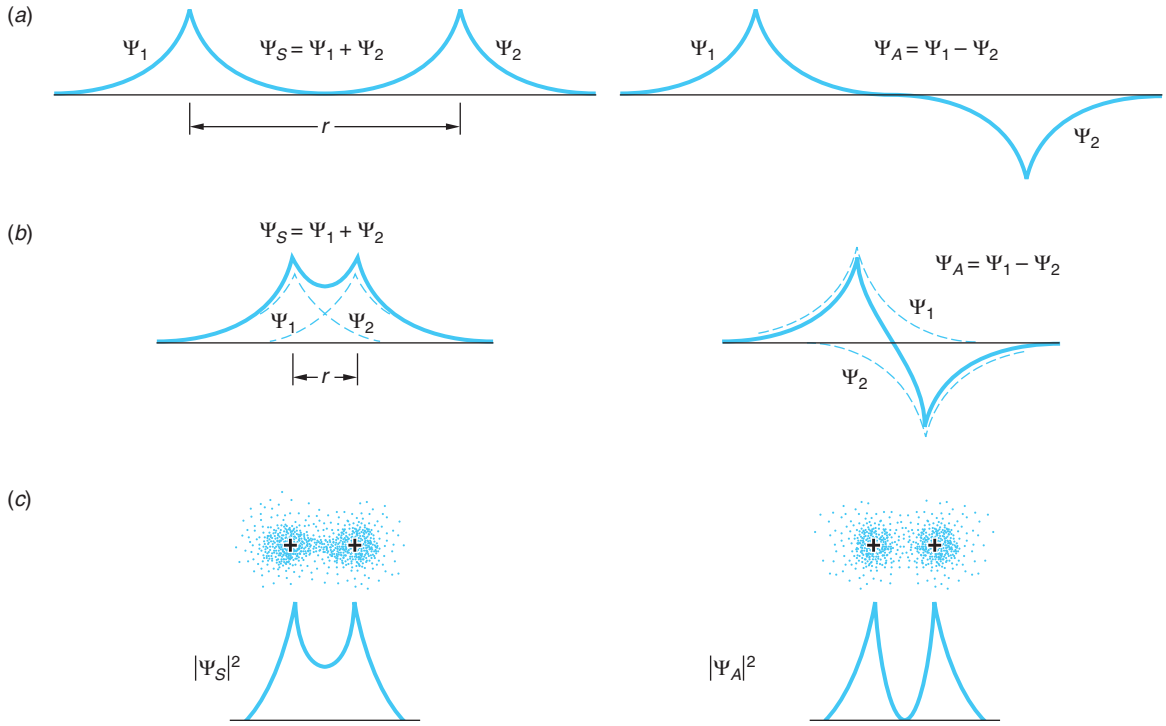

Figure 9-6 One-dimensional symmetric and antisymmetric electron space wave functions for (*a*) two protons far apart and (*b*) two protons close together. (*c*) Probability distributions for wave functions in (*b*). Computer-drawn electron density around the protons is shown above the probability densities.

The results are similar to the square-well case: Ψ_S is large in the region between the protons, while Ψ_A is small in that region. Only in the case where the electron wave function and, hence, the probability density is large near the center of the molecule do we expect a stable molecular bond to form. This concentration of negative charge between the protons for Ψ_S holds the protons together. Similarly, we would not expect Ψ_A to result in a stable molecule. The justification of this conclusion would be the solution of the Schrödinger equation and calculation of $|\Psi|^2$ for H_2^+.

The solution and calculation are quite difficult, so we will simply state the results for the energy of the molecule as a function of the separation r of the protons, describing in the process how, in general, the potential energy function arises. Referring first to Figure 9-6*a*, when the protons are far apart, the electron's energy is −13.6 eV. The potential energy U_p (repulsion) of the protons is negligibly small for large r and, since there is only a single electron in the system, there is no exclusion-principle repulsion. As the two protons are brought closer together as in Figure 9-6*b*, U_p increases and the energy of the electron decreases since the electron experiences a greater Coulomb force and becomes more tightly bound. Consider what is happening to the energy of the electron as the separation r of the protons is reduced. As $r \rightarrow 0$, the electron's wave function is approaching that of an atom with $Z = 2$. The symmetric wave function Ψ_S has a maximum at $r = 0$ and thus corresponds to the 1*s* (ground) state of the $Z = 2$ atom. As we have already seen (Equation 7-25), its energy is $E_1 = -13.6\ Z^2/n^2 = -54.4$ eV. For our discussion here, let us call the electron's energy E_S for the wave function Ψ_S.

Thus, $E_S = -13.6$ eV for $r \to \infty$ and $E_S = -54.4$ eV for $r \to 0$. The antisymmetric wave function Ψ_A is zero at $r = 0$ and thus corresponds to the $2p$ (first excited) state of the $Z = 2$ atom, this state being the lowest energy state with a wave function that vanishes at $r = 0$. (See Equation 7-26 and Table 7-2.) The energy of this state is $E_2 = -13.6\ Z^2/n^2 = -13.6$ eV. As above, if we call E_A the energy of the electron for the wave function Ψ_A, then $E_A = -13.6$ eV for $r \to \infty$ (where $|\Psi_S|^2$ and $|\Psi_A|^2$ are the same) and $E_A = -13.6$ eV for $r \to 0$. Recall that the smaller average slope of Ψ_S compared to Ψ_A as $r \to 0$ implies a smaller energy for the symmetric state. The variation of both E_S and E_A are shown in Figure 9-7.

The potential energy U_p of the protons as a function of their separation is, of course, $U_p = ke^2/r$, and the total energy of the H_2^+ molecule is then $U_p + E_S$ or $U_p + E_A$, depending on which of the electronic wave functions happens to exist. As can be seen in Figure 9-7, only one of the total energy functions has a minimum and therefore can result in bonding of the H_2^+ molecule. The potential energy function $E_{\text{total}} = U_p + E_S$ has a minimum at $r = 0.106$ nm. This tells us that the H_2^+ molecule is stable, with equilibrium separation $r_0 = 0.106$ nm and binding energy $= E_{\text{total}}(r \to \infty) - E_{\text{total}}(r_0) = -13.6 - (-16.3) = 2.7$ eV. In contrast, the potential energy function $E_{\text{total}} = U_p + E_A$ has no minimum; therefore, the antisymmetric wave function does not result in a stable molecule, as we expected at the outset of this discussion. Note that the H_2^+-type bond will tend to be unstable unless the nuclei have the same Z.

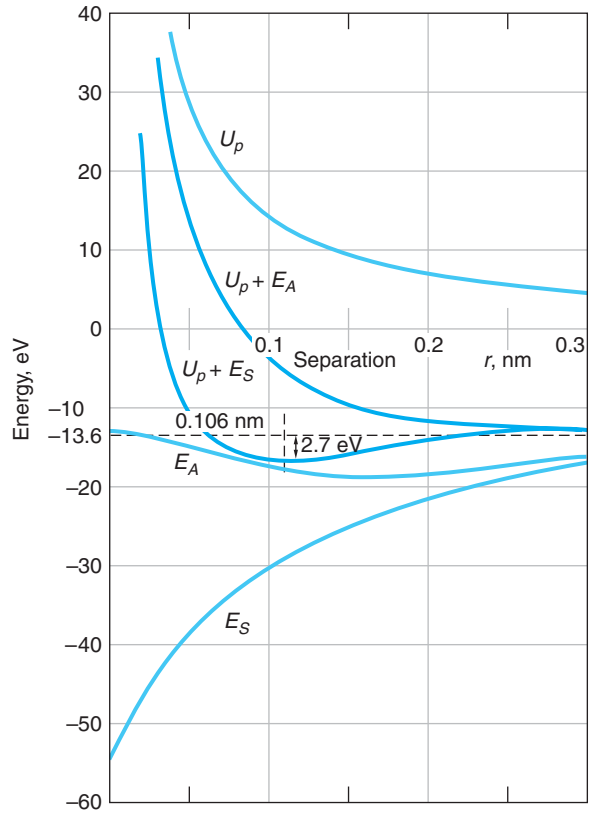

Figure 9-7 Dependence of the molecular potential energy on the separation of the protons and on the symmetry of the electron wave function for the H_2^+ system.

FÈUE WHE

H_2 Molecule

Formation of the H_2 molecule is very similar to that of H_2^+. We can think of it as two H atoms in their ground states, initially far apart. Each has a 1*s* electronic *orbital*,[1] i.e., an electron the space part of whose wave function is Ψ_{100}, with an energy of -13.6 eV. Thus, the total energy of the H_2 system for large r (i.e., $r \rightarrow \infty$) is -27.2 eV. As the two atoms approach each other, the wave functions begin to overlap, again as illustrated by Figure 9-6*a* and *b*, so that the two atoms (protons) share both electrons. Just as was discussed above, the two wave functions may add to produce a symmetric total wave function Ψ_S that results in a stable bound H_2 molecule or an antisymmetric one Ψ_A, which does not lead to a stable molecule. Since the *total* wave function Ψ must always be antisymmetric to an exchange of the electrons, the *space* wave function $\Psi_S (= R_{n\ell} Y_{\ell m})$ must be associated with an antisymmetric *spin* function χ_A (see Section 7-6). Thus, Ψ_S is a singlet state ($S = 0$) and Ψ_A is a triplet state ($S = 1$).

There is a difference between the H_2 molecule and the H_2^+ molecule that needs explanation. Just as H_2^+, the H_2 molecule has two *molecular* states whose total energy at large r is, as we have seen, -27.2 eV. As r gets smaller, the molecule still has two states, but their energies separate, as sketched in Figure 9-8*a*. The lower energy E_S is, as before, associated with Ψ_S, the electronic wave function of the stable molecule, known also as the *bonding orbital*. The wave function Ψ_A associated with the energy E_A that does not result in bonding is also called the *antibonding orbital*. The difference is that there are now two electrons whose probability density is large in the region between the protons, both in the Ψ_S molecular orbital. Since electrons obey the exclusion principle, their spins must be antiparallel ($S = 0$). Thus, a molecular orbital, just like an atomic orbital, can be occupied by no more than two electrons. For H_2 both electrons can occupy the bonding orbital. Both electrons being in *s* states, H_2 is referred to as being *s-bonded*.

Figure 9-8*b* illustrates the potential energy functions for H_2. The energy corresponding to Ψ_S, the bonding orbital, has a minimum of $E = -31.7$ eV at $r = 0.074$ nm—i.e., the equilibrium separation $r_0 = 0.074$ nm—and the binding

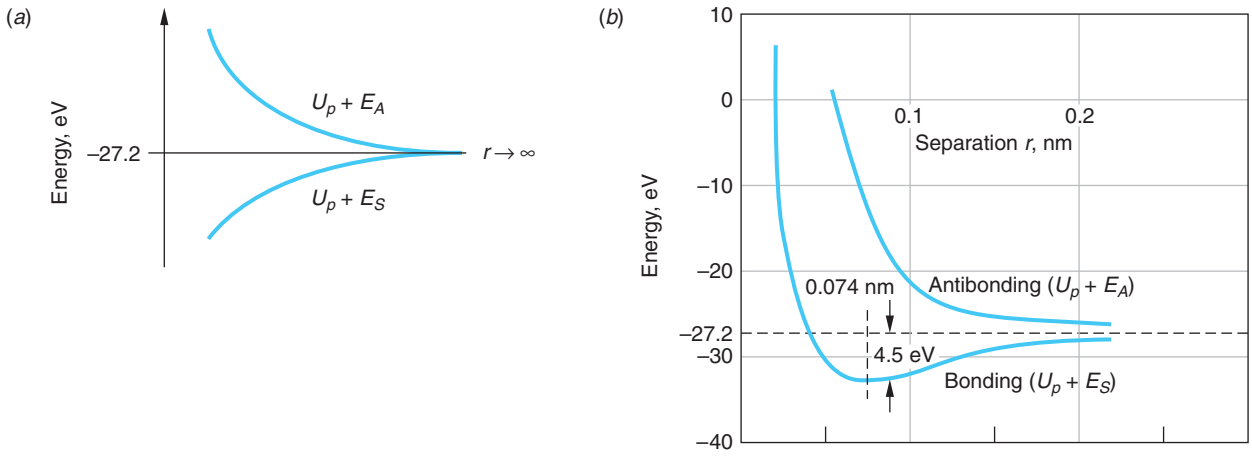

Figure 9-8 (*a*) The two levels of the H_2 system, which have the same energy for $r \rightarrow \infty$, have different energies as the atoms approach each other. (*b*) Potential energy versus separation for two hydrogen atoms. $U_p + E_S$ is for the symmetric (bonding) space wave function, and $U_p + E_A$ is for the antisymmetric (antibonding) space wave function. As the separation approaches zero, both curves approach $+\infty$.

FEUE WHE

energy is $E(r \to \infty) - E(r_0) = -27.2 - (-31.7) = 4.5$ eV. The effect of adding the second electron to H_2^+ to form H_2 is evident from a comparison of Figure 9-7 and Figure 9-8*b*. The increased charge concentration between the protons binds them more tightly, the binding energy increasing from 2.7 eV to 4.5 eV and the equilibrium separation decreasing by 30 percent. The sharing of the outer, or valence, electrons in a molecule, as in our H_2 example, is the mechanism of the *covalent* molecular bond. The basic requirement for covalent bonding is that the wave functions of the valence electrons of the participating atoms overlap as much as possible. Unlike the H_2^+ case, the covalent bond is just as strong for nonidentical nuclei as it is for identical nuclei.[2]

We can now see why three H atoms do not bond to form H_3. If a third H atom is brought near an H_2 molecule, the third electron cannot be in a 1*s* state and have its spin antiparallel to both the other electrons. It must therefore occupy the higher-energy, antibonding orbital. If it is in an antisymmetric state with respect to exchange with one of the electrons, the repulsion of this atom is greater than the attraction of the other. Thus, as the three atoms are pushed together, the third electron is in effect forced into a higher quantum state by the exclusion principle. The bond between two H atoms is called a *saturated bond* because there is no room for another electron. The two electrons being shared essentially fill the 1*s* states of both atoms. This is basically the reason why covalent bonds involving three (or more) electrons are typically unstable. However, be aware that the H_3^+ ion *is* stable. Discovered by J. J. Thomson in 1911, this simplest of all polyatomic molecules provides important cosmic spectral lines for astrophysicists and a calculation benchmark for quantum chemists.

Although the H_3 molecule is not bound, the H_3^+ ion is! Discovered by J. J. Thomson in 1911, and lacking a stable excited state, H_3^+ is used as a probe in Jupiter's atmosphere and serves as the benchmark for quantum chemistry calculations for polyatomic molecules.

It should also be clear now why He atoms do not bond together to form He_2. There are no valence electrons that can be shared. As two He atoms approach each other, the bonding and antibonding molecular orbitals form, just as they do for H_2; however, each orbital can accommodate only two electrons (with spins antiparallel), so two of the four electrons in the He_2 system cannot remain in the 1*s* atomic states but must be in the antibonding orbital. The net effect is that He_2 does not form as a stable bond. At low temperatures or high pressures, He atoms do bond together, but the bonds are very weak and are due to van der Waals forces, which we will discuss in Section 9-3. The bonding is so weak that at atmospheric pressure, He boils at 4.2 K, and it does not form a solid at any temperature unless the pressure is greater than about 20 atm.

Covalent or Ionic?

Covalently bonded fullerene molecules have been assembled into nanotubes, i.e., tubes with diameters in the nanometer range. Adding a few impurity atoms per molecule turns it into a superconductor. (See Section 10-8.)

When two identical atoms bond, as in homonuclear diatomic molecules such as O_2 or N_2, the bonding is purely covalent. Since the wave functions of the two atoms are exactly alike, neither atom dominates and the electrons are completely shared between them. However, the bonding of two dissimilar atoms is often a mixture of covalent and ionic bonding. Even in NaCl, the electron donated by sodium to chlorine has some probability of being at the sodium atom because its wave function does not suddenly fall to zero. Thus, this electron is partially shared in a covalent bond, although this bonding is only a small part of the total bond, which is mainly ionic.

A measure of the degree to which a bond is ionic or covalent can be obtained from the electric dipole moment of the molecule. For example, if the bonding in NaCl were purely ionic, the center of positive charge would be at the Na^+ ion and the center of negative charge would be at the Cl^- ion. The electric dipole moment would have the magnitude

$$p_{\text{ionic}} = er_0 \qquad \textbf{9-3}$$

where r_0 is the equilibrium separation of the ions. Thus, the dipole moment of NaCl would be

$$p_{\text{ionic}} = er_0 = (1.60 \times 10^{-19}\,\text{C})(2.36 \times 10^{-10}\,\text{m}) = 3.78 \times 10^{-29}\,\text{C}\cdot\text{m}$$

The actual measured electric dipole moment of NaCl is

$$p_{\text{measured}} = 3.00 \times 10^{-29}\,\text{C}\cdot\text{m}$$

A purely covalent molecule would be expected to have an electric dipole moment of zero. We can define the ratio of p_{measured} to p_{ionic} as the fractional amount of ionic bonding. For NaCl, this ratio is 3.00/3.78 = 0.79. Thus, the bonding in NaCl is about 79 percent ionic and 21 percent covalent.

EXAMPLE 9-3 Bonding in LiH The measured electric dipole moment of LiH is $1.96 \times 10^{-29}\,\text{C}\cdot\text{m}$. This molecule is among those listed in Table 9-3 (on the home page) as being covalently *s*-bonded. What portion of the LiH bond is covalent?

SOLUTION

The equilibrium separation of LiH from the table is 0.159 nm. If it were a purely ionically bonded molecule, its dipole moment p_{ionic} would be

$$p_{\text{ionic}} = (1.60 \times 10^{-19}\,\text{C})(0.159 \times 10^{-9}\,\text{m}) = 2.54 \times 10^{-29}\,\text{C}\cdot\text{m}$$

The fractional amount of the bond that is ionic is 1.96/2.54 = 0.77. Thus, LiH is only about 23 percent covalently *s*-bonded.

More

In addition to the *s*-bonded H_2 molecule, there are many other covalently bonded molecules involving shared pairs of *s* electrons, *s* and *p* electrons, and *p* electrons. Important among these are the *s*-*p* bonds involving carbon that are the basis for the vast array of hydrocarbon molecules and compounds. Several examples, including the remarkable fullerenes, are discussed in *Other Covalent Bonds* on the home page: www.whfreeman.com/tiplermodernphysics5e See also Equations 9-4 and 9-5 here, as well as Tables 9-3 through 9-6 and Figures 9-9 through 9-17.

EXPLORING
9-3 Other Bonding Mechanisms

The two bonding mechanisms that we have discussed thus far, ionic and covalent, account for a large fraction of the cases in which atoms combine to form molecules. As is described in Chapter 10, when atoms combine on a larger scale to form solids, these exact same mechanisms are responsible for the bonding in many solids. In addition to these types of bonding, two other types occur in solids. One of these, *molecular bonding*, or *dipole-dipole bonding*, also occurs in the formation of many large molecules from smaller molecules and will be discussed in this section. The second type, *metallic bonding*, is responsible for the structure of metals in the solid state and has no single-molecule version or counterpart. For that reason, our discussion of metallic bonding will be deferred to Chapter 10.

Dipole-Dipole Bonding

It was first suggested by J. D. van der Waals[5] in 1873 that any two separated molecules will be attracted toward each other by electrostatic forces. Similarly, atoms that do not otherwise form ionic or covalent bonds will be attracted to each other by the same sort of weak electrostatic bonds. The practical result of this is that at temperatures low enough so that the disruptive effects of thermal agitation are negligible, all substances will condense into a liquid and then a solid form. (Recall that helium is the only element that does not solidify at any temperature under its own vapor pressure.) The relatively weak electrostatic forces responsible for this sort of intermolecular attraction arise because of the electrostatic attraction of electric dipoles.

The electric field due to an electric dipole is illustrated in Figure 9-18*a*. The electric field $\mathbf{E}_d$ at point A due to the dipole is given by

$$\mathbf{E}_d = k\left[\frac{\mathbf{p}}{r^3} - \frac{3(\mathbf{p}\cdot\mathbf{r})}{r^5}\mathbf{r}\right] \qquad \textbf{9-6}$$

whose magnitude for $r \gg a$ is

$$E_d = \frac{kqa}{r^3} = \frac{kp_1}{r^3} \qquad \textbf{9-7}$$

where $|\mathbf{p}_1| = qa$ is the dipole moment.[6] Thus, the electric field of the dipole, and hence the electric force on a charge, falls off as $1/r^3$. This result, which is correct even if the point A is not on the perpendicular, is to be compared with the $1/r^2$ dependence of the Coulomb force that occurs in the covalent and ionic bonds: the force on a test charge due to the dipole qa is weaker at a distance r than that due to a charge q. A second dipole $\mathbf{p}_2$ that happens into the vicinity of $\mathbf{p}_1$ will then orient itself along the $\mathbf{E}_d$ field lines, as illustrated in Figure 9-18*b*, as a result of the electric force on the charges.

The potential energy of the second dipole $\mathbf{p}_2$ in the field of $\mathbf{p}_1$ is given by

$$U = -\mathbf{p}_2\cdot\mathbf{E}_d \qquad \textbf{9-8}$$

and, since $\mathbf{E}_d$ falls off like $1/r^3$, the electric force $\mathbf{F}$ $(= -\partial U/\partial r)$ between two *permanent* dipoles falls off as $1/r^4$. Thus, it is attractive ($\mathbf{F}$ is negative), relatively weak, and of short range.

Polar Molecules

It is then not hard to see physically why molecules with permanent electric dipole moments—so-called *polar molecules* such as H_2O and NaCl—will attract other polar molecules. Consider the H_2O molecule as an example. Although the molecule is electrically neutral, its bonding is partially ionic, so the electrons tend to be concentrated nearer the oxygen atom, making it look like the negative end of a dipole. The two protons then look like the positive end of the dipole. There will then be a mutual

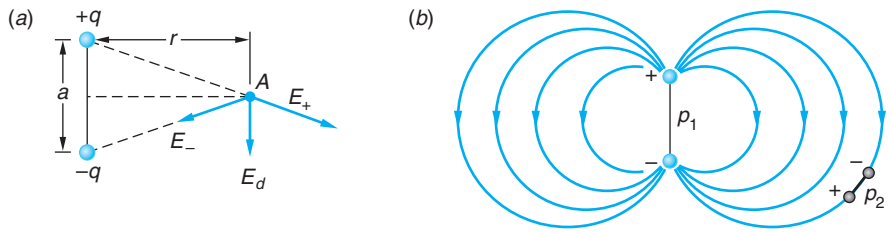

Figure 9-18 (*a*) The electric field $\mathbf{E}_d$ at a point A on a line perpendicular to the axis of an electric dipole $p_1 = qa$. (*b*) The field of $\mathbf{E}_d$ acts on a second dipole p_2 to orient it along the field lines. The force on a charge due to p_1 is $\propto 1/r^3$.

FEUE WHE

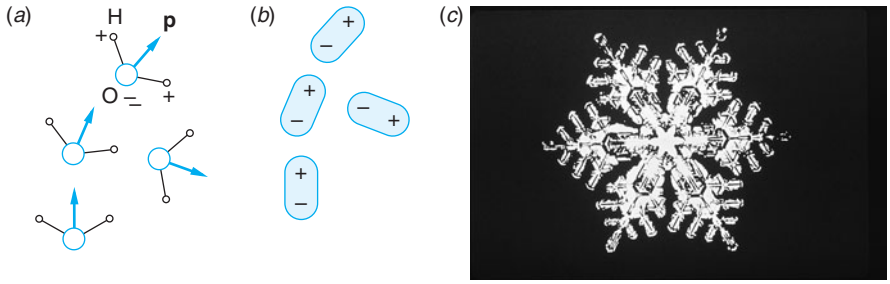

Figure 9-19 (*a*) Schematic of four H_2O molecules. The water molecules' permanent dipole moments are shown by the vectors **p**. (*b*) The four polar water molecules represented as electric dipoles. Notice that the attractive dipole-dipole force tends to align the dipoles so that the nearest neighbors of each charge are charges of the opposite sign. (*c*) A snowflake—one result of dipole-dipole bonding.

attraction between the molecule and other nearby molecules with potential energy given by Equation 9-8. (See Figure 9-19.) Pairs of polar molecules will thus move closer to each other, decreasing their potential energy, until the combined effects of the increasing nuclear repulsion and the exclusion principle produce a minimum in the total potential energy similar to the minima in Figures 9-2 and 9-8*b*. For H_2O the resulting bonding energy is about 0.5 eV per molecule. Although this is only about 10 percent of the strength of the H—OH bond in the water molecule, it is this dipole-dipole force that bonds H_2O molecules to each other to form ice and is responsible in part for the beautiful hexagonal patterns that we see in snowflakes (Figure 9-19*c*).

When dipole-dipole bonds between molecules with permanent dipole moments involve hydrogen, as is the case for water, the bond is referred to as a *hydrogen bond*. The hydrogen bond is of enormous importance since it is the bonding mechanism responsible for the cross-linking that allows giant biological molecules and polymers to hold their fixed shape. For example, it is the hydrogen bond that forms the linkage between the two strands of the double helix DNA molecule. It is the weakness of the hydrogen bonds relative to the covalent/ionic bonds along each strand that allows the two strands to unwind from each other in the DNA molecular replication process. Notice that the hydrogen bond can be viewed as the sharing of a proton by two negatively charged atoms, oxygen atoms in the case of water. (See Figure 9-19.) In this way it is similar to the sharing of electrons that is responsible for the covalent bond. Hydrogen bonding is facilitated by the small mass of the proton and the absence of inner-core electrons.

Nonpolar Molecules

A nonpolar molecule will be polarized by the field of a polar molecule and thus have an induced dipole moment and be attracted to the polar molecule. If $\mathbf{p}_2$ in Figure 9-18*b* is an induced dipole, then

$$\mathbf{p}_2 = \alpha \mathbf{E}_d \qquad \textbf{9-9}$$

where α is a constant characteristic of the nonpolar molecule called the *polarizability*. In this case we expect the potential energy of the interaction to fall off as $1/r^6$ since we have from Equations 9-8 and 9-9 that

$$U = -\mathbf{p}_2 \cdot \mathbf{E}_d = -\alpha E_d^2 = -\alpha k^2 p_1^2 / r^6 \qquad \textbf{9-10}$$

Once again, the energy is negative, signifying that the force between the dipoles is attractive. The force $F = -\partial U/\partial r$ is thus proportional to $1/r^7$, i.e., the force is very short range, dropping rapidly with increasing r. Indeed, increasing the separation of the molecules by a factor of 2 reduces the attractive force between them to only 0.008 of its original value.

Perhaps surprisingly, two molecules, neither of which has a permanent dipole moment, can also attract each other via the mechanism just described. It is somewhat harder to see why an attractive force exists between two nonpolar molecules. Though the *average* dipole moment $\overline{\mathbf{p}}$ of a nonpolar molecule is zero, the *average square* dipole moment $\overline{p^2}$ is not because the electrons are in constant motion and at any given instant there will be an excess or deficiency of them in one part or another of the molecule. A measurement that we might do in the laboratory reveals the average value (zero), not the instantaneous value. The instantaneous dipole moment of a nonpolar molecule is, in general, not zero. When two nonpolar molecules are nearby, the fluctuations in the instantaneous dipole moments tend to be correlated so as to produce attraction, as illustrated in Figure 9-20. The potential energy is again given approximately by Equation 9-10, so that the potential energy is proportional to $1/r^6$ and the attractive force is proportional to $1/r^7$. This attractive force between nonpolar molecules is called the *van der Waals force*[7] or, occasionally, the *London dispersion force*, after Fritz London, the German physicist who in 1930 first explained the physical origin of the interaction.

As van der Waals first suggested, dipole-dipole forces act between all molecules and, in addition, between all atoms. They are the only forces that occur between rare gas atoms, without which the atoms of these elements would not condense into liquids or form solids. (The single exception to the latter is He, whose quantum-mechanical zero-point energy exceeds the minimum of the potential energy resulting from Equation 9-10 and core repulsion.) The dipole-dipole forces between molecules, although relatively weak, are also responsible for the physical phenomena of surface tension and friction.

Scientists have recently succeeded in trapping a sample of *molecules* in a single quantum level at a temperature in the millikelvin range. This ability raises the possibilities for, among other things, high-precision molecular spectroscopy and producing a molecular Bose-Einstein condensate.

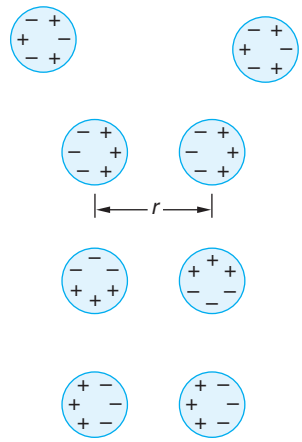

Figure 9-20 Nonpolar molecules have, on average, symmetric charge distributions, as illustrated by the pair of molecules at the top of the figure. However, instantaneous fluctuations in the electron distribution are asymmetric and tend to be correlated with those of nearby molecules, as shown in the other three examples. The correlated distributions lead to an attractive force proportional to $1/r^7$ that draws the molecules closer to each other as shown.

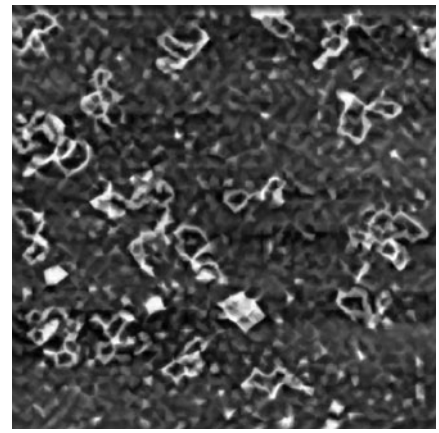

The 2-nm height of DNA molecules is readily imaged by an atomic force microscope (AFM). [*Taken from www.di.com, Digital Instruments, Veeco metrology Group, Santa Barbara, CA.*]

FEUE WHE

Questions

1. Why would you expect the separation distance between the two protons to be larger in the H_2^+ ion than in the H_2 molecule?
2. Would you expect the NaCl molecule to be polar or nonpolar?
3. Would you expect the N_2 molecule to be polar or nonpolar?
4. Does neon occur naturally as Ne or Ne_2? Why?

9-4 Energy Levels and Spectra of Diatomic Molecules

As is the case with an atom, a molecule often emits electromagnetic radiation when it makes a transition from an excited energy state to a state of lower energy. Conversely, a molecule can absorb radiation and make a transition from a lower energy state to a higher energy state. The study of molecular emission and absorption spectra thus provides us with information about the energy states of molecules. For simplicity, we will consider only diatomic molecules here.

As might be expected, the energy levels of molecular systems are even more complex than those of atoms. The energy of a molecule can be conveniently separated into three parts: electronic, due to the excitation of its electrons; vibrational, due to the oscillations of the atoms of the molecule; and rotational, due to the rotation of the molecule about an axis through its center of mass. Fortunately, the magnitudes of these energies are sufficiently different that they can be treated separately. Electrons in molecules can be excited to higher states, just as those in atoms. For example, a 1*s* electron in the H_2 molecule can be excited to a 2*p* level, emitting a photon as it returns to the ground state. The energies due to the electronic excitations of a molecule are of the order of magnitude of 1 eV, the same as for the excitation of atoms. We have already discussed such transitions and will not consider them further in this section. The energies of vibration and rotation are about 1/100 to 1/1000 times smaller and will be the focus of our attention.

Rotational Energy Levels

Classically, the kinetic energy of rotation is

$$E = \frac{1}{2}I\omega^2 = \frac{(I\omega)^2}{2I} = \frac{L^2}{2I} \qquad \textbf{9-11}$$

where I is the moment of inertia, ω the angular velocity of rotation, and $L = I\omega$ the angular momentum. The solution of the Schrödinger equation for the rotation of a rigid body leads to the quantization of the angular momentum, with values given by

$$L^2 = \ell(\ell + 1)\hbar^2 \qquad \ell = 0, 1, 2, \ldots \qquad \textbf{9-12}$$

where ℓ is the *rotational quantum number*. This is the same quantum condition on angular momentum that holds for the orbital angular momentum of an electron in an atom.

Note, however, that L in Equation 9-11 refers to the angular momentum of the entire molecule rotating about an axis through its center of mass. The energy levels of a rotating molecule are therefore given by

$$E = \frac{\ell(\ell + 1)\hbar^2}{2I} = \ell(\ell + 1)E_{0r} \quad \ell = 0, 1, 2, \ldots \tag{9-13}$$

where E_{0r} is the *characteristic rotational energy* of a particular molecule, which is inversely proportional to its moment of inertia:

$$E_{0r} = \frac{\hbar^2}{2I} \tag{9-14}$$

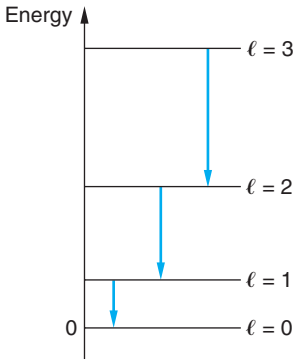

Figure 9-21 Energy levels and allowed transitions for a rotating rigid body as given by Equation 9-13.

The rotational-energy level scheme is shown in Figure 9-21. Transitions between these levels produce the *pure rotational spectrum* of a molecule. While all diatomic molecules have rotational energy levels, those without permanent dipole moments (symmetric molecules such as H_2, Cl_2, or CO_2) cannot emit or absorb electric dipole radiation by only changing the rotational quantum state and thus do not have a pure rotational spectrum. For molecules that do have dipole moments and emit pure rotational spectra, the quantum number ℓ is subject to the selection rule $\Delta\ell = \pm 1$, just as it was for the atomic electrons. Thus, the energy separation between adjacent rotation states is given by

$$\Delta E_{\ell,\,\ell+1} = \frac{[(\ell + 1)(\ell + 2) - \ell(\ell + 1)]\hbar^2}{2I} = \frac{(\ell + 1)\hbar^2}{I} \tag{9-15}$$

A measurement of the rotational energy of a molecule from its rotational spectrum can be used to determine the moment of inertia of the molecule, which can then be used to find the equilibrium separation of the atoms in the molecule, i.e., the bond length. The moment of inertia about an axis through the center of mass of a diatomic molecule (see Figure 9-22) is

$$I = m_1 r_1^2 + m_2 r_2^2$$

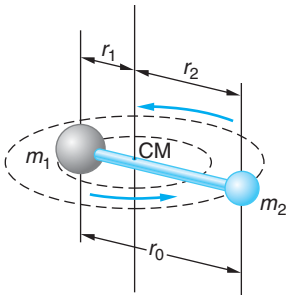

Figure 9-22 Diatomic molecule rotating about an axis through its center of mass.

Using $m_1 r_1 = m_2 r_2$, which relates the distances r_1 and r_2 from the atoms to the center of mass, and $r_0 = r_1 + r_2$ for the separation of the atoms, we can write the moment of inertia as

$$I = \mu r_0^2 \tag{9-16}$$

where μ, the reduced mass, is

$$\mu = \frac{m_1 m_2}{m_1 + m_2} \tag{9-17}$$

If the masses are equal ($m_1 = m_2$), as in H_2 and O_2, the reduced mass $\mu = m/2$ and

$$I = \frac{1}{2} m r_0^2 \tag{9-18}$$

A unit of mass convenient for discussing atomic and molecular masses is the *unified mass unit* u, which is defined as one-twelfth of the mass of a neutral carbon-12 (^{12}C) atom.

The mass of one ^{12}C atom is thus 12 u. The mass of an atom in unified mass units is therefore numerically equal to the molar mass of the atom in grams. The unified mass unit is related to the gram and kilogram by

$$1\text{ u} = \frac{1g}{N_A} = \frac{10^{-3}\text{ kg}}{6.0221 \times 10^{23}} = 1.6605 \times 10^{-27}\text{ kg} = 931.4940 \times 10^{6}\text{ eV}/c^2 \qquad \textbf{9-19}$$

where N_A is Avogadro's number.

EXAMPLE 9-4 The Reduced Mass of HCl Compute the reduced mass of the HCl molecule.

SOLUTION

1. The reduced mass μ is given by Equation 9-17:
$$\mu = \frac{m_1 m_2}{m_1 + m_2}$$
2. From the periodic table on the inside back cover of this book, the mass of the hydrogen atom is 1.01 u and that of the chlorine atom is 35.5 u. Substituting these gives
$$\mu = \frac{(1.01\text{ u})(35.5\text{ u})}{1.01\text{ u} + 35.5\text{ u}} = 0.98\text{ u}$$

Remarks: *Note that the reduced mass of the HCl molecule is less than that of a single hydrogen atom.*

EXAMPLE 9-5 Equilibrium Separation in CO The energy difference ΔE between the $\ell = 0$ and $\ell = 1$ rotational levels in the CO molecule is found experimentally from measurement of the wavelength $\lambda = 2.6$ mm of the corresponding transition. For CO, ΔE is equal to 4.77×10^{-4} eV. Find the equilibrium separation, or bond length r_0, of the CO molecule.

SOLUTION

1. The bond length r_0 is given in terms of the moment of inertia I of the molecule by Equation 9-16:
$$I = \mu r_0^2 \quad \text{or} \quad r_0 = \sqrt{\frac{I}{\mu}}$$
2. I in terms of ΔE is given by Equation 9-15:
$$\Delta E_{\ell,\,\ell+1} = \frac{(\ell + 1)\hbar^2}{I} \quad \text{or} \quad I = \frac{(\ell + 1)\hbar^2}{\Delta E_{\ell,\,\ell+1}}$$
3. Substituting $\ell = 0$ and $\Delta E = 4.77 \times 10^{-4}$ eV into step 2 gives
$$I = \frac{\hbar^2}{4.77 \times 10^{-4}\text{ eV}}$$
4. The reduced mass of the CO molecule is computed from Equation 9-17 using atomic mass values from the periodic table:
$$\mu = \frac{m_1 m_2}{m_1 + m_2} = \frac{(12\text{ u})(16\text{ u})}{12\text{ u} + 16\text{ u}} = 6.86\text{ u}$$

5. Substituting these results into step 1 gives

$$r_0 = \left(\frac{\hbar^2}{4.77 \times 10^{-4}\,\text{eV} \times 6.86\,\text{u}}\right)^{1/2}$$

$$= \frac{1.055 \times 10^{-34}}{[(4.77 \times 10^{-4}\,\text{eV})(1.60 \times 10^{-19}\,\text{J/eV})(6.86\,\text{u})(1.66 \times 10^{-27}\,\text{kg/u})]^{1/2}}$$

$$= 0.133\,\text{nm}$$

The rotational energy levels are several orders of magnitude smaller than those due to electron excitation, which have energies of the order of 1 eV or higher. For example, the characteristic rotational energy of the O_2 molecule, whose equilibrium separation is about 0.1 nm, is 2.59×10^{-4} eV, calculated from Equation 9-14. Transitions within a given set of rotational energy levels yield photons in the far infrared region of the electromagnetic spectrum. Notice that the rotational energies are also small compared with the typical thermal energy kT at normal temperatures. For $T = 300$ K, for example, kT is about 2.6×10^{-2} eV. Thus, at ordinary temperatures, a molecule can easily be excited to the lower rotational energy levels by collisions with other molecules. But such collisions cannot excite the molecule to electronic energy levels above the ground state.

Vibrational Energy Levels

The molecular vibrational energies are a bit harder to estimate than were the rotational energies. Our discussion is aided by the fact that the molecular potential energy functions of Figures 9-2, 9-7, and 9-8*b* can be closely approximated by parabolas in the vicinity of the equilibrium point. (See Figure 9-23*b*.) Thus, we can use the

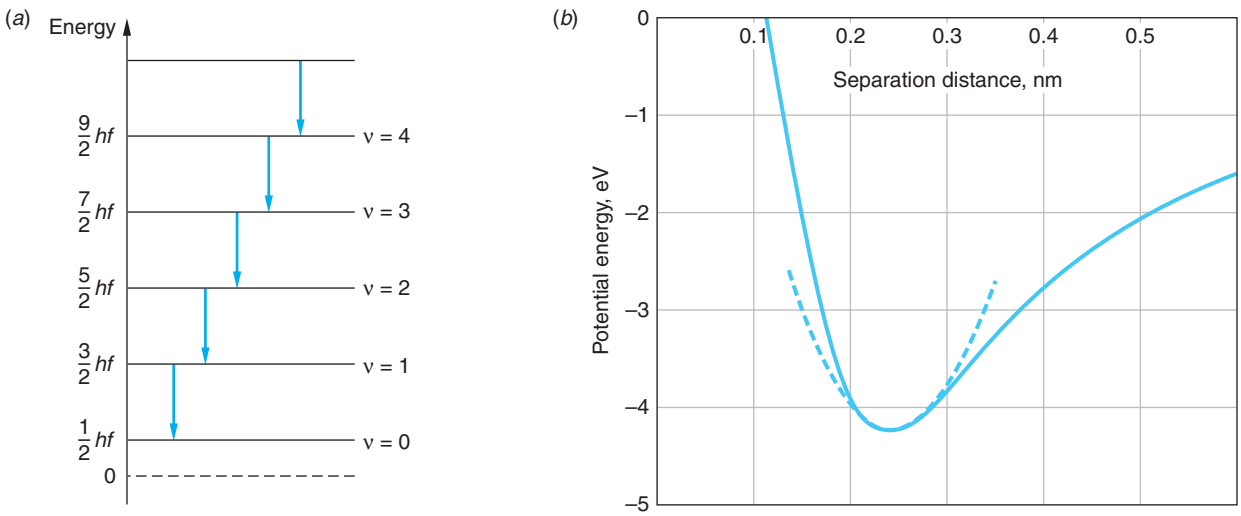

Figure 9-23 (*a*) The energy levels of the molecular vibrations are equally spaced in the vicinity of the equilibrium spacing of the atoms. (*b*) A harmonic oscillator potential fitted to the actual potential energy function of the NaCl molecule shown in Figure 9-2*b*.

results of our study of the simple harmonic oscillator in Chapter 6. The energy levels are given by

$$E_v = (v + 1/2)hf \qquad v = 0, 1, 2, 3, \ldots \tag{9-20}$$

where f is the frequency of the vibration and v is the *vibrational quantum number*.[8] An interesting feature of this result is that the energy levels are equally spaced with intervals $\Delta E_{v,\,v+1} = hf$, as shown in Figure 9-23*a*. The frequency of vibration of a diatomic molecule can be related to the force exerted by one atom on the other. Consider two objects of mass m_1 and m_2 connected by a spring of force constant K. The frequency of oscillation of this system is (see Section 6-5)

$$f = \frac{1}{2\pi}\sqrt{\frac{K}{\mu}} \tag{9-21}$$

where μ is the reduced mass given by Equation 9-17. The effective force constant of a diatomic molecule can thus be determined from a measurement of the frequency of oscillation of the molecule.

We could get a good estimate of f by fitting the one-dimensional parabolic harmonic oscillator potential energy function for the molecule as illustrated in Figure 9-23*b*, but for simplicity we can get a rough idea of the order of magnitude of the vibrational energies by observing that the energy of an atom of mass m in a square well of width r_0 is (Figure 9-24)

$$E_n = n^2\frac{h^2}{8mr_0^2} = n^2\frac{4\pi^2\hbar^2}{8mr_0^2} = n^2\frac{\pi^2}{2}\frac{\hbar^2}{mr_0^2}$$

Except for the factor $\pi^2/2 \approx 5$ (and the n^2), this expression is the same as the characteristic rotational energy E_{0r}; thus we expect the vibrational energies to be somewhat larger than the rotational energies.

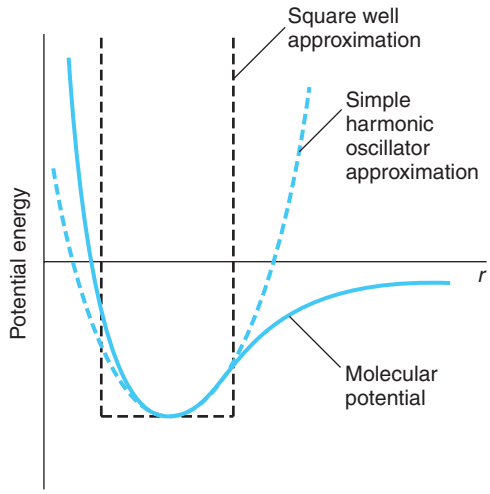

Figure 9-24 Molecular potential. The simple harmonic oscillator approximation, used to calculate the energy levels, and a square well approximation, used to estimate the order of magnitude of the energy levels, are each indicated by dashed curves.

The selection rule for transitions between vibrational states (of the same electronic state) requires that v change only by ± 1, so the energy of a photon emitted by such a transition is hf and the frequency is the same as the frequency of vibration. A typical measured frequency of a transition between vibrational states is 5×10^{13} Hz, which gives for the order of magnitude of vibrational energies

$$E \sim hf = (4.14 \times 10^{-15}\ \text{eV} \cdot \text{s})(5 \times 10^{13}\ \text{s}^{-1}) = 0.2\ \text{eV}$$

Thus, a typical vibrational energy is actually about 1000 times greater than the typical rotational energy E_{0r} of the O_2 molecule we noted above and about 8 times greater than the typical thermal energy $kT = 0.026$ eV at $T = 300$ K. In contrast with the rotational levels, the molecular vibrational states are not readily excited by collisions between molecules at ordinary temperatures.

EXAMPLE 9-6 **Force Constant of CO** The observed vibrational frequency of the CO molecule is 6.42×10^{13} Hz. What is the effective force constant for this molecule?

SOLUTION

1. The force constant K is given in terms of the vibrational frequency f by Equation 9-21: $$f = \frac{1}{2\pi}\sqrt{\frac{K}{\mu}}$$
2. The reduced mass μ of the CO molecule was computed in step 4 of Example 9-5: $$\mu = 6.86\ \text{u}$$
3. Solving Equation 9-21 for K and substituting the values of f and μ gives

$$\begin{aligned} K &= (2\pi f)^2\mu \\ &= (2\pi \times 6.42 \times 10^{13}\ \text{Hz})^2(6.86\ \text{u})(1.66 \times 10^{-27}\ \text{kg/u}) \\ &= 1.86 \times 10^{3}\ \text{N/m} \end{aligned}$$

Emission Spectra

Figure 9-25 shows schematically some electronic, vibrational, and rotational energy levels of a diatomic molecule. The vibrational levels are labeled with the quantum number v and the rotational levels with the quantum number ℓ. The lower vibrational levels are evenly spaced, with $\Delta E = hf$. For higher vibrational levels, the approximation that the vibration is simple harmonic is not valid and the levels are not quite evenly spaced. The actual potential spreads somewhat more rapidly, as can be seen in Figure 9-24, and the spacing of the vibrational levels becomes closer for large values of the quantum number v. Notice in Figure 9-25 that the potential energy curves representing the force between the two atoms in the molecule do not have exactly the same shape for the electronic ground and excited states. This implies that the fundamental frequency of vibration f is different for different electronic states. For transitions between vibrational states of different electronic states, the selection rule $\Delta v = \pm 1$ does not hold. Such transitions result in the emission of photons of wavelength in or near the visible spectrum.

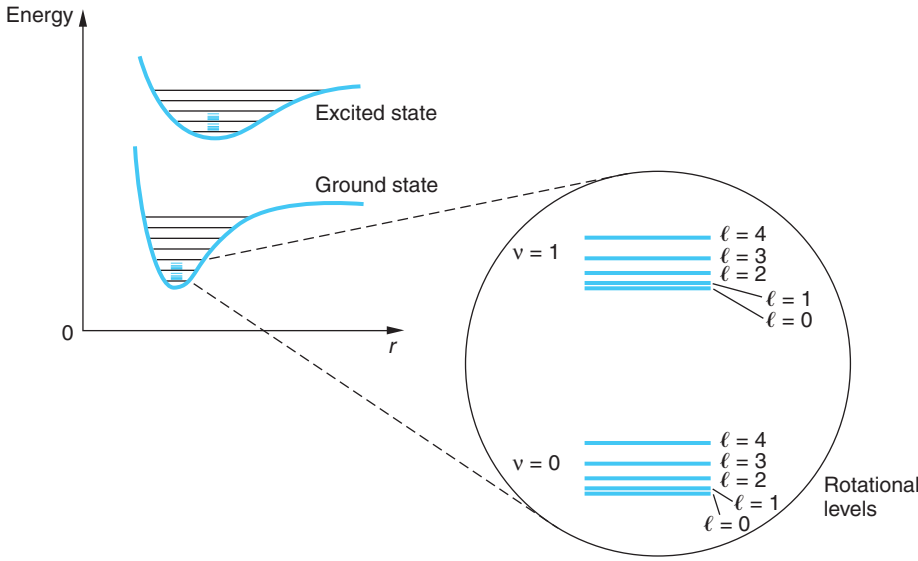

Figure 9-25 Electronic, vibrational, and rotational energy levels of a diatomic molecule. The rotational levels are shown in an enlargement of the $v = 0$ and $v = 1$ vibrational levels of the electronic ground state.

The spacing of the rotational levels increases with increasing values of ℓ. Since the energies of rotation are so much smaller than those of vibrational or electronic excitations of a molecule, molecular rotation shows up in molecular spectra as a fine-structure splitting of the spectral lines. When the fine structure is not resolved, the spectrum appears as bands, as shown in Figure 9-26*a* (page 386). Close inspection of these bands reveals that they have a fine structure due to the rotational energy levels, as shown in the enlargement in Figure 9-26*b*.

Absorption Spectra

Much molecular spectroscopy is done using infrared absorption techniques in which only the vibrational and rotational energy levels of the ground-state electronic level are excited. Consequently, we will now direct our attention to what is called the *vibration-rotation spectrum*. For ordinary temperatures, the vibrational energies are sufficiently large in comparison with the thermal energy kT that most of the molecules are in the lowest vibrational state $v = 0$, for which the energy is $E_0 = \frac{1}{2}hf$. The transition from $v = 0$ to $v = 1$ is the predominant transition in absorption. The rotational energies, however, are sufficiently smaller than kT that the molecules are distributed among several rotational energy states, the relative number in each state being determined by the Boltzmann factor. If the molecule is originally in a rotational state characterized by the quantum number ℓ, its initial energy, in addition to that of the electronic state, is

$$E_\ell = \tfrac{1}{2}hf + \ell(\ell + 1)E_{0r} \qquad \textbf{9-22}$$

where E_{0r} is given by Equation 9-14. From this state, two transitions are permitted by the selection rules. For a transition to the next highest vibrational state $v = 1$ and a rotational state characterized by $\ell + 1$, the final energy is

$$E_{\ell+1} = \tfrac{3}{2}hf + (\ell + 1)(\ell + 2)E_{0r} \qquad \textbf{9-23}$$

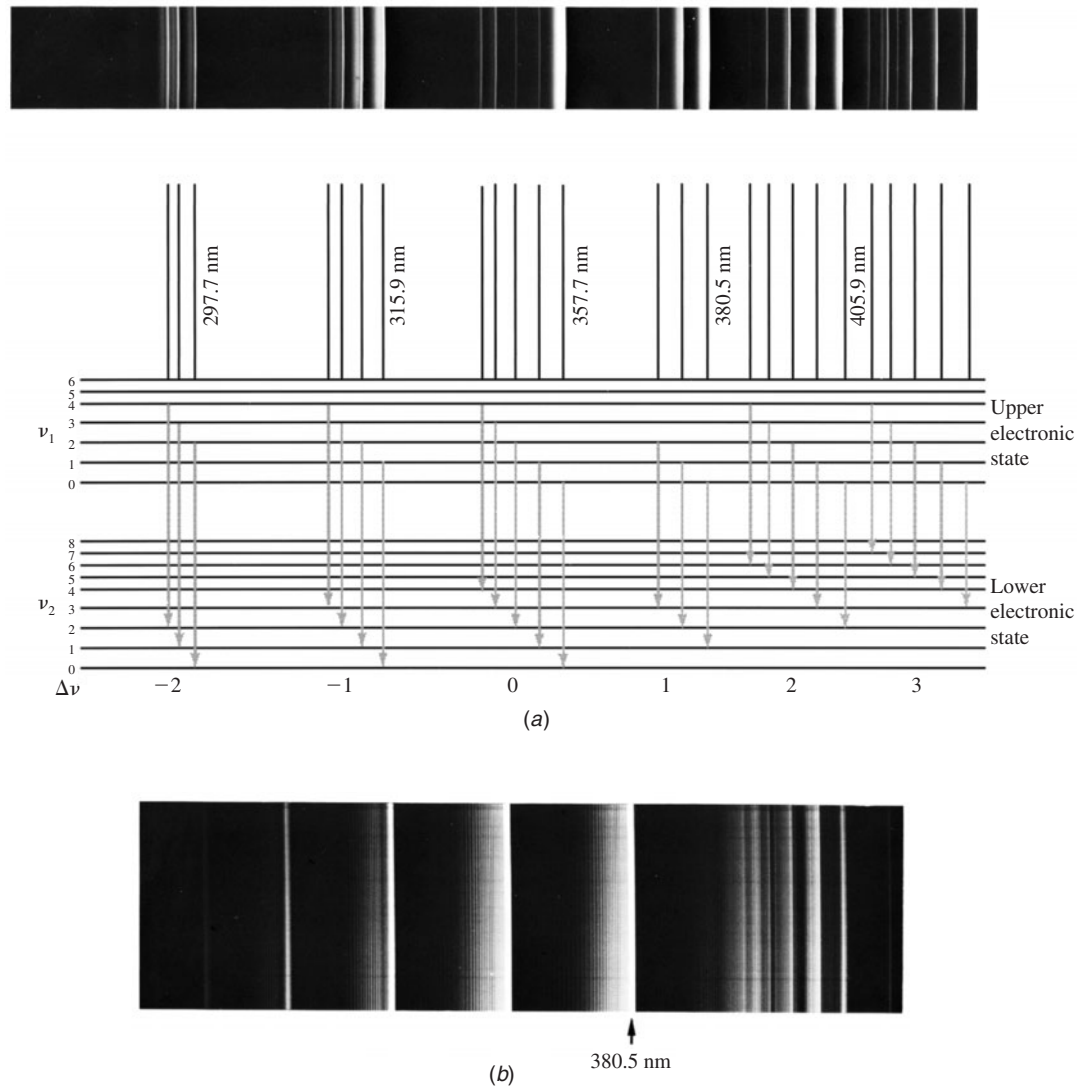

Figure 9-26 Part of the emission spectrum of N_2. (*a*) These components of the band are due to transitions between the vibrational levels of two electronic states, as indicated in the diagram. (*b*) An enlargement of part of (*a*) shows that the apparent lines in (*a*) are in fact band heads with structure caused by rotational levels. [*Courtesy of J. A. Marquisee.*]

For a transition to the next highest vibrational state and to a rotational state characterized by $\ell - 1$, the final energy is

$$E_{\ell-1} = \tfrac{3}{2}hf + (\ell - 1)\ell E_{0r} \qquad \textbf{9-24}$$

The energy differences are

$$\Delta E_{\ell \to \ell+1} = E_{\ell+1} - E_{\ell} = hf + 2(\ell + 1)E_{0r} \qquad \textbf{9-25}$$

where $\ell = 0, 1, 2, \ldots$, and

FÈUE WHE

$$\Delta E_{\ell \to \ell - 1} = E_{\ell - 1} - E_{\ell} = hf - 2\ell E_{0r} \qquad \textbf{9-26}$$

where $\ell = 1, 2, 3, \ldots$. (In Equation 9-26, ℓ begins at $\ell = 1$ because from $\ell = 0$ only the transition $\ell \to \ell + 1$ is possible.) Figure 9-27 illustrates these transitions. The frequencies of these transitions are given by

$$f_{\ell \to \ell + 1} = \frac{\Delta E_{\ell \to \ell + 1}}{h} = f + \frac{2(\ell + 1)E_{0r}}{h} \qquad \ell = 0, 1, 2, \ldots \qquad \textbf{9-27}$$

and

$$f_{\ell \to \ell - 1} = \frac{\Delta E_{\ell \to \ell - 1}}{h} = f - \frac{2\ell E_{0r}}{h} \qquad \ell = 1, 2, 3, \ldots \qquad \textbf{9-28}$$

The frequencies for the transitions $\ell = \ell + 1$ are thus, $f + 2(E_{0r}/h)$, $f + 4(E_{0r}/h)$, $f + 6(E_{0r}/h)$, and so forth; those corresponding to the transition $\ell \to \ell - 1$ are $f - 2(E_{0r}/h)$, $f - 4(E_{0r}/h)$, $f - 6(E_{0r}/h)$, and so forth. We thus expect the absorption spectrum to contain frequencies equally spaced by $2E_{0r}/h$ except for a gap of $4E_{0r}/h$ at the vibrational frequency f, as shown in Figure 9-28. A measurement of the position of the gap gives f and a measurement of the spacing of the absorption peaks gives E_{0r}, which is inversely proportional to the moment of inertia of the molecule.

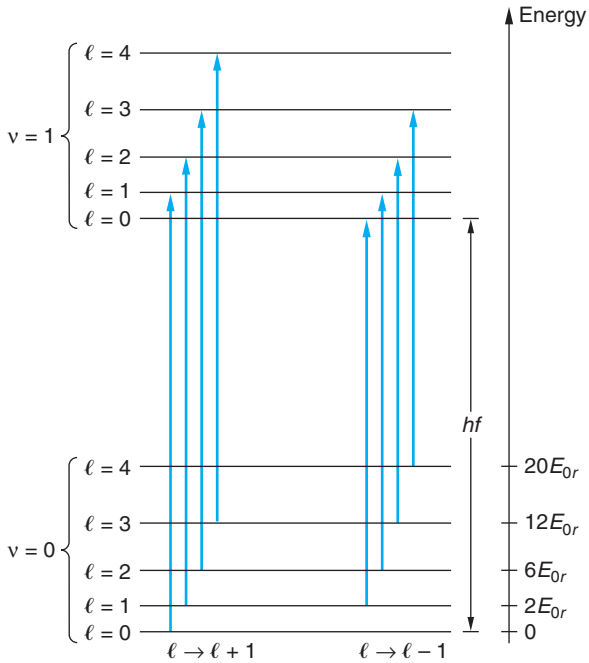

Figure 9-27 Absorptive transitions between the lowest vibrational states $v = 0$ and $v = 1$ in a diatomic molecule. These transitions obey the selection rule $\Delta\ell = \pm 1$ and fall into two bands. The energies of the $\ell \to \ell + 1$ band are $hf + 2E_{0r}$, $hf + 4E_{0r}$, $hf + 6E_{0r}$, and so forth, whereas the energies of the $\ell \to \ell - 1$ band are $hf - 2E_{0r}$, $hf - 4E_{0r}$, $hf - 6E_{0r}$, and so forth.

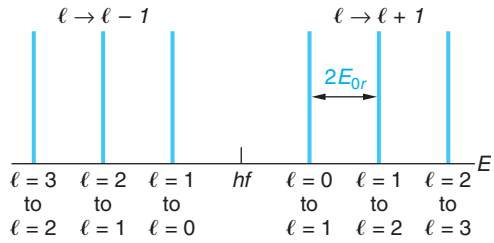

Figure 9-28 Expected absorption spectrum of a diatomic molecule. The right branch corresponds to the transitions $\ell \rightarrow \ell + 1$ and the left branch to the transitions $\ell \rightarrow \ell - 1$. The lines are equally spaced by $2E_{0r}$. The energy midway between the branches is hf, where f is the frequency of vibration of the molecule.

Figure 9-29 shows the absorption spectrum of HCl. The double-peak structure results from the fact that chlorine occurs naturally in two isotopes, ^{35}Cl and ^{37}Cl, which results in slightly different moments of inertia. If all of the rotational levels were equally populated initially, we would expect the intensities of each absorption line to be equal. However, the population $n(E_\ell)$ of a rotational level ℓ is proportional to the density of states $g(E_\ell)$, which equals the degeneracy of the level in this case, that is, the number of states with the same value of ℓ, which is $2\ell + 1$, and to the Boltzmann factor $e^{-E_\ell/kT}$,where E_ℓ is the energy of the state:

$$n(E_\ell) = g(E_\ell)e^{-E_\ell/kT} \qquad \textbf{9-29}$$

or

$$n(E_\ell) = (2\ell + 1)e^{-[\frac{1}{2}hf + \ell(\ell+1)E_{0r}]/kT} \qquad \textbf{9-30}$$

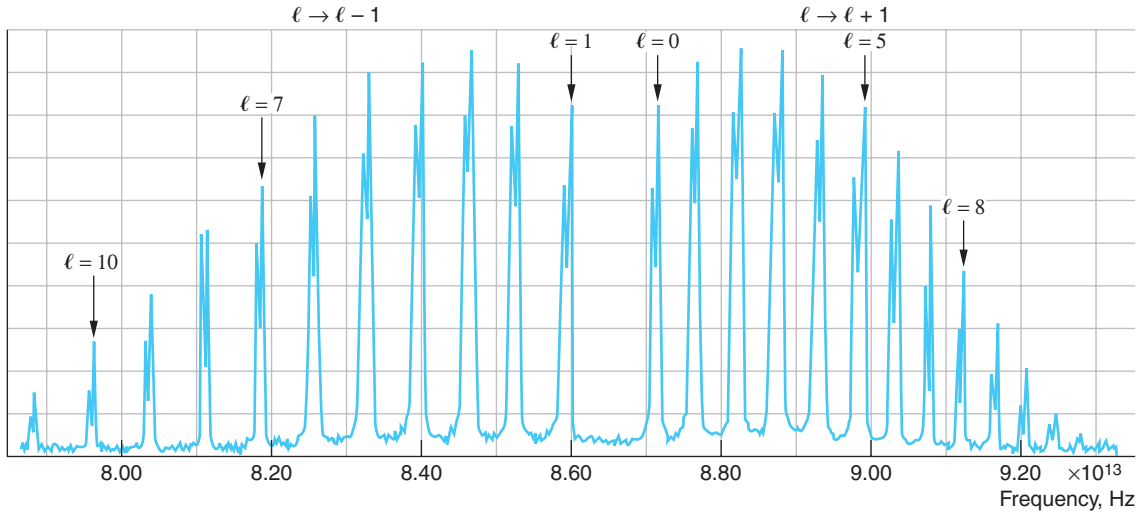

Figure 9-29 Absorption spectrum of the diatomic molecule HCl. The double-peak structure results from the two isotopes of chlorine, ^{35}Cl (abundance 75.5 percent) and ^{37}Cl (abundance 24.5 percent). The intensities of the peaks vary because the population of the initial state depends on ℓ.

FÈUE WHE

The $(2\ell + 1)$-fold degeneracy of the rotational state with angular momentum $\ell\hbar$ makes the thermal equilibrium population proportional to $(2\ell + 1) \exp [-\ell(\ell + 1)\hbar^2/2\, IkT]$. Therefore, the $\ell = 0$ state is usually not the most densely populated state at room temperature. For low values of ℓ, the population increases slightly because of the degeneracy factor, whereas for higher values of ℓ, the population decreases because of the Boltzmann factor. The intensities of the absorption lines therefore increase with ℓ for low values of ℓ and then decrease with ℓ for high values of ℓ, as can be seen from the figure. We can find out where the maximum population of the rotational states is located and hence which lines will be the most intense by differentiating Equation 9-30 with respect to ℓ and setting $dn/d\ell$ equal to zero. The result is

$$\ell_{\max} = \frac{1}{2}\left[\sqrt{\frac{4kT}{h^2/mr^2}} - 1\right] \qquad \textbf{9-31}$$

For a measurement made at room temperature, $kT = 0.026$ eV and thus $\ell_{\max} \approx 3$. This, too, can be seen in Figure 9-29.

Notice also in Figure 9-29 that the spacing between adjacent peaks, which we expected to be constant and equal to $2E_{0r}$ on the basis of our calculation above, is in fact not constant. The reason for this is our assumption that the moment of inertia of the molecule is constant. The rotation of the molecule tends to increase the separation of the atoms and hence increase the moment of inertia and decrease the rotational energy. As might be expected and the figure also shows, this effect becomes larger as ℓ increases.

As mentioned above, the gap in the spectrum in Figure 9-29 is due to the absence of a transition beginning on the $\ell = 0$ level in the $\ell \rightarrow \ell - 1$ group of peaks. The center of the gap is at the characteristic oscillation frequency f of the molecule given by Equation 9-21. From the figure we see that f for HCl is about 8.56×10^{13} Hz, or about 0.36 eV, corresponding to a force constant K of about 476 N/m. Table 9-7 lists the rotational and vibrational constants for several diatomic molecules. All diatomic

Table 9-7 Rotational and vibrational constants for selected diatomic molecules

Molecule	Equilibrium separation r_0 (nm)	Frequency f (Hz)	E_{0r} (eV)
H_2	0.074	1.32×10^{14}	7.56×10^{-3}
Li_2	0.267	1.05×10^{13}	8.39×10^{-5}
O_2	0.121	4.74×10^{13}	1.78×10^{-4}
LiH	0.160	4.22×10^{13}	9.27×10^{-4}
HCl^{35}	0.127	8.97×10^{13}	1.32×10^{-3}
$NaCl^{35}$	0.251	1.14×10^{13}	2.36×10^{-5}
KCl^{35}	0.279	8.40×10^{12}	1.43×10^{-5}
KBr^{79}	0.294	6.93×10^{12}	9.1×10^{-6}

Symmetric molecules such as H_2 or O_2 have no electric dipole moment. The vibration or rotation of these molecules does not involve a changing dipole moment, and there is no vibrational-rotational electric dipole absorption or radiation for these molecules.

molecules[9] have a gap at f in their vibration-rotation spectra; however, many polyatomic molecules have more complex vibrations and rotations, one result of which is that $\Delta\ell = 0$ may be allowed, i.e., vibrational energy may change without an accompanying rotational transition. In that event, a line will occur in the vibration-rotation spectrum at the frequency f. Such lines are given the rather enigmatic name of *Q branch*.[10]

9-5 Scattering, Absorption, and Stimulated Emission

Scattering

In the interactions between radiation incident on atomic or molecular systems, photons may also be scattered both elastically and inelastically. The process by which photons scatter elastically, i.e., without a change in their frequency, is called *elastic* or *Rayleigh scattering* since it was first described adequately by a classical scattering theory derived by Rayleigh in about 1900. Rayleigh scattering is illustrated in Figure 9-30*d*. In the classical theory, the oscillating electric field of the incident radiation produces an oscillating acceleration of the atomic electrons, causing them to radiate electromagnetic waves of the same frequency as and in phase with the incident wave. Thus, the electrons of the target atoms and molecules absorb energy from the incident wave and re-emit, or scatter it, in all directions without changing its frequency. The intensity of the scattered radiation is proportional to f^4. Rayleigh scattering is the origin of the unmodified line in our discussion of the Compton scattering of x rays in Section 3-4. (See Figure 3-17.) We saw there that if the incident wavelength λ_1 was large compared with the Compton shift $\lambda_2 — \lambda_1$, i.e., visible wavelengths or larger, then the scattered wave always included a wavelength equal to the incident wavelength to within experimental accuracy regardless of whether the electron mass or atomic mass is used in Equation 3-25. So as $\lambda \rightarrow \infty$, the quantum explanation of Chapter 3 and Rayleigh's classical explanation of elastic scattering agree. However, for incident wavelengths in the x-ray and gamma-ray regions of the spectrum, Compton scattering, shown in Figure 9-30*e*, becomes increasingly important for low-Z atoms whose electron binding energies are not large. In the gamma-ray region as $\lambda \rightarrow 0$, the photon energy becomes so large that even the most tightly bound electrons are freed in the process and Compton effect becomes the dominant process.

The incident and scattered photons are also correlated in the *inelastic* scattering process illustrated in Figure 9-30*f*. Such scattering of light from molecules was first observed by physicist C. V. Raman[11] and is known as *Raman scattering*, or sometimes as the *Raman effect*. The scattered photon may have less energy than the incident photon or it may have greater energy if the molecule is initially in an excited vibrational or rotational energy state. Both possibilities are illustrated in Figure 9-30*f*. Thus, the scattered frequency is not the same as the incident frequency, nor is it related to a characteristic frequency of the molecule. It is found that for incident monochromatic radiation of frequency f the scattered radiation contains not only the frequency f (Rayleigh scattering; see Figure 9-31), but also much weaker lines on either side of the Rayleigh line, with frequencies given by

$$f' = f \pm \Delta f \qquad \textbf{9-32}$$

These are the Raman lines illustrated in Figure 9-31. If the incident frequency is varied, the Raman lines are observed to move along the frequency axis at the same rate so that the *difference* Δf between f and f' remains constant. It is this difference Δf that corresponds to characteristic transitions of the scattering molecule.

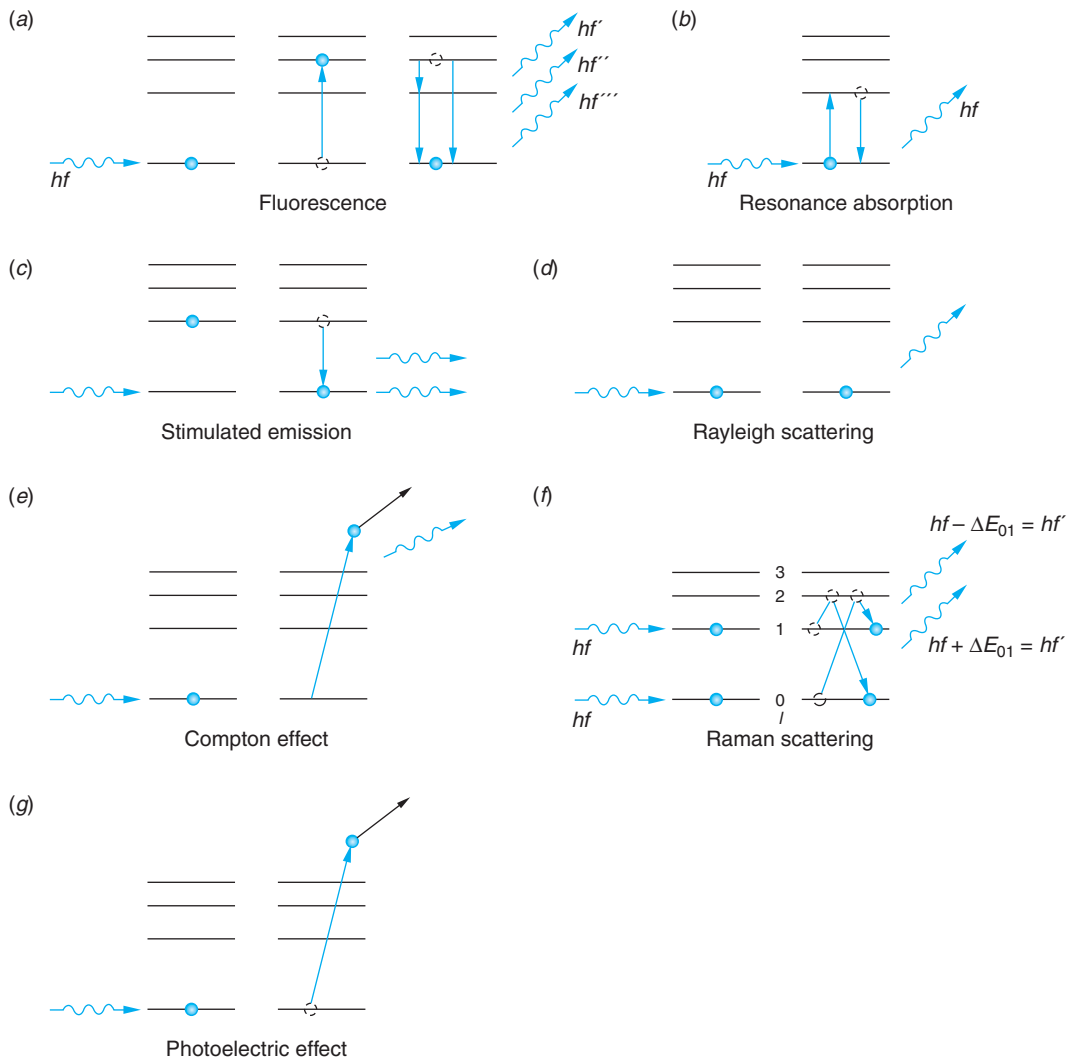

Figure 9-30 Description of photon interactions with an atom. (*a*) The photon is absorbed and the atom, in an excited state, later emits one or more photons as it decays to a state of lower energy. This is a two-step process called *fluorescence*, and the emitted photons are uncorrelated with the incident photon. (*b*) If the energy of the incident photon matches one of the excitation energies of the atom, resonance radiation results. (*c*) The atom, in an excited state, is stimulated to make a transition to a lower state by an incident photon of just the right energy. The emitted and incident photons have the same energy and are coherent. The Rayleigh scattering process (*d*) and Raman scattering (*f*) differ from (*a*) and (*b*) in that they are single-step processes and there is a correlation between the incident and emitted photons. Parts (*e*) and (*g*) illustrate Compton scattering and the photoelectric effect discussed in Chapter 3.

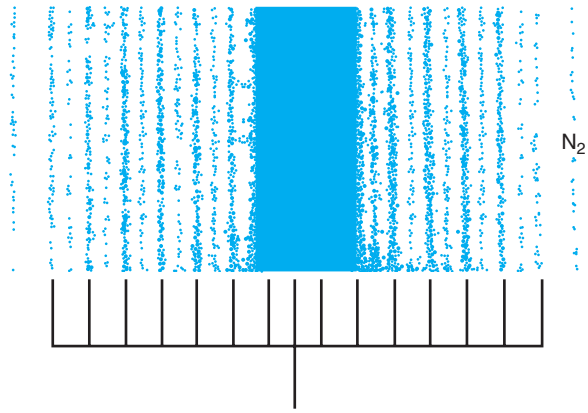

Figure 9-31 The rotational Raman spectrum of N_2. The alternating intensities, determined by the nuclear spins, are in the ratio of 1/2, corresponding with the $I = 1$ spin of the nitrogen nucleus. The dark central area is the result of the much more intense Rayleigh-scattered portion of the incident wave. [*R. Eisberg and R. Resnick, Quantum Physics, 2d ed. (New York: Wiley, 1985), p. 436.*]

Although the measurements of Δf for each line in the Raman spectrum makes possible construction of the rotational levels for a given molecule,[12] its quantum-mechanical explanation is different from that of the rotational spectrum. In particular, the selection rule for the rotational quantum number in the Raman effect is $\Delta\ell = 0, \pm 2$. The $\Delta\ell = 0$ value yields Rayleigh scattering, while $\Delta\ell = \pm 2$ yields the Raman lines. One can see how this comes about physically by studying the transitions shown in Figure 9-30*f*. An electron initially in the $\ell = 0$ state absorbs energy $\Delta E_{01} + \Delta E_{12}$ from the incident photon of frequency f and emits energy ΔE_{12}. Thus, the energy of the scattered photon is

$$hf' = hf - (\Delta E_{01} + \Delta E_{12}) + \Delta E_{12} = hf - \Delta E_{01} \qquad \textbf{9-33}$$

or

$$f' = f - \Delta f$$

where $\Delta f = \Delta E_{01}/h$. If the electron is initially in the $\ell = 1$ state, then it absorbs ΔE_{12} from the incident photon and emits $\Delta E_{12} + \Delta E_{01}$. Thus, the scattered photon has energy

$$hf' = hf - \Delta E_{12} + (\Delta E_{12} + \Delta E_{01}) = hf + \Delta E_{01} \qquad \textbf{9-34}$$

or

$$f' = f + \Delta f$$

Many Raman spectra have been studied. They provide a valuable source of information regarding molecular quantum states, including, as was pointed out earlier, the structure of the rotational levels for homonuclear diatomic molecules. For example, the detailed understanding of the complex vibrations and rotations of the ammonia molecule referred to in Section 6-6 that enabled the development of the first atomic clocks was made possible by studies of the Raman rotational-vibrational spectrum of the NH_3 molecule, the so-called *ammonia inversion spectrum*. Finally, Figure 9-30*g* illustrates the photoelectric effect, the final example of the interaction of radiation with matter, in which the absorption of the photon ionizes the atom or molecule. Like Compton scattering, this effect was discussed in Chapter 3 and will not be considered further here.

Absorption

Information about the energy levels of an atom or molecule is usually obtained from the radiation emitted when the atom or molecule makes a transition from an excited state to a state of lower energy. As mentioned in Section 9-4, we can also obtain information about such energy levels from the absorption spectrum. When atoms and molecules are irradiated with a continuous spectrum of radiation, the transmitted radiation shows dark lines corresponding to absorption of light at discrete wavelengths. Absorption spectra of atoms were the first line spectra observed. Fraunhofer in 1817 labeled the most prominent absorption lines in the spectrum of sunlight; it is for this reason that the two intense yellow lines in the spectrum of sodium are called the *Fraunhofer D lines*. Since at normal temperatures atoms and molecules are in their ground states or in low-lying excited states, the absorption spectra are usually simpler than the emission spectra. For example, only those lines corresponding to the Lyman emission series are seen in the absorption spectrum of atomic hydrogen because nearly all the atoms are originally in their ground states. In the Chapter 6 MORE section "Transitions Between Energy States," we described how transitions between quantum states in an atomic system occur as a result of interaction with oscillating electromagnetic fields. In particular, if the frequency greater than f_{12} is present in radiation incident on an atom whose ground-state and an excited-state energies are respectively E_1 and E_2, then there is a probability that the atom will undergo a transition from the lower energy state E_1, absorbing the energy $hf_{12} = E_2 - E_1$ from the radiation. This absorption of energy resulting from the interaction between the electric field of the radiation oscillating at f_{12} and the charge on the atomic electrons was first described quantum mechanically by Einstein, who expressed the probability of absorption per atom per unit time as $B_{12}u(f)$, where $u(f)$ is the energy density of the radiation per unit frequency and B_{12} is Einstein's coefficient of absorption.

In addition to absorption, several other interesting phenomena occur when electromagnetic radiation—i.e., photons—is incident on atoms or molecules. These are illustrated in Figure 9-30. In Figure 9-30*a* a photon of energy hf is absorbed and the system makes a transition to the excited state. Later, the system makes a transition to a lower state and/or back to the ground state with the *spontaneous emission* of one or more photons via the mechanism described on the home page in the Chapter 6 MORE section "Transitions Between Energy States." The radiation thus emitted is called *fluorescence*. If state 2 happens to be the first excited state, then this two-step process is called *resonance absorption* and the photon emitted is called *resonance radiation*, as shown in Figure 9-30*b*. As a result of motions that occur while the system is in state 2, there is no correlation in direction or phase between the incident and emitted photons. While in state 2 the system has definite probabilities of making spontaneous transitions to each of the lower states as determined by the probability density given by Equation 6-52*d* in the MORE section. For example, the probability per atom per unit time of returning to state 1 with the spontaneous emission of a photon can be expressed by the quantity A_{21} (transitions per unit time). Notice that the reciprocal $1/A_{21}$ has the units of time per transition; i.e., it is a measure of how long the system stays in state 2 before returning to state 1. This is t_s, the mean lifetime of the state, defined as $t_s = 1/A_{21}$. For most atomic (electric dipole) transitions this characteristic lifetime is of the order of 10^{-8} s. A_{21} is called Einstein's coefficient of spontaneous emission.

Stimulated Emission

In addition to the spontaneous emission of fluorescent and resonant radiation with probability A_{21}, which is independent of the energy density $u(f)$ of the incident radiation, emission can also be induced to occur by the oscillating electromagnetic field of the incident radiation. Called *stimulated emission*, its probability does depend upon $u(f)$. This phenomenon, like absorption and spontaneous emission, was first analyzed by Einstein, in 1917. The probability of stimulated emission per atom per unit time (transition rate) can be written as $B_{21}u(f)$, where B_{21} is called Einstein's coefficient of stimulated emission. In this process the electric field of an incident photon with energy hf equal to the energy difference $E_2 - E_1$ in Figure 9-30*c* stimulates the atom or molecule in state 2 to emit a photon with energy $E_2 - E_1 = hf$, which is propagated in the same direction and with the same phase as the incident photon. Such photons (or radiation) are said to be *coherent*.

The relation between the three Einstein coefficients can be found as follows. Consider a system of atoms and radiation in thermal equilibrium at temperature T. Let N_1 and N_2 be the number of atoms occupying the states with energies E_1 and E_2. The ratio N_2/N_1 is determined by the Boltzmann factor, given by Equation 8-2, assuming the two states have the same degeneracy:

$$\frac{N_2}{N_1} = e^{-(E_2 - E_1)/kT} = e^{-hf/kT} \tag{9-35}$$

This ratio represents a dynamic equilibrium in which the number of absorption transitions ($E_1 \rightarrow E_2$) per unit time equals the sum of the number of spontaneous and stimulated emissions ($E_2 \rightarrow E_1$) per unit time. Since the number of atoms making a transition (of any type) is proportional to the population of the state on which the transition begins and to the probability, we can express the dynamic equilibrium as

$$N_1 B_{12} u(f) = N_2(A_{21} + B_{21}u(f)) \tag{9-36}$$

Solving Equation 9-36 for the energy density $u(f)$ of the radiation yields

$$u(f) = \frac{\dfrac{A_{21}}{B_{21}}}{\dfrac{N_1}{N_2}\dfrac{B_{12}}{B_{21}} - 1} \tag{9-37}$$

Inserting N_1/N_2 from Equation 9-35, we have that

$$u(f) = \frac{\dfrac{A_{21}}{B_{21}}}{\dfrac{B_{12}}{B_{21}}e^{hf/kT} - 1} \tag{9-38}$$

This expression for the energy density of radiation of frequency f in thermal equilibrium at temperature T with atoms of energies E_1 and E_2 must be consistent with Planck's law for a blackbody spectrum at temperature T given by Equation 8-57:

$$u(f) = \frac{8\pi h f^3}{c^3}\left(\frac{1}{e^{hf/kT} - 1}\right) \tag{9-39}$$

FEUE WHE

Comparing Equation 9-38 and 9-39, we conclude that

$$\frac{B_{12}}{B_{21}} = 1 \qquad \textbf{9-40}$$

and that

$$\frac{A_{21}}{B_{21}} = \frac{8\pi hf^3}{c^3} \qquad \textbf{9-41}$$

Although this analysis gives us only the ratios of the coefficients, A_{21} can be computed from quantum mechanics, as was discussed in the home page MORE section "Transitions Between Energy States" in Chapter 6, and the other coefficients may then be computed from the result.

There are several points of interest in these equations. For instance, Equation 9-40 tells us that the coefficients for absorption and stimulated emission are the same for the same pair of states. Notice, too, that Equation 9-41 says that the ratio of the spontaneous emission coefficient to that for stimulated emission is proportional to f^3. This means that the larger $\Delta E = E_2 - E_1$, the more likely spontaneous emission will be comparable to stimulated emission. Rewriting Equation 9-39 as

$$\frac{A_{21}}{B_{21}u(f)} = e^{hf/kT} - 1 \qquad \textbf{9-42}$$

yields the result that, in equilibrium situations, spontaneous emission is far more probable than stimulated emission for $hf \gg kT$. Since this is usually the case for electronic transitions in both atoms and molecules, de-excitation of excited electronic states by stimulated emission is normally ignored in these transitions. Stimulated emission does become important when $hf \approx kT$ and may dominate de-excitation of excited states when $hf \ll kT$. This latter condition exists for ordinary temperatures in the microwave region of the spectrum. We will return to these matters in Section 9-6 in connection with the discussion of lasers and masers.

EXAMPLE 9-7 Spontaneous versus Stimulated Emission Compare the relative probabilities of spontaneous and stimulated emission in an equilibrium system at room temperature ($T = 300$ K) for transitions that occur in (*a*) the visible and (*b*) the microwave regions of the spectrum.

SOLUTION

Equation 9-42 gives the ratio of the probability for spontaneous emission A_{21} to that for stimulated emission $B_{21}u(f)$. At $T = 300$ K, $kT = 0.026$ eV.

(*a*) In the visible region of the spectrum, $hf \approx 2$ eV, so $hf/kT = 2/0.026 = 77$. Therefore,

$$\frac{A_{21}}{B_{21}u(f)} = e^{77} - 1$$

Clearly, under these conditions spontaneous emission is favored over stimulated emission by an enormous factor.

(*b*) In the microwave region of the spectrum, $hf \approx 10^{-4}$ eV, so $hf/kT = 10^{-4}/0.026 = 0.0038 \approx 1/260$ and stimulated emission is rather heavily favored.

FEUE WHE

Questions

5. How does Rayleigh scattering differ from resonance absorption?
6. How does the photoelectric effect differ from all the other processes illustrated in Figure 9-30?
7. Why is stimulated emission usually not observed?

9-6 Lasers and Masers

The *laser* (*l*ight *a*mplification by *s*timulated *e*mission of *r*adiation) is a device that produces a strong beam of coherent photons by stimulated emission. The *maser*, where *m*icrowave replaces *l*ight in the definition from which the acronym is formed, was the laser's predecessor. Both devices depend on stimulated emission for their operation. We will discuss it more fully here because of its application to these important devices. Stimulated emission occurs if the atom is initially in an excited state and if the energy of the photon incident on the atom is just $E_2 - E_1$, where E_2 is the excited energy of the atom and E_1 is the energy of a lower state or the ground state. In this case, the oscillating electromagnetic field of the incident photon accelerates the electron(s) at a rate that matches the photon's frequency and thus, we say, stimulates the excited atom, which may then emit a photon in the same direction as the incident photon and with the same phase. We have seen that the relative probabilities of stimulated emission and absorption B_{21} and B_{12} are equal (Equation 9-40). Ordinarily, at normal temperatures, nearly all atoms will initially be in the ground state, so absorption will be the main effect. That is, $N_1 \gg N_2$, so

$$N_1 u(f) B_{12} \gg N_2 u(f) B_{21}$$

where N_1 and N_2 are the populations of the two states. To produce more stimulated emission transitions than absorption transitions, we must arrange to have more atoms in the excited state than in the ground state ($N_2 > N_1$). This condition is called *population inversion*. It can be achieved if the excited state E_2 is a metastable state. Once population inversion is achieved, any light emitted by a spontaneous $E_2 \rightarrow E_1$ transition is amplified by stimulated emission from the excited atoms that it encounters. Population inversion is often obtained by a method called *optical pumping*, in which atoms are "pumped" up to energy levels greater than E_2 by the absorption of an intense auxiliary radiation. The atoms then decay down to the metastable state E_2 by either spontaneous emission or by nonradiative transitions such as those due to collisions.

The maser was the first of these devices to be constructed, an accomplishment of Charles Townes and his co-workers in 1953. Currently, the most important type of maser is the hydrogen maser, which is used as an atomic-frequency standard, one type of atomic clock. The hydrogen transition used in these masers is that between the hyperfine levels of the ground state, the same transition used to map hydrogen clouds in interstellar space (see Chapter 13). This transition between the $\Psi_{100+\frac{1}{2}}$ and $\Psi_{100-\frac{1}{2}}$ states is shown in Figure 9-32*a*. Townes shared the 1964 Nobel Prize in Physics for his contributions to the development of masers and lasers.

FEUE WHE

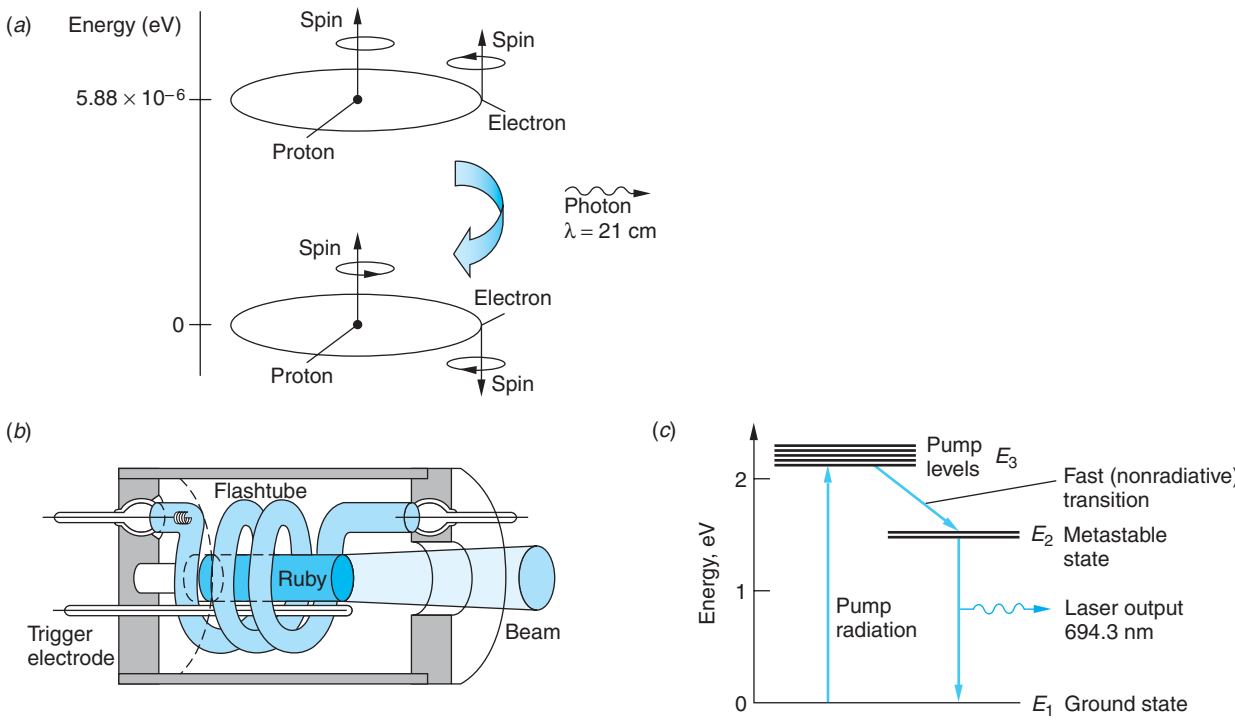

Figure 9-32 (*a*) Hyperfine levels used in the hydrogen maser. (*b*) Schematic diagram of the first ruby laser. (*c*) Energy levels of chromium in ruby, Al_2O_3.

The Ruby Laser

Figure 9-32*b* shows a schematic diagram of the first laser, a ruby laser built by Theodore Maiman in 1960.[13] It consists of a small rod of ruby (a few centimeters long) surrounded by a helical gaseous flashtube. The ends of the ruby rod are flat and perpendicular to the axis of the rod. Ruby is a transparent crystal of Al_2O_3 containing a small amount (about 0.05 percent) of chromium. It appears red because the chromium ions (Cr^{3+}) have strong absorption bands in the blue and green regions of the visible spectrum. The energy levels of chromium that are important for the operation of a ruby laser are shown in Figure 9-32*c*.

When the mercury- or xenon-filled flashtube is fired, there is an intense burst of light lasting a few milliseconds. Absorption excites many of the chromium ions to the bands of energy levels called *pump levels* in Figure 9-32*c*. The excited chromium ions give up their energy to the crystal in nonradiative transitions and drop down to a pair of metastable states labeled E_2 in the figure. These metastable states are about 1.79 eV above the ground state. If the flash is intense enough, more atoms will make the transition to the states E_2 than remain in the ground state. As a result, the populations of the ground state and the metastable states become inverted. When some of the atoms in the states E_2 decay to the ground state by spontaneous emission, they emit photons of energy 1.79 eV and wavelength 694.3 nm. Some of these photons then stimulate other excited atoms to emit photons of the same energy and wavelength, moving in the same direction with the same phase.

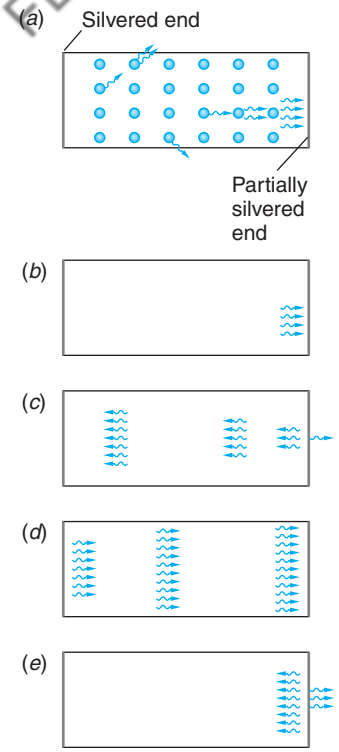

Figure 9-34 Buildup of photon beam in a laser. (*a*) Some of the atoms spontaneously emit photons, some of which travel to the right and stimulate other atoms to emit photons parallel to the axis of the crystal. The others are absorbed, transmitted through the walls, or otherwise lost to the lasing process. (*b*) Four photons strike the partially silvered right face of the laser. (*c*) One photon has been transmitted and the others have been reflected. As these photons traverse the laser crystal, they stimulate other excited atoms to emit photons and the beam intensity increases. By the time the beam reaches the right face again (*d*), it comprises many photons. (*e*) Some of these photons are transmitted to become part of the external laser beam and the rest are reflected to sustain the process.

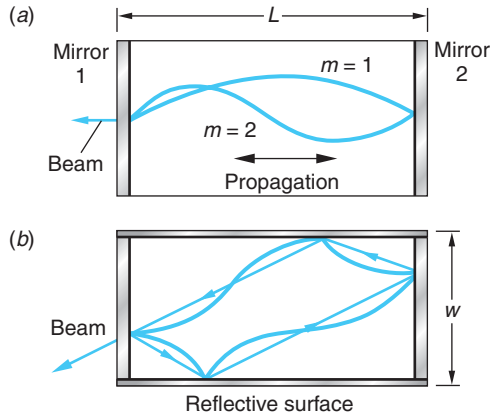

Figure 9-33 Laser as a resonating optical cavity. If mirror 1 is the partially reflecting end, then (*a*) illustrates the longitudinal standing-wave modes, for which $L = m\lambda/2$, where λ is the laser wavelength and m is integral. If the sides of the cavity are also reflective, as in (*b*), then standing-wave modes transverse to the long axis are also possible. Notice that the exit beam for these modes is not parallel to the long axis of the laser.

The ruby laser, like other conventional lasers, acts as a resonating optical cavity. In the ruby laser, both ends of the crystal are silvered such that one end is almost totally reflecting (about 99.9 percent) and the other end is only partially reflecting (about 99 percent) so that some of the beam is transmitted through that slightly transparent end. If the ends are parallel, standing waves are set up, as shown in Figure 9-33, and an intense beam of coherent light emerges through the partially silvered end. Figure 9-34 illustrates the buildup of the beam inside the laser. When photons traveling parallel to the axis of the crystal strike the silvered ends, all are reflected from the back face and most are reflected from the front face, with a few escaping through the partially silvered front face. During each pass through the crystal, the photons stimulate more and more atoms so that an intense photon beam is developed.

Modern ruby lasers generate intense light beams with energies ranging from 50 J to 100 J in pulses lasting a few milliseconds. This pulse length is approximately equal to that of the flash tube, whose output excites atoms into the pump levels shown in Figure 9-32*c*. The output of the laser during that time is actually a series of very short pulses, each of the order of a microsecond long, as illustrated in Figure 9-35. This is because the pump levels depopulate quickly compared to the pump rate. Therefore, the flash requires some time to reestablish the population inversion that generates the next short pulse.

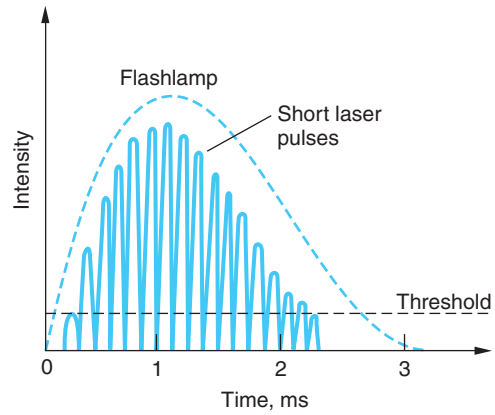

Figure 9-35 A single output pulse from a ruby laser. The pulse actually consists of a series of very short pulses each about 1 μs long. Flashlamp intensities below the threshold do not produce a sufficient population inversion to initiate lasing. Not shown is a weak background of incoherent spontaneous emission that accompanies the coherent laser light.

FÈUE WHE

Notice in Figure 9-35 that the first of the very brief laser pulses, or "spikes," begins very soon after the population inversion $N_2 > N_1$ occurs and ends when N_2 falls back to N_1 due to stimulated emissions. Extremely intense spikes can be generated via a technique called *Q-switching*, whereby the resonating property of the cavity is temporarily destroyed in order to sharply reduce the stimulated emissions so as to allow the pumping radiation to make $N_2 \ggg N_1$. The resonant status is then suddenly restored and an extremely intense laser pulse results. This is how the very high-energy pulses mentioned above are typically produced. The Q in *Q-switching* refers to the cavity's *quality factor*, or its ability to maintain the intensity of the reverberating wave. If the end mirrors are low loss and the medium very transparent to the laser frequency, then the wave will die out slowly and the cavity is of high quality, or high Q. If Q is low, then substantial light is lost in each pass and the wave will die out quickly. If Q is too low, lasing will not occur at all. Q can be made very low, for example, by replacing the totally reflecting end mirror with an external one of equal reflectivity that rotates. When the rotating mirror is not parallel to the one on the other end of the cavity, Q is very low and little stimulated emission occurs as the pumping flash builds the population of state E_2 so that $N_2 \ggg N_1$. When the rotating mirror becomes parallel to the other, Q suddenly becomes very high (hence the name Q-switch) and the extremely intense laser pulse is generated as E_2 depopulates.

Sustaining laser action requires that the increase in the number of coherent photons produced by stimulated emission per round trip through the resonating cavity to be greater than or equal to the decrease resulting from all losses, such as transmission through the partially reflecting end mirror and scattering. Although its a bit difficult, we have information to calculate the population inversion density necessary for lasing with the aid of the Einstein coefficients from Section 9-5, so let's try it. To begin, let's combine all of the various ways by which photons may be lost into a single characteristic time t_p. That is, the intensity of radiation I of a particular frequency f in the resonant cavity will decay due to the losses according to

$$I = I_0 e^{-t/t_p} \tag{9-43}$$

where I_0 is the intensity at $t = 0$. Thus, the rate at which intensity is lost is given by

$$\left(\frac{dI}{dt}\right)_{\text{loss}} = -\frac{I_0}{t_p} e^{-t/t_p} = -\frac{I}{t_p} \tag{9-44}$$

The net rate at which the intensity of the frequency f gains due to the difference between the gain from stimulated emissions $E_2 \rightarrow E_1$ and the offsetting loss from absorptions $E_1 \rightarrow E_2$ is equal to the difference in the populations $(N_2 - N_1)$ times the intensity per photon times the transition probability $u(f)B_{21}$. The transition probability $u(f)B_{21}$ must be corrected for the width Δf of the spectral line emitted in the $E_2 \rightarrow E_1$ transition arising from the finite width of the level E_2, as described in Chapter 5.[14] The correction is a multiplicative factor approximately equal to $2/\pi\Delta f$. Taking these together, we obtain

$$\left(\frac{dI}{dt}\right)_{\text{gain}} = (N_2 - N_1)\frac{hfc}{V}\frac{2}{\pi\Delta f}u(f)B_{21} \tag{9-45}$$

where V is the volume of the resonant cavity and hfc/V is the intensity per photon.

Using Equation 9-38 and the fact that A_{21} is the reciprocal of the lifetime for spontaneous emission t_s, Equation 9-45 can be written as

$$\left(\frac{dI}{dt}\right)_{\text{gain}} = \frac{(N_2 - N_1)}{V}(hfc)\left[\frac{u(f)c^3}{4\pi^2 hf^3 \Delta f\, t_s}\right] \qquad \textbf{9-46}$$

or

$$\left(\frac{dI}{dt}\right)_{\text{gain}} = (n_2 - n_1)\frac{c^3 I}{4\pi^2 f^2 \Delta f\, t_s} \qquad \textbf{9-47}$$

where $n_2 = N_2/V$ and $n_1 = N_1/V$ are the *population densities* of the states and $cu(f) = I$, the intensity.[15] If the density of states (degeneracies) $g(E)$ of E_2 and E_1 are not equal, then Equation 9-47 must be modified to

$$\left(\frac{dI}{dt}\right)_{\text{gain}} = \left[n_2 - n_1\left(\frac{g(E_2)}{g(E_1)}\right)\right]\frac{c^3 I}{4\pi^2 f^2 \Delta f\, t_s} \qquad \textbf{9-48}$$

Thus, the condition for laser action becomes

$$\left(\frac{dI}{dt}\right)_{\text{gain}} \geq \left(\frac{dI}{dt}\right)_{\text{loss}} \qquad \textbf{9-49}$$

or

$$\left[n_2 - n_1\left(\frac{g(E_2)}{g(E_1)}\right)\right]\frac{c^3 I}{4\pi^2 f^2 \Delta f\, t_s} \geq \frac{I}{t_p} \qquad \textbf{9-50}$$

The equal sign provides the threshold condition for the initiation of lasing. The greater-than sign represents sustained laser action. Solving the threshold condition yields the *critical population inversion density* Δn_c:

$$\Delta n_c = \frac{4\pi^2 f^2 \Delta f\, t_s}{c^3 t_p} \qquad \textbf{9-51}$$

where

$$n_2 - n_1\left(\frac{g(E_2)}{g(E_1)}\right) = \Delta n_c$$

Equation 9-51 describes the population inversion that must be established if laser action is to be achieved for a given frequency and spontaneous emission lifetime. It also points out that the only property of the cavity that affects Δn_c is its characteristic decay lifetime t_p.

The ruby laser is an example of a three-level laser, referring to the energy levels in Figure 9-32*c*. Such lasers have a practical disadvantage for many applications in that more than half of the atoms must be pumped from $E_1 \rightarrow E_3$ in order to obtain the necessary population inversion between levels E_2 and E_1. In addition, the source of the excitation energy, the flashlamp, produces light over a broad range of frequencies, most of which do not contribute to exciting the level E_3 and are thus wasted. The large pumping requirement and relatively low excitation efficiency mean that substantial energy must be dissipated as heat, so three-level solid-state lasers such as the ruby laser must be pulsed in order to allow the system time to cool periodically. A more advantageous

system is one that does not require such a large fraction of the atoms to be excited at any one time and avoids the excess heat produced by optical pumping. Such lasers provide continuous output and are called *continuous wave*, or *cw*, lasers.

Helium-Neon Lasers

In 1961, the first successful operation of a cw laser, a continuous helium-neon gas laser, was announced by Ali Javan, W. R. Bennet, Jr., and D. R. Herriott.[16] Figure 9-36 shows a schematic diagram of the type of helium-neon laser commonly used for physics demonstrations and laser pointers and by land surveyors and carpenters. It consists of a gas tube containing 15 percent helium gas and 85 percent neon gas. A totally reflecting flat mirror is mounted on one end of the gas tube and a partially reflecting concave mirror is placed at the other end. The concave mirror focuses parallel light at the flat mirror and also acts as a lens that transmits part of the light so that it emerges as a parallel beam.

Population inversion is achieved somewhat differently in the helium-neon laser than in the ruby laser. Figure 9-37 shows the energy levels of helium and neon that are important for operation of the laser. (The complete energy-level diagrams for helium and neon are considerably more complicated.) Helium has excited states, the 2^3S and 2^1S levels that lie 19.72 eV and 20.61 eV, respectively, above the 1^1S ground state. Both are metastable because of the $\Delta\ell = \pm 1$ selection rule, the 2^3S level being more strongly forbidden due to the $\Delta S = 0$ selection rule, discussed in the Chapter 7 home page MORE section "Multielectron Atoms," that prohibits intercombination lines. Helium atoms are excited to these states by an electrical discharge. Neon has closely spaced groups of excited states at 19.83 eV and 20.66 eV above its ground state—the energies of these neon states almost exactly match the excited states of helium. The neon atoms are excited to these levels by collisions with excited helium atoms. The kinetic energy of the helium atoms provides the extra energy, about 0.05 eV, needed to excite the neon atoms. There is another excited state of neon that is 18.70 eV above its ground state and 1.96 eV below the 20.66 eV state. Since this state is normally unoccupied, population inversion between these states is obtained immediately. The stimulated emission that occurs between these states results in photons of energy 1.96 eV and wavelength 632.8 nm, which produces a bright red light. After stimulated emission, the atoms in the 18.70 eV state decay to the ground state by spontaneous emission of a photon with a wavelength of about 600 nm followed by a nonradiative de-excitation, typically collision with the cavity wall. The collisions are an important part of the laser process since if the diameter of the tube (see Figure 9-36) is too large, the probability of collision with the wall decreases and the 600-nm radiation may re-excite the 18.70 eV level. This reduces the population inversion and decreases the laser gain. Stimulated emission also occurs from the state at 19.83 eV to the 18.70 eV level, producing laser light with a wavelength of 1100 nm (infrared).

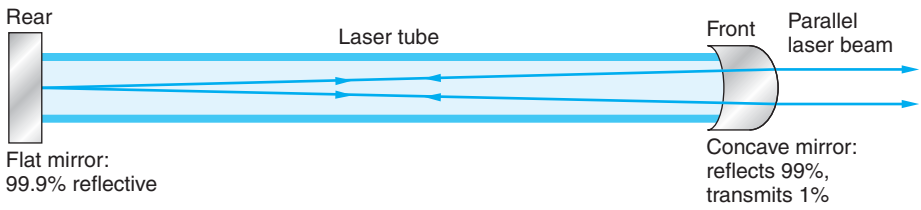

Figure 9-36 Schematic drawing of a helium-neon laser. The use of a concave mirror rather than a second plane mirror makes the alignment of the mirrors less critical than it is for the ruby laser. The concave mirror on the right also serves as a lens that focuses the emitted light into a parallel beam.

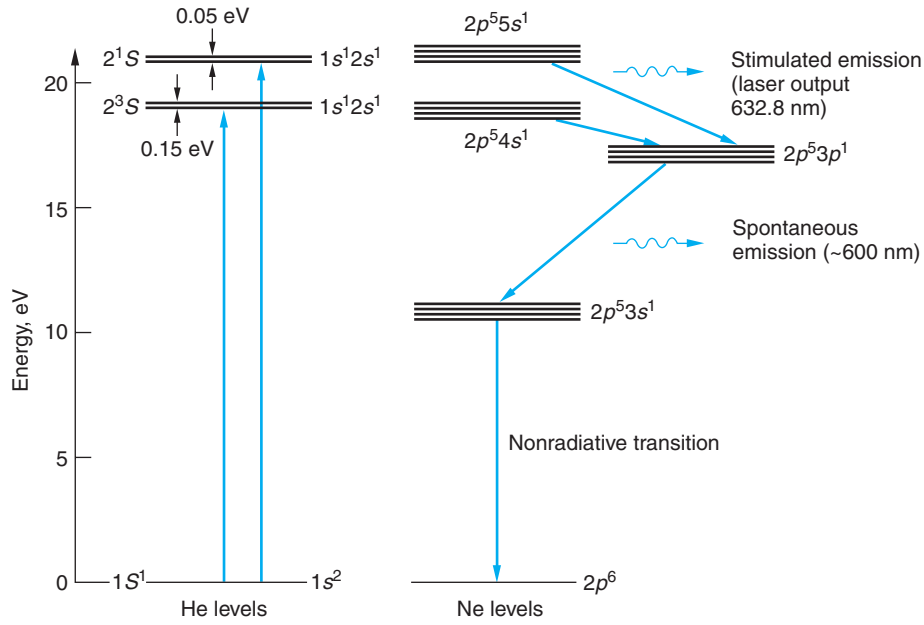

Figure 9-37 Energy levels of helium and neon that are important for the helium-neon laser. The helium atoms are excited by electrical discharge to energy states 19.72 eV and 20.61 eV above the ground state. They collide with neon atoms, exciting some neon atoms to energy states 19.83 eV and 20.66 eV above the ground state. Population inversion is thus achieved between these levels and one at 18.70 eV above the ground state. The spontaneous emission of photons of energy 1.96 eV from the upper state stimulates other atoms in the upper state to emit photons of energy 1.96 eV, producing the characteristic He-Ne red laser light. Emission from the 19.83 eV neon state to the 18.70 eV level also produces laser output at about 1100 nm.

Helium-neon lasers have recently been developed that lase at a number of other visible and infrared wavelengths. The several possible laser wavelengths are not present simultaneously since each device is designed to operate at a particular wavelength.

Note that there are four energy levels involved in producing the 632.8-nm helium-neon laser line, whereas the ruby laser involved only three levels. In a three-level laser, population inversion is difficult to achieve because more than half the atoms in the ground state must be excited, i.e., $N_2 > N_1/2$ in Equation 9-46. In a four-level laser, population inversion is easily achieved because the state after stimulated emission is not the ground state but an excited state that is normally unpopulated, so that $N_1 \approx 0$.

New Lasers and Applications

A laser beam is coherent, very narrow, and intense. Its coherence makes the laser beam useful in the production of holograms, such as those used on credit cards and "heads-up" displays; i.e., transparent data displays that don't obstruct the user's view. The precise direction and small angular spread of the beam make it useful as a surgical tool for destroying cancer cells or reattaching a detached retina. Lasers are also used by land surveyors and carpenters to ensure precise alignment over large distances. Distances can be accurately measured by reflecting a laser pulse from a mirror and measuring the time the pulse takes to travel to the mirror and back. The distance to the Moon is currently measured to within a few millimeters using corner reflectors placed on the Moon by Apollo astronauts for that purpose. Laser beams are also used in fusion research.

FEUE WHE

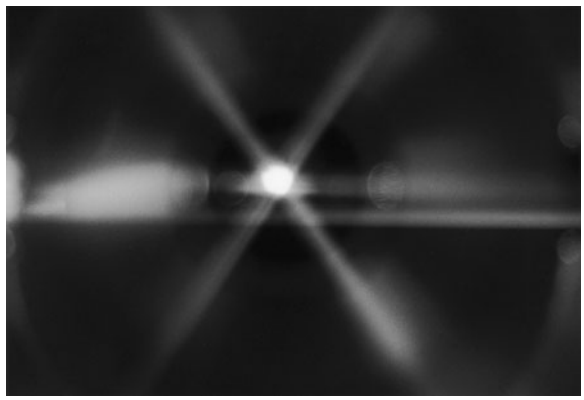

Three counterpropagating pairs of orthogonal laser beams illuminate about 100 million sodium atoms at their intersection. The pressure of the laser light cools the atoms, slowing them to rms velocities comparable to those resulting from recoil due to emission or absorption of a single photon. Systems incorporating laser cooling of sodium atoms have achieved a record low temperature of 450 pK. [*National Institute of Science and Technology.*]

An intense laser pulse is focused on tiny pellets of deuterium-tritium in a combustion chamber. The beam heats the pellets to temperatures of the order of 10^8 K in a very short time, causing the deuterium and tritium to fuse and release energy. (See Section 11-8.) At the other end of the temperature scale, using advanced cooling techniques that included the focusing of three orthogonal pairs of lasers (optical tweezers) on a sample containing 2500 cesium atoms, in 2003 W. Ketterle and his group achieved a record low temperature of 450 pK.[17] (See the photo above.) Orthogonal pairs of laser beams, called *optical traps*, capable of cooling samples containing millions of atoms down to the submicrokelvin range, are used in creating Bose-Einstein condensates and the degenerate Fermi gas, discussed in Chapter 8, and antihydrogen atoms, described in Chapter 12.

While cw lasers are the lasers of choice for many applications, many others require pulsed lasers, particularly those where very high power levels are important or even essential. For these applications the current state of the art is *chirped pulse amplification*. With this technique, invented in the 1980s by Gérhard Mourou, an input ultrashort pulse is stretched out (in time) by dispersing the wavelengths (frequencies) of the pulse with a suitable arrangement of gratings or prisms together with mirrors. After passing through the optical stretcher, the pulse duration is up to 10^5 times longer than the original pulse and the intensity has been correspondingly lowered as a result to avoid nonlinear effects that would damage or destroy the amplification medium. The laser pulse, amplified by a factor of 10^6 or more, is recompressed by an optical system that is essentially the reverse of the stretcher. Off-the-shelf chirped pulse lasers are available with peak power in the 10- to 100-gigawatt range. Several major research facilities operate chirped lasers with peak power in the petawatt range.

Long-range fiber optic communication lines will be enhanced by the recent development of the erbium-doped fiber optic amplifier. Light from a diode laser "pumps up" a segment of erbium-doped optical fiber in the line. A signal moving down the line stimulates emission from the erbium atoms, resulting in amplification of the signal.

Laser technology is advancing so fast that it is possible to mention only a few recent developments. In addition to the ruby laser, there are many other solid-state lasers with output wavelengths ranging from about 18 nm (soft x rays) to about 3900 nm (infrared). Lasers that generate more than 1 kW of continuous power have been constructed, and pulsed lasers can now deliver nanosecond pulses of power exceeding 10^9 W. Various gas lasers produce wavelengths ranging from the far infrared to the ultraviolet. Semiconductor lasers (also known as diode lasers or junction lasers; these will be discussed further in Chapter 10) the size of a pinhead can develop 200 mW of power.

FEUE WHE

In addition to the ubiquitous diode lasers used in supermarket checkout counters, compact disc players, copiers, and computer printers, through very recent developments in materials physicists have constructed reliable diode lasers that emit in the blue to ultraviolet region of the spectrum. These lasers should make possible significantly increased high-density optical storage on digital versatile discs (DVDs). Liquid lasers using chemical dyes can be tuned over a range of wavelengths (about 70 nm for continuous lasers and more than 170 nm for pulsed lasers). The free-electron laser extracts light energy from a beam of free electrons moving through a spatially varying magnetic field. It has the potential for very high power and high efficiency and can be tuned over a large range of wavelengths. The variety and uses of modern lasers seem limitless.

Questions

8. What are the advantages of a four-level laser over a three-level laser?
9. Why is helium needed in a helium-neon laser? Why not just use neon?

EXAMPLE 9-8 **Critical Population Inversion Comparison** Compare the critical population inversion necessary for laser action in the ruby and He-Ne lasers. Compute the corresponding power requirements.

SOLUTION

The critical population density Δn_c is given by Equation 9-51. The typical parameters of these systems are as follows:

Parameter	Ruby laser	He-Ne laser
λ	694.3 nm	632.8 nm
f	$4.32 \times 10^{14}\ s^{-1}$	$4.74 \times 10^{14}\ s^{-1}$
n (refractive index)	1.76	1.00
t_s	3×10^{-3} s	10^{-7} s
t_p	2.9×10^{-8} s	3.3×10^{-7} s
Δf	$3.3 \times 10^{11}\ s^{-1}$	$9 \times 10^{8}\ s^{-1}$
N (Cr^{3+} concentration)	$2 \times 10^{19}/cm^3$	—

For ruby laser:

$$\Delta n_c = \frac{4\pi^2 f^2 \Delta f\, t_s}{c^3 t_p} = \frac{4\pi^2(4.32 \times 10^{14})^2(3.3 \times 10^{11})(3 \times 10^{-3})}{(3.00 \times 10^8/1.76)^3(2.9 \times 10^{-8})}$$

$$\Delta n_c = 5.08 \times 10^{22}\ \text{atoms/m}^3 = 5.08 \times 10^{16}\ \text{atoms/cm}^3$$

For He-Ne laser:

$$\Delta n_c = \frac{4\pi^2 f^2 \Delta f\, t_s}{c^3 t_p} = \frac{4\pi^2(4.74 \times 10^{14})^2(9 \times 10^{8})(10^{-7})}{(3.00 \times 10^8)^3(3.3 \times 10^{-7})}$$

$$\Delta n_c = 8.96 \times 10^{13}\ \text{atoms/m}^3 = 8.96 \times 10^{7}\ \text{atoms/cm}^3$$

Thus, the critical population density is far smaller for the He-Ne laser.

The minimum power input P needed to maintain the laser action in the helium-neon system is approximately equal to $\Delta n_c(hf/t_s)$ since $N_1 \approx 0$, or

$$P(\text{He-Ne}) \approx \Delta n_c(hf/t_s) \approx \frac{(8.96 \times 10^7)(6.63 \times 10^{-34})(4.74 \times 10^{14})}{10^{-7}} \approx 2.8 \times 10^{-4}\ \text{W/cm}^3$$

For the ruby laser, about one-half of the Cr^{3+} ions must be in the pumped level E_3 in Figure 9-32*c*, and the power per unit volume necessary to maintain that population is approximately

$$P(\text{ruby}) \approx \frac{N}{2}\left(\frac{hf}{t_s}\right) \approx \frac{(2 \times 10^{19})(6.63 \times 10^{-34})(4.32 \times 10^{14})}{2 \times 3 \times 10^{-3}} \approx 955\ \text{W/cm}^3$$

Summary

TOPIC	RELEVANT EQUATIONS AND REMARKS
1. The ionic bond	The bonding mechanism typical of most salts, it involves the transfer of one or more electrons to form ions that are attracted by the Coulomb force. The exclusion principle limits the close approach of the ions, resulting in a minimum in the potential energy $U(r)$. For a diatomic molecule, $U(r) = -\frac{ke^2}{r} + E_{ex} + E_{ion}$ **9-1** where E_{ion} is the net ionization energy and E_{ex} is the exclusion-principle energy. The latter is given by $E_{ex} = \frac{A}{r^n}$ **9-2** where A and n are constants.
2. The covalent bond	This bond is a quantum-mechanical effect arising from the sharing of one or more electrons by identical or similar atoms. The symmetry of the molecular wave functions resulting from their superposition of electron orbitals determines whether bonding will occur. The wave function for the symmetric state Ψ_S is large between the atomic potential wells, resulting in minimum potential energy and bonding. The antisymmetric wave function Ψ_A is small in that region. Bonding of two nonidentical atoms is often a mixture of ionic and covalent bonding.
Other covalent bonds	Covalent bonds differ in detail, depending upon which electrons are shared. For example, H_2 with only *s* electrons, is *s*-bonded. O_2 is *p*-*p* bonded. There are also *s*-*p* bonds, of which H_2O is one example.
3. Dipole-dipole bonds	Bonding between atoms and molecules may arise due to interactions between dipole moments. The interaction may involve molecules with either permanent electric dipole moments (polar molecules) or induced dipole moments (nonpolar molecules). The potential energy U of a dipole $\mathbf{p}_2$ in the electric field $\mathbf{E}_d$ of dipole $\mathbf{p}_1$ is given by $U = -\mathbf{p}_2 \cdot \mathbf{E}_d$ **9-8** The force between permanent dipoles decreases as $1/r^4$. If one or both of the dipoles is an induced dipole, the force between them decreases as $1/r^7$.

TOPIC	RELEVANT EQUATIONS AND REMARKS
4. Molecular spectra	The energy states of diatomic molecules consist of rotational bands superimposed on more widely spaced vibrational levels, which are in turn superimposed on the much more widely spaced atomic electron levels.
Rotational energies	The rotational energies of a diatomic molecule are $E = \frac{\ell(\ell+1)\hbar^2}{2I} = \ell(\ell+1)E_{0r} \qquad \ell = 0, 1, 2, \ldots$ **9-13** where I is the moment of inertia, $E_{0r} = \hbar^2/2I$ is the characteristic rotational energy, and ℓ is the rotational quantum number, which obeys the selection rule $\Delta\ell = \pm 1$.
Vibrational energies	The vibrational energies of a diatomic molecule are $E_v = (v + 1/2)hf \qquad v = 0, 1, 2, \ldots$ **9-20** where f is the vibrational frequency and v is the vibrational quantum number, which obeys the selection rule $\Delta v = \pm 1$.
5. Scattering, absorption, and stimulated emission	A photon incident on an atom can be absorbed, producing fluorescence or resonance radiation, or scattered elastically (Rayleigh scattering) or inelastically (Raman scattering). If the photon energy is greater than the ionization energy of the atom, Compton scattering or the photoelectric effect can occur. If the atom is initially in an excited state, an incident photon of the proper energy can stimulate emission of another photon of the same energy. The incident and emitted photons are in phase and travel parallel to each other. In an equilibrium system the probabilities (Einstein coefficients) for absorption and for stimulated emission between two states are equal.
6. Lasers and masers	Lasers and masers are important applications of stimulated emission, differing only in the wavelengths of their outputs. Amplification by stimulated emission depends on the possibility of obtaining population inversion, in which there are more atoms in an excited state than in the ground state or another excited state of lower energy. Population inversion is usually obtained by optical pumping and is produced more readily in four-level systems than in three-level systems.

General References

The following general references are written at a level appropriate for the readers of this book.

Brehm, J. J., and W. J. Mullin, *Introduction to the Structure of Matter*, Wiley, New York, 1989.

Eisberg, R., and R. Resnick, *Quantum Physics of Atoms, Molecules, Solids, Nuclei, and Particles*, 2d ed., Wiley, New York, 1985.

Herzberg, G., *Atomic Spectra & Atomic Structure*, Dover, New York, 1944.

Pauling, L., *The Chemical Bond*, Cornell University Press, Ithaca, NY, 1967.

Schawlow, A. L., "Laser Light," *Scientific American*, September 1968. This article and several other excellent articles on lasers and masers are reprinted in *Lasers and Light*, W. H. Freeman and Co., New York, 1969.

Serway, R. A., C. J. Moses, and Curt A. Moyer, *Modern Physics*, 3d ed., Thomson, Belmont, CA, 2005.

Zeilinger, A., "Quantum Teleportation," *Scientific American*, April 2000.

FÈUE WHE

Notes

1. The term *orbital* is frequently used in molecular physics and in chemistry to refer to the space part of the electron wave functions, that is, the quantum numbers n, ℓ, and m_ℓ. In molecular physics the electrons of interest are usually the outermost (valence) ones of the constituent atoms, which become associated with the entire molecule rather than their original atoms, so we speak of "molecular orbitals" as well as "atomic orbitals."

2. Molecules whose atoms are identical, such as H_2, are sometimes called *homopolar* or *homonuclear*. Those whose atoms are not identical are called *heteropolar* or *heteronuclear*.

3. C_{60} and the other fullerenes are named after the philosopher and engineer R. Buckminster Fuller, who invented the architectural geodesic dome structure. Such domes, as Fuller pointed out, can be considered as networks of pentagons and hexagons.

4. Leonhard Euler (1707–1783), Swiss mathematician. Arguably the most prolific mathematician of all time, he published 866 papers during his lifetime and, despite having lost his sight in 1766 (in part due to his earlier observations of the Sun), he left so many manuscripts at his death that it took another 35 years to get them all published. He introduced the symbol e as the base of the natural logarithms and i as the square root of -1.

5. Johannes D. van der Waals (1837–1923), Dutch physicist. Largely self-taught, he became interested in the fact that the ideal gas law derived from kinetic theory does not hold exactly for real gases. This led him to question the assumption that no forces act between individual gas molecules except during collisions, which resulted in his development of an equation, the van der Waals equation, which more accurately describes real gases. He was awarded the 1910 Nobel Prize in Physics for his work.

6. This result is derived in most introductory physics books. See, e.g., P. A. Tipler and G. Mosca, *Physics for Scientists and Engineers,* 6th ed., W. H. Freeman and Co., New York, 2008, p. 671.

7. Terminology concerning the dipole-dipole forces is a bit confused. Some textbooks use *van der Waals* to describe all three types of dipole-dipole forces. We will follow the more common (and traditional) use, reserving *van der Waals* for the attractive force between induced dipoles only.

8. We use v (the Greek letter nu) here rather than n so as not to confuse the vibrational quantum number with the principal quantum number n for electronic energy levels.

9. The nitric oxide (NO) molecule is an exception due to its odd electron.

10. Also, the $\ell \rightarrow \ell - 1$ group of lines are called the *P branch* and the $\ell \rightarrow \ell + 1$ group the *R branch*.

11. Chandrasekhara V. Raman (1888–1970), Indian physicist. Graduating from college at the age of 16, like Einstein he became a civil servant and worked at science in his spare time. He had predicted that visible light should be inelastically scattered even before Heisenberg had predicted and Compton had found the effect for x rays. He was awarded the 1930 Nobel Prize in Physics for his work, becoming the first Asian to be so recognized in the sciences.

12. There is also a Raman effect for the vibrational and electronic levels of molecules.

13. T. H. Maiman, "Stimulated Optical Radiation in Ruby," *Nature*, **187**, 493 (1960).

14. The correction essentially accounts for the fact that, due to the finite line width, the energy density $u(f)$ in the transition probability must include a narrow range of frequencies Δf rather than just the single frequency f.

15. Recall that the energy per unit volume $u(f)$ times c is the intensity, e.g., W/m^2 in SI units.

16. A. Javan, W. B. Bennet, Jr., and D. R. Herriott, *Physical Review Letters*, **6**, 106 (1961).

17. W. Ketterle et al., *Science*, **301**, 1513 (2003).

Problems

Level I

Section 9-1 The Ionic Bond

9-1. The dissociation energy is sometimes expressed in kilocalories per mole. (*a*) Find the relation between electron volts per molecule and kilocalories per mole. (*b*) Find the dissociation energy of molecular NaCl in kilocalories per mole. (*c*) The dissociation energy of the Li_2 molecule is 106 kJ/mole. Find the value in eV per molecule.

9-2. The dissociation energy of Cl_2 is 2.48 eV. Consider the formation of an NaCl molecule by the reaction

$$Na + \tfrac{1}{2}Cl_2 \longrightarrow NaCl$$

Is this reaction endothermic (requiring energy) or exothermic (giving off energy)? How much energy per molecule is required or given off?

9-3. Using the data in Table 9-1, compute the net energy required to transfer an electron between the following pairs of atoms: Cs to F, Li to I, and Rb to Br.

9-4. Using the data in Tables 9-1 and 9-2, estimate the dissociation energy of the three ionically bonded molecules CsI, NaF, and LiI. Your results are probably all higher than those in Table 9-2. Explain why.

9-5. The equilibrium separation of the Rb^+ and Cl^- ions in RbCl is about 0.267 nm. (*a*) Calculate the potential energy of attraction of the ions, assuming them to be point charges. (*b*) The ionization energy of rubidium is 4.18 eV, and the electron affinity of Cl is 3.62 eV. Find the dissociation energy, neglecting the energy of repulsion. (*c*) The measured dissociation energy is 4.37 eV. What is the energy due to repulsion of the ions?

9-6. Compute the Coulomb energy of the KBr molecule at the equilibrium separation. Use that result to compute the exclusion-principle repulsion at r_0.

9-7. If the exclusion-principle repulsion in Problem 9-6 is given by Equation 9-2, compute the coefficient A and the exponent n.

9-8. Compute the dissociation energy of molecular NaBr in kilocalories per mole.

9-9. Note in Table 9-2 that the equilibrium separations of the KBr and RbCl molecules are very nearly equal. Compute the exclusion-principle repulsion for these molecules.

Section 9-2 The Covalent Bond

9-10. Hydrogen can bond covalently with many atoms besides those listed in Tables 9-3 and 9-5, including sulfur, tellurium, phosphorus, and antimony. What would you expect to be the chemical formula of the resulting molecules? (*Hint:* Use the table of electron configurations in Appendix C.)

9-11. What kind of bonding mechanism would you expect for (*a*) the KCl molecule, (*b*) the O_2 molecule, and (*c*) the CH_4 molecule?

9-12. The equilibrium separation of the atoms in the HF molecule is 0.0917 nm, and its measured electric dipole moment is 6.40×10^{-30} C · m. What percentage of the bonding is ionic?

9-13. The equilibrium separation of CsF is 0.2345 nm. If its bonding is 70 percent ionic, what should its measured electric dipole moment be?

9-14. Ionic bonding in the BaO molecule involves the transfer of two electrons from the Ba atom. If the equilibrium separation is 0.193 nm and the measured electric dipole moment is 26.7×10^{-30} C · m, to what extent is the bond actually ionic?

Section 9-3 Other Bonding Mechanisms

9-15. Find three other elements with the same subshell electron configuration in the two outermost orbits as carbon. Would you expect the same kind of hybrid bonding for these elements as for carbon? Support your answer.

9-16. The dipole moment $\mathbf{p}$ of the water molecule, illustrated in Figure 9-19, is actually the vector sum of two equal dipoles $\mathbf{p}_1$ and $\mathbf{p}_2$ directed from the oxygen atom to each of the hydrogen atoms. The measured value of the angle between the two hydrogen atoms is 104.5°, the O–H bond length is 0.0956 nm, and the magnitude of $\mathbf{p}$ is 6.46×10^{-30} C · m. Compute the fraction of the electron charge that is transferred from each hydrogen to the oxygen.

9-17. The polarizability of Ne is 1.1×10^{-37} m · C^2/N. (*a*) At what separation would the dipole-dipole energy between a molecule of H_2O and an atom of Ne in the atmosphere be sufficient to withstand collision with an N_2 molecule moving with the average kinetic energy for $T = 300$ K? (*b*) At what separation does this energy occur for a typically bonded molecule? (*c*) On the basis of these results, do you expect H_2O–Ne bonds to be very likely? Explain your answer.

9-18. The hydrogen bonds linking the two helical strands of DNA have bond strengths of about 0.3 eV, or approximately 15 percent of the strengths of the ionic/covalent bonds along the strands. (*a*) What is the wavelength of a photon with sufficient energy to break this bond? (*b*) In what part of the spectrum does this wavelength lie? (*c*) Since a significant intensity exists at this wavelength in the environment, why haven't all the DNA hydrogen bonds long since broken?

9-19. Would you expect the following molecules to be polar or nonpolar? Explain your answer in each case. (*a*) NaCl; (*b*) O_2.

Section 9-4 Molecular Spectra

9-20. The characteristic rotational energy E_{0r} for N_2 molecules is 2.48×10^{-4} eV. From this, find the separation distance of the nitrogen atoms in N_2.

9-21. For the O_2 molecule, the separation of the atoms is 0.121 nm. Calculate the characteristic rotational energy $E_{0r} = \hbar^2/2I$ in eV.

9-22. The CO molecule undergoes a transition from the $v = 1$ vibrational state to the $v = 0$ state. (*a*) What is the wavelength of the emitted photon? (*b*) At what temperature would 1 percent of the CO molecules be in the $v = 1$ vibrational state?

9-23. Using data from Table 9-7, (*a*) compute the vibrational energy of the LiH molecule in its lowest vibrational state. (*b*) Compute the reduced mass of LiH. (*c*) Determine the force constant for LiH. (*d*) From those results, compute an estimate of the LiH bond length and compare your result with the value in the table.

9-24. Calculate the reduced mass in unified mass units for (*a*) H_2, (*b*) N_2, (*c*) CO, and (*d*) HCl.

9-25. The characteristic rotational energy $E_{0r} = \hbar^2/2I$ for KCl is 1.43×10^{-5} eV. (*a*) Find the reduced mass for the KCl molecule. (*b*) Find the separation distance of the K^+ and Cl^- ions.

9-26. Use the data from Table 9-7 to find the force constant for (*a*) the $H^{35}Cl$ and (*b*) the $K^{79}Br$ molecules.

9-27. The equilibrium separation of HBr is 0.141 nm. Treating the Br atom as fixed, compute the four lowest rotational energies of the HBr molecule and show them in a carefully sketched energy-level diagram.

9-28. The vibrational spectrum of Li_2 consists of a series of equally spaced lines in the microwave region 1.05×10^{13} Hz apart. Compute the equilibrium separation for Li_2.

9-29. Compute the difference in the rotational energy E_{0r} for $K^{35}Cl$ and $K^{37}Cl$.

9-30. What type of bonding mechanism would you expect for (*a*) NaF, (*b*) KBr, (*c*) N_2, and (*d*) Ne?

9-31. For NaCl compute (*a*) the energy in eV necessary to excite the first rotational state and (b) the wavelength and frequency of the photon emitted in the transition back to the ground state. (Assume that the molecule is in the electronic and vibrational ground states.)

Section 9-5 Scattering, Absorption, and Stimulated Emission

9-32. The five lowest levels of a certain monatomic gas have the values $E_1 = 0$, $E_2 = 3.80$ eV, $E_3 = 4.30$ eV, $E_4 = 7.2$ eV, and $E_5 = 7.5$ eV. (*a*) If the temperature is high enough that all levels are occupied and the gas is illuminated with light of wavelength 2400 nm, what transitions can occur? (*b*) Which of those found in part (*a*) will still occur if the temperature is so low that only the state E_1 is occupied? (*c*) Repeat (*a*) and (*b*) for light of 250 nm wavelength. (*d*) What wavelength of the incident light would stimulate emission from state E_4?

9-33. A hydrogen discharge tube is operated at about 300 K in the laboratory in order to produce the Balmer series. Compute the ratio of the probability for spontaneous emission of the H_α line to that for stimulated emission.

9-34. Determine the ratio of the number of molecules in the $v = 1$ state to the number in the $v = 0$ state for a sample of O_2 molecules at 273 K. Repeat the calculation for 77 K. (Ignore rotational motion.)

9-35. The nuclei in the F_2 molecule are separated by 0.14 nm. (*a*) Compute the energy separations and sketch an energy-level diagram for the lowest four rotational levels with $v = 0$. (*b*) What are the wavelengths of possible transitions between these levels?

Section 9-6 Lasers and Masers

9-36. A pulse from a ruby laser has an average power of 10 MW and lasts 1.5 ns. (*a*) What is the total energy of the pulse? (*b*) How many photons are emitted in this pulse?

9-37. A helium-neon laser emits light of wavelength 632.8 nm and has a power output of 4 mW. How many photons are emitted per second by this laser?

9-38. A laser beam is aimed at the Moon, a distance 3.84×10^8 m away. The angular spread of the beam is given by the diffraction formula (Rayleigh's criterion), $\sin\theta = 1.22\,\lambda/D$, where D is the diameter of the laser tube or rod. (a) Calculate the size of the beam on the Moon for $D = 10$ cm and $\lambda = 600$ nm. (*b*) Repeat the calculation if the laser beam is projected toward the Moon through a 1.0-m-diameter telescope.

9-39. A particular atom has two energy levels with a transition wavelength of 420 nm. At 297 K there are 2.5×10^{21} atoms in the lower state. (*a*) How many atoms are in the upper state? (*b*) Suppose that 1.8×10^{21} of the atoms in the lower state are pumped to the upper state. How much energy could this system release in a single laser pulse?

Level II

9-40. (*a*) Calculate the electrostatic potential energy of Na^+ and Cl^- ions at their equilibrium separation distance of 0.24 nm, assuming the ions to be point charges. (*b*) What is the energy of repulsion at this separation? (*c*) Assume that the energy of repulsion is given by Equation 9-2. From Figure 9-2*b*, this energy equals ke^2/r at about $r = 0.14$ nm. Use this and your answer to part (*b*) to calculate n and A. (Although this calculation is not very accurate, the energy of repulsion does vary much more rapidly with r than does the energy of attraction.)

9-41. The angular width of a ruby laser beam is determined by Rayleigh's criterion (see Problem 9-38). For this laser the diameter of the ruby rod is 1.0 cm and $\lambda = 694.3$ nm. (*a*) What is the diameter of the spot projected by the ruby laser at a distance of 1.0 km? (*b*) If the laser is emitting 10^{18} photons/s, what is the power deposited per square centimeter on the target at 1.0 km?

9-42. The equilibrium separation of the K^+ and Cl^- ions in KCl is about 0.267 nm. (*a*) Calculate the potential energy of attraction of the ions assuming them to be point charges at this separation. (*b*) The ionization energy of potassium is 4.34 eV and the electron affinity of chlorine is 3.62 eV. Find the dissociation energy for KCl, neglecting any energy of repulsion (see Figure 9-2*a*). (*c*) The measured dissociation energy is 4.40 eV. What is the energy due to repulsion of the ions at the equilibrium separation?

9-43. Use the equilibrium separation for the K^+ and Cl^- ions given in Problem 9-42 and the reduced mass of KCl to calculate the characteristic rotational energy E_{0r} of KCl.

9-44. In this problem, you are to find how the van der Waals force between a polar and a nonpolar molecule depends on the distance between the molecules. Let the dipole moment of the polar molecule be in the x direction and the nonpolar molecule be a distance x away. (*a*) How does the electric field due to an electric dipole depend on the distance x? (*b*) Use the facts that the potential energy of an electric dipole of moment $\mathbf{p}$ in an electric field $\mathbf{E}$ is $U = -\mathbf{p} \cdot \mathbf{E}$ and that the induced dipole moment of the nonpolar molecule is proportional to $\mathbf{E}$ to find how the potential energy of interaction of the two molecules depends on separation distance. (*c*) Using $F_x = -dU/dx$, find the x dependence of the force between the two molecules.

9-45. The microwave spectrum of CO has lines at 0.86 mm, 1.29 mm, and 2.59 mm. (*a*) Compute the photon energies and carefully sketch the energy level diagram that corresponds. What molecular motion produces these lines? (*b*) Compute the equilibrium separation (bond length) of CO.

FÈUE WHE

9-46. Carefully draw a potential energy curve for a diatomic molecule (like Figure 9-2*b*) and indicate the mean values of r for two vibrational levels. Show that because of the asymmetry of the curve, r_{av} increases with increasing vibrational energy and therefore solids expand when heated.

9-47. A sample of HCl is illuminated with light of wavelength 435.8 nm. (*a*) Compute the wavelengths of the four lines in the rotational Raman spectrum that are closest to that of the incident light. (*b*) Compare the difference in their frequencies with the corresponding lines in Figure 9-29.

9-48. Use data from Table 9-7 to compute the first excited vibrational and the first excited rotational states of (*a*) the Li_2 and (*b*) the $K^{79}Br$ molecules.

9-49. Calculate the effective force constant for HCl from its reduced mass and the fundamental vibrational frequency obtained from Figure 9-29.

9-50. Notice in Figure 9-32*c* that the level E_2 in Cr^{3+} is a doublet, the pair of states being separated by only 0.0036 eV. (*a*) Assume that all of the Cr^{3+} ions in a certain laser are in the three states E_1 and E_2 (doublet) and compute the relative populations of these levels. (*b*) If only the lower state of the E_2 doublet can produce laser light but both levels must be pumped together, determine the pumping power necessary for laser action to occur. The density of states (degeneracy) of level E_1 is 4 and for *each* of the E_2 levels is 2.

9-51. The central frequency for the absorption band of HCl shown in Figure 9-29 is at $f = 8.66 \times 10^{13}$ Hz, and the absorption peaks are separated by about $\Delta f = 6 \times 10^6$ Hz. Using this information, find (*a*) the lowest (zero-point) vibrational energy for HCl, (*b*) the moment of inertia of HCl, and (*c*) the equilibrium separation of the atoms.

Level III

9-52. The potential energy between two atoms in a molecule can often be described rather well by the Lenard-Jones potential, which can be written

$$U(r) = U_0\left[\left(\frac{a}{r}\right)^{12} - 2\left(\frac{a}{r}\right)^{6}\right]$$

where U_0 and a are constants. (*a*) Find the interatomic separation r_0 in terms of a for which the potential energy is minimum. (*b*) Find the corresponding value of U_{min}. (*c*) Use Figure 9-8*b* to obtain numerical values for r_0 and U_0 for the H_2 molecule. Express your answer in nanometers and electron volts. (*d*) Make a plot of the potential energy $U(r)$ versus the internuclear separation r for the H_2 molecule. Plot each term separately, together with the total $U(r)$.

9-53. (*a*) Find the exclusion-principle repulsion for NaCl. (*b*) Use Equation 9-2 to find A and n.

9-54. Show that the H^+–H^- system cannot be ionically bonded. (*Hint:* Show that $U(r)$ has no negative minimum.)

9-55. (*a*) Calculate the fractional difference $\Delta\mu/\mu$ for the reduced masses of the $H^{35}Cl$ and $H^{37}Cl$ molecules. (*b*) Show that the mixture of isotopes in HCl leads to a fractional difference in the frequency of a transition from one rotational state to another given by $\Delta f/f = -\Delta\mu/\mu$. (*c*) Compute $\Delta f/f$ and compare your result with Figure 9-29.

9-56. For a molecule such as CO, which has a permanent electric dipole moment, radiative transitions obeying the selection rule $\Delta\ell = \pm 1$ between two rotational energy levels of the same vibrational energy state are allowed. (That is, the selection rule $\Delta v = \pm 1$ does not hold.) (*a*) Find the moment of inertia of CO for which $r_0 = 0.113$ nm, and calculate the characteristic rotational energy E_{0r} in electron volts. (*b*) Make an energy-level diagram for the rotational levels for $\ell = 0$ to $\ell = 5$ for some vibrational level. Label the energies in electron

volts, starting with $E = 0$ for $\ell = 0$. (*c*) Indicate on your diagram transitions that obey $\Delta\ell = -1$ and calculate the energy of the photons emitted. (*d*) Find the wavelength of the photon emitted for each transition in (*c*). In what region of the electromagnetic spectrum are these photons?

9-57. An H_2 molecule in its ground electronic, vibrational, and rotational state absorbs a photon of frequency 1.356×10^{14} Hz, undergoing a transition to the $v = 1$, $\ell = 1$ state while remaining in the electronic ground state. It then undergoes a transition to the $v = 0$, $\ell = 2$ state, emitting a photon of frequency 1.246×10^{14} Hz. (*a*) Compute the moment of inertia of the H_2 molecule about an axis through the center of mass. (*b*) Determine the vibrational frequency and r_0 for H_2 and compare these with the values in Table 9-7.

CHAPTER 10

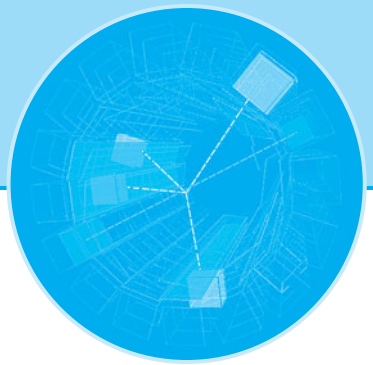

Solid State Physics

The many and varied properties of solids have intrigued us for centuries. Technological developments involving metals and alloys have shaped the courses of civilizations, and the symmetry and beauty of naturally occurring, large single crystals have consistently captured our imaginations. However, the origins of the physical properties of solids were not understood even in rudimentary form until the development of quantum mechanics. The application of quantum mechanics to solids has provided the basis for much of the technological progress of modern times. We will study briefly some aspects of the structure of solids in Section 10-1 and then concentrate on the electrical and magnetic properties of solids.

10-1 The Structure of Solids

In our everyday world we see matter in three phases: gases, liquids, and solids. In a gas the average distance between two atoms or molecules is large compared with the size of an atom or molecule. The molecules have little influence on one another except during their frequent but brief collisions. In a liquid or solid the atoms or molecules are close together and exert forces on one another comparable to the forces that bind atoms into molecules. (There is a fourth phase of matter, plasma, which occurs when the matter consists largely—or entirely—of ions and free electrons. Usually this condition exists only at very high temperatures, such as inside stars, in intense electrical discharges—e.g., lightning—and in the laboratory. The properties of a plasma are very different from those of an ordinary gas because of the long-range electrical and magnetic effects arising from the charges of the particles. The recently discovered low-temperature gas phase of matter, the Bose-Einstein condensate, was discussed in Chapter 8.) In a liquid, the molecules form temporary short-range bonds that are continually broken and re-formed as the result of the thermal kinetic energy of the molecules. The strength of the bonds depends on the type of molecule. For example, as we discussed in Section 9-3, the bonds between helium atoms are very weak van der Waals bonds, and He does not liquefy at atmospheric pressure until the very low temperature of 4.2 K is reached.

FEUE WHE

If a liquid is slowly cooled, the kinetic energy of its molecules is reduced and the molecules will arrange themselves in a regular crystalline array, producing the maximum number of bonds and leading to a minimum potential energy. However, if the liquid is cooled rapidly so that its internal energy is removed before the molecules have a chance to arrange themselves, a solid is often formed that is not crystalline but resembles a "snapshot" of a liquid. Such a solid is called *amorphous*; it displays short-range order but not the long-range order (over many atomic diameters) characteristic of a crystal. Glass is a typical amorphous solid. A characteristic of the long-range ordering of a crystal is that it has a well-defined melting point, whereas an amorphous solid merely softens as its temperature is increased. Many materials may solidify in either an amorphous or a crystalline state, depending on how they are prepared. Others exist only in one form or the other. Most common solids are polycrystalline—i.e., they are collections of single crystals. The size of such single crystals is typically a fraction of a millimeter; however, large single crystals occur naturally and can be produced artificially (Figure 10-1). We will discuss only simple crystalline solids in this chapter.

The most important property of a single crystal is its symmetry and regularity of structure: it can be thought of as a single unit structure repeated throughout the solid.

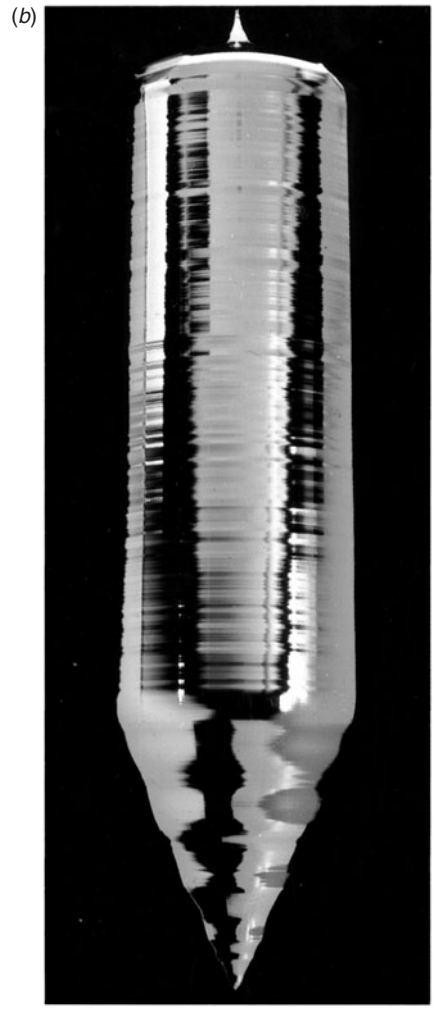

Figure 10-1 (*a*) A single crystal of quartz, one of several naturally occurring crystalline forms of SiO_2. [*Courtesy of Sawyer Research Products, Inc.*] (*b*) A synthetic silicon crystal is created beginning with a raw material containing silicon (for instance, common beach sand), purifying out the silicon, and melting it. From a seed crystal, the molten silicon grows into a cylindrical crystal, such as the one shown here. The crystals (typically about 1.3 m long) are formed under highly controlled conditions to ensure that they are flawless and sliced into thousands of thin wafers, onto which the layers of an integrated circuit are etched. [*Courtesy of the Museum of Modern Art, New York City.*]

The smallest unit of a crystal is called the *unit cell*. The structure of the unit cell depends on the type of bonding between the atoms, ions, or molecules in the crystal. If more than one kind of atom is present, the structure will also depend on their relative size. The structure may also change in response to changes in pressure and/or temperature. The bonding mechanisms are those discussed in Chapter 9: ionic, covalent, and dipole-dipole, the latter including the hydrogen and van der Waals bonds. In addition, a quantum-mechanical mechanism responsible for bonding metals in the solid state, *metallic bonding*, will be described later in this section.

Ionic and Covalent Solids

Figure 10-2 shows the structure of the ionic crystal NaCl. The Na^+ and Cl^- ions are spherically symmetric (see Section 9-1) with the Cl^- ions approximately twice as large as the Na^+ ions. The minimum potential energy of this crystal occurs when an ion of either kind has six nearest neighbors of the other kind. This structure is called *face-centered-cubic* (*fcc*) because the unit cell is a cube and an ion, in this case Cl^-, occupies the center of each face. Note that the Na^+ and Cl^- ions are *not* paired into NaCl molecules in solid NaCl.

The net attractive part of the potential energy of an ion in a crystal can be written

$$U_{\text{att}} = -\alpha\frac{ke^2}{r} \qquad \textbf{10-1}$$

where r is the separation distance between neighboring ions (which is 0.282 nm for the Na^+ and Cl^- ions in crystalline NaCl) and α, called the *Madelung constant*, depends on the geometry of the crystal. If only the six nearest neighbors of each ion were important, α would be 6. However, in addition to the six neighbors of opposite charge at a distance r there are 12 ions of the same charge at a distance $2^{1/2}r$, 8 ions of opposite charge at distance $3^{1/2}r$, and so on. The Madelung constant is thus an infinite sum:

$$\alpha = 6 - \frac{12}{\sqrt{2}} + \frac{8}{\sqrt{3}} - \frac{6}{2} + \frac{20}{\sqrt{5}} - \cdots \qquad \textbf{10-2}$$

Unfortunately, the sum in Equation 10-2 does not converge! We are saved by the fact that NaCl crystals are not spherical, as the analysis above implies. A better physical approach is to use cubic shells rather than spherical ones; then the cubic-shell equivalent

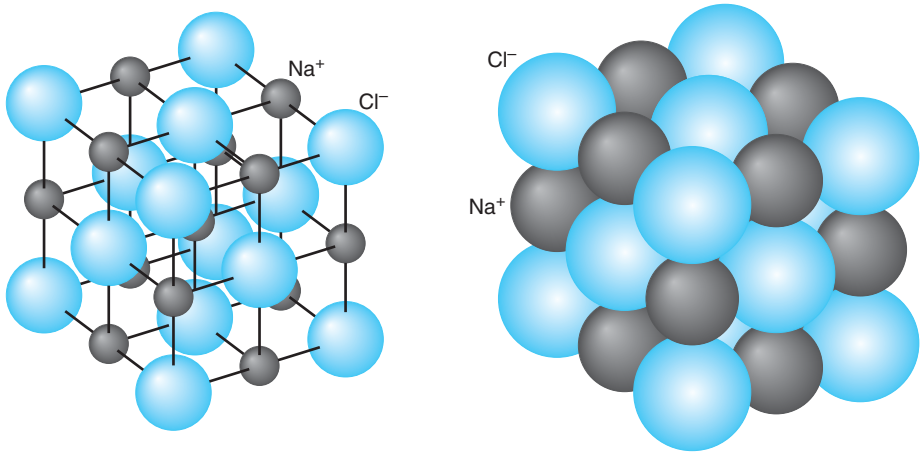

Figure 10-2 Structure of the face-centered-cubic (fcc) NaCl crystal.

FEUE WHE

Table 10-1 Properties of selected crystalline solids

Solid	Bonding	Equilibrium separation (nm)	Crystal symmetry	Madelung constant	Cohesive energy (eV/atom)	Melting point (K)
NaCl	ionic	0.282	fcc	1.7476	3.19	1074
LiBr	ionic	0.275	fcc	1.7476	3.10	823
KCl	ionic	0.315	fcc	1.7476	3.24	1043
RbF	ionic	0.282	fcc	1.7476	3.55	1068
CsCl	ionic	0.348	sc	1.7627	3.27	918
ZnO	ionic	0.222	hcp	1.4985	7.22	2248
Li	metallic	0.302	bcc	—	1.63	454
Fe	metallic	0.248	bcc	—	4.28	1811
Au	metallic	0.288	fcc	—	3.81	1338
Zn	metallic	0.266	hcp	—	1.35	693
C	covalent	0.154	fcc	—	7.37	†
Si	covalent	0.235	fcc	—	4.63	1687
Ge	covalent	0.245	fcc	—	3.85	1211
H_2O	dipole-dipole	0.367	hcp	—	0.52*	273
C_{60}	dipole-dipole	1.00	fcc	—	1.5*	?
Ne	dipole-dipole	0.313	fcc	—	0.020	24

* eV/molecule.

† Diamond transforms to graphite at high temperature. The latter then sublimes at about 3800 K.

of Equation 10-2 does converge, albeit slowly. The result for face-centered-cubic structures such as NaCl is $\alpha = 1.7476$. The geometric details of other ionic arrangements results in slightly different values for α. (See Table 10-1.)

When Na^+ and Cl^- ions are very close together, they repel each other because of the overlap of the wave functions of their electrons and the exclusion principle repulsion discussed in Section 9-1. A simple empirical expression for the potential energy associated with this repulsion that works fairly well is

$$U_{\text{rep}} = \frac{A}{r^n}$$

where A and n are constants.[1] The total potential energy of an ion is then

$$U = -\alpha\frac{ke^2}{r} + \frac{A}{r^n} \qquad \textbf{10-3}$$

The equilibrium separation $r = r_0$ is that at which the force $F = -dU/dr$ is zero. Differentiating Equation 10-3 and setting $dU/dr = 0$ at $r = r_0$, we obtain

$$A = \frac{\alpha k e^2 r_0^{n-1}}{n} \qquad \textbf{10-4}$$

The total potential energy of an ion in the crystal can thus be written

$$U = -\alpha \frac{ke^2}{r_0}\left[\frac{r_0}{r} - \frac{1}{n}\left(\frac{r_0}{r}\right)^n\right] \qquad \textbf{10-5}$$

At $r = r_0$, we have

$$U(r_0) = -\alpha \frac{ke^2}{r_0}\left[1 - \frac{1}{n}\right] \qquad \textbf{10-6}$$

If we know the equilibrium separation r_0, which can be found from x-ray diffraction experiments or computed from the crystal density, the value of n can be found approximately from the *dissociation energy* or *lattice energy* of the ionic crystal, which is the energy needed to break up the crystal into its constituent ions. In the case of NaCl the measured dissociation energy is 770 kJ/mol. Using 1 eV $= 1.602 \times 10^{-19}$ J and the fact that 1 mol of NaCl contains N_A pairs of ions, we can express the dissociation energy in electron volts per ion pair, which makes possible an easier comparison with, e.g., the binding energy per molecule. The conversion between electron volts per ion pair and kilojoules per mole is

$$1\frac{\text{eV}}{\text{ion pair}} \times \frac{6.022 \times 10^{23}\ \text{ion pairs}}{\text{mol}} \times \frac{1.602 \times 10^{-19}\ \text{J}}{1\ \text{eV}} = 96.47\frac{\text{kJ}}{\text{mol}} \qquad \textbf{10-7}$$

Thus, 770 kJ/mol = 7.98 eV per ion pair. Substituting −7.98 eV for $U(r_0)$, 0.282 nm for r_0 (see Example 10-1), and 1.75 for α in Equation 10-6, we can solve for n. The result is $n = 9.35 \approx 9$.

The dissociation energy is also used to compute the *cohesive energy* of a crystal, which is the potential energy per atom or per atomic pair rather than per ion pair and is the term used for all crystalline bonding mechanisms. For the NaCl illustration above, 7.98 eV is the energy needed to remove an Na^+ and Cl^- pair from the crystal. Forming Cl from Cl^- requires the input of 3.62 eV, and forming Na from Na^+ releases 5.14 eV. Therefore, the energy necessary to remove the neutral Na and Cl pair from the crystal is 7.98 eV + 3.62 eV − 5.14 eV = 6.46 eV, and the cohesive energy of NaCl is 6.46 eV per Na and Cl pair. This result is in good agreement with the observed value of 3.19 eV/atom in Table 10-1. A large cohesive energy implies a high melting point and vice versa.

EXAMPLE 10-1 **Equilibrium Spacing r_0 in an NaCl Crystal** Calculate the equilibrium spacing r_0 for NaCl from the measured density of NaCl, which is $\rho = 2.16\ \text{g/cm}^3$.

SOLUTION

We consider each ion to occupy a cubic volume of side r_0. The mass of 1 mol of NaCl is 58.4 g, which is the sum of the atomic masses of sodium and chlorine. The ions occupy a volume of $2N_A r_0^3$, where $N_A = 6.02 \times 10^{23}$ is Avogadro's number. The density is thus related to r_0 by

$$\rho = \frac{m}{V} = \frac{m}{2N_A r_0^3}$$

Then

$$r_0^3 = \frac{m}{2N_A\rho} = \frac{58.4\ \text{g}}{2(6.02 \times 10^{23})(2.16\ \text{g/cm}^3)} = 2.24 \times 10^{-23}\ \text{cm}^3$$

$$r_0 = 2.82 \times 10^{-8}\ \text{cm} = 0.282\ \text{nm}$$

FEUE WHE

EXAMPLE 10-2 **Measuring r_0 from X-Ray Diffraction** Molybdenum K_α x rays ($\lambda = 0.071$ nm) strike the diagonal Bragg planes of the NaCl crystal shown on the right in Figure 3-15 such that a diffraction maximum (a bright Laue spot) is observed for $\theta = 10.25°$. Determine the value of r_0.

SOLUTION

1. Since NaCl is a cubic crystal, the distance d between the diagonal Bragg planes is related to the equilibrium separation r_0 by

$$d = \frac{r_0}{\sqrt{2}}$$

2. The x-ray diffraction maxima satisfy the Bragg condition, Equation 3-23:

$$2d \sin\theta = m\lambda$$

3. For $m = 1$ and substituting d from above:

$$2\left(\frac{r_0}{\sqrt{2}}\right)\sin\theta = \lambda$$

4. Solving this for r_0 and substituting values from above gives

$$r_0 = \frac{\sqrt{2}\,\lambda}{2\sin\theta}$$
$$= \frac{(\sqrt{2})(0.071\text{ nm})}{(2)(\sin 10.25°)}$$
$$= 0.282\text{ nm}$$

Remarks: *This result agrees with the value calculated from the density of NaCl in Example 10-1.*

Most ionic crystals, such as LiF, KF, KCl, KI, AgCl, and others formed by molecules in Table 9-2, have a face-centered-cubic structure. Some elemental solids that also have this structure are Ag, Al, Au, Ca, Cu, Ni, and Pb.

Figure 10-3 illustrates the structure of another ionic crystal, CsCl, which is called *simple cubic* (*sc*) because it can be considered as two interpenetrating cubic structures, one of Cs^+ ions and the other of Cl^- ions. In this structure, each ion has eight nearest-neighbor ions of the opposite charge. The Madelung constant for ionic crystals with simple cubic structure is 1.7627. Other crystals with this structure include CsI, TlI, TlBr, LiHg, and NH_4Cl. Some elemental solids, such as Ba, Cs, Fe, K, Li, Mo, and Na, also crystallize with the structure shown in Figure 10-3; when the atoms are the same at the vertices and in the center of the cube, the structure is called *body-centered-cubic* (*bcc*).

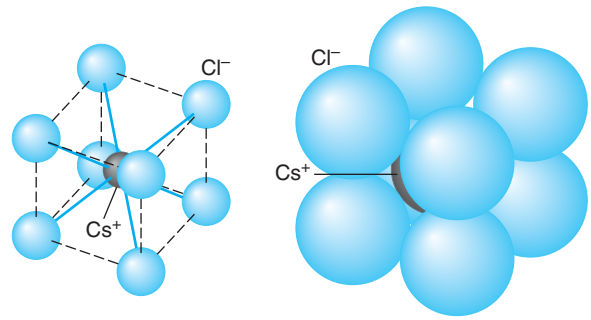

Figure 10-3 Structure of the simple cubic (sc) crystal CsCl.

Figure 10-4 illustrates another important crystal structure, called *hexagonal close-packed* (*hcp*). This is the structure obtained by stacking identical spheres such as Ping-Pong balls. In one layer, each ball touches six others; hence the name *hexagonal*. In the next layer, each ball fits into the triangular depressions of the first layer. In the third layer, each ball fits into a triangular depression of the second layer such that it lies directly over a ball in the first layer. Elements with a hexagonal close-packed crystal structure include Be, Cd, Ce, Mg, Os, Zn, and Zr. There are a total of 14 different types of three-dimensional crystal lattice structures, of which we have discussed only a few of the most common ones. (See Appendix B3.)

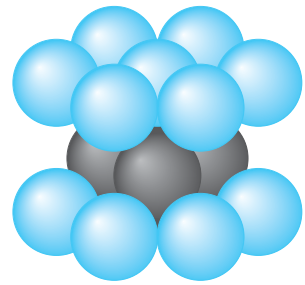

Figure 10-4 Hexagonal close-packed (hcp) crystal structure.

EXAMPLE 10-3 **Madelung Constant for a Two-Dimensional Crystal** Calculate out to four terms in the series the Madelung constant for the hypothetical univalent, two-dimensional ionic crystal shown in Figure 10-5.

SOLUTION

The net attractive potential is given by Equation 10-1. When the negative ion at the origin of Figure 10-5 is considered, there are four positive ions located a distance r away, as indicated by circle A in the diagram. There are four negative ions lying on circle B, whose radius is $2^{1/2}r$. Four negative ions are located on circle C, whose distance from the ion at the origin is $2r$, and finally, eight positive ions lie on circle D at $5^{1/2}r$ from the origin. Therefore, to four terms the net attractive potential is

$$U_{\text{att}} = -ke^2\left(\frac{4}{r} - \frac{4}{\sqrt{2}\,r} - \frac{4}{2r} + \frac{8}{\sqrt{5}\,r}\right)$$

or

$$U_{\text{att}} = -\frac{ke^2}{r}\left(4 - \frac{4}{\sqrt{2}} - 2 + \frac{8}{\sqrt{5}}\right)$$

The quantity in parentheses is the Madelung constant α correct to four terms in the infinite expansion; thus we have that $\alpha \approx 2.749$.

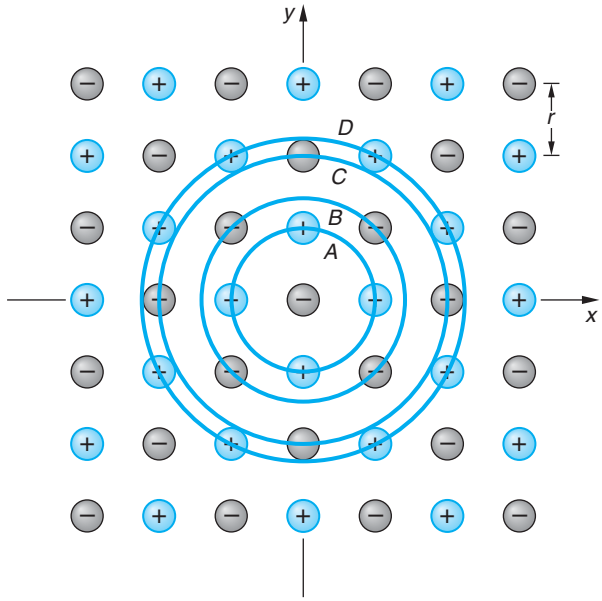

Figure 10-5 A hypothetical univalent two-dimensional ionic crystal (Example 10-3).

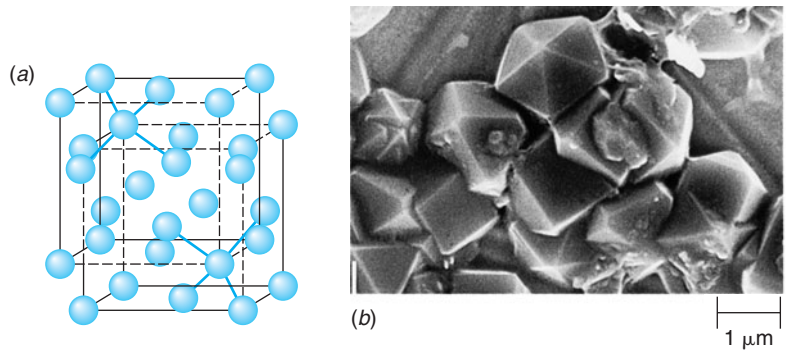

Figure 10-6 (*a*) Diamond crystal structure showing how this structure can be considered to be a combination of two interpenetrating face-centered-cubic structures. (*b*) Synthetic diamonds magnified about 50,000 times. In diamond, each carbon atom is at the center of a tetrahedron formed by four other carbon atoms. [*Courtesy of Chris Kovach/Discover Publications.*]

In covalently bonded crystals the nature of the individual bonds is just like that in covalently bonded molecules, as was described in Section 9-2. The electron-sharing character of the bond enhances its effectiveness in crystals, for example, enabling tetravalent carbon atoms to form bonds with as many as four other carbon atoms. The crystal structure is determined by the directional nature of the bonds. Figure 10-6 illustrates the diamond structure of carbon (which is also the structure of Ge and Si), in which each atom is bonded to four others located at the vertices of a regular tetrahedron as a result of the sp^3 hybridization discussed in the Chapter 9 MORE section *Other Covalent Bonds* on the home page. The diamond structure can be considered to be two interpenetrating face-centered-cubic structures. This arrangement with equal bond angles is particularly tightly bound and results in the carbon diamond structure having one of the largest atomic cohesive energies of all solids, about 7.37 eV per carbon atom. Carbon has two other well-defined crystalline structures, graphite and solid fullerenes,[2] both the result of carbon orbitals hybridized in the sp^2 configuration. In graphite, illustrated in Figure 10-7*a*, three of the valence electrons link each atom to

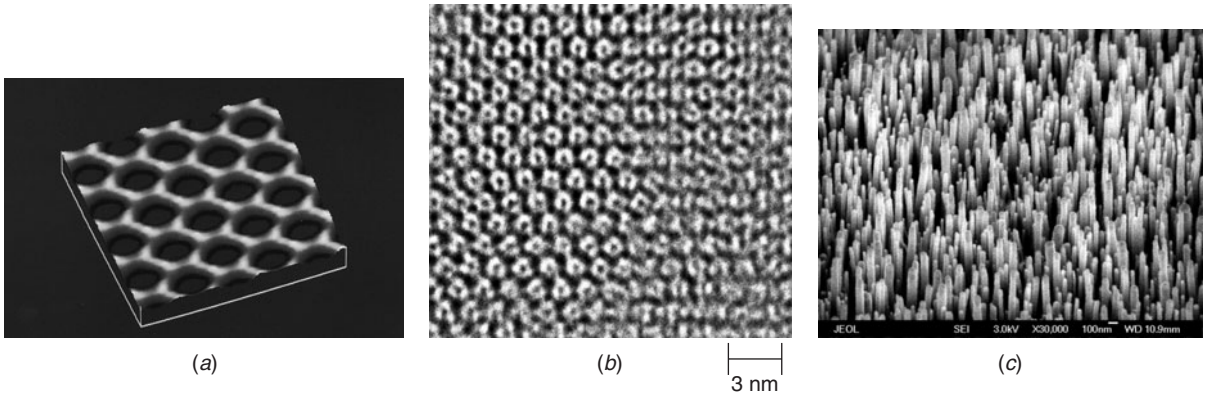

Figure 10-7 (*a*) An atomic-force micrograph of graphite. The brighter spots at each vertex are single carbon atoms. In graphite, carbon atoms are arranged in sheets, each sheet made up of atoms in hexagonal rings. The sheets slide easily across one another, a property that allows graphite to function as a lubricant. [*Courtesy of Srinivas Manne, University of California at Santa Barbara.*] (*b*) This high-resolution transmission electron micrograph shows clearly the close-packed fcc arrangement of the C_{60} molecules in the solid fullerene. [*Courtesy of P. R. Buseck, Science,* ***257****, 215 (1992).*] (*c*) Carbon nanotubes grown on a titanium substrate. The nanotubes are perpendicular to the substrate and range between 40 nm and 100 nm in diameter. [*Courtesy of Z. F. Ren et al., Boston College.*]

three near neighbors via directed bonds, forming a planar hexagonal structure. The planes thus formed are connected by much weaker dipole-dipole forces. This results in a structure consisting of strong sheets that can be readily separated from one another. The structure of the fullerenes, using solid C_{60} as an example, is quite different from that of both diamond and graphite. As described in Section 9-2, the C_{60} molecule achieves its spheroid shape by incorporating 12 pentagons into the hexagonal structure, thus distorting the graphite planes into the soccer-ball configuration. The C_{60} molecules are then bonded to each other by dipole-dipole forces, just as are the sheets of graphite. As a result, the cohesive energy per atom is quite high, about 7.4 eV, or nearly equal to that of diamond, but the cohesive energy per molecule is low, only 1.5 eV. The C_{60} crystal, shown in Figure 10-7*b*, is face-centered-cubic. The equilibrium separation between the molecules is 1.00 nm. The nanotubes shown in Figure 10-7*c* are a remarkable example of carbon's possible bonding configurations.

Racing bicycles and Formula 1 race cars are constructed from woven carbon fibers. They absorb shock extremely well and are lighter and stronger than older bikes and race cars made of steel or aluminum.

Metallic Bonding in Solids

All solid metals, formed from the metal elements that make up more than half of the periodic table, are bonded by the *metallic bond*, which, as was noted earlier, has no single-molecule counterpart. It is somewhat analogous to the covalent bond, in which the atoms of the molecule share one or more electrons. In the metallic bond one or two of the valence electrons of each atom are free to move throughout the solid, and *all* of the atoms share all of those electrons. Thus, the metallic crystal can be pictured as a lattice of fixed, positive ions immersed in an electron gas. It is the attraction between the positively charged lattice and the negatively charged electron gas that results in bonding of the solid.[3]

To see how metallic bonding occurs, let us consider a specific simple example, the bonding of solid lithium. The electron structure of the lithium atom is $1s^2 2s$, and the radial wave function of the $2s$ electron, which "sees" a hydrogenlike core consisting of the nucleus and the completed $1s$ shell, is

$$\psi_{20} = C_{20}\left(2 - \frac{r}{a_0}\right)e^{-r/2a_0} \qquad \textbf{10-8}$$

where C_{20} is a normalization constant and a_0 is the Bohr radius. The probability density corresponding to this wave function for a single lithium atom located at $r = 0$ is shown in one dimension in Figure 10-8*a*. The probability density decays exponentially to zero as r approaches $\pm\infty$. Figure 10-8*b* illustrates the probability density of the electrons in the metal, which must be the same around each Li ion core. The peaks of the probability density are now closer to the positive Li ion core than was the case for the isolated atom. Thus, the potential energy of the electrons has been reduced. However, the effect of assembling the atoms into a lattice has also been to effectively confine the electrons to within about ± 0.3 nm of the ion core rather than the larger volume of the isolated atom. The uncertainty principle then implies an increase in the momentum, hence kinetic energy, of the electrons. The metallic bond is stable because the rise in kinetic energy is more than offset by the decrease in the potential energy, thus lowering the total energy of the system of atoms. The net effect is greatest when the difference in size between the atom and the core is large (so that the magnitude of the potential energy reduction is large) and when the number of valence electrons is small (so that the increase in kinetic energy is as small as possible). These conditions are increasingly satisfied as one moves toward the left across the periodic table.

Even hydrogen becomes a metal under ultrahigh pressure. The pressure reduces the conduction-valence band gap (see Section 10-6) from about 15 eV to 0.3 eV. Understanding metallic hydrogen will be of significant benefit to fusion energy research (see Section 11-8).

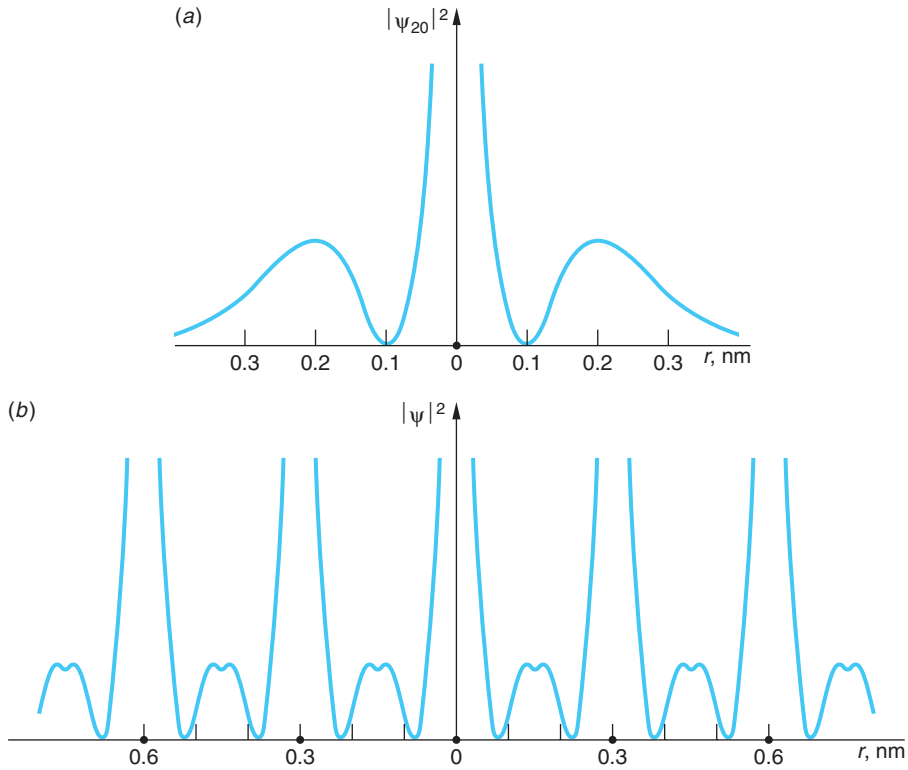

Figure 10-8 (*a*) Probability density for the 2*s* electron in an isolated Li atom. (*b*) Probability density for the 2*s* electrons in a (one-dimensional) Li crystal. The large dots on the *r* axis represent Li nuclei. Note that $|\psi|^2$ is compressed relative to that of the single atom and that an electron is, on the average, confined to within about ± 0.3 nm of a Li nucleus rather than between $\pm\infty$.

Questions

1. Why is r_0 different for solid NaCl than for the diatomic molecule?
2. Why would you not expect NaCl to have an hcp structure?
3. How can you account for the difference in the Madelung constants of NaCl and CsCl?
4. Although it is in the same column of the periodic table as Li, why is solid hydrogen not metallically bonded?

10-2 Classical Theory of Conduction

Because metals conduct electricity so readily, there must be charges in metals that are relatively free to move. The idea that metals contain electrons free to move about through a lattice of relatively fixed positive ions was proposed by the German physicist Paul Drude around 1900, just three years after Thomson's discovery of the electron, and was developed by H. A. Lorentz in about 1909. This microscopic model, now called the *classical model of electrical conduction*, successfully predicts Ohm's law and relates electrical conduction and heat conduction to the motion of free electrons in conductors. However, the model gives the wrong temperature dependence for electrical conductivity, and it predicts that the heat capacity of metals should be greater than that of insulators by $(3/2)R$ per mole, which is not observed. Despite these failures, the classical free-electron theory is a good starting point for a more sophisticated treatment

FEUE WHE

of metals based on quantum mechanics. For that reason, a discussion of the classical theory is included in the Classical Concept Review on the Web page. In this section we will briefly outline those predictions from classical theory that are pertinent to our subsequent discussion of the quantum mechanical theory of conduction. As we will see, the main defects in the classical theory are the use of the classical Maxwell-Boltzmann distribution function for electrons in a conductor and the treatment of the scattering of electrons by the lattice as a classical particle scattering.

Electrical Conduction

The classical model of a metal is a regular three-dimensional array of atoms or ions with a large number of electrons free to move throughout the entire metal. In the absence of an applied electric field the average speed of these electrons is quite high. For example, at $T = 300$ K, their average speed is

$$\langle v \rangle = \sqrt{\frac{8kT}{\pi m_e}} = \sqrt{\frac{8(1.38 \times 10^{-23}\ \text{J/K})(300\ \text{K})}{\pi(9.11 \times 10^{-31}\ \text{kg})}} = 1.08 \times 10^5\ \text{m/s} \qquad \textbf{10-9}$$

Applying an electric field $\mathscr{E}$ superimposes a *drift velocity* $\mathbf{v}_d$ on the free electrons that is opposite to the field direction. For n electrons per unit volume, the resulting current I in the conductor, the charge ΔQ through a cross-sectional area A per unit time (see Figure 10-9), is

$$I = \frac{\Delta Q}{\Delta t} = neAv_d \qquad \textbf{10-10}$$

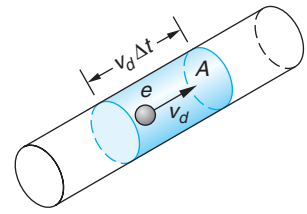

Figure 10-9 In time Δt, all the charges in the shaded volume pass through A. If there are n charge carriers per unit volume, each with charge e, the total charge in this volume is $\Delta Q = nev_dA\ \Delta t$, where v_d is the drift velocity of the charge carriers. The total current is then $I = \Delta Q/\Delta t = nev_dA$.

In contrast to the average speed of the electrons due to their thermal motion, the drift velocity is quite low, as Example 10-4 illustrates for copper.

EXAMPLE 10-4 **Drift Velocity of Electrons in Copper** What is the magnitude of the drift velocity of electrons in a typical copper wire of radius 0.815 mm carrying a current of 1 A?

SOLUTION

If we assume one free electron per copper atom, the density of free electrons is the same as the density of atoms n_a, which is related to the mass density ρ, Avogadro's number N_A, and the molar mass M by

$$n_a = \frac{\rho N_A}{M}$$

For copper $\rho = 8.92\ \text{g/cm}^3$ and $M = 63.5\ \text{g/mol}$. Then

$$n_a = \frac{(8.93\ \text{g/cm}^3)(6.02 \times 10^{23}\ \text{atoms/mol})}{63.5\ \text{g/mol}} = 8.47 \times 10^{22}\ \text{atoms/cm}^3$$

The density of electrons is then

$$8.47 \times 10^{22}\ \text{electrons/cm}^3 = 8.47 \times 10^{28}\ \text{electrons/m}^3$$

The magnitude of the drift velocity is therefore

$$v_d = \frac{I}{Ane} = \frac{1\ \text{C/s}}{\pi(0.000815\ \text{m})^2(8.47 \times 10^{28}\ \text{m}^{-3})(1.60 \times 10^{-19}\ \text{C})} \approx 3.54 \times 10^{-5}\ \text{m/s}$$

We see that typical drift velocities are of the order of 0.01 mm/s, which is quite small. Notice in particular that the magnitude of the drift velocity is very small compared with the average speed of the electrons due to their thermal energy as given by Equation 10-9. Indeed, the difference is approximately 10 orders of magnitude.

According to Ohm's law, the current in a conducting wire segment is proportional to the voltage drop across the segment $I \propto V$. The constant of proportionality is $1/R$, so that $I = V/R$. The resistance R of the wire is independent of both I and V, being proportional to the length of the wire L divided by its cross-sectional area A: $R = \rho L/A$. The constant of proportionality ρ is called the *resistivity* of the conductor material. Combining these two expressions and recalling that the electric field in the wire is $\mathscr{E} = V/L$, Equation 10-10 enables us to write

$$v_d = \frac{j}{ne} \qquad \textbf{10-11}$$

where $j = I/A$ is the *current density*. For materials that obey Ohm's law, the resistivity and, of course, its reciprocal the *conductivity* σ must be independent of $\mathscr{E}$.

Mean Free Path λ

The objective of the classical theory of conduction is to find an expression for ρ in terms of the properties of the conductor, a task that is aided by a consideration of the average distance an electron travels in the conductor between collisions, called the *mean free path* λ. It is the product of the average speed $\langle v \rangle$ and the average time between collisions τ, called the *relaxation time*:

$$\lambda = \langle v \rangle \tau = 1/n_a \pi r^2 \qquad \textbf{10-12}$$

where n_a is the number of ions per unit volume and r is the ion radius. As an example, λ for copper is about 0.38 nm. In terms of λ the resistivity and conductivity are given by

$$\rho = \frac{m_e \langle v \rangle}{ne^2 \lambda} \quad \text{and} \quad \sigma = \frac{ne^2 \lambda}{m_e \langle v \rangle} \qquad \textbf{10-13}$$

In Example 10-5 we compute the classical values for the resistivity and conductivity for copper, which illustrates a basic defect in the classical theory of conduction.

EXAMPLE 10-5 Conductivity and Resistivity of Copper Calculate the values of the resistivity and the conductivity of copper at 300 K.

SOLUTION

Using Equations 10-12 and 10-13, we have

$$\tau = \lambda/\langle v \rangle = (0.38 \times 10^{-9}\,\text{m})/(1.08 \times 10^{5}\,\text{m/s}) = 3.52 \times 10^{-15}\,\text{s}$$

and then

$$\begin{aligned} \rho &= \frac{m_e \langle v \rangle}{ne^2 \lambda} = \frac{m_e}{ne^2 \tau} \\ &= \frac{9.11 \times 10^{-31}\,\text{kg}}{(8.47 \times 10^{28}\,\text{electrons/m}^3)(1.60 \times 10^{-19}\,\text{C})^2(3.52 \times 10^{-15}\,\text{s})} \\ &= 1.19 \times 10^{-7}\,\Omega \cdot \text{m} \end{aligned}$$

FÈUE WHE

and $$\sigma = 1/\rho = 8.33 \times 10^6 (\Omega \cdot \mathrm{m})^{-1}$$

Remarks: *This value for the resistivity is about 7 times greater than the measured value of* $1.7 \times 10^{-8}\ \Omega \cdot m$.

Defects in the Classical Theory

At first glance it is surprising that any material obeys Ohm's law since in the presence of an electric field, a free electron experiences a force of magnitude $e\mathscr{E}$. If this were the only force acting on the electron, it would have acceleration $e\mathscr{E}/m_e$ and its velocity would steadily increase. However, the agreement of Ohm's law with experiment implies that there is a steady-state situation in which the drift velocity of the electron is proportional to the field $\mathscr{E}$ because the current I is proportional to both $\mathscr{E}$ and v_d, i.e., $v_d = j/ne = \sigma\mathscr{E}/ne$. In the classical model, it is assumed that a free electron is accelerated for a short time and then collides with a lattice ion. After the collision, the velocity of the electron is assumed to be completely unrelated to that before the collision. The justification for this assumption is that, as we have seen, the drift velocity is very small compared to the average thermal velocity. With the average speed given by Equation 10-9 and the mean free path by Equation 10-12, the resistivity has been expressed in terms of the properties of metals, which was the objective of the classical theory of conduction. According to Ohm's law, the resistivity is independent of the electric field $\mathscr{E}$. The only quantities in Equation 10-13 that might depend on the electric field are the average speed $\langle v \rangle$ and the mean free path λ. As we have seen, the drift velocity, a result of the applied electric field, is very much smaller than the average thermal speed of the electrons in equilibrium with the lattice ions. Thus, the electric field has essentially no effect on the average speed of the electrons. The mean free path of the electrons depends on the size of the lattice ions and on the density of the ions, neither of which depends on the electric field $\mathscr{E}$. Thus the classical model predicts Ohm's law with the resistivity as given by Equation 10-13.

Although successful in predicting Ohm's law, the classical theory of conduction has several defects. We saw from Example 10-5 that the magnitude of the resistivity of copper calculated from Equation 10-13 is about 7 times the measured value at $T = 300$ K. The temperature dependence of ρ is also not correct. Experimentally, the resistivity varies linearly with temperature over a wide range of temperatures. The temperature dependence of resistivity in Equation 10-13 is given completely by the speed $\langle v \rangle$, which according to Equation 10-9 is proportional to $T^{1/2}$. Thus, this calculation does not give a linear dependence on temperature. Finally, the classical model says nothing about why some materials are conductors, others insulators, and still others semiconductors.

In the quantum-mechanical theory of electrical conduction, which is discussed in Section 10-4, the resistivity is again given by Equation 10-13, but the average speed and the mean free path are interpreted in terms of quantum theory. We discovered in Section 8-5 that the average energy of the electrons, hence their average speed, is not proportional to $T^{1/2}$, but is approximately independent of T because electrons do not obey the Boltzmann distribution law, but instead obey the Fermi-Dirac distribution. Also, in the quantum-mechanical calculation of the mean free path the wave nature of the electron is important and must be taken into account.

FEUE WHE

Heat Capacity

If the electron gas in metals were a classical ensemble of identical distinguishable particles, it would obey Boltzmann statistics (see Chapter 8) and have the Maxwell distribution of speeds. It should then have an average kinetic energy $(3/2)kT$, and we would expect the molar heat capacity of a metal to be $(3/2)R$ greater than that of an insulator—that is, $3R$ from the lattice vibrations (rule of Dulong and Petit—see Section 8-1) and $(3/2)R$ from the electron gas:

$$C_v = (3R)_{\text{lattice vibrations}} + (3/2)R_{\text{electron gas}} = (9/2)R$$

As was noted in Section 8-5, this is not observed. The molar heat capacity of metals is very nearly $3R$. At higher temperatures it is slightly greater, but the increase is nowhere near the value of $(3/2)R$ predicted by the classical theory. The increase is, in fact, proportional to temperature, and at $T = 300$ K, it is only about $0.02R$.

10-3 Free-Electron Gas in Metals

Classically, at $T = 0$, all the electrons in a metal would have zero kinetic energy. As a conductor is heated, the lattice ions acquire an average kinetic energy of $(3/2)kT$, which is imparted to the electron gas by interactions of the lattice with the electrons. The electrons classically would be expected to have a mean kinetic energy of $(3/2)kT$ in equilibrium. Quantum mechanically, however, since the electrons are confined to the space occupied by the metal, it is clear from the uncertainty principle that even at $T = 0$, an electron cannot have zero kinetic energy. Furthermore, the exclusion principle prevents more than two electrons (with opposite spins) from being in the lowest energy level. At $T = 0$, we expect the electrons to have the lowest energies consistent with the exclusion principle. This is illustrated clearly by first considering a one-dimensional model that provides us with the foundation needed for the quantum theory of conduction in Section 10-4.

One-Dimensional Model

To simplify visualization, let us first consider N electrons in a one-dimensional infinite square well of width L. The physical analog of such a model could be a long, thin metal wire. As we have seen previously, the allowed energies are given by

$$E_n = \frac{n^2h^2}{8mL^2} = n^2E_1 \qquad \textbf{10-14}$$

where m is the electron mass and $E_1 = h^2/8mL^2$ is the energy of the ground state. Since two electrons can be put in the $n = 1$ level, two in the $n = 2$ level, etc., at $T = 0$, the N electrons in the system will fill $N/2$ levels, i.e., from the $n = 1$ to the $n = N/2$ state. (See Figure 10-10*a*.) The energy of the last filled level (or half-filled level, if N happens to be odd) is the Fermi energy, which for our one-dimensional system is

$$E_F = E_{N/2} = \frac{(N/2)^2h^2}{8mL^2} = \frac{h^2}{32m}\left(\frac{N}{L}\right)^2 \qquad \textbf{10-15}$$

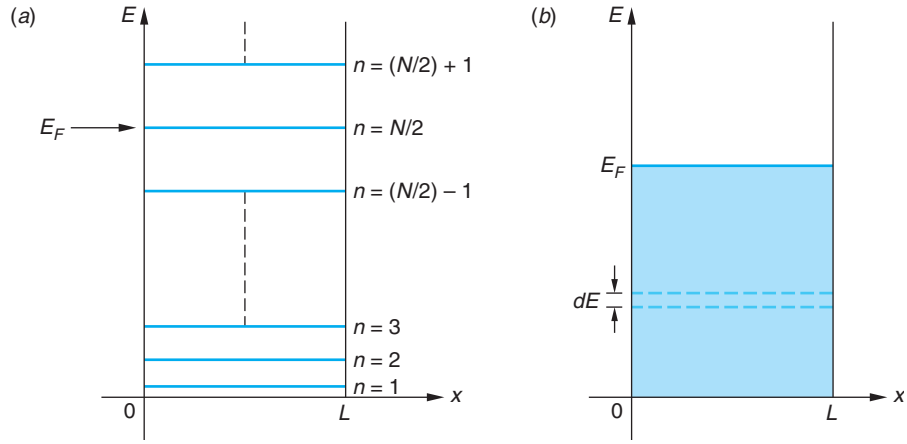

Figure 10-10 (*a*) A one-dimensional infinite square well for N electrons at $T = 0$ K. Two electrons, one with spin up and one with spin down, occupy each level. The Fermi energy is the energy of the level with $n = N/2$, the highest occupied level. (*b*) The levels are so closely spaced, they can be assumed to be continuous. The density of states $g(E)$ is the number of states between E and $E + dE$ divided by dE.

We see that the Fermi energy is a function of the number of electrons per unit length, which is the *number density* or number per unit volume in one dimension. The number density of electrons in copper, computed in Example 10-4, is $8.47 \times 10^{28}/\text{m}^3$. In one dimension this corresponds to

$$\frac{N}{L} = (8.47 \times 10^{28}/\text{m}^3)^{1/3} = 4.40 \times 10^9/\text{m} = 0.440/\text{Å} = 4.40/\text{nm}$$

Using this value, we see that the Fermi energy for a one-dimensional copper system, such as a wire, is

$$E_F = \frac{(hc)^2}{32mc^2}\left(\frac{N}{L}\right)^2 = \frac{(1240\ \text{eV}\cdot\text{nm})^2(4.40/\text{nm})^2}{(32)(5.11 \times 10^5\ \text{eV})} = 1.82\ \text{eV}$$

This value is much larger than the room temperature value of kT, which is about 0.026 eV. The average energy of the electrons is the total energy divided by N:

$$\langle E \rangle = \frac{1}{N}\sum_{n=1}^{N/2} 2n^2 E_1$$

where the factor of 2 accounts for the two electrons in each energy state. Since $N/2 \gg 1$, the summation can be replaced by an integral, so we have that

$$\langle E \rangle = \frac{E_1}{N}\int_0^{N/2} 2n^2\, dn = \frac{E_1}{N}\frac{2}{3}\left(\frac{N}{2}\right)^3 = \frac{h^2}{8mL^2}\frac{2}{3N}\left(\frac{N}{2}\right)^3 = \frac{1}{3}E_F \qquad \textbf{10-16}$$

Our one-dimensional calculation thus gives an average energy for copper's free electrons of about 0.6 eV at $T = 0$. This is 15 times the room-temperature average kinetic energy of molecules in the atmosphere. The temperature at which the average energy would be 0.6 eV for a one-dimensional Boltzmann distribution is about 14,000 K, obtained from $\frac{1}{2}kT = 0.6$ eV.

The expression for the number $n(E)$ of electrons with energy E in the one-dimensional system follows from Equation 8-37*c*:

$$n(E)\,dE = g(E)f_{FD}(E)\,dE$$

where $f_{FD}(E) = 1$ for $T = 0$ K and $E < E_F$ and $f_{FD}(E) = 0$ for $T = 0$ K and $E > E_F$. The density of states $g(E)$ is the number dn of states between E and $E + dE$ divided by dE and multiplied by 2 to account for the two spin states per space state (see Figure 10-10*b*):

$$g(E) = 2\frac{dn}{dE}$$

Since $E = n^2E_1$, then $dE = 2E_1 n\,dn = 2E_1^{1/2}E^{1/2}\,dn$ and we have that

$$g(E) = E_1^{-1/2}E^{-1/2}$$

The number of electrons with energy E at $T = 0$ K in the one-dimensional conductor is then

$$n(E) = \begin{cases} E_1^{-1/2}E^{-1/2} & \text{for} \quad E < E_F \\ 0 & \text{for} \quad E > E_F \end{cases} \qquad \textbf{10-17}$$

Three-Dimensional Electron Gas

Now let us extend the discussion to three-dimensional systems. The Fermi energy can be computed from the general expression for the number of fermions $n_{FD}(E)$ given by Equation 8-37*c*. The number density N/V of electrons in three dimensions, where V is the volume of the metal, is

$$\frac{N}{V} = \frac{1}{V}\int_0^\infty n_{FD}(E)\,dE = \frac{\pi}{2}\left(\frac{8m}{h^2}\right)^{3/2}\int_0^\infty \frac{E^{1/2}\,dE}{e^{(E-E_F)/kT} + 1} \qquad \textbf{10-18}$$

For arbitrary values of T, Equation 10-18 must be evaluated numerically, but for $T = 0$ K, the solution is straightforward since, as noted above, $f_{FD}(E) = 0$ or 1 as E is greater than or less than E_F. In that event, we have that

$$\frac{N}{V} = \frac{\pi}{2}\left(\frac{8m}{h^2}\right)^{3/2}\int_0^{E_F} E^{1/2}\,dE = \frac{\pi}{2}\left(\frac{8m}{h^2}\right)^{3/2}\frac{2}{3}E_F^{3/2} \qquad \textbf{10-19}$$

Solving for E_F we have for $T = 0$ K that

$$E_F = \frac{h^2}{2m}\left(\frac{3N}{8\pi V}\right)^{2/3} \qquad \textbf{10-20}$$

Table 10-3 lists the number density of free electrons for several elements. Notice that E_F increases slowly with N/V, as would be expected at $T = 0$ K since all states up to E_F are being filled and an increasing N/V requires more states to be filled, i.e., a larger value of E_F. The number $n(E)$ of electrons with energy E is then given by

$$n(E) = \frac{\pi}{2}\left(\frac{8m}{h^2}\right)^{3/2}VE^{1/2} = \frac{3N}{2}E_F^{-3/2}E^{1/2} \qquad \textbf{10-21}$$

FEUE WHE

Table 10-3 Free-electron number densities, Fermi energies, and Fermi temperatures for selected elements

Element	$N/V(\times 10^{28}\ \mathrm{m}^{-3})$	Fermi energy (eV)	Fermi temperature ($\times 10^4$ K)
Al	18.1	11.7	13.6
Ag	5.86	5.53	6.41
Au	5.90	5.55	6.43
Cu	8.47	7.06	8.19
Fe	17.0	11.2	13.0
K	1.40	2.13	2.47
Li	4.70	4.77	5.53
Mg	8.61	7.14	8.28
Mn	16.5	11.0	12.8
Na	2.65	3.26	3.78
Sn	14.8	10.3	11.9
Zn	13.2	9.50	11.0

and the average energy of an electron at $T = 0$ K by

$$\langle E\rangle = \frac{1}{N}\int_0^{E_F} E\,n(E)\,dE = \frac{3}{2}E_F^{-3/2}\int_0^{E_F} E^{3/2}\,dE = \frac{3}{5}E_F \qquad \textbf{10-22}$$

At temperatures greater than zero, some electrons will gain energy and occupy higher energy states. However, electrons cannot move to a higher or lower energy state unless the state is unoccupied. Since the kinetic energy of the lattice ions is of the order of kT, electrons cannot gain much more energy than kT in collisions with the lattice; therefore, only those electrons with energies within about kT of the Fermi energy can gain energy as the temperature is increased.

At $T = 300$ K, kT is only 0.026 eV, so the exclusion principle prevents all but a very few electrons near the top of the energy distribution from gaining energy by random collisions. Figure 10-11 shows the small fraction of the free electrons that move at $T = 300$ K (shaded rectangle at the Fermi energy of the $T = 0$ K curve). *Even for temperatures as high as several thousand degrees, the energy distribution of an electron gas does not differ very much from that at* $T = 0$ K.

For values of $T > 0$, we must remember that the Fermi energy is defined by Equation 8-68, since for $T > 0$, there is no state below which all states are full and above which all states are empty. Equation 8-68 defines the Fermi energy as that energy for which $f_{FD}(E) = \frac{1}{2}$. For all but extremely high temperatures, the difference between the Fermi energy at temperature T, $E_F(T)$ and that at $T = 0$ K, $E_F(0)$ is essentially negligible. As is clear from Equation 8-68 and Figure 8-31*b*, the value of $f_{FD}(E)$ at arbitrary T differs from that at $T = 0$ K only for those energies within about kT of the Fermi energy.

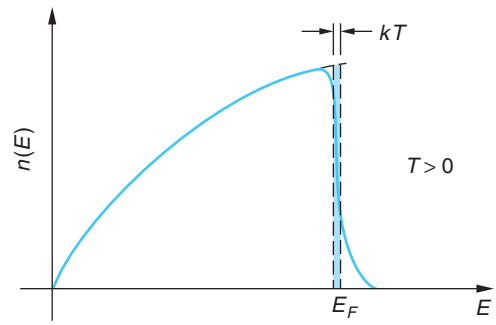

Figure 10-11 The fraction of the N electrons in the metal that contribute to C_v is the ratio of the shaded rectangle to the total area under the $n(E)$ versus E curve.

Fermi Temperature

It is convenient to define the *Fermi temperature* T_F by

$$E_F = kT_F \tag{10-23}$$

For temperatures much lower than the Fermi temperature, the average energy of the lattice ions will be much less than the Fermi energy; thus the electron energy distribution will not differ greatly from that at $T = 0$. The Fermi temperature corresponding to $E_F = 7.0$ eV for copper is about 81,900 K. Table 10-3 lists the Fermi temperatures for several elements. At temperatures much larger than the Fermi temperature (i.e., much larger than 81,900 K for copper) $f_{FD}(E)$ approaches $e^{-E/kT}$ and the Fermi-Dirac distribution approaches the Boltzmann distribution. This result is not very important for the understanding of the behavior of conductors since there are no conductors that remain as solids or even liquids at such extreme temperatures.

EXAMPLE 10-6 **Fermi Energy and Temperature of Silver** Compute (*a*) the Fermi energy and (*b*) the Fermi temperature for silver at 0 K.

SOLUTION

The density of silver is 10.50 gm/cm^3, and its molecular weight is 107.9 gm/mol. If each silver atom is assumed to contribute one electron to the Fermi gas, the number density N/V is computed as follows:

$$\frac{N}{V} = (10.50 \text{ g/cm}^3)(1/107.9 \text{ g/mol})(6.02 \times 10^{23} \text{ electrons/mol})$$
$$= 5.86 \times 10^{22} \text{ electrons/cm}^3 = 5.86 \times 10^{28} \text{ electrons/m}^3$$

which agrees with the entry in Table 10-3.

(*a*) The Fermi energy is then, from Equation 10-20,

$$E_F = \frac{(6.63 \times 10^{-34} \text{ J} \cdot \text{s})^2}{2(9.11 \times 10^{-31} \text{ kg})} \left(\frac{3 \times 5.86 \times 10^{28}}{8\pi} \right)^{2/3}$$
$$= 8.84 \times 10^{-19} \text{ J} = 5.53 \text{ eV}$$

in agreement with the entry for Ag in Table 10-3.

(*b*) The Fermi temperature is then

$$T_F = \frac{E_F}{k} = \frac{8.84 \times 10^{-19} \text{ J}}{1.38 \times 10^{-23} \text{ J/K}} = 6.41 \times 10^4 \text{ K}$$

again, in agreement with Table 10-3.

10-4 Quantum Theory of Conduction

With two relatively simple but important quantum-mechanical modifications of the classical free-electron theory, we can understand the electrical conductivity, heat capacity, and thermal conductivity of metals. First, we must replace the classical Boltzmann distribution with the Fermi distribution of energies in the electron gas, as was discussed in Section 8-5. Second, we must consider the effect of the wave properties of the electrons on their scattering by the lattice ions. We will discuss the latter modification qualitatively.

FEUE WHE

Electrical Conduction

We might expect that most of the electrons would not participate in the conduction of electricity because of the exclusion principle, but this is not the case because the electric field accelerates all the electrons together. Figure 10-12 shows the Fermi-Dirac distribution function versus velocity for some temperature T that is small compared with T_F (such as $T = 300$ K). The function is approximately 1 for $-u_F < v_x < +u_F$, where the *Fermi speed* u_F is the speed corresponding to the Fermi energy:

$$u_F = \left(\frac{2E_F}{m_e}\right)^{1/2} \qquad \textbf{10-24}$$

EXAMPLE 10-7 Fermi Speed in Al Compute the Fermi speed of electrons in aluminum.

SOLUTION

From Table 10-3, the Fermi energy E_F of Al is 11.7 eV. Thus,

$$u_F(\text{Al}) = \left(\frac{2 \times 11.7\ \text{eV} \times 1.60 \times 10^{-19}\ \text{J/eV}}{9.11 \times 10^{-31}\ \text{kg}}\right)^{1/2} = 2.03 \times 10^6\ \text{m/s}$$

The dashed curve in Figure 10-12 shows the Fermi distribution after the electric field has been acting for some time t. Although all of the electrons have been shifted to higher velocities, the net effect is equivalent to shifting only the electrons near the Fermi level; therefore, we can use the classical equations for the resistivity and conductivity (Equations 10-13) if we use the Fermi speed u_F in place of $\langle v \rangle$:

$$\rho = \frac{1}{\sigma} = \frac{m_e u_F}{ne^2\lambda} \qquad \textbf{10-25}$$

We now have two problems. First, since u_F is independent of temperature (to a very good approximation), the above expression for σ and ρ is independent of temperature unless the mean free path depends on it. The second problem concerns the magnitudes. We saw in Example 10-5 that the classical expression for σ yielded a result that was too small by a factor of 7, using $\langle v \rangle$ calculated from the Maxwell-Boltzmann distribution. Since u_F is about 19 times the value of $\langle v \rangle$, the magnitude of σ predicted from Equation 10-25 will be even smaller by another factor of 19 and the magnitude of ρ will, correspondingly, be larger than the observed value by the same factor.

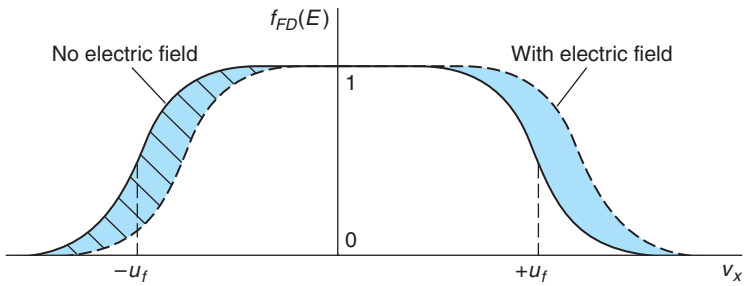

Figure 10-12 Occupation probability $f_{FD}(E)$ versus velocity in one dimension, with no electric field and with an electric field in the $+x$ direction. The difference is greatly exaggerated.

The resolution of both of these problems lies in the way that the value of the mean free path is calculated. If we use u_F from Equation 10-24 and the experimental value $\rho \approx 1.7 \times 10^{-8}\ \Omega \cdot \text{m}$ for copper in Equation 10-25, we obtain for the mean free path $\lambda \approx 39$ nm, about 100 times the value of 0.38 nm, which was noted in Section 10-2 for Cu ions.

We shouldn't be too surprised that the mean free path of electrons in the copper lattice is not given correctly by classical kinetic theory. The reason for this large discrepancy between the classical calculation of the mean free path and the "experimental" result calculated from Equation 10-25 is that the wave nature of the electron must be taken into account. The collision of an electron with a lattice ion is not similar to the collision of a baseball and a tree. Instead, it involves the scattering of the electron wave by the regularly spaced ions of the lattice. If the wavelength is long compared with the crystal spacing, as is approximately the case here (see Problem 10-55), Bragg scattering cannot occur. Detailed calculations of the scattering of electron waves by a *perfectly* ordered crystal of infinite extent show that there is *no scattering*, and the mean free path is infinite. *Thus, the scattering of electron waves must arise from imperfections in the crystal lattice.* The most common imperfections are due to impurities and to thermal vibrations of the lattice ions.

In Equation 10-12, for the classical mean free path, the quantity πr^2 can be thought of as the cross-sectional area of the lattice ions as seen by the electron, where r is the ion radius. Figure 10-13*a* depicts the classical picture in which the lattice ions have area πr^2. According to quantum mechanics applied to the scattering of electron waves, however, the "area" of the ion's cross section seen by the electron wave has nothing to do with the size of the ion. Instead, it depends upon the *deviations* of the lattice ions from a perfectly ordered array. We can estimate the magnitude of the deviations and thus compute a more accurate value for the mean free path in the following way.

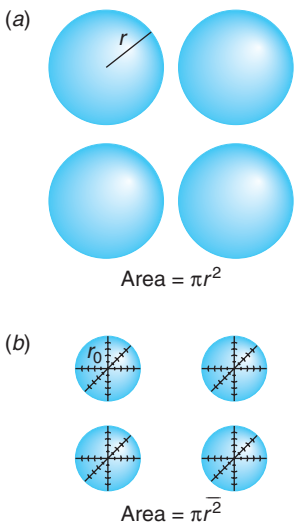

Figure 10-13 (*a*) Classical picture of the lattice ions as spherical balls of radius r that present an area πr^2 to the electrons. (*b*) Quantum-mechanical picture of the lattice ions as points that are vibrating in three dimensions. The area presented to the electrons is $\pi \overline{r_0^2}$, where r_0 is the amplitude of oscillation of the ions.

Let us assume that the lattice ions are *points* that are vibrating because of their thermal energy. (See Figure 10-13*b*.) We will take for the scattering cross section $\pi \overline{r^2}$, where $\overline{r^2} = \overline{x^2} + \overline{y^2}$ is the mean-square displacement of the point atom in a plane perpendicular to the direction of the electron's motion and represents a measure of the deviation of the ion from its equilibrium location. We can calculate $\overline{r^2}$ from the equipartition theorem. We have

$$\frac{1}{2}K\overline{r^2} = \frac{1}{2}M\omega^2\overline{r^2} = kT \qquad \textbf{10-26}$$

where K is the force constant, M is the mass of the ion, and $\omega = (K/M)^{1/2}$ is the angular frequency of vibration. The mean free path is then

$$\lambda = \frac{1}{n\pi\overline{r^2}} = \frac{M\omega^2}{2\pi nk}\frac{1}{T} \qquad \textbf{10-27}$$

We thus see that this argument gives the correct temperature dependence for σ and ρ; that is, $\rho \propto 1/\lambda$ (Equation 10-25), and so $\rho \propto T$ rather than $\rho \propto T^{1/2}$, as was obtained from the classical calculation.

We can then calculate the magnitude of $\overline{r^2}$, and therefore λ, using the Einstein model of a solid, which is fairly accurate except at very low temperatures. In the Einstein model (see Section 8-4) all the atoms vibrate with the same frequency. The Einstein temperature was defined by Equation 8-63 as

$$kT_E = hf = \hbar\omega$$

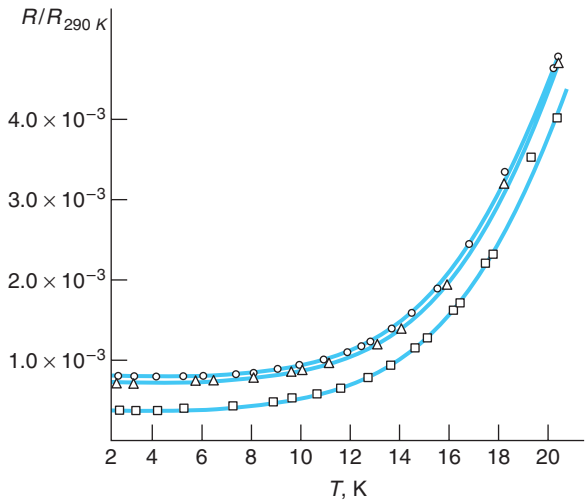

Figure 10-14 Relative resistance versus temperature for three samples of sodium. The three curves have the same temperature dependence but have different magnitudes because of differing amounts of impurities in the samples. [*From D. MacDonald and K. Mendelssohn, Proceedings of the Royal Society, A202, 103 (1950).*]

Using this for ω, we have

$$\overline{r^2} = \frac{2kT}{M\omega^2} = \frac{2T\hbar^2}{MkT_E^2} = \frac{2(\hbar c)^2}{Mc^2kT_E}\frac{T}{T_E} \qquad \textbf{10-28}$$

The Einstein temperature for copper is about 200 K, corresponding to an energy of $kT_E = 0.0172$ eV. Using this and $Mc^2 = 63.5 \times 931$ MeV for the mass of a copper ion, the value of $\overline{r^2}$ at $T = 300$ K is

$$\overline{r^2} = \frac{2(197.3 \text{ eV} \cdot \text{nm})^2}{(63.5 \times 931 \times 10^6 \text{ eV})(0.0172 \text{ eV})}\frac{300 \text{ K}}{200 \text{ K}} = 1.14 \times 10^{-4} \text{ nm}^2$$

Since this is about 100 times smaller than the area presented by a copper ion of radius 0.1 nm, the mean free path is about 100 times larger than that calculated from the classical model, in agreement with that calculated from the measured value of the conductivity. We see, therefore, that *the free-electron model of metals gives a good account of electrical conduction if the classical average speed is replaced by the Fermi speed u_F and if collisions are interpreted in terms of the scattering of electron waves for which only deviations from a perfectly ordered lattice are important.*

The presence of impurities in a metal also causes deviations from perfect regularity in the crystal. The effects of impurities on resistivity are approximately independent of temperature. The resistivity of a metal containing impurities can be written $\rho = \rho_t + \rho_I$, where ρ_t is due to the thermal motion of the lattice and ρ_I is due to impurities. Figure 10-14 shows a typical resistance versus temperature curve for a metal with impurities. As the temperature approaches zero, ρ_t approaches zero and the resistivity approaches the constant ρ_I.

Heat Capacity

Next, let's estimate the contribution of the electron gas to the molar heat capacity. At $T = 0$, the average energy of the electron, given by Equation 10-22, is $(3/5)E_F$, so the total energy for N electrons is $U = (3/5)NE_F$. At a temperature T, only those electrons near the Fermi level can be excited by random collisions with the lattice ions, which have

FEUE WHE

an average energy of the order of kT. The fraction of the electrons that are excited is of the order kT/E_F, and their energy is increased from that at $T = 0$ by an amount of the order of kT. We can thus write for the energy of the N electrons at temperature T,

$$U = \frac{3}{5}NE_F + \alpha N\frac{kT}{E_F}kT \qquad \textbf{10-29}$$

where α is some constant, which we expect to be of the order of 1 if our reasoning is correct. The calculation of α requires the use of the complete Fermi electron distribution at an arbitrary temperature T and is quite difficult. Such a calculation, first carried out by A. A. Sommerfeld, shows that this equation is correct with $\alpha = \pi^2/4$. Using this result, the contribution of the electrons to the molar heat capacity is

$$C_v(\text{electrons}) = \frac{dU}{dT} = 2\alpha Nk\frac{kT}{E_F} = \frac{\pi^2}{2}R\frac{T}{T_F} \qquad \textbf{10-30}$$

Understanding quantum theory of heat conduction and heat capacity has made possible such devices as "high-tech" frozen yogurt/ice cream makers for consumers. Using specially designed working fluids, they are replacing the old salt/ice-in-a-bucket freezers because of their convenience.

where $Nk = R$ for 1 mole and $T_F = E_F/k$ is the Fermi temperature. We see that because of the large value of T_F, the contribution of the electron gas is a small fraction of R at ordinary temperatures. Using $T_F = 81{,}900$ K for copper, the molar heat capacity of the electron gas at $T = 300$ K is

$$C_v = \frac{\pi^2}{2}\left(\frac{300}{81{,}900}\right)R = 0.018R$$

which is in reasonable agreement with the value estimated from the small fraction of electrons with energies greater than E_F in Figure 10-11 and in good agreement with experiment.

More

Quantum theory readily accounts for heat conduction, predicting results in good agreement with observations. *Thermal Conduction—The Quantum Model* is outlined briefly on the home page: www.whfreeman.com/tiplermodernphysics5e. See also Equations 10-31 and 10-32 here.

Questions

5. When the temperature is lowered from 300 K to 4 K, the resistivity of pure copper drops by a much greater factor than that of brass. Why?
6. Explain why, physically, you would expect the mean free path of electrons in a metal to decrease as the temperature increases.

10-5 Magnetism in Solids

Electron spins with their associated magnetic moments are the origin of magnetism in solids. If the atoms of the solid have unpaired spins, the solid itself may have a net magnetic moment. Since the atoms are effectively fixed in one or another of the several crystalline structures, the interactions between them may have a substantial effect on the magnetism exhibited by the solid. Several types of magnetism are observed in solids, *ferromagnetism* being perhaps the most familiar, though hardly the most common, among elements and compounds. In this section we will describe each of the several types.

FEUE WHE

Paramagnetism

Consider a solid consisting of atoms that each have an unpaired electron spin; that is, each atom has a net spin of $\frac{1}{2}$ (actually $\sqrt{3/4}\hbar$, of course) and the atoms do not interact magnetically. Examples of such solids are the rare earth elements and many of the transition elements. In that event, the only magnetic energy the system may have results from interaction with an applied external field **B**. Such a solid, one with no net magnetic moment in the absence of an applied external field, is called *paramagnetic*.

The magnetic moment of each atom is thus that of the unpaired electron $\boldsymbol{\mu} = g_s \mu_s \mathbf{s}/\hbar$. Its z component is given by Equation 7-49:

$$\mu_z = -m_s g_s \mu_B \qquad \textbf{7-49}$$

where g_s is the g factor for the electron and μ_B is the Bohr magneton. In an applied field **B**, whose direction provides the atom with an external z axis, the possible energies of the magnetic moment are

$$U = -\mu_z B \qquad \textbf{7-47}$$

or

$$U = m_s g_s \mu_B B \qquad \textbf{10-33}$$

Since $m_s = \pm 1/2$, the $m_s = -1/2$ orientation of **s** (called "spin down" because **s** is antiparallel to **B**) is of lower energy than the $m_s = +1/2$ orientation (called "spin up," of course). Thus, in a thermal distribution the spin-down states will contain more atoms than the spin-up states and the solid will have a net magnetic moment per unit volume **M** whose magnitude is given by

$$M = \mu(\rho_+ - \rho_-)$$

where ρ_+ and ρ_- are the densities of electrons with spin-up and spin-down, respectively. Since $\rho_- > \rho_+$ and μ is negative, M is positive. For sufficiently small fields **M** is proportional to **B**:

$$\mu_0 \mathbf{M} = \chi \mathbf{B} \qquad \textbf{10-34}$$

where χ is called the *magnetic susceptibility*. For high temperatures such that $\mu B \ll kT$, it can be shown that (see Problem 10-60)

$$\chi = \frac{\mu_0 M}{B} = \frac{\rho \mu^2}{kT} \qquad \textbf{10-35}$$

where $\rho = (\rho_+ + \rho_-)$ is the total electron density. Equation 10-35 is known as *Curie's law*, after Pierre Curie. Thus, as T increases, the ability of the magnetic field to align the spins decreases. Many solids exhibit Curie's law behavior. For low temperatures where $\mu B \gg kT$, $M \rightarrow \mu\rho$ as $T \rightarrow 0$, corresponding to the alignment of all the magnetic moments with the field.

Equation 10-35 does not apply to the magnetism arising from electrons in metals. The reason is that $T \ll T_F$, since $T_F = 10^4 - 10^5$ K for metals. Thus, the electrons are highly degenerate, with each allowed level containing two with paired spins. When an external **B** field is applied, spins cannot just "flip" to align with the field since doing so would violate the exclusion principle. A spin flip must be accompanied by raising that electron to a higher, unoccupied energy state. Thus, even at $T = 0$ K, metals have a finite susceptibility. This type of magnetic behavior is called *Pauli paramagnetism*.

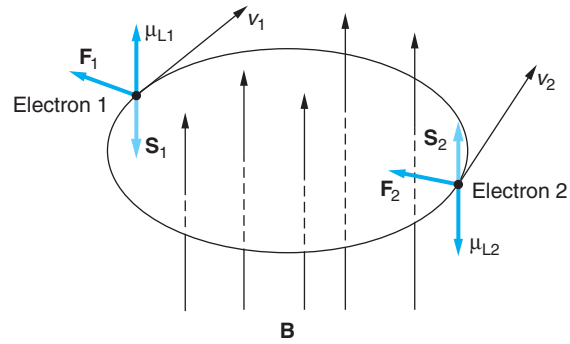

Figure 10-15 Electrons 1 and 2 orbit the atomic core (not shown) in opposite directions. The magnetic field **B** is perpendicular to the plane of the orbits. The magnetic forces $\mathbf{F}_1$ and $\mathbf{F}_2$ increase the orbital magnetic moment of electron 2 and decrease that of electron 1, resulting in a net moment opposite to **B**.

Diamagnetism

Recall that a free electron moving perpendicular to a magnetic field experiences a magnetic force $\mathbf{F} = -e(\mathbf{v} \times \mathbf{B})$. The resulting circular motion produces a current loop with a magnetic moment *opposite* to the direction of the applied field. (To see this, use the right-hand rule.) Now consider two electrons with paired spins orbiting in opposite directions in an atom. (See Figure 10-15.) If an external **B** field perpendicular to the plane of the orbits is turned on, the net force ($\mathbf{F}_{\text{Coulomb}} - \mathbf{F}_{\text{magnetic}}$) on electron 1 is reduced, reducing its *orbital* magnetic moment, which is parallel to **B**. The net force on electron 2 is increased, increasing its magnetic moment. The result is a net magnetic moment opposite to the direction of the applied field. This magnetic behavior is called *diamagnetism*. The diamagnetic effect is seen only in solids consisting of atoms whose electron spins are all paired. As we will see in Section 10-9, the "test" of superconductivity is that the material exhibit perfect diamagnetism.

Ferromagnetism

The first magnetic effect discovered, a result of its existence in iron that led to its early use as a compass, *ferromagnetism* is the consequence of a phase transition in certain materials. At high temperatures a piece of iron is unmagnetized, the spin directions of the atoms having rotational symmetry—all spin directions are equally probable. (In an applied **B** field iron is paramagnetic at high temperatures.) As the temperature decreases, at a certain temperature T_C, called the *Curie temperature*, the magnetic interaction between the atoms exceeds the randomizing effect of thermal agitation, spontaneously breaking the rotational symmetry and causing a phase transition in the solid that tends to align the spins parallel to each other, converting the sample into a permanent magnet. Only four elements besides iron exhibit ferromagnetism: nickel, cobalt, gadolinium, and dysprosium. There are also several ferromagnetic compounds, including some that contain none of the ferromagnetic elements.

In certain compounds the magnetic interaction between the atoms tends to align the spins on adjacent atoms antiparallel below a certain temperature, analogous to the Curie temperature, called the *Neel temperature* T_N. Such materials are called *antiferromagnetic*. Examples are FeO, $NiCl_2$, MnO, and MnS. In a few other materials the spins on adjacent sites are antiparallel below T_N, but because they contain two different types of positive ions, the spins do not exactly cancel and the material is left with a small net magnetization. Such materials are called *ferrimagnetic*. The most common example is the iron ore magnetite, $FeO \cdot Fe_2O_3$.

FEUE WHE

EXPLORING
Spintronics

A relatively new field of research with almost immediate applications, s*pintronics*, or *spin electronics*, is the manipulation of electron spin currents rather than charge currents. N. F. Mott was the first to suggest the possibility of spin-polarized currents in ferromagnetic materials more than 30 years ago. Utilization of spin currents was first realized with the discovery of the giant magnetoresistance (GMR) of magnetic multilayers in 1988. A magnetic multilayer film consists of a stack of alternate ferromagnetic and nonmagnetic layers. The resistance to current flow is low when the electron spins, hence magnetic moments, of the ferromagnetic layers are aligned parallel. The resistance is high when the spins of the ferromagnetic layers are aligned antiparallel, a result of spin-dependent scattering. The resulting relative resistance change can be as large as 200 percent (although 10–20 percent is more typical); hence the name *giant* magnetoresistance. Depending on the design of the layers, the direction of the spins (magnetic moments) can be changed very quickly by an applied magnetic field of only about 10^{-6} tesla. These so-called *spin valves* can detect very small magnetic fields, such as those of the magnetic bits on CDs and DVDs.

Spin valves, the first spintronic devices, form the read/write heads on the hard drives of essentially all modern computers. In addition, recent commercial development of magnetoresistive random access memory (MRAM) chips have read/write speeds much faster than flash memory and, like the latter, do not degrade over time.

Another spintronic device with enormous potential applications is the *magnetic tunnel junction*. In these devices the ferromagnetic layers are separated by very thin insulating layers, typically aluminum oxide (see Figure 10-16). Electrons can tunnel through the insulating layer (see Sections 6-6 and 10-8) and, since the tunneling probability from a ferromagnetic layer depends on the spin direction, the resistance of the junction is different by as much as 75 percent between the parallel and antiparallel configurations. Extremely small junctions can be mass-produced making possible random access memory for portable permanent computer memory with write speeds three orders of magnitude faster than current flash memory devices. The magnetic tunnel junction was also the key element in the recent direct electrical detection of the potential due to the *spin Hall effect* (see page 452), opening opportunities for controlling spin currents with electric fields.

Yet another intriguing future possibility is the application of spintronic devices to the development of quantum computers. The use of electron charge states for information storage is currently a barrier to their development since such states are readily destroyed by scattering. Spin states, on the other hand, have very long relaxation times.

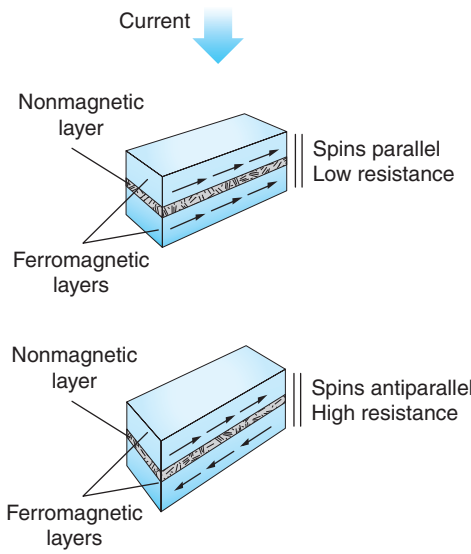

Figure 10-16 A magnetic tunnel junction consists of two ferromagnetic layers separated by a very thin nonmagnetic insulating layer. (*a*) The probability of electrons tunneling through the barrier layer is dependent on the spin direction, being highest when the spins, hence the magnetic moments, of the electrons in the ferromagnetic layers are parallel. This is the configuration of low resistance. (*b*) The tunneling probability is low when the spins are antiparallel, resulting in high resistance. Thus, each junction can store one bit of data, (*a*) representing, e.g., "0" and (*b*) representing "1."

10-6 Band Theory of Solids

We have seen that, if the electron gas is treated as a Fermi gas and the electron-lattice collisions treated as the scattering of electron waves, the free-electron model gives a good account of the electrical and thermal properties of conductors. This simple model, however, gives no indication why one material is a good conductor and another is an insulator. The conductivity (and its reciprocal, the resistivity) vary enormously from the best insulators to the best conductors. For example, the resistivity of a typical insulator (such as quartz) is of the order of $10^{16}\ \Omega \cdot \text{m}$, whereas that of a typical conductor (most metals) is of the order of $10^{-8}\ \Omega \cdot \text{m}$ and that of a superconductor is less than $10^{-19}\ \Omega \cdot \text{m}$.

To understand why some materials conduct and others do not, we must refine the free-electron model and consider the effect of the lattice on the electron energy levels. There are two standard approaches to this problem of determining the energy levels of electrons in a crystal. One is to consider the problem of an electron moving in a periodic potential and to determine the possible energies by solving the Schrödinger equation. The other is to determine the energy levels of the electrons in a solid by following the behavior of the energy levels of individual atoms as they are brought together to form the solid, in much the same way that we did in Section 9-2 in the explanation of the covalent bonding in the H_2 molecule. Both approaches lead to the result that the energy levels are grouped into allowed and forbidden bands. The details of the band structure of a particular material determine whether that material is a conductor, an insulator, or a semiconductor. Qualitative discussion of the first of these methods is given in this section. The second is described in the MORE section *Energy Bands in Solids—An Alternate Approach* on the home page.

Kronig-Penney Model

Consider first the problem of an electron moving in a periodic potential. Figure 10-17*a* shows a one-dimensional sketch of the potential energy function for a lattice of positive ions. The most important feature of this potential is not the shape, but the fact that it is periodic. A simpler periodic potential consisting of finite square wells is shown in Figure 10-17*b*. The model based on this potential is called the *Kronig-Penney model*. It has the important feature of periodicity and is easier to treat mathematically; however, even for this model the mathematical solution of the Schrödinger equation is

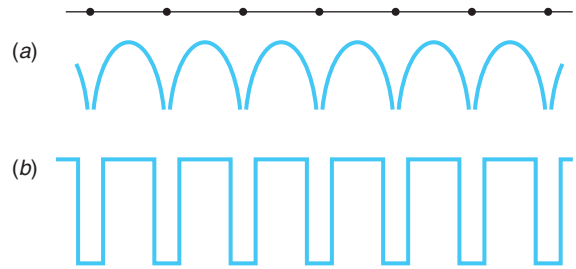

Figure 10-17 (*a*) One-dimensional potential energy of an electron in a crystal. $U(x)$ approaches $\pm\infty$ at the atom sites. (*b*) Simplified (Kronig-Penney) model of potential energy of an electron in a crystal.

FEUE WHE

quite involved, and we will only outline it here. For both potential functions shown in Figure 10-17, for certain ranges of energy traveling-wave-type solutions of the Schrödinger equation exist. This result is based on an important discovery made by Felix Bloch[4] that solutions to the Schrödinger equation for periodic potentials must be of the form (in one dimension)

$$\psi(x) = u_k(x)e^{ikx} \qquad \textbf{10-36}$$

where $u_k(x) = u_k(x + L) = u_k(x + nL)$, L is the periodic spacing of the potential wells, and n is an integer. The function e^{ikx} is a plane wave, i.e., a free electron (see Section 6-6) with wave number $k = 2\pi/\lambda$. As Bloch himself described it:

> I felt that the main problem was to explain how the electrons could sneak by all the ions in a metal. . . . I found to my delight the wave differed from the plane wave of free electrons only by a periodic modulation.

Thus, we require that the solutions of the Schrödinger equation

$$-\frac{\hbar^2}{2m}\frac{d^2\psi(x)}{dx^2} + U(x)\psi(x) = E\psi(x) \qquad \textbf{10-37}$$

where $U(x)$ is the Kronig-Penney potential of periodic square wells and $\psi(x)$ has the form of the *Bloch function* given by Equation 10-36. The solution for the region $0 < x < a$ in Figure 10-18 is

$$\psi(x) = A_1e^{ik'x} + A_2e^{-ik'x} \qquad \textbf{10-38}$$

where $k' = 2\pi/\lambda = (2mE)^{1/2}/\hbar^2$. In the region $-b < x < 0$, the solutions are of the form

$$\psi(x) = B_1e^{\alpha x} + B_2e^{-\alpha x} \qquad \textbf{10-39}$$

where $\alpha = [2m(U_0 - E)]^{1/2}/\hbar^2$. The requirement that $\psi(x)$ have the form of Equation 10-36 means that

$$\begin{aligned}\psi(x + a + b) &= u_k(x + a + b)e^{ik(x+a+b)}\\ \psi(x + a + b) &= u_k(x)e^{ikx}e^{ik(a+b)}\\ \psi(x + a + b) &= \psi(x)e^{ik(a+b)}\end{aligned} \qquad \textbf{10-40}\boldsymbol{a}$$

where $a + b$ is the periodic spacing of the wells. In general,

$$\psi(x + n(a + b)) = \psi(x)e^{ikn(a+b)} \qquad \textbf{10-40}\boldsymbol{b}$$

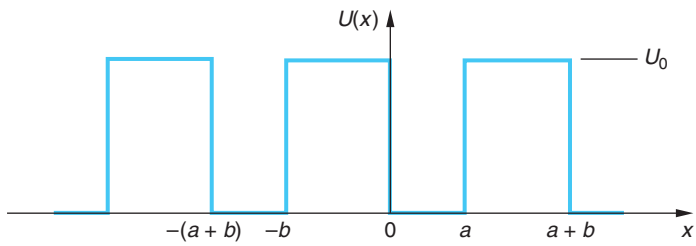

Figure 10-18 A portion of the Kronig-Penney potential of Figure 10-17*b* showing the width of the square wells a and their periodic spacing $(a + b)$.

FEUE WHE

As was done in Section 6-3 for solving the finite one-dimensional square well, the constants A_1, A_2, B_1, and B_2 are chosen so as to make $\psi(x)$ and $d\psi/dx$ continuous at $x = 0$ and $x = a$. Obtaining the constants is beyond the scope of our discussion here, but as in Chapter 6, doing so yields a conditional equation connecting k, k', and α with a and b, the parameters of the lattice. The result is that, in order to satisfy the requirement of Equation 10-40, only certain ranges of electron energies are allowed. These energy ranges, called *bands*, are separated by forbidden energy regions called *energy gaps*, in which no traveling wave can exist. Figure 10-19*a* shows the energy versus the wave number k for a completely free electron. This is, of course, merely a sketch of $E = \hbar^2 k^2/2m$. Figure 10-19*b* shows E versus k for an electron in the periodic potential of Figure 10-18. The energy gaps occur at

$$ka = \pm n\pi \qquad \textbf{10-41}$$

where n is an integer and a is the lattice spacing.[5] We can understand this result in terms of the Bragg reflection of the electron waves. Consider E to be small (near zero in Figure 10-19*b*) so that k is small; hence λ is large. As E increases, k eventually becomes large enough so that λ becomes small enough to suffer a Bragg reflection (constructive interference) from the lattice. (See Section 3-4.) Bragg reflection is governed by the Bragg condition (Equation 3-23):

$$n\lambda = 2a \sin\theta$$

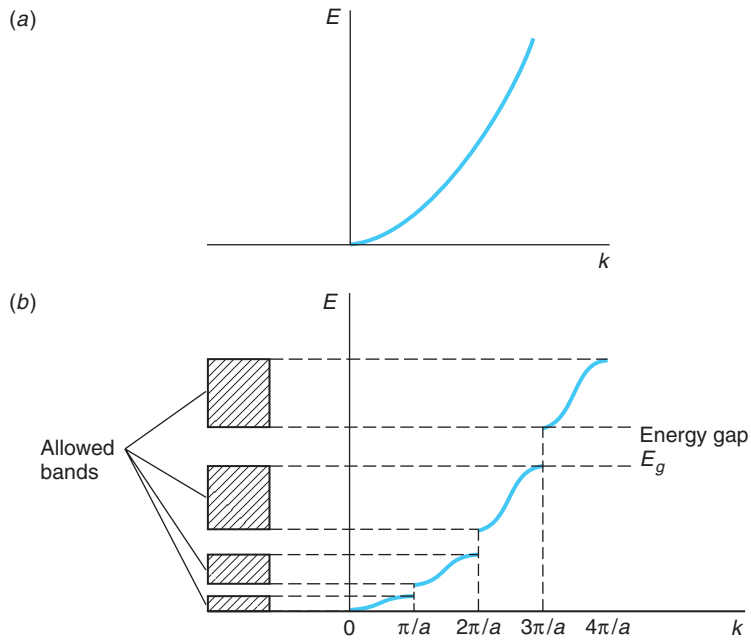

Figure 10-19 (*a*) Energy versus k for a free electron. (*b*) Energy versus k for a nearly free electron in the one-dimensional periodic potential of Figure 10-18 with $b = 0$ and $U_0 \rightarrow \infty$. Energy gaps occur at the k values which satisfy the Bragg scattering condition. In each case only the portions with $k > 0$ are shown. The complete curves are symmetric about $k = 0$.

FEUE WHE

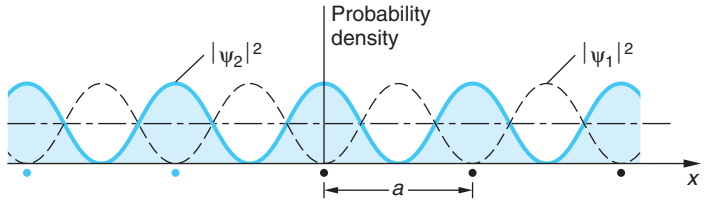

Figure 10-20 Probability density (proportional to the charge distribution) for standing waves of wave number $k = \pi/a$ in a one-dimensional crystal. The solid curve $|\psi_2|^2$ is a maximum at the lattice ion sites and has a lower potential energy than the dashed curve $|\psi_1|^2$.

In a one-dimensional system such as we are considering here, reflection means $\theta = 90°$. Since $k = 2\pi/\lambda$, Equation 10-41 becomes the condition for Bragg reflection. The reason that traveling waves cannot exist for these wave numbers is that the amplitude of the reflection from one atom in the chain becomes equal to and in phase with the forward electron wave from the preceding atom, so that standing waves are set up. Figure 10-20 shows a sketch of the electron probability density $|\psi|^2$ for the two types of standing waves for the lowest energy gap, where the value $k = \pi/a$:

$$\psi_1 = \sin kx = \sin\frac{\pi x}{a} \qquad \psi_2 = \cos kx = \cos\frac{\pi x}{a}$$

Since ψ_2 gives a higher concentration of electron charge density near the ion sites than ψ_1, the potential energy is less for ψ_2 than for ψ_1. The difference in the potential energies corresponds to the magnitude of the energy gap. Within the allowed energy bands, the energy has a continuous range if the number of atoms in the chain is infinite; for N atoms, there are N allowed energy levels in each band. Since the number of atoms is very large in a macroscopic solid, the energy bands can be considered continuous. Calculations in three dimensions are more difficult, of course, but the results are similar. The allowed ranges of the wave vector **k** are called *Brillouin zones*. Referring to Figure 10-19*a*, the first Brillouin zone has $-\pi/a < k < +\pi/a$, the second has $-2\pi/a < k < -\pi/a$ and $\pi/a < k < 2\pi/a$, and so on.

Conductors, Insulators, and Semiconductors

Conductors We can now understand why some solids are conductors and others are insulators. Consider sodium. There is room for two electrons in the 3*s* state of each atom, but each sodium atom has only one 3*s* electron. Therefore, when N sodium atoms are bound in a solid, the 3*s* energy band is only half filled. In addition, the empty 3*p* band overlaps the 3*s* band. The allowed energy bands of sodium are shown schematically in Figure 10-21. We can see that many allowed energy states are available immediately above the filled lower half of the 3*s* band, so the valence electrons can easily be raised to a higher energy state by an electric field. Accordingly, sodium is a good conductor. Magnesium, on the other hand, has two 3*s* electrons, so the 3*s* band is filled. However, like sodium, the empty 3*p* band overlaps the 3*s* band, so magnesium is also a conductor. The band occupied by the outer, or valence electrons, is called the *valence band*. The next (higher) allowed band is called the *conduction band*.

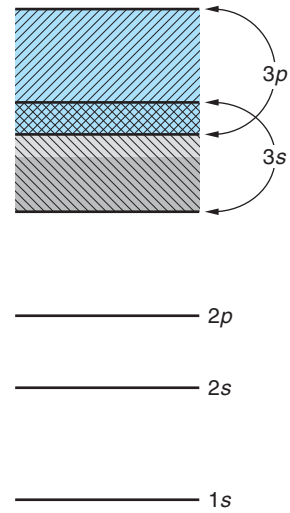

Figure 10-21 Energy-band structure of sodium. The empty 3*p* band overlaps the half-filled 3*s* band. Just above the filled states are many empty states into which electrons can be excited by an electric field, so sodium is a conductor.

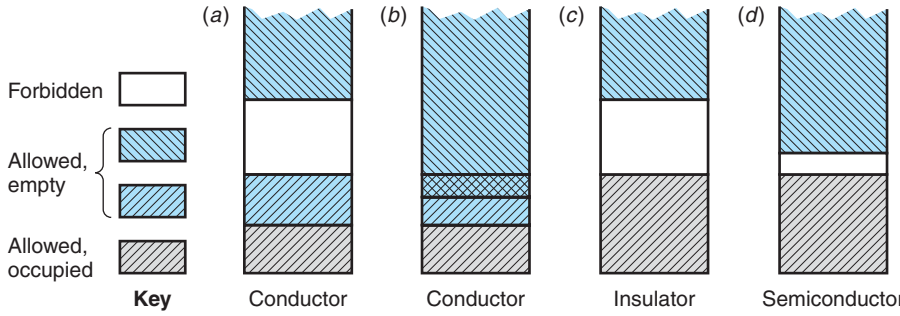

Figure 10-22 Four possible band structures for a solid. (*a*) The allowed band is only partially full, so electrons can be excited to nearby energy states. At 0 K the Fermi level is at the top of the filled states. (*a*) is a conductor. (*b*) is a conductor because the allowed bands overlap. In (*c*) there is a forbidden band with a large energy gap between the filled band and the next allowed band; this is an insulator. (*d*) The energy gap between the filled band and the next allowed band is very small, so some electrons are excited to the conduction band at normal temperatures, leaving holes in the valence band. The Fermi level is approximately in the middle of the gap. (*d*) is a semiconductor.

Thus, a conductor is a solid whose valence band is only partly filled or whose conduction band overlaps its valence band. There are a few elements, notably antimony, arsenic, and bismuth, whose conduction band overlaps the valence band only very slightly, limiting the number of available empty states. These materials are called *semimetals*. (See Figures 10-22*a* and *b*.)

Insulators A solid that has a completely filled valence band is an insulator if the energy gap between the valence band and the empty conduction band is larger than about 2eV, as illustrated in Figure 10-22*c*. For example, ionic crystals are insulators. The band structure of an ionic crystal, such as NaCl, is quite different from that of a metal. The energy bands arise from the energy levels of the Na^+ and Cl^- ions. Both of these ions have a closed-shell configuration, so the highest occupied band in NaCl is completely full. The next allowed band, which is empty, arises from the excited states of Na^+ and Cl^-. There is a large energy gap between the filled band and this empty band. Typical electric fields applied to NaCl will be too weak to excite an electron from the upper energy levels of the filled valence band across the large gap into the lower energy levels of the empty conduction band, so NaCl is an insulator. When an applied electric field is sufficiently strong to cause an electron to be excited to the empty band, the phenomenon called *dielectric breakdown* occurs.

Intrinsic Semiconductors If the gap between a filled valence band and an empty conduction band is small, the solid is a semiconductor. Consider carbon, which has two 2*s* electrons and two 2*p* electrons. We might expect carbon to be a conductor because of the four unfilled 2*p* states. However, the 2*s* and 2*p* levels mix when carbon forms covalent bonds.[6] Figure 10-23 shows the splitting of the eight $2s - 2p$ levels when carbon bonds in the diamond structure. This splitting is due to the nature of the covalent bond and is similar to the splitting of the 1*s* levels in hydrogen discussed in Section 9-2. The energy of the levels corresponding to the four space-symmetric wave functions (one for the 2*s* levels and three for the 2*p* levels) is lowered while the energy of the other four levels (one 2*s* and three 2*p*) is raised. The valence band therefore contains four levels per atom that are filled, and the conduction band is empty.

FÈUE WHE

At the diamond lattice spacing of about 0.154 nm, the energy gap between the filled valence band and the empty conduction band is about 7 eV. Since this gap is large compared to the energy that an electron might receive by thermal excitation due to scattering from the lattice ions, which on the average is of the order of $kT \approx 0.026$ eV at $T = 300$ K, very few electrons can reach the conduction band. Thus, diamond is an insulator. The band structure is similar for silicon, which has two 3*s* and two 3*p* electrons, and for germanium, which has two 4*s* and two 4*p* electrons. At the silicon lattice spacing of 0.235 nm the energy gap is about 1 eV; at the germanium lattice spacing of 0.243 nm the energy gap is only about 0.7 eV. For these gaps, at ordinary temperatures there are an appreciable number of electrons in the conduction band due to thermal excitation, although the number is still small compared with the number in a typical conductor. Solids such as these are called *intrinsic semiconductors*. Figure 10-22*d* illustrates the band structure of intrinsic semiconductors.

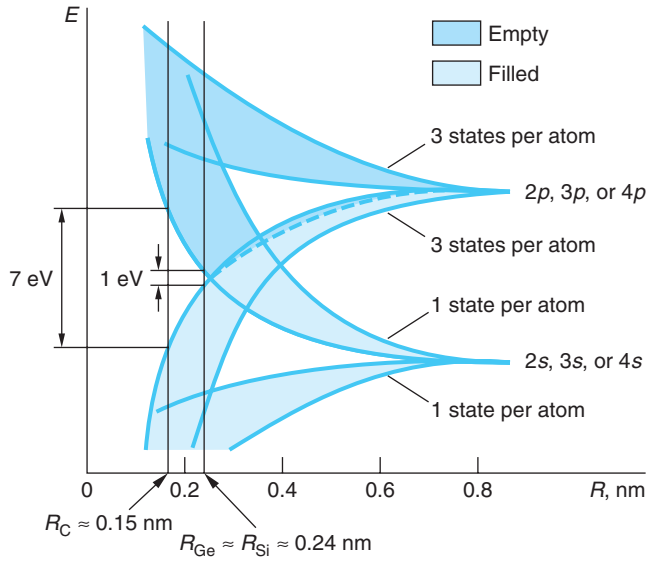

Figure 10-23 Splitting of the 2*s* and 2*p* states of carbon, the 3*s* and 3*p* states of silicon, or the 4*s* and 4*p* states of germanium versus separation of the atoms. The energy gap between the four filled states in the valence band and the empty states in the conduction band is 7 eV for the diamond-lattice spacing, $R_C = 0.154$ nm. For the silicon spacing $R_{Si} = 0.235$ nm, the energy gap is 1.09 eV. The splitting is similar for the 4*s* and 4*p* levels in germanium, which has an atom spacing of 0.243 nm, giving an energy gap of only 0.7 eV.

In the presence of an electric field, the electrons in the conduction band of an intrinsic semiconductor can be accelerated because there are empty states nearby. Also, for each electron that has been excited to the conduction band there is a vacancy, or hole, in the nearby filled valence band. In the presence of an electric field, other electrons in this band can be excited to the vacant energy level, thus filling that hole but creating another hole. This contributes to the electric current and is most easily described as the motion of a hole in the direction of the field and opposite to the motion of the electrons. The hole thus acts like a positive charge. An analogy of a two-lane, one-way road with one lane full of parked cars and the other empty may help in visualizing the conduction of holes. If a car moves out of the filled lane into the empty lane, it can move ahead freely. As the other cars move up to occupy the space left, the empty space propagates backward in the direction opposite to the motion of the cars. Both the forward motion of the car in the nearby empty lane and the backward propagation of the empty space contribute to a net forward propagation of the cars.

An interesting characteristic of semiconductors is that the conductivity increases (and the resistivity decreases) as the temperature increases, which is contrary to the case for normal conductors. The reason is that as the temperature is increased, the number of free electrons is increased because there are more electrons in the conduction band. The number of holes in the valence band is also increased, of course. In semiconductors, the effect of the increase in the number of charge carriers, both electrons and holes, exceeds the effect of the increase in resistivity due to the increased scattering of the electrons by the lattice ions due to thermal vibrations. Semiconductors therefore have negative temperature coefficients of resistivity.

Whether a solid with a filled valence band will be a semiconductor or an insulator depends critically on the width of the energy gap E_g, as Figure 10-23 suggests. A comparison of the relative numbers of electrons with various energies that *could* be

FEUE WHE

Table 10-4 Values of $f_{FD}(E)$ for $T = 293$ K

$E - E_F$ (eV)	0.05	0.10	0.25	1.0	2.5	7.5
Multiple of kT	2	4	10	40	100	300
$f_{FD}(E)$	1.2×10^{-1}	1.8×10^{-2}	5.1×10^{-5}	6.5×10^{-18}	1.1×10^{-43}	1.3×10^{-129}

above the Fermi level (located at the center of the band gap) at ordinary temperatures illustrates why this is true. Those numbers are given by the Fermi-Dirac distribution $f_{FD}(E)$ given by Equation 8-68:

$$f_{FD}(E) = \frac{1}{E^{(E-E_F)/kT} + 1} \qquad \textbf{8-68}$$

At $T = 293$ K, $kT = 0.025$ eV. Recall that for $E = E_F$, $f_{FD}(E) = 1/2$ (see Section 8-5). For $(E - E_F) = 0.10$, or $4(kT)$, we have

$$f_{FD}(E) = \frac{1}{e^{0.10/0.025} + 1} = 0.018$$

Repeating this calculation for several additional values of $(E - E_F)$ yields the relative numbers of electrons in Table 10-4. From the numbers in the table we see that, if a certain material has an energy gap E_g between the valence and conduction bands of 0.25 eV, for example, then approximately 10^{-5} of the electrons within kT of the Fermi level would be excited to the conduction band and thus able to participate in the conduction of electricity. This is a sizable number, given the numbers of electrons near the Fermi level, so we expect this material to have a higher electrical conductivity than materials with larger values of E_g.

For a gap of 1.0 eV, just four times that of the previous example, the relative number of electrons excited to the conduction band decreases by more than 12 orders of magnitude, illustrating the sharp decline of $f_{FD}(E)$ as the energy gap increases. The calculation of $f_{FD}(E)$ above also illustrates the increased conductivity of semiconductors as the temperature increases described earlier. If the temperature of a material with an energy gap of 1.0 eV is increased to 393 K from 293 K, as in Table 10-4, $f_{FD}(E)$ increases to 1.5×10^{-13}, thus increasing the relative number of electrons in the conduction band by nearly four orders of magnitude. Table 10-5 lists the energy gaps for several semiconducting elements and compounds. Notice that the energy gap is slightly temperature dependent.

A concept that is helpful in understanding a number of characteristics of semiconductors is that of *effective mass*. As pointed out above, Figure 10-19*a* is a graph of $E = \hbar^2 k^2/2m_e$, the energy of a free electron of wavelength $\lambda = 2\pi/k$. The curvature of the E versus k graph is given by $d^2E/dk^2 = \hbar^2/m_e$, and we may say that the curvature is determined by $1/m_e$, the reciprocal mass. In Figure 10-19*a* $1/m_e$ is of course constant; however, in regions near the energy gaps in Figure 10-19*b* the curvature is much higher than that for the free electron. Since the behavior of electrons near the band/gap boundary is of considerable interest, particularly in the discussion of impurity semiconductors and devices in Section 10-7, it is helpful to continue to describe the curvature of the E versus k curve near the boundary in terms of a reciprocal mass. Accordingly, we define the effective mass m^* as

$$\frac{1}{m^*} = \frac{1}{\hbar^2}\frac{d^2E}{dk^2} \qquad \textbf{10-42}$$

FEUE WHE

Table 10-5 Energy gap E_g and dielectric constant κ for selected semiconductors

	E_g (eV)				E_g (eV)		
Material	0 K	293 K	κ	Material	0 K	293 K	κ
Si	1.15	1.11	11.8	CdTe	1.56	1.44	10.2
Ge	0.74	0.67	15.9	PbS	0.28	0.37	17.0
Te	—	0.33	—	InP	1.41	1.27	12.4
GaAs	1.53	1.35	13.1	CdSe	1.85	1.74	10.1
InSb	0.23	0.16	17.8	GaP	2.40	2.24	11.1
ZnS	—	3.54	5.2	PbTe	0.19	0.25	30.1

Then, as in the case of the free electron, the curvature of E versus k for electrons bound in the crystal energy bands is also described in terms of a reciprocal mass, $1/m^*$. For a free electron $m^* = m_e$, as is also the case for electrons that are not close to the boundaries in Figure 10-19*b*. Close to the band/gap boundaries, however, is a different matter. Starting from $k = 0$ in the figure, the curvature is initially constant and equal to that of a free electron, thus $m^* = m_e$, but near the boundary where $k = \pi/a$, the curvature becomes large and, very close to the boundary, negative; hence m^* becomes smaller than m_e and also eventually negative! Just above the gap, the curvature is large and positive, so $m^* < m_e$ and positive. For the situation where E_g is small compared to the width of the band, the values of the effective mass are typically of the order of $0.01-0.1$ of the mass of a free electron. We will make further use of the effective mass in Section 10-7.

Questions

7. How does the change in resistivity of copper compare with that of silicon when the temperature increases?
8. Suppose an electron is excited from the valence band of a semiconductor to a state several levels above the lower edge of the conduction band. Devise an explanation for why it will quickly "decay" to a level at the bottom of the conduction band.

More

An alternative to the Kronig-Penny model of a solid is based on the molecular bonding model discussed in Section 9-2 for hydrogen. *Energy Bands in Solids—An Alternate Approach* is described briefly on the home page: www.whfreeman.com/tiplermodernphysics5e. See also Figures 10-24 and 10-25 here.

10-7 Impurity Semiconductors

Most semiconductor devices, such as the semiconductor diode and the transistor, make use of *impurity semiconductors*, which are created through the controlled addition of certain impurities to intrinsic semiconductors. This process is called *doping*.

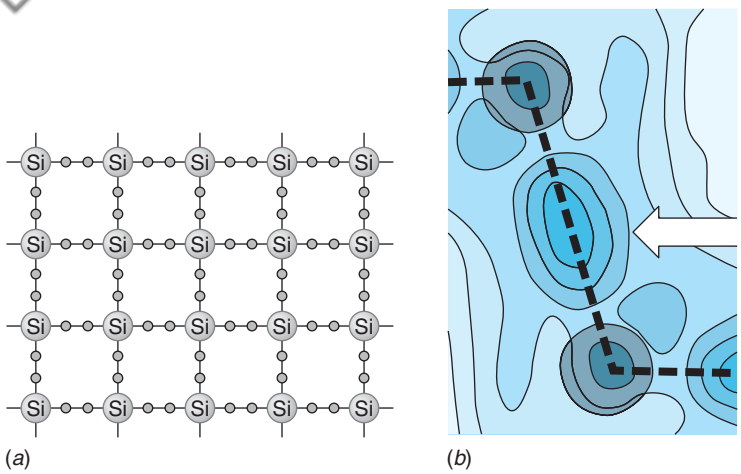

Figure 10-26 (a) A two-dimensional schematic illustration of solid silicon. Each atom forms a covalent bond with four neighbors, sharing one of its four valence electrons with each neighbor. (*b*) X-ray scattering measurement of electron density in the vicinity of two atoms in an Si crystal. The arrow points to the high electron density of the covalent bond. [*Adapted from Y. W. Yang, P. Coppens, Solid State Comm., 15, 1555 (1974).*]

Figure 10-26*a* illustrates the lattice structure of pure silicon, and Figure 10-27*a* is a schematic illustration of silicon doped with a small amount of arsenic such that arsenic atoms replace a few of the silicon atoms in the crystal lattice. Arsenic has five valence electrons in the $n = 4$ shell, whereas silicon has four valence electrons in the $n = 3$ shell. Four of the five arsenic electrons take part in covalent bonds with the four neighboring silicon atoms, and the fifth electron is very loosely bound to the atom. This extra electron occupies an energy level that is just slightly below the conduction band in the solid and is easily excited into the conduction band, where it can contribute to electrical conduction. The fifth arsenic valence electron and the arsenic ion core form a hydrogenlike system. Thus, Bohr theory (see Section 4-3) can be used to calculate the approximate values of the energies available to it, provided only that we make allowance for the fact that the electron-arsenic ion system is embedded in the semiconductor crystal rather than being isolated from other atoms. First, the crystal is a medium with a high dielectric constant; thus the potential energy function in the Schrödinger equation for a hydrogenlike atom (Equation 7-6) becomes[7] $V(r) = (-Zke^2/R)(1/\kappa)$ where κ is the dielectric constant of the material and $k = 1/4\pi\epsilon_0$. Second, the electron mass in the Schrödinger equation must be replaced by the effective mass m^*, which accounts for the fact that the electron "sees" a three-dimensional version of the periodic potential of Figure 10-17. With these two modifications the solution of the Schrödinger equation is carried out just as in Chapter 7. The results for the allowed energies and average values of the radii of the Bohr orbits for the fifth arsenic electron are given by

$$E_n = -\frac{1}{2}\left(\frac{ke^2}{\hbar}\right)^2 \frac{m_e}{n^2} \times \frac{m^*}{m_e} \times \frac{1}{\kappa^2} = -\frac{1}{2}\left(\frac{ke^2}{\hbar}\right)^2 \frac{m^*}{\kappa^2}\frac{1}{n^2} \qquad \textbf{10-43}$$

$$\langle r_n \rangle = a_0 n^2 \times \frac{m_e}{m^*} \times \kappa \qquad \textbf{10-44}$$

where a_0 is the Bohr radius, equal to 0.0529 nm (see Equation 4-19), and n is the principal quantum number.

To understand where these energy levels lie relative to the bands and gap of the silicon, consider that when the arsenic atom is ionized by removing the fifth electron, that electron is then free to move about and to participate in electrical conduction; i.e., it is then in the conduction band. Thus, we conclude that $E_\infty = 0$ is at the bottom edge of the conduction band and the other E_n hydrogenlike levels lie below it in the gap. The energy of the ground state E_1 can be calculated from the experimentally determined value of the electron's effective mass in silicon, about 0.2 m_e, and the dielectric constant of silicon given in Table 10-5. Substituting these into Equation 10-43 yields $E_1 = -0.020$ eV below the conduction band, which is substantially smaller than the -13.6-eV ground state for hydrogen. Similarly, substitution into Equation 10-44 yields $\langle r_1 \rangle = 3.1$ nm, or about 60 times the ground-state radius of hydrogen.[8]

FÈUE WHE

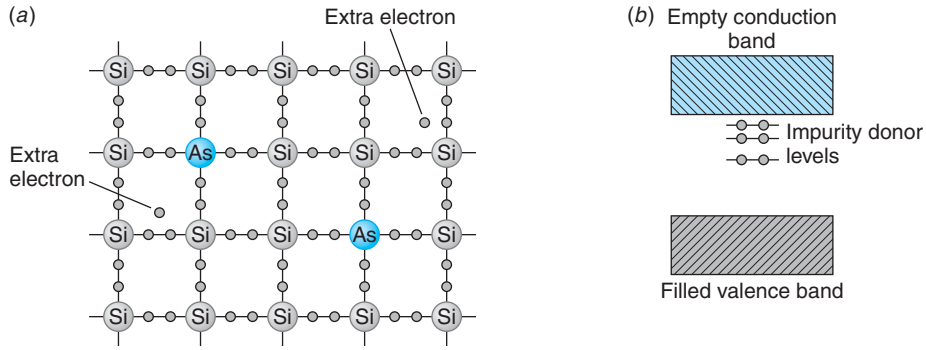

Figure 10-27 (*a*) A two-dimensional schematic illustration of silicon doped with arsenic. Because arsenic has five valence electrons, there is an extra, weakly bound electron that is easily excited to the conduction band, where it can contribute to electrical conduction. (*b*) Band structure of an *n*-type semiconductor such as silicon doped with arsenic. The impurity atoms provide filled energy levels that are just below the conduction band. These levels donate electrons to the conduction band.

These energies are quite close to the conduction band, as illustrated in Figure 10-27*b*; thus these electrons can be easily excited to the conduction band since their ionization energy is comparable to kT at room temperature.

These hydrogenlike levels just below the conduction band are called *donor levels* because they donate electrons to the conduction band without leaving holes in the valence band. Such a semiconductor is called an *n-type semiconductor* because the major charge carriers are *negative* electrons. The conductivity of a doped semiconductor can be controlled by controlling the amount of impurity added. The addition of just one part per million can increase the conductivity by several orders of magnitude.

Another type of impurity semiconductor can be made by replacing a silicon atom in the crystal lattice with a gallium atom, which has three electrons in its valence level rather than four (see Figure 10-28*a*). The gallium atom accepts electrons from the valence band of the silicon in order to complete its four covalent bonds, thus creating a hole in the valence band. The effect on the band structure of silicon achieved by doping it with

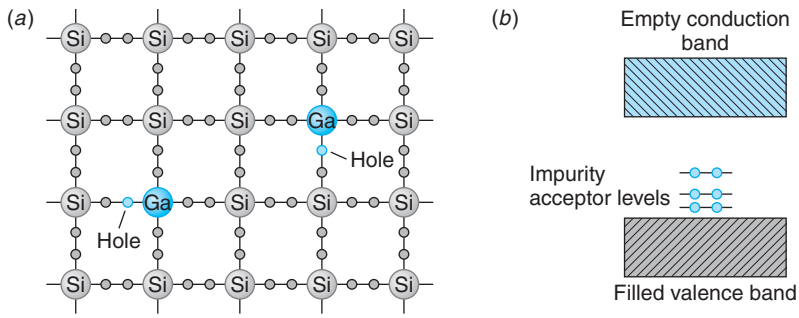

Figure 10-28 (*a*) Two-dimensional schematic illustration of silicon doped with gallium. Because gallium has only three valence electrons, there is a hole in one of its bonds. As electrons move into the hole, the hole moves about, contributing to the conduction of electric current. (*b*) Band structure of a *p*-type semiconductor such as silicon doped with gallium. The impurity atoms provide empty energy levels just above the filled valence band that accept electrons from the valence band.

gallium is shown in Figure 10-28*b*. The empty levels shown just above the valence band are due to the holes resulting from the ionization of the gallium atoms. These levels are called *acceptor levels* because they accept electrons from the filled valence band when these electrons are thermally excited to a higher energy state. They arise because the holes, which act like positive charges, may be bound to the negative gallium core much like the fifth electron was bound to the positive arsenic core. Thus, the hole-gallium ion system also forms a hydrogenlike system and the energy levels of the hole can also be calculated approximately using the Bohr model with results similar to Equation 10-43. Since the energy-band diagrams like Figure 10-27*b* and 10-28*b* are drawn with electron energy increasing upward, hole energy in those diagrams increases downward. Ionizing the hole-gallium system means returning the hole to the valence band; hence these levels are just above the top of the valence band, as shown in Figure 10-28*b*, and their magnitudes are of the same order as those of the donor levels discussed previously. Increasing the energy of holes is equivalent to promoting electrons from the valence band into the acceptor levels. This creates holes in the valence band that are free to propagate in the direction of an electric field. Such a semiconductor is called a *p-type semiconductor* because the charge carriers are *positive* holes. The fact that conduction is due to the motion of holes can be verified by the Hall effect, described in the Exploring section on page 449.

EXAMPLE 10-8 **Donor Ionization Energy in Ge** If phosphorus is used to dope germanium to form an *n*-type semiconductor, what is the ionization energy of the levels? What is the radius of the electron's orbit? Phosphorus has five valence electrons. (The effective mass for electrons in germanium is about 0.1 m_e.)

SOLUTION

1. The magnitude of the ionization energy is computed from Equation 10-43 with $n = 1$:
$$E_1 = \frac{1}{2}\left(\frac{ke^2}{\hbar}\right)^2 \frac{m^*}{\kappa^2}$$

2. The dielectric constant κ for germanium is given in Table 10-5:
$$\kappa = 15.9$$

3. Substituting values into Equation 10-43 gives
$$E_1 = \frac{1}{2}\left(\frac{9 \times 10^9\ \mathrm{N \cdot m^2/C^2} \times (1.60 \times 10^{-19}\ \mathrm{C})^2}{1.055 \times 10^{-34}\ \mathrm{J \cdot s}}\right)^2 \frac{(0.1 \times 9.11 \times 10^{-31}\ \mathrm{kg})}{(15.9)^2}$$
$$= 8.6 \times 10^{-22}\ \mathrm{J} = 5.4 \times 10^{-3}\ \mathrm{eV}$$

4. The orbit radius $\langle r_1 \rangle$ of the fifth phosphorus electron is computed from Equation 10-44 with $n = 1$:
$$\langle r_1 \rangle = a_0 \frac{m_e}{m^*} \kappa$$

5. Substituting values, where the Bohr radius $a_0 = 0.0529$ nm, gives
$$\langle r_1 \rangle = 0.0529 \times \frac{m_e}{0.1 m_e} \times 15.9$$
$$= 8.4\ \mathrm{nm}$$

Remarks: *The value computed above for E_1 is very close to the experimental value of 12.0×10^{-3} eV, even though our calculation is a Bohr model approximation.*

FEUE WHE

EXPLORING
Hall Effect

The number of donated electrons in a doped *n*-type semiconductor, or holes in a doped *p*-type semiconductor, is typically much greater than the intrinsic number of electron-hole pairs created by thermal excitation of electrons from the valence band to the conduction band. In an electric field, the current will therefore consist of both majority carriers (electrons in an *n*-type or holes in a *p*-type semiconductor) and minority carriers. The reality of conduction by motion of positive holes is clearly evident in the Hall effect, illustrated in Figure 10-29*a*. In this figure a thin strip of a doped semiconductor is connected to a battery (not shown), so that there is a current to the right. A uniform magnetic field B is applied perpendicular to the current. For the direction of the current and magnetic field shown, the magnetic force on a moving charged particle $q\,\mathbf{v}_d \times \mathbf{B}$ is upward (where $\mathbf{v}_d$ is the drift velocity) independent of whether the current is due to a positive charge moving to the right or a negative charge moving to the left. Let us assume for the moment that the charge carriers are electrons, as in Figure 10-29*b*. The magnetic force will then cause the electrons to drift up to the top of the strip, leaving the bottom of the strip with an excess positive charge. This will continue until the electrostatic field $\mathscr{E}$ caused by the charge separation produces an electric force on the charge carriers just balancing the magnetic force. The condition for balance is $q\mathscr{E} = qv_dB$. If w is the width of the strip, there will be a potential difference called the Hall voltage

$$V_H = \mathscr{E}w = v_dBw \qquad \textbf{10-45}$$

between the top and bottom of the strip. This potential difference can be measured with a high-resistance voltmeter. A measurement of the sign of the potential difference (i.e., whether the top of the strip is at a higher potential due to positive charge or lower potential due to negative charge) determines the sign of the majority carriers. Such measurements reveal that, indeed, the charge carriers are negative in *n*-type and positive in *p*-type semiconductors. The value of the Hall voltage provides a measurement of the drift velocity v_d. Since the current density $j = nqv_d$ can be easily measured from the total current and cross-sectional area of the strip, measurement of the drift velocity determines n, the number of charge carriers per unit volume.

Hall-effect probes are frequently used to measure magnetic field strengths. A current is established in a calibrated metal strip. Measuring the Hall voltage then yields the value of B (see Equation 10-46).

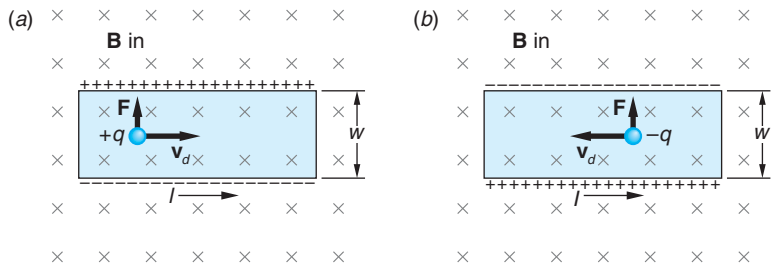

Figure 10-29 The Hall effect. The force on the charge carriers is up whether the carriers are positive charges moving to the right (*a*) or negative charges moving to the left (*b*). The sign of the charge carriers can be determined by the sign of the potential difference between the top and bottom of the strip, and the drift velocity can be determined by the magnitude of this potential difference. The thickness t of the strip is not shown.

EXAMPLE 10-9 **Hall Effect in Aluminum** A strip of aluminum of width $w = 1.5$ cm and thickness $t = 250$ μm is placed in a uniform magnetic field of 0.55 T oriented perpendicular to the plane of the strip. When a current of 25 A is established in the strip, a voltage of 1.64 μV is measured across the width of the strip. What is the density of charge carriers in aluminum and how many charge carriers are provided, on average, by each atom?

SOLUTION

Substituting for the drift velocity v_d in terms of the current density (Equation 10-11) in Equation 10-45 yields

$$V_H = v_d Bw = \frac{jBw}{nq} = \frac{iB}{qnt} \qquad \textbf{10-46}$$

since $j = i/wt$. The density of the charge carriers in aluminum is then given by

$$n = \frac{iB}{qtV_H} = \frac{(25\text{ A})(0.55\text{ T})}{(1.60 \times 10^{-19}\text{ C})(250 \times 10^{-6}\text{ m})(1.64 \times 10^{-6}\text{ V})}$$

$$= 2.10 \times 10^{29}\text{ carriers/m}^3$$

The density of atoms N in aluminum is given by the following, where the density $\rho(\text{Al}) = 2.72 \times 10^3\text{ kg/m}^3$ and the molar mass $M = 26.98$ kg/mol:

$$N = \frac{N_A \rho}{M} = \frac{(6.02 \times 10^{26}\text{ atoms/mol})(2.702 \times 10^3\text{ kg/m}^3)}{26.98\text{ kg/mol}}$$

$$= 6.02 \times 10^{28}\text{ atoms/m}^3$$

Thus, each aluminum atom contributes on average $n/N = 3.5$ charge carriers.

The Quantum Hall Effect

According to Equation 10-46, the Hall voltage should increase linearly with the magnetic field B for a given current. In 1980, while studying the Hall effect in thin semiconductors at very low temperatures and very large magnetic fields, Klaus von Klitzing[9] discovered that a plot of V_H versus B was *not* linear, but included a series of plateaus, as shown in Figure 10-30*a*. That is, the Hall voltage is quantized. More specifically, if we define the Hall resistance $R_H = V_H/i$, it is the Hall resistance that is quantized, taking on only the values

$$R_H = \frac{V_H}{i} = \frac{R_K}{n} \qquad \textbf{10-47}$$

where R_K, called the *von Klitzing constant*, is related to the fundamental electron charge e and Planck's constant h by

$$R_K = \frac{h}{e^2} = \frac{6.626 \times 10^{-34}\text{ J} \cdot \text{s}}{(1.602 \times 10^{-19}\text{ C})^2} = 25{,}813\ \Omega \qquad \textbf{10-48}$$

FÈUE WHE

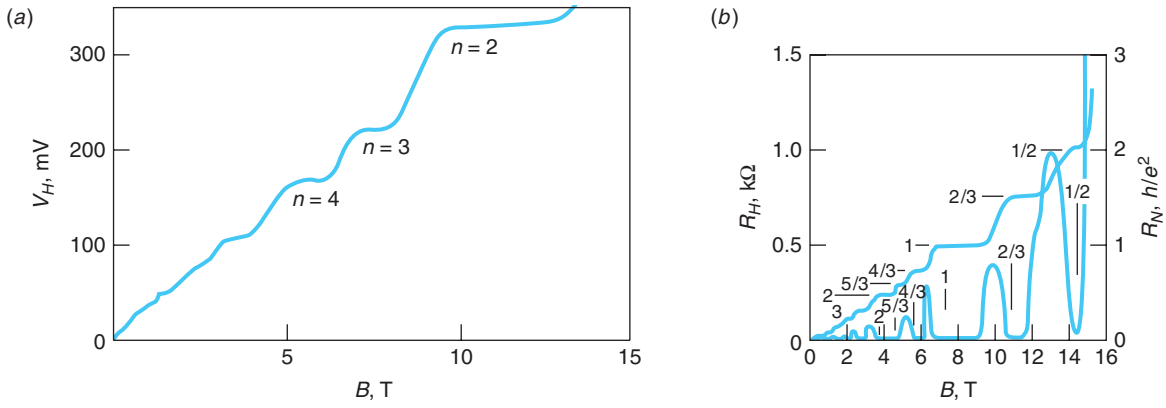

Figure 10-30 (*a*) A plot of the Hall voltage versus applied magnetic field shows plateaus, indicating that the Hall voltage is quantized. These data were taken at a temperature of 1.39 K with the current i held fixed at 25.52 μA. (*b*) The fractional quantum Hall effect. The Hall resistance R_H (the curve with the plateaus) is read on the left vertical axis, the normal resistance R_N (the curve with the peaks) on the right vertical axis. [*Data collected by Y. W. Suen and co-workers at Princeton University.*]

The values of n found by von Klitzing were small positive integers ($n = 1, 2, 3, \ldots$), as indicated in Figure 10-30*a*. Then, in 1982, Daniel Tsui and his co-workers,[10] while investigating the quantum Hall effect in ultrapure semiconductors, discovered quantized values of the Hall resistance for values of ν that were series of rational fractions formed from small integers. Values of R_H have been found thus far for more than 30 values of ν where $\nu = a, b$, where a and b are integers with no common factors. Several of these are seen in Figure 10-30*b*.

Von Klitzing's discovery is referred to as the integral quantized Hall effect (IQHE) and that of Tsui and his colleagues as the fractional quantized Hall effect (FQHE). The theoretical models that have been developed to explain these phenomena are as yet incomplete and, in any case, beyond the scope of our discussion here; however, we can give a brief qualitative description of the IQHE. In the "normal" Hall effect the material carries a current i due to an applied electric field $\mathscr{E}$. The electric field is perpendicular to the applied magnetic field $\mathbf{B}$, and as a result, the charge carriers move in a circular path, or orbit, of radius $r = m^*v/qB$. The fact that electrons obey the Pauli exclusion principle prevents the orbits from overlapping and determines how closely the electrons can group together on the negative side of the sample. Recalling that the orbital motion of electrons is quantized with only certain radii being allowed—namely those for which the orbit circumference equals an integral number of de Broglie wavelengths—we see that increasing the magnetic field decreases the orbit radius, but such decreases must occur suddenly and result in another, smaller allowed radius. Thus, more electron orbits can fit without overlapping in a given area and the density of charge carriers increases on the edges of the semiconductor sample. This increases the frequency of collisions and hence the Hall resistance. Since the orbit radii change only in quantized steps, so must the Hall resistance. Surprisingly, when the Hall resistance is on one of the plateaus, the ordinary resistance $R = V/i$ falls to zero, as illustrated by the multiple peaked curve in Figure 10-30*b*. The additional plateaus that occur in the FQHE are due to electron-electron spin interactions.

Because the von Klitzing constant can be measured with a precision of better than 1 part in 10^{10}, the quantum Hall effect is now used to define the standard of resistance. The ohm is now defined so that R_K has the value 25,812.807 Ω exactly.

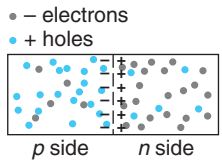

Figure 10-31 A *pn* junction. Because of the difference in their concentrations, holes diffuse from the *p* side to the *n* side and electrons diffuse from the *n* side to the *p* side. As a result, there is a double layer of charge at the junction, with the *p* side negative and the *n* side positive.

Spin Hall Effect

A new vista for spintronics was opened in 2004 with the observation of the spin Hall effect in GeAs at 20 K by David Awschalom and his group. In the spin Hall effect the electrons of a charge current flow in a nonmagnetic material in the absence of an external magnetic field but with an applied external electric field separate perpendicular to the conventional current direction into spin-up and spin-down populations that accumulate on opposite sides of the conducting material. The same phenomenon was detected at 295 K (room temperature) in ZnSe in 2006 by the same researchers. Although the effect is small, the potential useful applications, e.g., injecting spin-polarized electrons into semiconductor devices, would be enormous if current experiments to improve the size of the effect are successful.

10-8 Semiconductor Junctions and Devices

Semiconductor devices such as diodes and transistors make use of *n*-type and *p*-type semiconductors joined together as shown in Figure 10-31. In practice, the two types of semiconductors are often a single silicon crystal doped with donor impurities on one side and acceptor impurities on the other. The region in which the semiconductor changes from a *p*-type to an *n*-type is called a *junction*.

When an *n*-type and *p*-type semiconductor are placed in contact, the initially unequal concentrations of electrons and holes result in the diffusion of electrons across the junction from the *n* side to the *p* side until equilibrium is established. The result of this diffusion is a net transport of positive charge from the *p* side to the *n* side. Unlike the case when two different metals are in contact, there are fewer electrons available to participate in this diffusion because the semiconductor is not a particularly good conductor. The diffusion of electrons and holes creates a double layer of charge at the junction similar to that on a parallel-plate capacitor. There is thus a potential difference V across the junction, which tends to inhibit further diffusion. In equilibrium, the *n* side with its net positive charge will be at a higher potential than the *p* side with its net negative charge. In the junction region, there will be very few charge carriers of either type, so the junction region has a high resistance. Figure 10-32 shows the energy-level diagram for a *pn* junction. The junction region is also called the *depletion region* because it has been depleted of charge carriers.

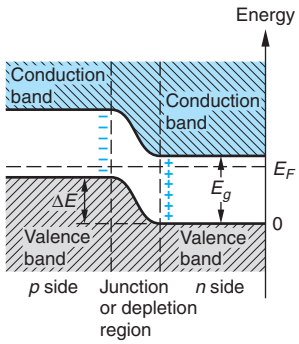

Figure 10-32 Electron energy levels for an unbiased *pn* junction.

Diodes

A semiconductor with a *pn* junction can be used as a simple diode rectifier. In Figure 10-33, an external potential difference has been applied across the junction by connecting a battery and resistor to the semiconductor. When the positive terminal of the battery is connected to the *p* side of the junction, as shown in Figure 10-33*a*, the diode is said to be *forward biased*. Forward biasing lowers the potential across the junction. The diffusion of electrons and holes is thereby increased as they attempt to reestablish equilibrium, resulting in a current in the circuit. If the positive terminal of the battery is connected to the *n* side of the junction, as shown in Figure 10-33*b*, the diode is said to be

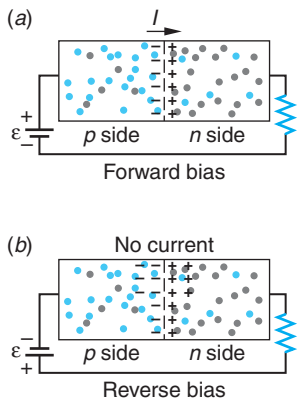

Figure 10-33 A *pn*-junction diode. (*a*) Forward-biased *pn* junction. The applied potential difference enhances the diffusion of holes from the *p* side to the *n* side and electrons from the *n* side to the *p* side, resulting in a current I. (*b*) Reverse-biased *pn* junction. The applied potential difference inhibits the further diffusion of holes and electrons, so there is no current.

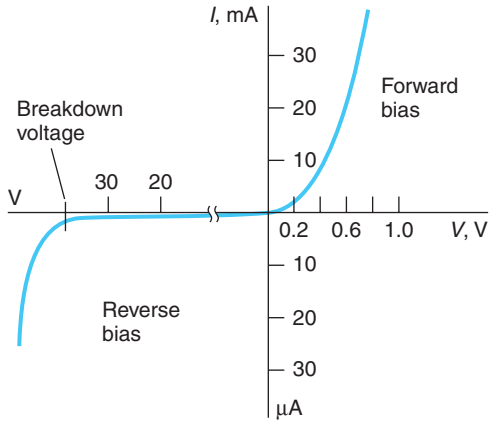

Figure 10-34 Current versus applied voltage across a *pn* junction. Note the different scales for the forward- and reverse-bias conditions.

reverse biased. Reverse biasing tends to increase the potential difference across the junction, thereby further inhibiting diffusion. Figure 10-34 shows a plot of current versus voltage for a typical semiconductor junction. Essentially, the junction conducts only in one direction, the same as a vacuum-tube diode. Junction diodes have replaced vacuum diodes in nearly all applications except when a very high current is required.

We can get an idea of how the current depends on applied voltage quantitatively if we note that the electrons and holes, being at the high energy end of the distribution, are approximately described by the Maxwell-Boltzmann distribution. Let N_e be the number of conduction electrons in the n region. With no external voltage, only a small fraction given by $N_e e^{-eV/kT}$ will have enough energy to diffuse across the contact potential difference. When a forward bias V_b is applied, the number that can cross the barrier becomes

$$N_e e^{-e(V-V_b)/kT} = (N_e e^{-eV/kT}) e^{+eV_b/kT}$$

The current due to the majority electron carriers in the n region will be

$$I = I_0 e^{+eV_b/kT}$$

where I_0 is the current with no bias. The current due to the minority carriers, the holes from the n side, will be merely I_0, the same as with no bias. (The minority carriers are swept across the junction by the contact potential V with or without a bias voltage.) The net current due to carriers from the n side will therefore be

$$I_{\text{net}} = I_0(e^{+eV_b/kT} - 1) \qquad \textbf{10-49}$$

If we now consider the current due to the majority and minority carriers from the p side, we obtain the same results. We can use Equation 10-49 for the total current if we interpret I_0 as the total current due to both kinds of minority carriers, holes in the n region and electrons in the p region. For positive V_b the exponential quickly dominates. For $V_b = 0$, the current is 0, and for V_b less than zero, the current saturates at $-I_0$, due to the flow of minority carriers. Note that the current in Figure 10-35 suddenly increases in magnitude at extreme values of reverse bias. In such large electric fields, two things can happen: either electrons are stripped from their atomic bonds or the few free electrons that exist in a reversed-biased junction are accelerated across the junction and gain enough energy to cause others to break loose. The first effect is

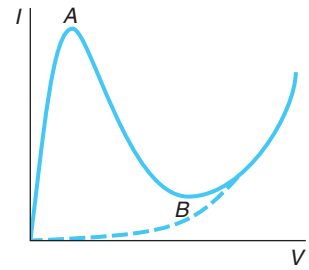

Figure 10-35 Current versus applied voltage for a tunnel diode. Up to point *A*, an increase in the bias voltage enhances tunneling. Between points *A* and *B*, an increase in the bias voltage inhibits tunneling, i.e., the diode acts as if it has negative resistance. After point *B*, the tunneling is negligible, and the diode behaves like an ordinary *pn*-junction diode, shown by the dashed line.

called *Zener breakdown*; the second, *avalanche breakdown*. Although such a breakdown can be disastrous in a circuit where it is not intended, the fact that it occurs at a sharp voltage value makes it of use in a special voltage reference standard known as a *Zener diode*.

An interesting effect that we can discuss only qualitatively occurs if both the *n* side and the *p* side of a *pn*-junction diode are so heavily doped that the bottom of the conduction band lies below the top of the valence band. Figure 10-36*a* shows the energy-level diagram for this situation. Since there are states on the *p* side with the same energy as states on the *n* side and the depletion region is now so narrow, electrons can tunnel across the potential barrier (see Section 6-6). This flow of electrons is called *tunneling current*, and such a heavily doped diode is called a *tunnel diode*.

At equilibrium with no bias, there is an equal tunneling current in each direction. When a small bias voltage is applied across the junction, the energy-level diagram is as shown in Figure 10-36*b* and the tunneling of electrons from the *n* to the *p* side is increased, whereas that in the opposite direction is decreased. This tunneling current in addition to the usual current due to diffusion results in a considerable net current. When the bias voltage is increased slightly, the tunneling current decreases because there are fewer states on the *p* side with the same energy as states on the *n* side. Although the diffusion current is increased, the net current is decreased. At large bias voltages the energy-level diagram is as shown in Figure 10-36*c*, the tunneling current is completely negligible, and the total current increases with increasing bias voltage due to diffusion as in an ordinary *pn*-junction diode. Figure 10-35 shows the current versus voltage curve for a tunnel diode. Such diodes are used in electric circuits because of their very fast response time. When operated near the peak in the current versus voltage curve, a small change in bias voltage results in a large change in the current.

Among the many applications of semiconductors with *pn* junctions are particle detectors called *surface-barrier detectors*. These consist of a *pn*-junction semiconductor with a large reverse bias so that there is ordinarily no current. When a high-energy particle, such as an electron, passes through the semiconductor, it excites electrons into the conduction band, creating many electron-hole pairs as it loses energy. The intrinsic electric field sweeps the electrons toward the positive (*n*) side of the junction and the holes toward the negative (*p*) side. The resulting current pulse signals the passage of the particles and records the energy lost by the particle in the detector. The pulses are of short duration ($10^{-8} - 10^{-7}$ seconds), making possible high-energy-resolution measurements.

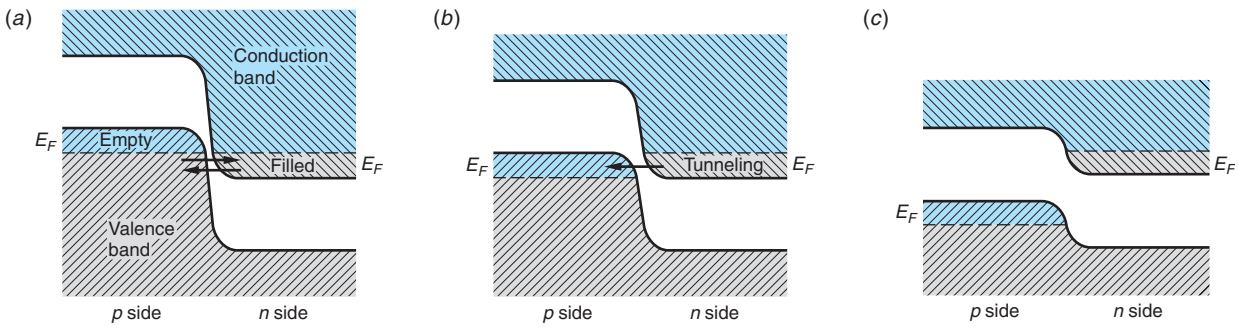

Figure 10-36 Electron energy levels for a heavily doped *pn*-junction tunnel diode. (*a*) With no bias voltage, some electrons tunnel in each direction. (*b*) With a small bias voltage, the tunneling current is enhanced in one direction, making a sizable contribution to the net current. (*c*) With further increases in the bias voltage, the tunneling current decreases dramatically.

FÈUE WHE

Light-emitting and light-absorbing *pn*-junction semiconductors function similar to gaseous atoms emitting and absorbing light, with the conduction and valence bands analogous to the atomic energy levels. The light-absorbing *pn*-junction semiconductor diode, or *solar cell*, is illustrated schematically in Figure 10-37*a*. When photons with energy greater than the gap energy (1.1 eV in silicon) strike the *pn*-junction, they can excite electrons from the valence band into the conduction band, leaving holes in the valence band. This region is already rich in holes. Some of the electrons created by the photons will recombine with holes, but some will migrate to the junction. From there they are accelerated into the *n*-type region by the intrinsic electric field between the double layers of charge. This creates an excess negative charge in the *n*-type region and excess positive charge in the *p*-type region. The result is a potential difference, a *photovoltage*, between the two regions, which in practice is about 0.6 V. If a load resistance is connected across the two regions, a charge flows through the resistance. Some of the incident light energy is thus converted into electrical energy. The current in the resistor is proportional to the number of incident photons, which is in turn proportional to the intensity of the incident light.

Light-emitting diodes (*LEDs*) are *pn*-junction semiconductors with a large forward bias that produces a large excess concentration of electrons on the *p* side and holes on the *n* side of the junction. (See Figure 10-37*b*.) Under these conditions, the diode emits light as the electrons and holes recombine. This is essentially the reverse of the process that occurs in a solar cell. Following the first practical demonstration of an LED (in 1962), the performance of LEDs has steadily improved. (See Figure 10-38.) They can be fabricated in all of the primary colors and, more recently, white light as well, portending them as a common source of white light in the future. LEDs already provide a viable alternative to filtered incandescent lighting in applications requiring monochromatic light. They are used, for example, as indicator lamps in appliances,

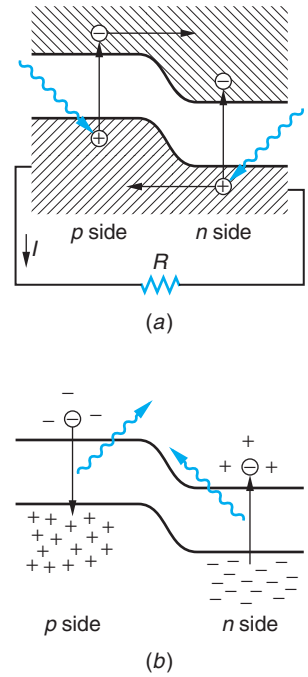

Figure 10-37 (*a*) A *pn* junction as a solar cell. Radiation striking the junction produces electrons and holes. The electrons are swept from the *p* side and holes from the *n* side by the intrinsic electric field. The accumulated charge results in a potential difference that produces a current through an external load. (*b*) A *pn* junction as an LED. Large forward bias produces current of electrons moving to the left and holes moving to the right. When they recombine, radiation is emitted.

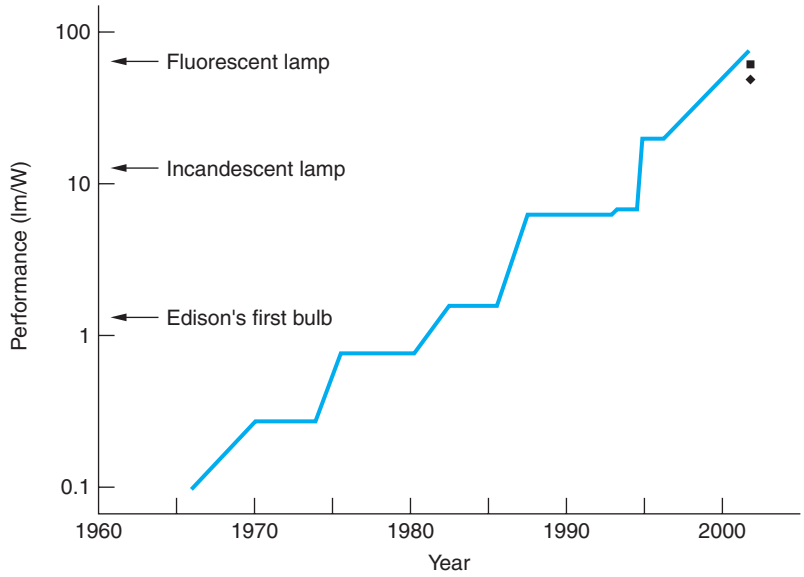

Figure 10-38 Summary of the performance improvements in LEDs over the span of their existence. The ■ marks the current performance of small-molecule OLEDs; the ◆ marks that of the polymer OLEDs. A few performance benchmarks are indicated on the vertical axis.

The development of InGaAlP HB LEDs in the early 1990s led to their rapid application to automotive rear lighting. The recent development of high-powered, large area, white GaN HB LEDs makes automobile headlights using these LEDs a possibility for the near future.

electronic equipment, calculators, and digital watches. In automobiles they are used in instrument panel lighting, and high-brightness (HB) LEDs are now often used for rear, stop, and turn lights. In traffic signals the red, amber, and green LED arrays now in common use require only 10 percent of the power consumed by the standard 140-W incandescent lamps, are brighter, and have a much longer lifetime. Rapid development of organic semiconductor light-emitting diodes (OLEDs) in the 1990s was catalyzed by worldwide efforts to construct large, full-color, flat-screen displays. Fabricated from small organic molecules and various polymers, OLEDs have an advantage over LEDs in that they can be produced on a large scale at very low cost. In LEDs high forward currents result in a very large population inversion, i.e., electrons on the *p* side and holes on the *n* side, so that stimulated emission dominates the light emission process and lasing results. By appropriate construction of the diode, a resonant cavity can be formed, leading to the production of a coherent beam of laser light in a selected direction (see Figure 10-39).

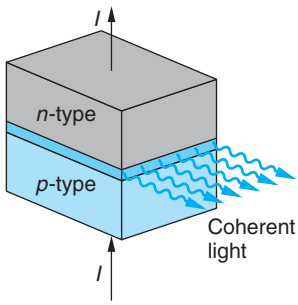

Figure 10-39 The resonant cavity is formed by cleaving the ends of the diode crystal parallel to one another and with the proper separation. Gallium arsenide and similar compounds, which have much higher photon-production efficiency than silicon, are typically used as diode laser semiconductors. Their light-energy-out to electrical-energy-in ratios are greater than 50 percent.

Transistors

The transistor, invented in 1948 by William Shockley, John Bardeen, and Walter Brattain,[11] has revolutionized the electronics industry and our everyday world. A simple junction transistor consists of three distinct semiconductor regions called the *emitter*, the *base*, and the *collector*. The base is a very thin region of one type of semiconductor sandwiched between two regions of the opposite type. The emitter semiconductor is much more heavily doped than either the base or the collector. In an *npn* transistor, the emitter and collector are *n*-type semiconductors and the base is a *p*-type semiconductor; in a *pnp* transistor, the base is an *n*-type semiconductor and the emitter and collector are *p*-type semiconductors. In a *pnp* transistor holes are emitted by the emitter; in an *npn* transistor electrons are emitted.

Figures 10-40 and 10-41 show, respectively, a *pnp* transistor and an *npn* transistor with the symbols used to represent each transistor in circuit diagrams. Notice that a transistor consists of two *pn* junctions. The operation of a *pnp* transistor is described in the MORE section *How Transistors Work*. The operation of an *npn* transistor is similar.

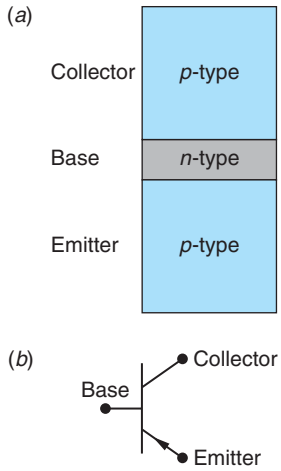

Figure 10-40 (*a*) A *pnp* transistor. The heavily doped emitter emits holes that pass through the thin base to the collector. (*b*) Symbol for a *pnp* transistor in a circuit. The arrow points in the direction of the conventional current, which is the same as that of the emitted holes.

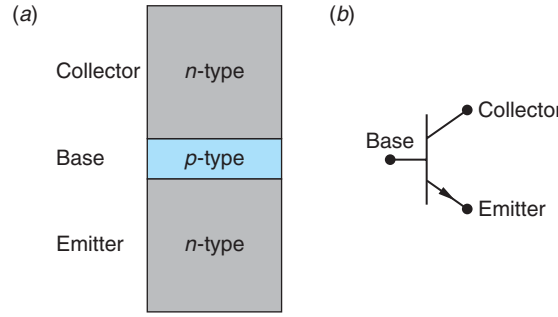

Figure 10-41 (*a*) An *npn* transistor. The heavily doped emitter emits electrons that pass through the thin base to the collector. (*b*) Symbol for an *npn* transistor. The arrow points in the direction of the conventional current, which is opposite the direction of the emitted electrons.

(*a*)

(*a*) LED traffic lights use 10 percent of the power of the old 140-W signal lamps, last far longer, and are collectively brighter. (*b*) Automobile LED rear lighting and brake lights have become ubiquitous, as have LED traffic signals. Pictured here are examples of the scores of different colors, shapes, and sizes of vehicle clearance and safety LED lights one sees every day on the streets and highways. [*Photos by Francisco Roman.*]

(*b*)

More

How Transistors Work, on the home page at www.whfreeman.com/tiplermodernphysics5e, describes the way transistors function in electrical circuits. Also located here are Equations 10-50 through 10-54, Example 10-10, and Figures 10-42 and 10-43.

Questions

9. Why is a semiconductor diode less effective at high temperatures?
10. Explain why adding impurities to metals decreases their conductivity but adding impurities to semiconductors increases their conductivity.
11. What would you expect to be the effect on the conductivity when impurities are added to an insulator?

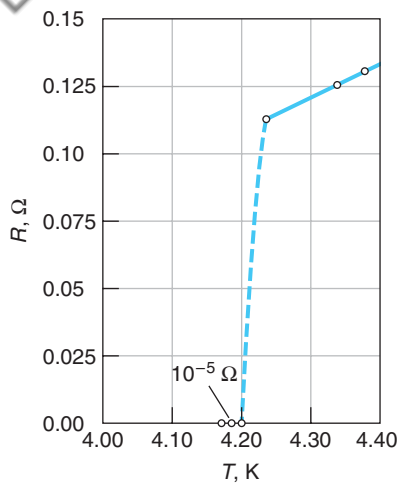

Figure 10-44 Plot by Kamerlingh Onnes of the resistance of mercury versus temperature, showing sudden decrease at the critical temperature $T = 4.2$ K signifying the onset of superconductivity.

10-9 Superconductivity

In 1911, just a few years after he had succeeded in liquefying helium and while he was investigating the properties of materials at liquid helium temperatures, the Dutch physicist H. Kamerlingh Onnes discovered that for some materials a certain temperature exists, called the *critical temperature* T_c, below which the resistivity is zero and the conductivity $\sigma = 1/\rho \rightarrow \infty$. He called this phenomenon *superconductivity*. Figure 10-44 shows the plot Kamerlingh Onnes obtained of the resistance of mercury versus temperature. The critical temperature for mercury is 4.2 K. The critical temperature varies from material to material, but below this temperature the electrical resistance of the material is zero. Critical temperatures for other superconducting elements range from less than 0.1 K for hafnium and iridium to 9.2 K for niobium. The critical temperatures of several superconducting materials are given in Table 10-6. In the presence of a magnetic field B, the critical temperature is lower than it is when there is no field. As the magnetic field increases, the critical temperature decreases, as illustrated in Figure 10-45. If the magnetic field is greater than some critical field B_c, superconductivity does not exist at any temperature. The values of T_c in the table are for $B = 0$.

Many metallic compounds are also superconductors. For example, the superconducting alloy Nb_3Ge, discovered in 1973, has a critical temperature of 23.2 K, which was the highest known until 1986, when the first of the complex high-T_c cuprate ceramic superconductors was discovered. More recently, in 2001 Jun Akimitsu discovered that the metal compound MgB_2, available "off the shelf" for about \$2/g, became superconducting at 39 K, as of this writing the highest T_c yet for a conventional superconductor. (See Table 10-6.) Despite the cost and inconvenience of refrigeration with expensive liquid helium, which boils at 4.2 K, many superconducting magnets have been built using such materials.

Electromagnets wound with superconducting wire are used in applications ranging from medical diagnostic MRI systems to beam-focusing and beam-bending magnets at large particle accelerators worldwide.

Table 10-6 T_c and B_c values for some type I and type II superconductors

Type I element	T_c (K)	B_c (at 0 K; T)	Type II compound	T_c (K)	B_{c2} (at 0 K; T)
Al	1.175	0.0105	Nb_3Sn	18.1	24.5
Cd	0.517	0.0028	Nb_3Ge	23.2	34.0
Hg	4.154	0.0411	NbN	16.0	15.3
In	3.408	0.0282	V_3Ga	16.5	35.0
Nb	9.25	0.2060	V_3Si	17.1	15.6
Os	0.66	0.0070	PbMoS	14.4	6.0
Pb	7.196	0.0803	CNb	8.0	1.7
Sn	3.722	0.0305	MgB_2	39.0	16
Tl	2.38	0.0178	Rb_3C_{60}	29.0	?
Zn	0.85	0.0054	Cs_2RbC_{60}	33.0	?

FÈUE WHE

The conductivity of a superconductor cannot be defined since its resistance is zero. There can be a current in a superconductor even when the electric field in the superconductor is zero. Such currents are called *supercurrents*. Indeed, steady currents have been observed to persist for years without apparent loss in superconducting rings in which there was no electric field.

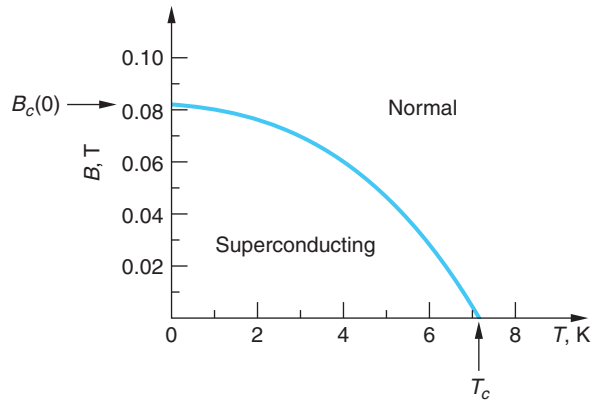

Figure 10-45 Variation of the critical temperature with magnetic field for lead. Note that B_c approaches zero as T approaches T_c.

Meissner Effect

Consider a superconducting material that is originally at a temperature greater than the critical temperature and is in the presence of a small external magnetic field $B < B_c$. We now cool the material below the critical temperature so that it becomes superconducting. Since the resistance is now zero, there can be no emf in the superconductor. Thus, from Faraday's law, the magnetic field in the superconductor cannot change. We therefore expect from classical physics that the magnetic field in the superconductor will remain constant. However, it is observed experimentally that when a superconductor is cooled below the critical temperature in an external magnetic field, the magnetic field lines are expelled from the superconductor and thus the magnetic field inside the superconductor is zero. (See Figure 10-46.) This effect was discovered by H. W. Meissner

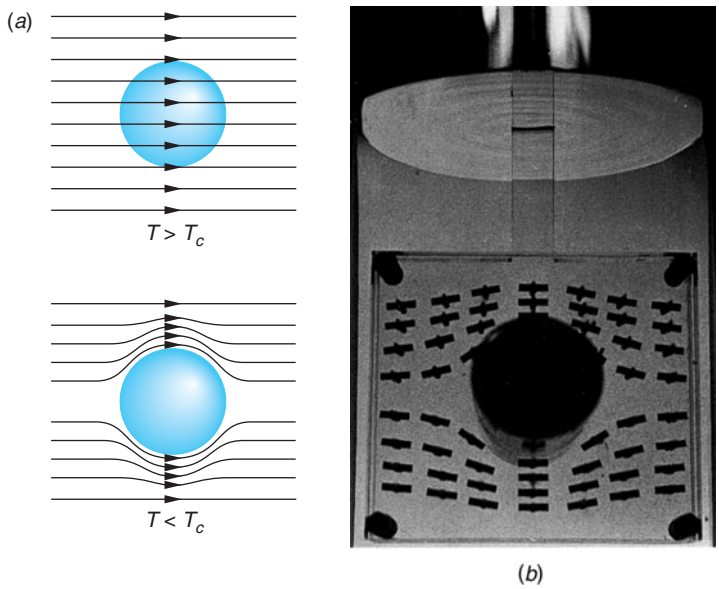

Figure 10-46 (*a*) The Meissner effect in a superconducting sphere cooled in a constant applied magnetic field. As the temperature drops below the critical temperature T_c, the magnetic field lines are expelled from the sphere. (*b*) Demonstration of the Meissner effect. A superconducting tin cylinder is situated with its axis perpendicular to a horizontal magnetic field. The directions of the field lines near the cylinder are indicated by weakly magnetized compass needles mounted in a Lucite sandwich so that they are free to turn. [*Courtesy of A. Leitner, Rensselaer Polytechnic Institute.*]

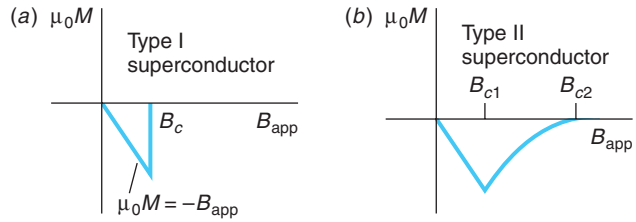

Figure 10-47 Plots of μ_0 times the magnetization M versus applied magnetic field for type I and type II superconductors. (*a*) In a type I superconductor, the resultant magnetic field is zero below a critical applied field B_c because the field due to induced currents on the surface of the superconductor exactly cancels the applied field. Above the critical field, the material is a normal conductor and the magnetization is too small to be seen on this scale. (*b*) In a type II superconductor, the magnetic field starts to penetrate the superconductor at a field B_{c1}, but the material remains superconducting up to the field B_{c2}, after which it becomes a normal conductor.

and R. Ochsenfeld in 1933 and is now known as the *Meissner effect*. It, not zero resistance, is the criterion that determines if a material is a superconductor. The mechanism by which the magnetic field lines are expelled or, more specifically, canceled within the bulk of the superconductor is that a supercurrent (called a screening current) is induced on the surface in such a direction as to exactly cancel the external field within the material.[12] Thus, the superconductor exhibits perfect diamagnetism. Establishing the supercurrent "costs" the superconductor an amount of energy per unit volume equal to $B^2/2\mu_0$, where μ_0 is the permeability of the vacuum. When the field B becomes larger than B_c, there is insufficient energy available and the material reverts to its "normal" resistive state. The magnetic levitation shown in the photograph below results from the repulsion between the permanent magnet producing the external field and the magnetic field produced by the currents induced in the superconductor.

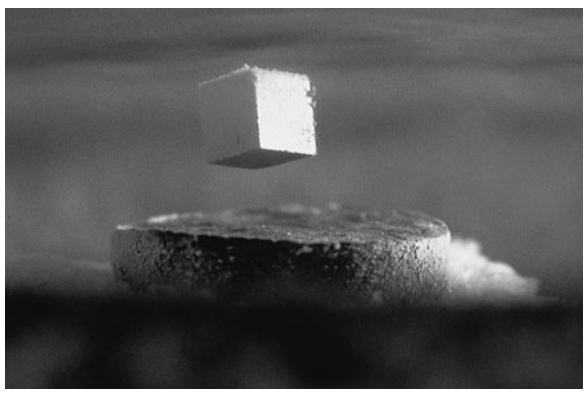

A small, cubicle permanent magnet levitates above a disk of the superconductor yttrium-barium-copper oxide, cooled by liquid nitrogen to 77 K. At temperatures below 92 K, the disk becomes superconducting. The magnetic field of the cube sets up circulating electric supercurrents in the superconducting disk, such that the resultant magnetic field in the superconductor is zero. These currents produce a magnetic field opposite to that of the cube, and thus the cube is repelled. [*Courtesy of IBM Research.*]

Only certain superconductors called *type I*, or *"soft,"* superconductors exhibit the complete Meissner effect. Type I superconductors are primarily very pure metal elements. Figure 10-47*a* shows a plot of the magnetization M times μ_0 versus the applied magnetic field B_{app} for a type I superconductor. For a magnetic field less than the critical field B_c, the magnetic field $\mu_0 M$ induced in the superconductor is equal and opposite to the external magnetic field; that is, the superconductor is a perfect diamagnet. The values of B_c for type I superconductors are all too small for such materials to be useful in the coils of a superconducting magnet. (See Table 10-6.)

Other materials, known as *type II*, or *"hard," superconductors*, have a magnetization curve similar to that in Figure 10-47*b*. Such materials are usually alloys or metals that have large resistivities in the normal state. Type II superconductors exhibit *two* critical magnetic fields, B_{c1} and B_{c2}, as shown in Figure 10-48 for tantalum. Applied fields less than B_{c1} result in the Meissner effect of total magnetic flux cancellation and the entire sample is superconducting, as in type I superconductors. Applied fields greater than B_{c2} result in complete penetration of the magnetic field throughout the sample, and the resistivity of

FÈUE WHE

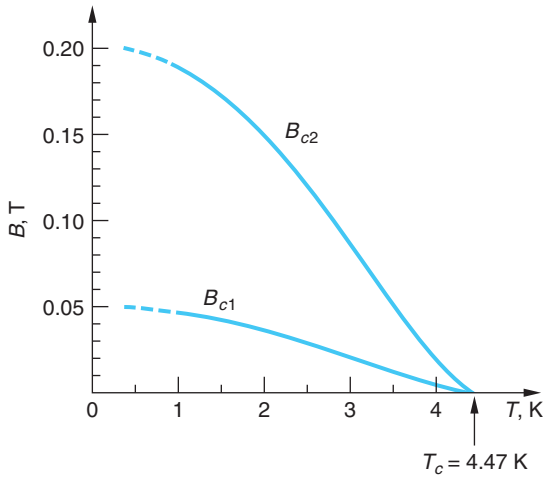

Figure 10-48 Critical magnetic fields B_{c1} and B_{c2} for Ta (99.95 percent) as a function of temperature. Below the B_{c1} curve Ta exhibits the Meissner effect. Between the two curves is a mixed, or vortex, state with filaments of normal Ta penetrating the superconducting state. Above the B_{c2} curve there is complete magnetic field penetration and the entire sample has normal resistivity.

the material returns to normal. However, in the region between B_{c1} and B_{c2} there is partial penetration of the magnetic field, the field lines being confined to *flux tubes*, also called *vortices*, in which the material has normal resistivity. The surrounding material remains field free and superconducting, as illustrated schematically in Figure 10-49. Each flux tube contains one quantized unit of magnetic flux, as will be described later in this section. For many type II superconductors the critical field B_{c2} may be several hundred times larger than the typical values of critical fields for type I superconductors (see Table 10-6). For example, the alloy Nb_3Ge has a critical field $B_{c2} = 34$ T. Such materials can be used to construct high-field superconducting magnets.

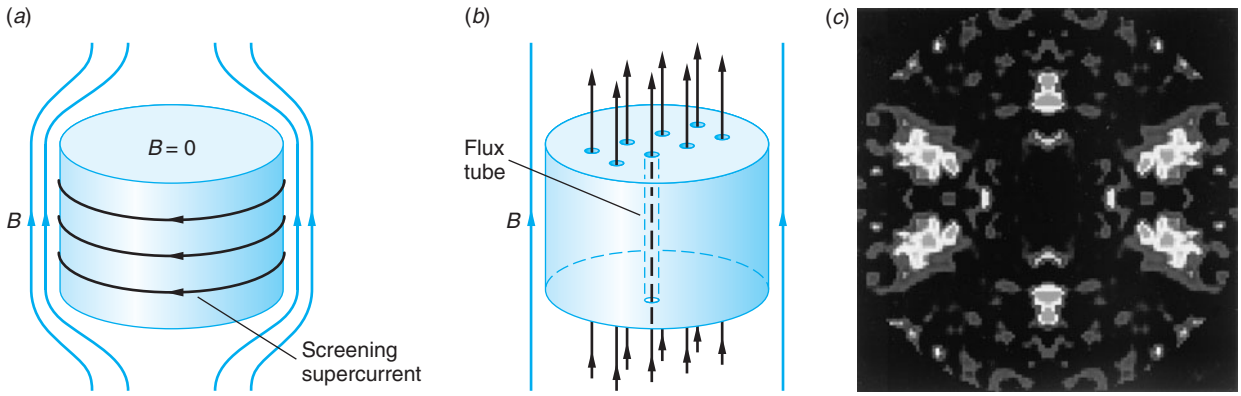

Figure 10-49 (*a*) Below B_{c1} the type II material shows the Meissner effect. For temperatures below T_c the material is superconducting and $B = 0$ throughout the volume. (*b*) For $B_{c1} < B < B_{c2}$, magnetic field lines penetrate the material but are confined to flux tubes of normally resistive material that form the so-called vortex lattice. For a given $T < T_c$, as the applied field B approaches B_{c2}, the size of the superconducting region shrinks as more flux tubes occupy the volume. When $B > B_{c2}$, the entire material has normal resistivity. (*c*) The lattice of magnetic vortices in UPt_3, a strongly type II superconductor, is shown clearly by neutron diffraction.

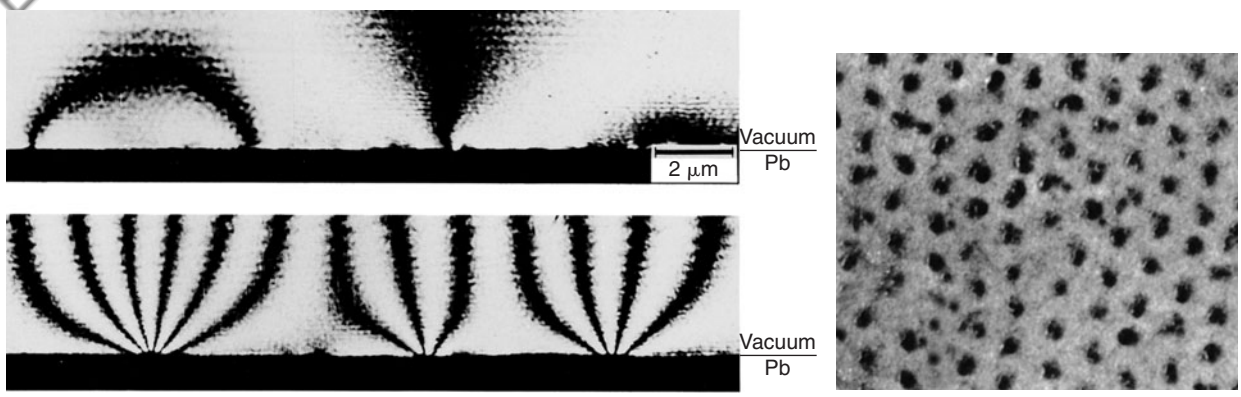

(*a*) (*b*)

Fluxoids penetrating a superconducting film. The image has been formed by the technique of electron holography, in which coherent electron beams are used in place of coherent light beams to create a hologram. Electrons passing by a magnetic field are phase-shifted; i.e., the phase term in their wave function changes. (The shift arises from a phenomenon known as the Aharonov-Bohm effect.) By superposing such a phase-shifted beam with an unshifted reference beam, an interference pattern is created that can be interpreted as an image of the magnetic field. For the upper images, a magnetic field was applied perpendicular to a thin superconducting lead film. When the field was weak, it was expelled by the Meissner effect. A stronger field, however, penetrated the film. The fluxoids shown arose from vortices of current set up in the superconductor—not from the applied field directly. In the upper right is an isolated fluxoid; in the upper left is an antiparallel pair of fluxoids. The lower micrograph, in which the lead film is thicker, shows penetration by bundles of fluxoids. [*Courtesy of Akira Tonomura, Hitachi Ltd., Saitama, Japan.*] (*b*) A lattice of fluxoid vortices penetrating the surface of a superconductor. They were made visible for the photograph by a dusting of fine ferromagnetic particles. [*Courtesy of U. Essmann.*]

EXPLORING
Flux Quantization

Consider a superconducting loop of area A carrying a current. There can be a magnetic flux $\phi_m = B_n A$ through the loop due to the current in the loop. According to Faraday's law of induction, if the flux changes, an emf will be induced in the loop that is proportional to the rate of change of the flux. But for a superconductor there can be no emf in the loop because there is no resistance. Therefore, the flux through the ring is frozen and cannot change. Indeed, the quantum-mechanical treatment of superconductivity reveals that the total flux through the loop is quantized and is given by

$$\phi_m = n\frac{h}{2e} \qquad n = 1, 2, 3, \ldots$$

The quantum of flux, called a *fluxoid*, is

$$\phi_0 = \frac{h}{2e} = 2.0678 \times 10^{-15}\ \mathrm{T \cdot m^2}$$

Each flux tube in a type II superconductor with $B_{c1} < B < B_{c2}$ contains one quantum of flux.

FEUE WHE

BCS Theory

Our discussion of the classical free-electron theory in Section 10-2 considered the ions of the crystal lattice to be fixed. Resistivity was due to the interactions of the electrons with the ions of the lattice, and both electron-electron interactions and the effects of lattice vibrations, i.e., electron-phonon interactions, were ignored. In the quantum theory of conduction, lattice vibrations were explicitly taken into account (see Equations 10-41 to 10-43). Lattice vibrations are also responsible for the *isotope effect*[13] in superconductivity, discovered in 1950. This experimental observation revealed that the critical temperature depended on the isotopic mass of the crystal according to

$$M^{\alpha}T_c = \text{constant} \qquad \textbf{10-55}$$

where M is the average isotopic mass and α varies from material to material. For example, for mercury $\alpha = 0.50$ and $T_c = 4.185$ K for samples of average isotopic mass $M = 199.5$ u, whereas $T_c = 4.146$ K for samples with $M = 203.4$ u. Table 10-7 lists experimental values for α for a few superconductors.

The importance of the discovery represented by Equation 10-55 is to tell us that the lattice vibrations, hence the electron-phonon interactions, cannot be ignored. The assumption of fixed lattice ions is equivalent to assuming that $M \rightarrow \infty$ for electron-lattice ion interactions. But if $M \rightarrow \infty$, then T_c would be zero for all materials.

It had been recognized for some time that superconductivity is due to a collective behavior of the conducting electrons, and discovery of the isotope effect pointed to the crucial interaction as being with the phonons. In 1957, John Bardeen, Leon Cooper, and Bob Schrieffer published a successful theory of superconductivity now known as the *BCS theory*.[14] According to this theory, the electrons in a superconductor are coupled in pairs at low temperatures. The coupling comes about because of the interaction between electrons and the crystal lattice. An electron moving through the lattice of positive ions interacts with and perturbs it, as illustrated in Figure 10-50. The electron attracts the positive ions nearby, displacing them slightly, resulting in a region of increased positive charge density. Because the ions are bound to the lattice by elastic forces, this region of increased charge density propagates through the material as a vibrational wave in the lattice, i.e., a *phonon*. The momentum of the phonon has been provided by the electron, and we can think of the electron as having emitted a phonon.

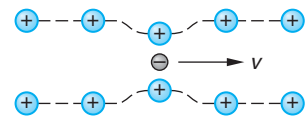

Figure 10-50 An electron traveling through the lattice of positive ions generates a wave of increased charge density, shown in two dimensions by the dashed lines. The momentum of the wave comes at the expense of the electron's momentum. A second electron may encounter the wave and absorb its momentum. The net effect is an attraction between the two electrons and the production, for $T < T_c$, of a Cooper pair.

Table 10-7 Experimental values of α for a few superconductors

Material	α	Material	α
Cd	0.32	Nb_3Sn	0.08
Hg	0.50	Os	0.15
Pb	0.49	Zn	0.45

Data from C. Kittel, *Introduction to Solid State Physics,* 8th ed. (New York: Wiley, 2005).

A second electron that encounters the wave of increased positive charge concentration is attracted toward it by the Coulomb interaction and can absorb the momentum carried by the wave; i.e., it may absorb the phonon. Thus, the two electrons can interact via the phonon and (very important) the interaction is an attractive one since both electrons experience an attractive force toward the region of increased positive charge density. At low temperatures ($T < T_c$) the attraction between the two electrons can exceed the Coulomb repulsion between them. Then the electrons can form a bound state called a *Cooper pair*, provided the temperature is low enough so that the number and energy of randomly generated thermal phonons will not disrupt its formation. The electrons in a Cooper pair have opposite spins and equal and opposite linear momenta. Thus, they form a system with zero spin and zero momentum. Each Cooper pair may be considered as a single particle with zero spin. Such a particle does not obey the Pauli exclusion principle, so any number of Cooper pairs may be in the same quantum state with the same energy.[15] In the ground state of a superconductor (at $T = 0$), all the electrons are in Cooper pairs and all the Cooper pairs are in the same energy state. In the superconducting state, the Cooper pairs are correlated, so that they all act together. In order for the electrons in a superconducting state to absorb or emit energy, the binding of the Cooper pairs must be broken. The energy needed to break up a Cooper pair is analogous to that needed to break up a molecule into its constituent atoms. This energy is called the *superconducting energy gap* E_g. In the BCS theory, this energy at absolute zero is predicted to be

$$E_g = 3.5kT_c \qquad \textbf{10-56}$$

In agreement with experimental observations, BCS theory also predicts the flux quantization described in the Exploring section on page 462 and the temperature dependence of B_c.

$$B_c(T)/B_c(0) = 1 - (T/T_c)^2$$

EXAMPLE 10-11 **Energy Gap of Cadmium** (*a*) Calculate the superconducting energy gap at $T = 0$ K predicted by the BCS theory for cadmium and compare the result with the measured result of 1.50×10^{-4} eV. (*b*) Compute the wavelength of a photon whose energy is just sufficient to break up a Cooper pair in cadmium.

SOLUTION

(*a*) From Table 10-6, we have that $T_c = 0.517$ K for cadmium. The BCS prediction of the energy gap is then

$$E_g = 3.5kT_c = \frac{3.5(1.38 \times 10^{-23}\ J/K)(0.517\ \text{K})}{(1.60 \times 10^{-19}\ \text{J/eV})} = 1.56 \times 10^{-4}\ \text{eV}$$

This differs from the measured values of 1.50×10^{-4} eV by about 4 percent.

(*b*) $E_g = hf = hc/\lambda$, or we have that

$$\lambda = hc/E_g = \frac{(6.63 \times 10^{-34}\ \text{J} \cdot \text{s})(3.00 \times 10^{8}\ \text{m/s})}{(1.56 \times 10^{-4}\ \text{eV})(1.60 \times 10^{-19}\ \text{J/eV})} = 7.97 \times 10^{-3}\ \text{m}$$

Remarks: This wavelength is in the short-wavelength microwave region of the electromagnetic spectrum.

Note that the energy gap for a typical superconductor is much smaller than the energy gap for a typical semiconductor, which is of the order of 1 eV. As the temperature is increased from $T = 0$, some of the Cooper pairs are broken. The resulting individual (unpaired) electrons interact with the remaining Cooper pairs, reducing the energy gap until at $T = T_c$ the energy gap is zero (see Figure 10-51). Notice, too, that the gap

energy is typically larger than that available from the thermal energy of the system. For example, for $T = 0.5\,T_c$, $E_g(T) = (0.95)\,E_g(0) \approx (3.3)\,kT_c$, whereas the thermal energy $kT = (0.5)kT_c$.

The Cooper pairs that we have discussed so far have zero momentum, so there are as many electrons traveling in one direction as the other and there is no current. Cooper pairs can also be formed with a net momentum **p** rather than zero momentum, but all the pairs have the same momentum. In this state, current is carried by the Cooper pairs. In ordinary conductors, resistance is present because the current carriers can be scattered with a change in momentum. As we have discussed, this scattering may be due to impurity atoms or thermal vibrations of the lattice ions. In a superconductor, the Cooper pairs are constantly scattering each other, but since the total momentum remains constant in this process, there is no change in the current. A Cooper pair cannot be scattered by a lattice ion because all the pairs act together. The only way that the current can be decreased by scattering is if a pair is broken up, which requires energy greater than or equal to the energy gap E_g. At reasonably low currents, scattering events in which the total momentum of a Cooper pair is changed are completely prohibited, so there is no resistance.

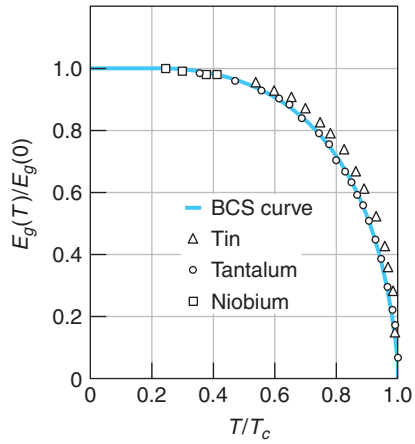

Figure 10-51 Ratio of the energy gap at temperature T to that at $T = 0$ as a function of the relative temperature T/T_c. The solid curve is that predicted by the BCS theory.

EXAMPLE 10-12 How Big Is a Cooper Pair? Calculate an estimate of the separation Δx of the electrons forming a Cooper pair, assuming that the binding energy of the pair equals the gap energy E_g and that, like semiconductors, the gap is centered on the Fermi energy E_F.

SOLUTION

The energy of either electron is, with the aid of the de Broglie relation, given by

$$E = \frac{p^2}{2m^*} = \frac{\hbar^2 k^2}{2m^*}$$

and

$$\Delta E = \frac{2k\hbar^2\,\Delta k}{2m^*}$$

If we associate E with the Fermi energy and ΔE with the gap, then

$$\frac{\Delta E}{E} \approx \frac{E_g}{E_F} \approx \frac{2k\hbar^2\,\Delta k}{2m^*} \times \frac{2m^*}{\hbar^2 k^2} \approx \frac{2\,\Delta k}{k}$$

Since the Fermi energy is typically of the order of 1 eV and the gap of the order 10^{-4} eV, as computed in Example 10-12, then $E_g/E_F \approx 10^{-4}$ and

$$\Delta k \approx 0.5 \times 10^{-4} k$$

where k refers to the value at the Fermi level. As was discussed in Section 10-6 and illustrated in Figure 10-19, $k = \pi/a$ at the top of the first allowed band, where the energy is approximately E_F. The lattice spacing $a \approx 0.1$ nm, so we have that $k \approx \pi/0.1\ \text{nm}^{-1}$ and $\Delta k = 10^{-3}\ \text{nm}^{-1}$. From the uncertainty relation (Equation 5-17), we then have that the uncertainty in the location of either electron, i.e., the extent of their wave functions in space, is

$$\Delta x = \frac{1}{\Delta k} = 10^3\ \text{nm}$$

or roughly equal to 10,000 atomic diameters and approximately equal to the wavelength of visible light.

High-Temperature Superconductivity

For many years, the highest known critical temperature for a superconductor was 23.2 K for the alloy Nb_3Ge. Then in 1986 J. G. Bednorz and K. A. Müller found that an oxide of lanthanum, barium, and copper became superconducting at 30 K. Soon afterward, in 1987, superconductivity with a critical temperature of 92 K was found in a ceramic of copper oxide containing yttrium and barium ($YBa_2Cu_3O_7$). Since then, several copper oxides have been found with critical temperatures as high as 164 K. Table 10-8 lists some of the high-temperature superconductors along with their critical temperatures. These discoveries have revolutionized the study of superconductivity because relatively inexpensive liquid nitrogen, which boils at 77 K, can be used for a coolant. However, there are many problems, such as the brittleness of ceramics, that thus far make these new superconductors difficult to use. High-temperature superconductors are all type II superconductors with very high upper critical fields. For some, B_{c2} is estimated to be as high as 100 T. Although the BCS theory appears to be the correct starting place for understanding these new superconductors, they have many features that are not clearly understood, and the theoretical explanation of the phenomenon is not yet in hand. Thus, there is much work, both experimental and theoretical, to be done.

Table 10-8 Critical temperatures of some high T_c superconductors

Material	T_c, K
LaBaCuO	30
La_2CuO_4	40
$YBa_2Cu_3O_7$	92
$DyBa_2Cu_3O_7$	92.5
$C_{60}(CHBr_3)$	117
BiSrCaCuO	120
$Tl_2Ba_2Ca_2Cu_3O_{10}$	120
$Hg_{.8}Tl_{.2}Ba_2Ca_2Cu_3O_{8.33}$	138

EXPLORING
Josephson Junction

In Section 6-6, we discussed barrier penetration—the tunneling of a single particle through a potential barrier. The tunneling of electrons from one metal to another can be observed by separating the two metals with a thin layer only a few nanometers thick of an insulating material such as aluminum oxide. When both metals are normal metals (not superconductors), the current resulting from the tunneling of

FÈUE WHE

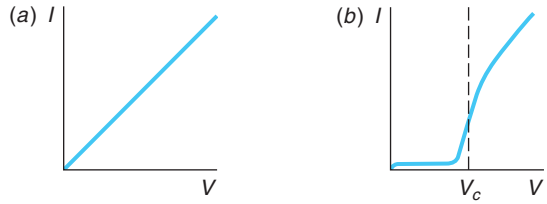

Figure 10-52 Tunneling current versus voltage for a junction of two metals separated by a thin oxide layer. (*a*) When both metals are normal metals, the current is proportional to the voltage as predicted by Ohm's law. (*b*) When one metal is a normal metal and one is a superconductor, the current is approximately zero until the applied voltage exceeds the critical voltage $V_c = E_g/2e$.

electrons through the insulating layer obeys Ohm's law for low applied voltages (see Figure 10-52*a*). When one of the metals is a normal metal and the other is a superconductor, there is no current (at absolute zero) unless the applied voltage V is greater than a critical voltage $V_c = E_g/2e$, where E_g is the superconductor energy gap. Figure 10-52*b* shows the plot of current versus voltage for this situation. The current jumps abruptly when V is great enough to break up a Cooper pair. (At temperatures above absolute zero, there is a small current because some of the electrons in the superconductor are thermally excited above the energy gap and therefore are not paired.) The superconducting energy gap can thus be accurately measured by measuring the critical voltage V_c.

In 1962, Brian Josephson[16] proposed that when two superconductors form a junction, now called a *Josephson junction*, Cooper pairs could tunnel from one superconductor to the other with no resistance. The current is observed with no voltage applied across the junction and is given by

$$I = I_{\max} \sin(\phi_2 - \phi_1) \qquad \textbf{10-57}$$

where $I_{\max}$ is the maximum current, which depends on the thickness of the barrier, ϕ_1 is the phase of the wave function for the Cooper pairs in one of the superconductors, and ϕ_2 is the phase of the corresponding wave function in the other superconductor. (The phase of a wave function is the exponent $Et/\hbar = \omega t$ of the time part of the total wave function. See Section 6-1.) This result has been observed experimentally and is known as the *dc Josephson effect*.

Josephson also predicted that if a dc voltage were applied across a Josephson junction, there would be a current that alternates with frequency f given by

$$f = \frac{2eV}{h} \qquad \textbf{10-58}$$

This result, known as the *ac Josephson effect*, has also been observed experimentally, and careful measurement of the frequency allows a precise determination of the ratio e/h. Because frequency can be measured so accurately, the ac Josephson effect is also used to establish precise voltage standards. The inverse effect, in which the application of an alternating voltage across a Josephson junction results in a dc current, has also been observed.

FEUE WHE

EXAMPLE 10-13 **AC Josephson Effect** Using $e = 1.602 \times 10^{-19}$ C and $h = 6.626 \times 10^{-34}$ J · s, calculate the frequency of the Josephson current if the applied voltage is 1 μV.

SOLUTION

From Equation 10-58, we obtain

$$f = \frac{2eV}{h} = \left(\frac{2(1.602 \times 10^{-19}\ \text{C})(10^{-6}\ \text{V})}{6.616 \times 10^{-34}\ \text{J} \cdot \text{s}}\right) = 4.836 \times 10^{8}\ \text{Hz}$$
$$= 483.6\ \text{MHz}$$

There is a third effect observed with Josephson junctions. When a dc magnetic field is applied through a superconducting ring containing two Josephson junctions, the total supercurrent shows interference effects that depend on the intensity of the magnetic field (Figure 10-53). This effect can be used to measure very weak magnetic fields. It is the basis for a device called a *SQUID* (for *S*uperconducting *Qu*antum *I*nterference *D*evice) that can detect magnetic fields as low as 10^{-14} T. Such a device can detect the magnetic fields produced by the tiny currents flowing in the heart and brain.

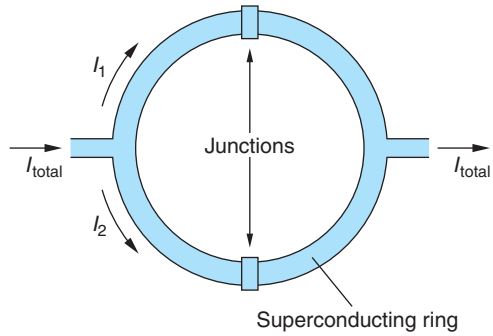

Figure 10-53 A superconducting ring with two Josephson junctions. When there is no applied magnetic field through the ring, the currents I_1 and I_2 are in phase. A very small applied magnetic field produces a phase difference in the two currents that produces interference in the total current exiting the ring.

Summary

TOPIC	RELEVANT EQUATIONS AND REMARKS
1. Structure of solids	Solids are often found in crystalline form, in which a small structure called the *unit cell* is repeated over and over. The structure of the unit cell depends on the type of bonding between the atoms, ions, or molecules forming the crystal.
Ionic and covalent solids	The attractive part of the potential energy of an ion in an ionic crystal is $U_{att} = -\alpha\frac{ke^2}{r}$ **10-1** where r is the separation between neighboring ions and α is the Madelung constant, which depends on the crystal geometry. The constant α is 1.7476 for face-centered-cubic crystals.

TOPIC	RELEVANT EQUATIONS AND REMARKS
	In covalently bonded crystals the individual bonds are just like those in covalently bonded molecules. The metallic bond has no single-molecule counterpart. One or more valence electrons are free to move throughout the solid, and *all* of the atoms share all of the free electrons, making this bond roughly analogous to the covalent bond.
2. Classical free-electron theory	Electrical resistivity ρ and conductivity σ are given by $\rho = \frac{m_e\langle v\rangle}{ne^2\lambda}$ and $\sigma = \frac{ne^2\lambda}{m_e\langle v\rangle}$ **10-13** where $\langle v\rangle$ is the mean speed of the electrons and λ is the mean free path between collisions. The latter is given by $\lambda = \frac{1}{n_a\pi r^2}$ **10-12** where n_a is the ion density. These yield Ohm's law correctly but result in the wrong temperature dependence of the resistivity.
3. Electron gas in metals	The average energy of the electrons at ordinary temperatures is much larger than kT: $\langle E\rangle = \frac{3}{5}E_F$ **10-22** where typical values of the Fermi energy E_F are 1 to 2 eV.
4. Quantum theory of conduction	This theory results from making two important corrections to the classical free-electron theory. First, the Fermi-Dirac distribution of electron energies is used rather than the Maxwell-Boltzmann distribution. Second, the effect of the wave characteristics of the electrons is considered in their scattering from the lattice ions. The resulting theory is in good agreement with observations.
5. Magnetism in solids	The origin of magnetism in solids is the electron spins and their associated magnetic moments.
6. Band theory of solids	When many atoms are brought together to form a solid, the individual energy levels are split into bands of allowed energies. The splitting depends on the type of bonding and the lattice separation. In a conductor, the uppermost band containing electrons is only partially full, so there are many available states for excited electrons. In an insulator, the uppermost band containing electrons, the valence band, is completely full and there is a large energy gap between it and the next allowed band, the conduction band. In a semiconductor, the energy gap between the filled valence band and the empty conduction band is small, so at ordinary temperatures an appreciable number of electrons are thermally excited into the conduction band.
Kronig-Penney model	The solid is modeled as a periodic potential. The wave functions are then $\psi(x) = u_k(x)e^{ikx}$ **10-36** where the function $u_k(x)$ is periodic with a period equal to that of the spacing of the potential wells and e^{ikx} is a free electron, i.e., a plane wave. The energy gaps occur at $ka = \pm n\pi$ **10-41** for integer n and a equal to the lattice spacing.

TOPIC	RELEVANT EQUATIONS AND REMARKS
7. Impurity semiconductors	The conductivity of a semiconductor can be greatly increasing by doping. In an *n*-type semiconductor, the doping adds electrons just below the conduction band. In a *p*-type semiconductor, holes are added just above the valence band. A junction between an *n*-type and *p*-type semiconductors has applications in many devices, such as diodes, solar cells, and light-emitting diodes. A transistor consists of a very thin semiconductor of one type sandwiched between two semiconductors of the opposite type. Transistors are used in amplifiers because a small variation in the base current results in a large variation in the collector current.
8. Superconductivity	In a superconductor the resistance drops suddenly to zero below a critical temperature T_c. Magnetic field lines are expelled and $B = 0$ inside a type I semiconductor, a phenomenon called the Meissner effect. Superconductivity at low temperatures is described by BCS theory, in which free electrons form Cooper pairs. Recently discovered high-temperature semiconductors are only partially understood in terms of BCS theory.

General References

The following general references are written at a level appropriate for the readers of this book.

Anderson, B., *Fundamentals of Semiconductor Devices*, McGraw-Hill, New York, 2005.

Blatt, F., *Modern Physics*, McGraw-Hill, New York, 1992.

Burns, G., *Solid State Physics*, Academic Press, Orlando, FL, 1985.

Eisberg, R., and R. Resnick, *Quantum Physics of Atoms, Molecules, Solids, Nuclei, and Particles,* 2d ed., Wiley, New York, 1985.

Fermi, E., *Molecules, Crystals, and Quantum Statistics* (trans. M. Ferro-Luzzi), W. A. Benjamin, New York, 1966.

Holden, A., *The Nature of Solids*, Columbia University Press, 1968. An excellent nonmathematical treatment of the properties of solids.

Kittel, C., *Introduction to Solid State Physics*, 8th ed., Wiley, New York, 2005.

Leitner, A., *Introduction to Superconductivity*, Michigan State University, East Lansing, 1965. This excellent film, running 48 minutes, is probably one of the best introductions to superconductivity available.

Shockley, W., *Electrons and Holes in Semiconductors*, Van Nostrand, Princeton, NJ, 1950.

Notes

1. The constant n is often called the Born exponent.

2. Carbon also has a fourth solid form, charcoal, which has no well-defined crystalline structure.

3. Notice that this view of the metal fits the definition of a plasma set forth in the opening paragraph of the chapter. Though not usually thought of in that way, metals are indeed low-temperature plasmas.

4. Felix Bloch (1905–1983), Swiss American physicist. He devised a method for measuring atomic magnetic fields in liquids and solids that led to the development of nuclear magnetic resonance (NMR) spectroscopy and earned for him a share (with E. M. Purcell) of the 1952 Nobel Prize in Physics. He was the first director-general of CERN, the European Center for Nuclear Research.

5. The graph of the energy bands and gaps of Figure 10-19*b* results from a simplified version of the conditional equation connecting k, k', and α in which $b \rightarrow 0$ and $U_0 \rightarrow \infty$. In that limit the lattice spacing is a, rather than $a + b$, as in Figure 10-18.

6. This mixing, called hybridization, was discussed in Section 9-2.

7. See, e.g., Section 25-5 in P. Tipler and G. Mosca, *Physics for Scientists and Engineers*, 6th ed. (W. H. Freeman and Co., New York, 2008).

8. The fact that the radius of the bound electron is several times the equilibrium spacing of the atoms helps justify our tacit assumption that the fifth electron sees a uniform dielectric constant in the crystal.

9. Klaus von Klitzing (b. 1943), German physicist. He received the 1985 Nobel Prize in Physics for this discovery.
10. Daniel C. Tsui (b. 1939), Chinese American physicist. He received the 1998 Nobel Prize in Physics with H. L. Stormer and R. B. Laughlin for their discovery.
11. William B. Shockley (1910–1989), John Bardeen (1908–1991), and Walter H. Brattain (1902–1987), American physicists. Shockley discovered that doped germanium crystals were excellent rectifiers, and subsequently the three Bell Laboratories colleagues discovered that two such "solid-state rectifiers" combined would amplify current. The discovery of this device, the transistor, earned them the 1956 Nobel Prize in Physics.
12. Actually, the field decreases exponentially across the surface, reaching zero at a depth of about 10 nm.
13. Isotopes are atoms with the same atomic number Z but different atomic mass numbers A. Isotopes will be discussed in Chapter 11.
14. John Bardeen (1908–1991), Leon N. Cooper (b. 1930), and J. Robert Schrieffer (b. 1931), American physicists. Developed at the University of Illinois, the BCS theory earned the collaborators the 1972 Nobel Prize in Physics, and Bardeen became the only person thus far to win two physics Nobel Prizes (see note 11).
15. This may make it seem like the Cooper pair is a boson and superconductivity another example of Bose-Einstein condensation (see Section 8-3); however, the large size of the Cooper pair (see Example 10-12) means many pairs overlap and that the symmetry of the pair with respect to an exchange of electrons must also take into account exchanges involving electrons in different pairs. The result is that the Cooper pair is neither a pure boson nor a pure fermion.
16. Brian D. Josephson (b. 1940), Welsh physicist. For this discovery, made while he was still a graduate student, he shared the 1973 Nobel Prize in Physics with L. Esaki and I. Giaever. Bardeen had strongly opposed Josephson's tunneling prediction until experiments, led by those of Giaever (also done while he was a graduate student), confirmed tunneling by Cooper pairs.

Problems

Level I

Section 10-1 The Structure of Solids

10-1. Find the value of n in Equation 10-6 that gives the measured dissociation energy of 741 kJ/mol for LiCl, which has the same structure as NaCl and for which $r_0 = 0.257$ nm.
10-2. Calculate the distance r_0 between the K^+ and Cl^- ions in KCl, assuming that each ion occupies a cubic volume of side r_0. The molar mass of KCl is 74.55 g/mol and its density is 1.984 g/cm^3.
10-3. The distance between the Li^+ and Cl^- ions in LiCl is 0.257 nm. Use this and the molecular mass of LiCl (42.4 g/mol) to compute the density of LiCl.
10-4. The crystal structure of KCl is the same as that of NaCl. (*a*) Calculate the electrostatic potential energy of attraction of KCl, assuming that r_0 is 0.314 nm. (*b*) Assuming that $n = 9$ in Equation 10-6, calculate the dissociation energy in eV per ion pair and in kcal/mol. (*c*) The measured dissociation energy is 165.5 kcal/mol. Use this to determine n in Equation 10-6.
10-5. The observed dissociation energy of solid LiBr is 788 kJ/mol. Compute the cohesive energy of LiBr and compare the result with the value in Table 10-1. (Ionization energies for Li and Br are in Table 9-1.)
10-6. The density of NaCl (an fcc crystal) is 2.16 g/cm^3. Find the distance between ions that are nearest neighbors.
10-7. The separation of nearest neighbor ions in the KCl crystal (an fcc structure) is 0.315 nm. Use this information to determine the density of KCl.
10-8. Using the data for ionic and metallic crystals from Table 10-1, (*a*) graph cohesive energy versus melting point and put the best straight line through the points. (*b*) Determine the cohesive energies of cobalt, silver, and sodium, whose melting temperatures are 1495°C, 962°C, and 98°C, respectively. (The measured values are cobalt 4.43 eV, silver 2.97 eV, and sodium 1.13 eV.)
10-9. Figure 10-54 shows a one-dimensional ionic lattice consisting of doubly charged positive ions and twice as many singly charged negative ions. Compute the Madelung constant for this "crystal" to within 1 percent.

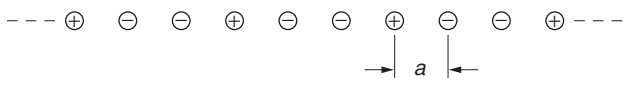

Figure 10-54

Section 10-2 Classical Theory of Conduction

10-10. (*a*) Given a mean free path $\lambda = 0.4$ nm and a mean speed $\langle v \rangle = 1.17 \times 10^5$ m/s for the current flow in copper at a temperature of 300 K, calculate the classical value for the resistivity ρ of copper. (*b*) The classical model suggests that the mean free path is temperature independent and that $\langle v \rangle$ depends on temperature. From this model, what would ρ be at 100 K?

10-11. Find (*a*) the current density and (*b*) the drift velocity if there is a current of 1 mA in a No. 14 copper wire. (The diameter of No. 14 wire, which is often used in household wiring, is 0.064 in = 0.163 cm.)

10-12. A measure of the density of the free-electron gas in a metal is the distance r_s, which is defined as the radius of the sphere whose volume equals the volume per conduction electron. (*a*) Show that $r_s = (3/4\pi n_a)$, where n_a is the free-electron number density. (*b*) Calculate r_s for copper in nanometers.

10-13. Calculate the number density of free electrons in (*a*) Ag ($\rho = 10.5$ g/cm^3) and (*b*) Au ($\rho = 19.3$ g/cm^3), assuming one free electron per atom, and compare your results with the values listed in Table10-3.

10-14. Calculate the number density of free electrons for (*a*) Mg ($\rho = 1.74$ g/cm^3) and (*b*) Zn ($\rho = 7.1$ g/cm^3), assuming two free electrons per atom, and compare your results with the values listed in Table 10-3.

10-15. (*a*) Using $\lambda = 0.37$ nm and $\langle v \rangle = 1.08 \times 10^5$ m/s at $T = 300$ K, calculate σ and ρ for copper from Equations 10-13. Using the same value of λ, find σ and ρ at (*b*) $T = 200$ K and (*c*) $T = 100$ K.

Section 10-3 Free-Electron Gas in Metals

10-16. Find the average energy of the electrons at $T = 0$ K in (*a*) copper ($E_F = 7.06$ eV) and (*b*) Li ($E_F = 4.77$ eV).

10-17. Calculate the Fermi energy for magnesium in a long, very thin wire.

10-18. Compute (*a*) the Fermi energy and (*b*) the Fermi temperature for silver and for iron and compare your results with the corresponding values in Table 10-3.

10-19. Show that for $T = 300$ K about 0.1 percent of the free electrons in metallic silver have an energy greater than E_F.

Section 10-4 Quantum Theory of Conduction

10-20. What is the Fermi speed, i.e., the speed of a conduction electron whose energy is equal to the Fermi energy E_F, for (*a*) Na, (*b*) Au, and (*c*) Sn? (See Table 10-3.)

10-21. The resistivities of Na, Au, and Sn at $T = 273$ K are 4.2 $\mu\Omega \cdot$cm, 2.04 $\mu\Omega \cdot$cm, and 10.6 $\mu\Omega \cdot$cm, respectively. Use these values and the Fermi speeds calculated in Problem 10-20 to find the mean free paths λ for the conduction electrons in these elements.

10-22. At what temperature is the heat capacity due to the electron gas in copper equal to 10 percent of that due to lattice vibrations?

10-23. Use Equation 10-29 with $\alpha = \pi^2/4$ to calculate the average energy of an electron in copper at $T = 300$ K. Compare your result with the average energy at $T = 0$ and the classical result of $(3/2)kT$.

10-24. Compute the maximum fractional contribution to the heat capacity of solid iron that can be made by the electrons.

Section 10-5 Magnetism in Solids

10-25. The magnetic polarization P of any material is defined as $P = (\rho_+ - \rho_-)/\rho$. Compute the high-temperature polarization of a paramagnetic solid at $T = 200$ K in a magnetic field of 2.0 T.

10-26. Show that the magnetic susceptibility χ is a dimensionless quantity.

Section 10-6 Band Theory of Solids

10-27. (*a*) The energy gap between the valence band and the conduction band in silicon is 1.14 eV at room temperature. What is the wavelength of a photon that will excite an electron from the top of the valence band to the bottom of the conduction band? Do the same calculation for (*b*) germanium, for which the energy gap is 0.72 eV, and (*c*) for diamond, for which the energy gap is 7.0 eV.

10-28. (*a*) The energy band gap in germanium is 0.72 eV. What wavelength range of visible light will be transmitted by a germanium crystal? (Think about it carefully!) (*b*) Now consider a crystal of an insulator whose energy band gap is 3.6 eV. What wavelength range of visible light will this crystal transmit? (*c*) Justify each of your answers to (*a*) and (*b*).

10-29. A photon of wavelength 3.35 μm has just enough energy to raise an electron from the valence band to the conduction band in a lead sulfide crystal. (*a*) Find the energy gap between these bands in lead sulfide. (*b*) Find the temperature T for which kT equals this energy gap.

10-30. Consider a small silicon crystal measuring 100 nm on each side. (*a*) Compute the total number N of silicon atoms in the crystal. (The density of silicon is 2.33 g/cm^3.) (*b*) If the conduction band in silicon is 13 eV wide and recalling that there are $4N$ states in this band, compute an approximate value for the energy spacing between adjacent conduction band states for the crystal.

Section 10-7 Impurity Semiconductors

10-31. Arsenic has five valence electrons. If arsenic is used as a dopant in silicon, compute (*a*) the ionization energy and (*b*) the orbit radius of the fifth arsenic electron. The effective mass for electrons in silicon is 0.2 m_e. (*c*) What is the ratio of the ionization energy of the fifth electron to the energy gap in silicon?

10-32. Gallium has three valence electrons. If gallium is used to dope germanium, compute (*a*) the ionization energy of the hole and (*b*) the orbit radius of the hole. The effective mass of holes in germanium is 0.34 m_e.

10-33. What type of semiconductor is obtained if silicon is doped with (*a*) aluminum and (*b*) phosphorus? (See Appendix C for the electron configurations of these elements.)

10-34. The donor energy levels in an *n*-type semiconductor are 0.01 eV below the conduction band. Find the temperature for which $kT = 0.01$ eV.

10-35. A strip of tin is 10 mm wide and 0.2 mm thick. When a current of 20 A is established in the strip and a uniform magnetic field of 0.25 T is oriented perpendicular to the plane of the strip, a Hall voltage of 2.20 μV is measured across the width of the strip. Compute (*a*) the density of charge carriers in tin and (*b*) the average number of charge carriers contributed by each tin atom. The density of tin is 5.75×10^3 kg/m^3 and its molecular mass is 118.7.

Section 10-8 Semiconductor Junctions and Devices

10-36. For a temperature of 300 K, use Equation 10-49 to find the bias voltage V_b for which the exponential term has the value (*a*) 10 and (*b*) 0.1.

10-37. For what value of bias voltage V_b does the exponential in Equation 10-49 have the value (*a*) 5, and (*b*) 0.5 for $T = 200$ K?

10-38. Compute the fractional change in the current through a *pn* junction diode when the forward bias is changed from +0.1 V to +0.2 V.

10-39. For $T = 300$ K, use Equation 10-49 to find the bias voltage V_b for which the exponential term had the value (*a*) 10 and (*b*) 0.1.

10-40. When light of wavelength no larger than 484 nm illuminates a CdS solar cell, the cell produces electric current. Determine the energy gap in CdS.

Section 10-9 Superconductivity

10-41. Three naturally occurring isotopes of lead are ^{206}Pb, ^{207}Pb, and ^{208}Pb. Using the value of α from Table 10-7 and the isotopic masses from Appendix A, compute the critical temperatures of these isotopes.

10-42. Compute (*a*) the superconducting energy gap for indium and (*b*) the wavelength of a photon that could just break up a Cooper pair in indium at $T = 0$ K.

10-43. (*a*) Use Equation 10-56 to calculate the superconducting energy gap for tin and compare your result with the measured value of 6×10^{-4} eV. (*b*) Use the measured value to calculate the wavelength of a photon having sufficient energy to break up a Cooper pair in tin at $T = 0$ K.

10-44. Use the BCS curve in Figure 10-51 to estimate the energy gaps in (*a*) tin, (*b*) niobium, (*c*) aluminum, and (*d*) zinc, all at $T = 0.5T_c$.

10-45. Expressing the temperature T as a fraction of the critical temperature T_c, according to BCS theory at what temperature is (*a*) $B_c = 0.1B_c(0)$, (*b*) $B_c = 0.5B_c(0)$, (*c*) $B_c = 0.9B_c(0)$?

Level II

10-46. Estimate the fraction of free electrons in copper that are in excited states above the Fermi energy at (*a*) room temperature of 300 K and (*b*) 1000 K.

10-47. A one-dimensional model of an ionic crystal consists of a line of alternating positive and negative ions with distance r_0 between adjacent ions. (*a*) Show that the potential energy of attraction of one ion in the line is

$$V = -\frac{2ke^2}{r_0}\left(1 - \frac{1}{2} + \frac{1}{3} - \frac{1}{4} + \frac{1}{5} - \ldots\right)$$

(*b*) Using the result that

$$\ln(1 + x) = x - \frac{x^2}{2} + \frac{x^3}{3} - \frac{x^4}{4} + \ldots$$

show that the Madelung constant for this one-dimensional model is $\alpha = 2 \ln 2 = 1.386$.

10-48. Estimate the Fermi energy of zinc from its electronic molar heat capacity of $(3.74 \times 10^{-4}\ \text{J/mol} \cdot \text{K})T$.

10-49. The density of the electron states in a metal can be written $g(E) = AE^{1/2}$, where A is a constant and E is measured from the bottom of the conduction band. (*a*) Show that the total number of states is $(2/3)A(E_F)^{3/2}$. (*b*) About what fraction of the conduction electrons are within kT of the Fermi energy? (*c*) Evaluate this fraction for copper at $T = 300$ K.

10-50. High-purity germanium (HPGe) crystals are used as detectors for x rays and gamma rays. On interacting with the crystal, incoming photons produce electron-hole pairs, exciting many electrons across the 0.72-eV energy gap into the conduction band. The decay of the radioisotope ^{60}Co results in the emission of two gamma rays with energies 1.17 MeV and 1.33 MeV (see Chapter 11). (*a*) Compute the numbers of electrons N_1 and N_2 excited across the energy gap by each of the two gamma rays. (*b*) The numbers N_1 and N_2 are subject to statistical fluctuations of $\pm\sqrt{N_1}$ and $\pm\sqrt{N_2}$. Compute the fractional uncertainties in N_1 and N_2. (*c*) Compute the corresponding fractional uncertainties in the energies of the two gamma rays. This is a measure of the energy resolution of the HPGe crystal.

10-51. A doped *n*-type silicon sample with 10^{16} electrons per cubic centimeter in the conduction band has a resistivity of $5 \times 10^{-3}\ \Omega \cdot \text{m}$ at 300 K. Find the mean free path of the electrons. Use $0.2\ m_e$ for the effective mass of the electron. Compare your result with the mean free path of electrons in copper at 300 K.

10-52. A "good" silicon diode has a current-voltage characteristic given by

$$I = I_0(e^{eV_b/kT} - 1)$$

Let $kT = 0.025$ eV (room temperature) and the saturation current $I_0 = 1$ nA. (*a*) Show that for small reverse-bias voltages, the resistance is 25 MΩ. (*Hint:* Do a Taylor expansion of the exponential function or use your calculator and enter small values for V_b.) (*b*) Find the dc resistance for a reverse bias of 0.5 V. (*c*) Find the dc resistance for a 0.5-V forward bias. What is the current in this case? (*d*) Calculate the ac resistance dV/dI for a 0.5-V forward bias.

FEUE WHE

10-53. The relative binding of the extra electron in the arsenic atom that replaces an atom in silicon or germanium can be understood from a calculation of the first Bohr orbit of this electron in these materials. Four of arsenic's outer electrons form covalent bonds, so the fifth electron sees a singularly charged center of attraction. This model is a modified hydrogen atom. In the Bohr model of the hydrogen atom, the electron moves in free space at a radius a_0 given by

$$a_0 = \frac{\epsilon_0 h^2}{\pi m_e e^2}$$

When an electron moves in a crystal, we can approximate the effect of the other atoms by replacing ϵ_0 with $\kappa\epsilon_0$ and m_e with an effective mass for the electron. For silicon κ is 12 and the effective mass is about $0.2m_e$, and for germanium κ is 16 and the effective mass is about $0.1m_e$. Estimate the Bohr radii for the outer electron as it orbits the impurity arsenic atom in silicon and germanium.

10-54. InSb is a semiconductor. The energy gap E_g between its valence and conduction bands is 0.23 eV, and its dielectric constant $\kappa = 18$. In the InSb crystal the electron's effective mass $m^* = 0.015m_e$. (*a*) Compute the ionization energy for an electron donor in InSb. (*b*) What is the radius of the ground-state orbit? (*c*) At approximately what donor concentration will the orbits of adjacent donor atoms begin to overlap?

10-55. The mean free path of an electron in a metal depends on both the lattice oscillations of the metal ions and those of any impurity ions according to $1/\lambda = 1/\lambda_m + 1/\lambda_i$. The resistivity of pure copper is increased by about $1.2 \times 10^{-8}\ \Omega \cdot \text{m}$ by the addition of 1 percent (by number of atoms) of a certain impurity dispersed evenly throughout the metal. (*a*) Estimate λ_i from this information. (*b*) The impurity atoms are "seen" by the electrons to have an effective diameter d. Estimate the scattering cross section d^2 from Equation 10-12, where $d = 2r$.

Level III

10-56. When arsenic is used to dope silicon, the fifth arsenic electron and the As^+ ion act like a hydrogen atom system except that the potential function $V(r)$ and the electron mass must be modified as described in Section 10-7 to account for the crystal lattice. With these modifications, (*a*) solve the Schrödinger equation, using the solution in Chapter 7 as a guide. (*b*) Obtain Equation 10-43, and (*c*) sketch a properly scaled energy-level diagram for the fifth electron for $n = 1$ through 5.

10-57. The quantity K is the force constant for a "spring" consisting of a line of alternating positive and negative ions. If these ions are displaced slightly from their equilibrium separation r_0, they will vibrate with a frequency

$$f = \frac{1}{2\pi}\sqrt{\frac{K}{m}}$$

(*a*) Use the values of α, n, and r_0 for NaCl and the reduced mass for the NaCl molecule to calculate this frequency. (*b*) Calculate the wavelength of electromagnetic radiation corresponding to this frequency, and compare your result with the characteristic strong infrared absorption bands in the region of about $\lambda = 61\ \mu\text{m}$ that are observed for NaCl.

10-58. Consider a model for a metal in which the lattice of positive ions forms a container for a classical electron gas with n electrons per unit volume. In equilibrium, the average electron velocity is zero, but the application of an electric field produces an acceleration of the electrons. If we use a relaxation time τ to account for the electron-lattice collisions, then we have the equation

$$m\frac{dv}{dt} + \frac{m}{\tau}v = -eE$$

(*a*) Solve the equation for the drift velocity in the direction of the applied electric field. (*b*) Verify that Ohm's law is valid, and find the resistivity as a function of n, e, m, and the relaxation time τ.

10-59. Imagine a cubic crystal like NaCl, with a negative charge at the center of a Cartesian coordinate system with scale units equal to the interatomic distance (*a*) Show that an ion at a position r units along the x axis, s units along the y axis, and t units along the z axis has a charge of $e(-1)^r \cdot (-1)^s \cdot (-1)^t = e(-1)^{r+s+t}$, where e is the electron charge. (*b*) Using Equation 10-2 as a guide, calculate the Madelung constant for a cube 2 units on a side. Do the same for cubes of sides 4, 6, 8, 10, 12, 16, and 20 units (You will probably want to use a computer spreadsheet to write a program to do the calculations for the larger cubes). Are your answers approaching the value $\alpha = 1.7476$?

10-60. (*a*) Show that for a paramagnetic solid with electron energies given by Equation 10-33 the magnetization per unit volume M is given by

$$M = \mu\rho \tanh (\mu B/kT)$$

(*b*) For $\mu B \ll kT$ show that the susceptibility is given by Equation 10-35.

CHAPTER 11

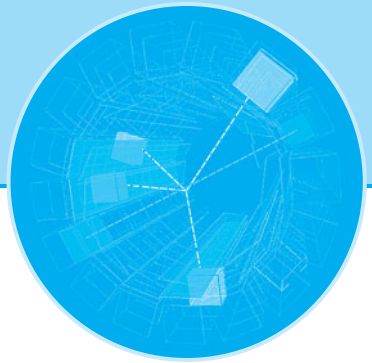

Nuclear Physics

The first information about the atomic nucleus came with the discovery of radioactivity by A. H. Becquerel[1] in 1896. Intrigued by Roentgen's discovery of x rays the previous year, Becquerel was investigating the possibility that minerals that exhibit fluorescence after exposure to sunlight might also be emitting x rays. He used the simple technique of placing a sample of such a mineral, potassium uranyl sulfate, on top of a photographic plate wrapped in black paper lying in the sunlight on a window ledge. Sure enough, an image of the sample appeared on the developed plate, and Becquerel concluded that x rays had indeed been emitted. But when a similar sample lying on a wrapped photographic plate in a drawer without exposure to sunlight during a period of cloudy weather produced an image just as dark, he investigated further and found that the sample was spontaneously emitting a previously unknown penetrating radiation. He had discovered radioactivity.[2]

The rays emitted by radioactive nuclei were first classified by Rutherford as α, β, and γ, according to their ability to penetrate matter and to ionize air: α radiation penetrates the least and produces the most ionization, γ radiation penetrates the most with the least ionization, and β radiation is intermediate between them. In a classic experiment, Rutherford soon found that α rays are ^{4}He nuclei. It was also quickly discovered that β rays are electrons and γ rays are very short-wavelength electromagnetic radiation. Geiger and Marsden's α-particle-scattering experiments in 1911 (see Section 4-2) and the successes of the Bohr model of the atom led to the modern view of an atom as consisting of a tiny, massive nucleus with a radius of 1 to 10 femtometer (fm; 1 fm $= 10^{-15}$ m) surrounded by a cloud of electrons at a relatively great distance, of the order of 0.1 nm ($=$ 100,000 fm) from the nucleus.

In 1928, the correct explanation of α radioactivity as a quantum-mechanical, barrier-penetration phenomenon was given by G. Gamow, R. W. Gurney, and E. U. Condon. Then, in rapid succession in 1932, the *neutron* was discovered by J. Chadwick and the *positron* by C. D. Anderson, and the first nuclear reaction using artificially accelerated particles (protons) was observed by J. D. Cockcroft and E. T. S. Walton.[3] Thus, it is quite reasonable to mark that year as the beginning of modern nuclear physics. Much of the information about nuclei is obtained by bombarding them with various particles and observing the results. The advent of particle accelerators, the Van de Graaff electrostatic generator in 1931 and the cyclotron in 1932,

made many experimental studies possible without the severe limitations on particle type and energy imposed by naturally radioactive sources. Since then, an enormous technology has been developed for accelerating and detecting particles, and many nuclear reactions and fundamental particle interactions have been studied.

Among the myriad nuclear reactions that have been investigated are two types of special interest: *fission* and *fusion*. Both are processes by which nuclear mass is converted into other forms of energy, such as thermal energy, just as some atomic mass is converted in chemical reactions such as oxidation. Fission reactions currently provide a significant, albeit controversial, means of producing electrical energy in 30 countries, accounting for 6.0 percent of the world's total consumption of energy in 2005.[4] The similar potential of fusion reactions has not yet been realized at a practical level; however, of far more intrinsic importance is the role of fusion in the production of energy in stars. The grim reality that both fission and fusion are also the basis for weapons of enormous destructive power means that this application of nuclear reactions influences political debate to a greater degree than has perhaps any other scientific discovery in history.

In this chapter we will discuss some of the general properties of atomic nuclei and the important features of radioactivity. While our discussions will of necessity be only semiquantitative, we will consider the nature of the nuclear force as it is currently understood and describe one of the most useful models in terms of which many nuclear properties may be explained. The applications of radioactivity and nuclear reactions are by no means limited to fission and fusion. The radiations emitted by radioisotopes have long been used in medical diagnosis and treatment. These contributions were measurably enhanced with the development of *computer assisted tomography*[5] (CAT) in the 1970s, which made possible not only x-ray CAT scans, but also the more recent development of *positron emission tomography*, called PET. Neutron-induced nuclear reactions provide an extremely sensitive technique, called *neutron activation analysis* (NAA), for measuring trace amounts of certain isotopes for most elements in the periodic table. These and many other applications will be discussed in this chapter.

11-1 The Composition of the Nucleus

The experiments of Moseley (see Section 4-4) showed that the nuclear charge is Z times the proton charge, where Z is the *atomic number*, which is about half the *atomic mass number* A (except for hydrogen, for which $Z = A$). Thus, the nucleus has a mass about equal to that of A protons but a charge of only $Z \approx \frac{1}{2}A$ protons. Before the discovery of the neutron, it was difficult to understand this unless there were A–Z electrons in the nucleus to balance the charge without changing the mass very much. The idea that the nucleus contained electrons was supported by the observation of β decay, in which electrons are ejected by certain radioactive nuclei. However, there were serious difficulties with this model. A relatively simple calculation from the uncertainty principle (see Problem 11-2) shows that an electron has a minimum kinetic energy of about 100 MeV if it is confined in the region of $r < 10^{-14}$ m; however, the energies of the electrons emitted in β decay are only of the order of 1 or 2 MeV. In addition, there is no evidence for such a strong attractive force between nuclei and electrons as would be implied by a negative potential energy of 50 to 100 MeV inside the nucleus. Furthermore, since the electrostatic potential energy of the electron and nucleus is negative, there is no barrier to be overcome, as there is in α decay (Figure 11-1). If the electron's total energy were positive, as required for β decay, the electron should escape from the nucleus immediately and most naturally occurring β emitters should

FEUE WHE

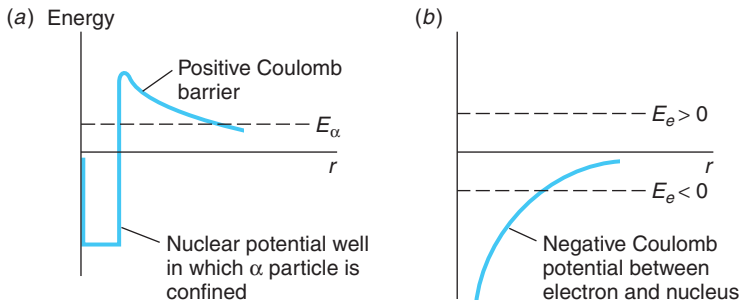

Figure 11-1 (*a*) Potential barrier for an α particle compared with (*b*), potential for a negative electron. Because there is no barrier for the electron, it will not be bound at all unless the total energy is negative, in which case it can never escape. The very narrow steep rise to the potential in (*a*) as $r \rightarrow 0$ represents the "hard core" of the nucleus.

have long since disappeared. A further difficulty is the observation that the magnetic moments of nuclei are of the order of nuclear magnetons, $\mu_N = e\hbar/2m_p$, about 2000 times smaller than a Bohr magneton $\mu_B = e\hbar/2m_e$, which would be expected if there were electrons inside the nucleus.

A further convincing argument against electrons existing in the nucleus concerns angular momentum. Protons and neutrons are fermions with spins of 1/2 and as such both obey the exclusion principle. The angular momentum of the nitrogen nucleus has a quantum number of 1, which can be inferred from a very small splitting of atomic spectral lines called *hyperfine structure* (see Section 11-2). It is also known (from molecular spectra—see Section 9-4) that the nitrogen nucleus obeys Bose-Einstein rather than Fermi-Dirac statistics. If ^{14}N contained 14 protons and 7 electrons, each with spin 1/2, the resultant angular momentum would have to be 1/2, 3/2, 5/2, etc., and the nucleus would obey Fermi-Dirac statistics.

In 1920 Rutherford suggested that there might be a neutral particle, possibly a proton and an electron tightly bound together, which he called a *neutron*. When such a particle was found by Chadwick in 1932, the idea that electrons were permanent constituents of nuclei was abandoned. Instead, the nucleus was assumed to contain N neutrons and Z protons, a total of $A = N + Z$ particles. N is referred to as the *neutron number*. The notion of the neutron being a proton and electron bound together has also been abandoned since the spin of the neutron is 1/2. Thus, the nucleus is composed of protons and neutrons, the *nucleons*, which collectively occupy a volume whose radius is of the order of 1 to 10 fm. All of the large variety of nuclei with their broad diversity of properties are assembled from various numbers of these two particles. The fundamental properties of the individual nucleons are given in Table 11-1. We should note at this point that the nucleons are not fundamental particles. Each of the two types of nucleons is composed of a set of three *quarks*, fundamental particles that interact with each other via the strong force, which accounts for the fact that the nucleons also feel that force. Quarks and their interactions will be discussed in Chapter 12.

Table 11-1 Fundamental properties of atomic constituents

Particle	Charge	Mass (u)	Mass (kg)	Spin	Magnetic moment
Proton	$+e$	1.007276	1.6726×10^{-27}	1/2	$2.79285\ \mu_N$
Neutron	0	1.008665	1.6749×10^{-27}	1/2	$-1.91304\ \mu_N$
Deuteron	$+e$	2.013553	3.3436×10^{-27}	1	$0.85744\ \mu_N$
Electron	$-e$	5.4858×10^{-4}	9.1094×10^{-31}	1/2	$1.00116\ \mu_B$

11-2 Ground-State Properties of Nuclei

Understanding nuclei, like atoms, requires the application of quantum theory. It was the study of nuclear spectra, the energy and particles emitted spontaneously by radioactive nuclei, that provided the first indication of the existence of quantized energy levels, angular momenta, and magnetic moments in nuclei, just as the regularities in atomic spectra had earlier pointed the way to Bohr's theory and, ultimately, to wave mechanics. Interpreting the nuclear studies presents more complex problems due to the existence of two nucleons, the possible emission of several different particles in addition to photons from excited energy states, and our incomplete knowledge of the nuclear potential function.

In this section we will discuss some of the properties of nuclei in the ground state and mention a few methods of determining these properties. In Section 11-3 we will study radioactivity, which provides information about the excited states of nuclei. Several of the general references at the end of this chapter contain good discussions of the experimental methods used in measuring nuclear properties. We will use the following standard terminology: the letter N stands for the number of neutrons in a nucleus and Z for the number of protons (the atomic number); $A = N + Z$ is the total number of nucleons, the mass number. The mass number is an integer approximately equal to the atomic weight. A particular nuclear species is called a *nuclide*. Nuclides are denoted by the chemical symbol with a presuperscript giving the value of A, such as ^{16}O or ^{15}O. Sometimes Z is given as a pre-subscript, such as $^{15}_{8}O$, although this is not necessary because each element (Z number) has a unique chemical symbol. Occasionally, N is also given as a subscript, such as $^{15}_{8}O_7$, although this, too, is unnecessary since $N = A - Z$. Nuclides with the same Z, such as ^{15}O and ^{16}O, are called *isotopes*. Nuclides with the same N, such as $^{13}_{6}C_7$ and $^{14}_{7}N_7$, are called *isotones*, while nuclides with the same A, such as ^{14}C and ^{14}N, are called *isobars*.

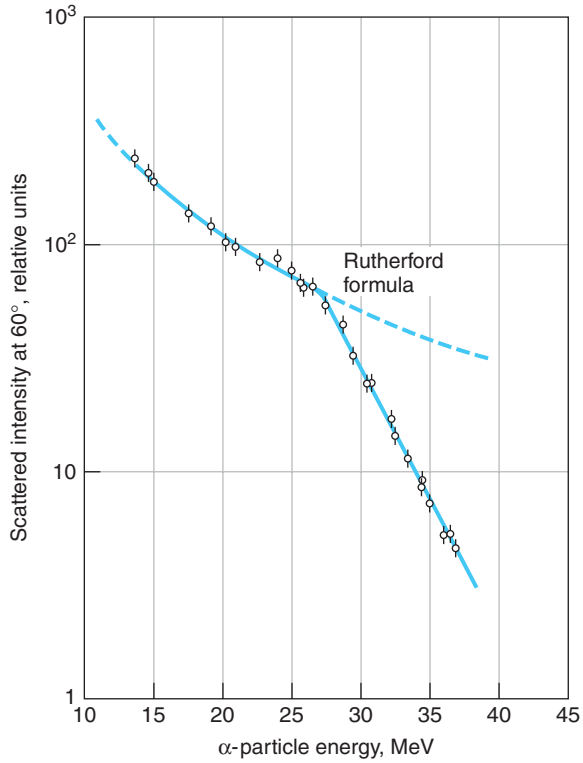

Figure 11-2 Rutherford's α-scattering formula (Equation 4-6) is shown by the dashed line. α particles of increasing energy incident on the nuclei of a Pb target scattered as would be expected by the Rutherford formula until their energy reached about 27 MeV. At greater energies the α particles approach the Pb nuclei closely enough so that the nucleons of the α and the Pb interact via the attractive nuclear force and the scattered intensity falls below that predicted by the Rutherford equation. [*Data from R. M. Eisberg and C. E. Porter, Rev. Mod. Phys., 33, 190 (1961).*]

Size and Shape of Nuclei

Nuclear Radii All of the methods for measuring nuclear radii agree that the radii are proportional to the cube root of the mass number. The nuclear radius can be determined by scattering experiments similar to the first ones of Rutherford or in some cases from measurements of radioactivity. Indeed, as we discussed in Section 4-2 and as illustrated in Figure 11-2, Rutherford's original α-particle-scattering experiment furnished the first measurement of the nuclear radius. An interesting, nearly classical method of determining the nuclear radius involves the measurement of the energy of β decay between *mirror nuclides*, which are nuclides whose Z and N numbers are interchanged (Figure 11-3). For example, ^{15}O, with eight protons and seven neutrons, and ^{15}N, with

FÈUE WHE

eight neutrons and seven protons, are mirror nuclides. If one assumes that the nuclear force between nucleons is independent of the kind of nucleons, the only difference in energy between ^{15}O and ^{15}N is electrostatic. The electrostatic energy of a ball of uniform charge is given by

$$U = \frac{3}{5}\frac{1}{4\pi\epsilon_0}\frac{q^2}{R} \qquad \textbf{11-1}$$

where q is the charge and R is the radius. ^{15}O is radioactive and, as we will discuss further in a later section, decays to ^{15}N by emitting a positron and a neutrino. The energy difference between ^{15}O and ^{15}N, the beta-decay energy, is then

$$\Delta U = \frac{3}{5}\frac{1}{4\pi\epsilon_0}\frac{e^2}{R}\left[Z^2 - (Z-1)^2\right] \qquad \textbf{11-2}$$

with $Z = 8$. A measurement of the energy of decay, equal to ΔU, thus gives a measurement of R. If one assumes a uniform charge distribution, measurements of the positron-decay energies (see Section 11-4) for 18 pairs of mirror nuclides give for the nuclear radius

$$R = R_0 A^{1/3} \quad \text{with} \quad R_0 = 1.2 \pm 0.2 \text{ fm} \qquad \textbf{11-3}$$

where A is the atomic mass number. The value of R_0 in Equation 11-3 includes the effect of a quantum-mechanical correction using a charge distribution calculated from the nuclear shell model discussed in Section 11-6. The consistency of these results with other methods of determining R is a strong indication that the nuclear part of the potential energy is the same for each pair of mirror nuclei.

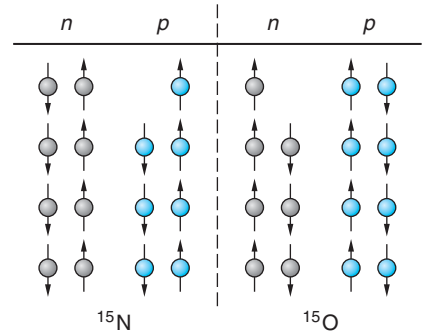

Figure 11-3 Mirror nuclides. If all the neutrons are changed to protons and all the protons are changed to neutrons, ^{15}N becomes its mirror, ^{15}O. The ground-state energy of mirror pairs differs only in the electrostatic energy.

The most extensive measurements of nuclear radii were carried out by Robert Hofstadter and his co-workers in a series of experiments begun in 1953.[6] In these experiments at the Stanford Linear Accelerator (SLAC), nuclei were bombarded with electrons having energies of about 200 to 500 MeV. The wavelength of a 500-MeV electron is about 2.5 fm, which is smaller than the radius of heavy nuclei. It is thus possible to learn something about the detailed structure of the charge distribution of nuclei by analyzing the diffraction pattern that results from the scattering of these electrons. The analysis is fairly complicated because the electrons are relativistic. Figure 11-4 shows the diffraction pattern of high-energy electrons scattered by ^{16}O and ^{12}C nuclei. If we consider the incoming electron beam to be a plane wave of wavelength λ, the scattering process is similar to the diffraction of light from a circular hole of radius R, discussed in most introductory physics textbooks, where R in this case is the nuclear radius. The first minimum of the diffraction pattern is then given approximately by

$$\sin\theta = 0.16\lambda/R \qquad \textbf{11-4}$$

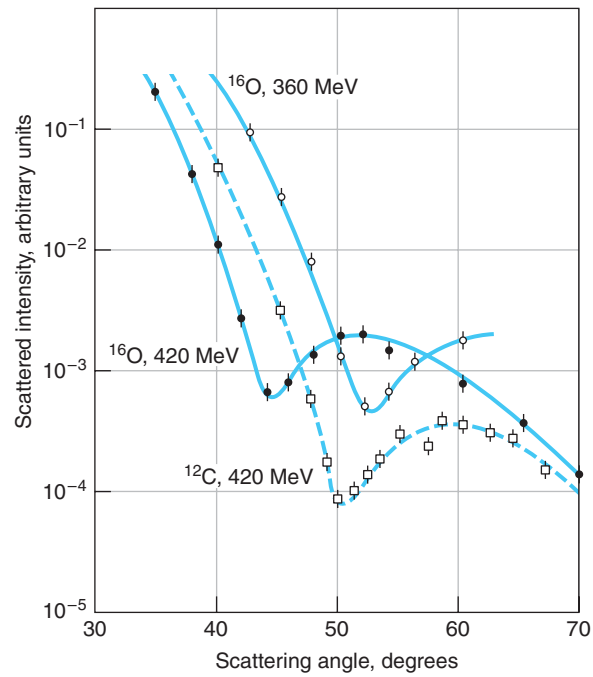

Figure 11-4 Diffraction pattern of high-energy electrons scattered by ^{16}O and ^{12}C. The angle at which the minimum occurs in each pattern is given by Equation 11-4.

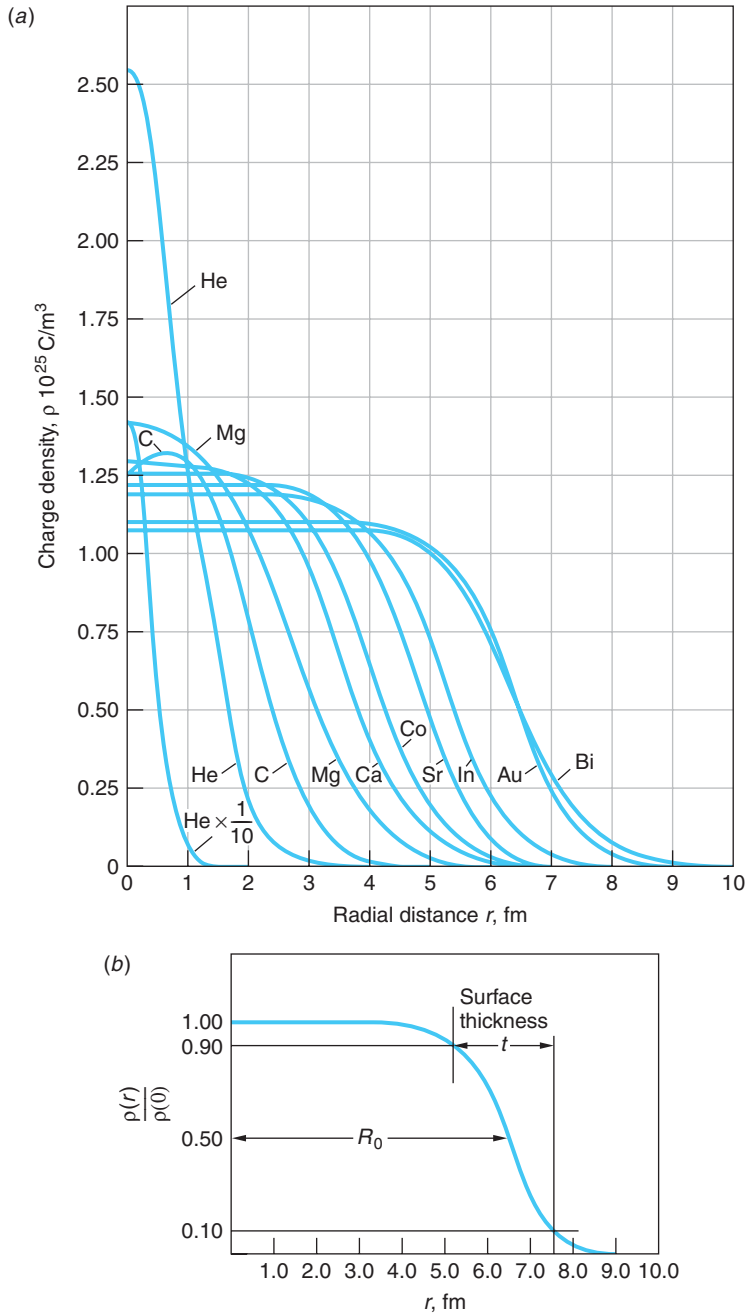

Figure 11-5 (*a*) Charge density versus distance for several nuclei as determined by high-energy electron scattering experiments. (*b*) Definitions of parameters R_0 and t used to describe nuclear charge density. The skin thickness t is measured from 10 percent to 90 percent of the central core density. [*From R. Hofstadter, Annual Review of Nuclear Science, 7, 231 (1957).*]

Example 11-2 shows how the nuclear radius can be calculated from Equation 11-4 with the aid of Figure 11-4. Figure 11-5*a* shows some charge distributions obtained from detailed analysis of these experiments. The mean electromagnetic radius R and the surface thickness t, defined in Figure 11-5*b*, are given by

$$R = (1.07 \pm 0.02)A^{1/3} \text{ fm}$$
$$t = 2.4 \pm 0.3 \text{ fm} \qquad \textbf{11-5}$$

These results are consistent with those obtained from the β-decay studies of mirror nuclides.

EXAMPLE 11-1 Nuclear Radii of ^{4}He and ^{238}U Use Equation 11-3 to compute the radii of ^{4}He and ^{238}U.

SOLUTION

For ^{4}He: $R_{He} = 1.2(4)^{1/3} = 1.90$ fm

For ^{238}U: $R_U = 1.2(238)^{1/3} = 7.42$ fm

Thus, the nuclear radius varies only by a factor of about 4 from the lightest nuclides to the heaviest.

EXAMPLE 11-2 Nuclear Radius of ^{16}O Using the data for 420-MeV electrons scattered from ^{16}O in Figure 11-4, compute a value for the radius of the ^{16}O nucleus.

SOLUTION

1. The radius R of the ^{16}O nucleus is computed from Equation 11-4:
$$\sin\theta = \frac{0.61\lambda}{R} \quad \text{or} \quad R = \frac{0.61\lambda}{\sin\theta}$$

2. The angle θ in Equation 11-4 is the first minimum of the diffraction pattern. From Figure 11-4 we see that the first minimum occurs at about:
$$\theta = 44°$$

3. The de Broglie wavelength λ of the electrons is
$$\lambda = \frac{h}{p}$$

4. The momentum p of the 420-MeV electrons is computed from the relativistic expression, Equation 2-32:
$$p^2c^2 = E^2 - (mc^2)^2$$
$$= (420)^2 - (0.511)^2$$
$$\approx (420 \text{ MeV})^2$$
or
$$p = 420 \text{ MeV}/c = 2.24 \times 10^{-19} \text{ kg} \cdot \text{m/s}$$

5. Substituting this value in λ from step 3 gives
$$\lambda = \frac{6.63 \times 10^{-34} \text{ J} \cdot \text{s}}{2.24 \times 10^{-19} \text{ kg} \cdot \text{m/s}}$$
$$= 2.96 \times 10^{-15} \text{ m} = 2.96 \text{ fm}$$

6. The radius R is computed by substituting the values for θ and λ into Equation 11-4:
$$R = \frac{(0.61)(2.96 \text{ fm})}{\sin 44°} = 2.60 \text{ fm}$$

Remarks: This result agrees well with the values of R_0 for the low-Z nuclei in Figure 11-5a.

A different kind of measurement of the nuclear radius can be made using the attenuation of a beam of fast neutrons as it moves through a sample. The total cross section for attenuation can be shown to be

$$\sigma = 2\pi\left(R + \frac{\lambda}{2\pi}\right)^2 \qquad \textbf{11-6}$$

where R is the nuclear radius and λ is the de Broglie wavelength of the neutron. The neutrons must be fast enough so that $\lambda/2\pi < R$ in order to gain information about R from measurement of σ. These experiments do not measure the charge distribution but instead measure the "radius" of the nuclear force between a neutron and the nucleus. The results of these measurements are

$$R = R_0 A^{1/3} \quad \text{with} \quad R_0 = 1.4 \text{ fm} \qquad \textbf{11-7}$$

These different types of experiments thus give comparable but not identical results, depending on whether the particular experiment measures the nuclear force radius (neutrons) or the nuclear charge radius (electrons). The fact that the radius is proportional to $A^{1/3}$ implies that the volume of the nucleus is proportional to A. Since the mass of the nucleus is also approximately proportional to A, the densities of all nuclei are approximately the same. A drop of liquid also has a constant density independent of its size, and this fact has led to a model in which the nucleus is viewed as analogous to a liquid drop. This model has been helpful in computing nuclear masses and in understanding certain types of nuclear behavior, particularly the fission of heavy elements. The numerical value of the nuclear density is about 10^{17} kg/m^3. This fantastically high density, compared with 10^3 kg/m^3 for atoms, is a consequence of the fact that nearly all the mass of the atom is concentrated in a region whose radius is only about 10^{-5} that of the atom. A cubic millimeter of nuclear matter has a mass of about 200,000 metric tons, or about the same mass as a supertanker filled with petroleum!

EXAMPLE 11-3 Radius of a Neutron Star In certain supernova events, the outer layer of the star is blown away, leaving a core consisting entirely of neutrons. This stellar remnant is called a *neutron star*, and its density is approximately the same as that of atomic nuclei. Compute the radius of a neutron star whose mass is equal to that of the Sun, 1.99×10^{30} kg.

SOLUTION

The mass of the neutron star is $M = \rho V$, where V is the volume and the density ρ is approximately 10^{17} kg/m^3. Assuming the neutron star to be a sphere, we have that

$$M = 1.99 \times 10^{30} \text{ kg} = \rho V = (10^{17} \text{ kg/m}^3)(4\pi R^3/3)$$

where R is the radius of the star in meters. Solving for R^3 yields

$$R^3 = \frac{(3)(1.99 \times 10^{30} \text{ kg})}{(4\pi)(10^{17} \text{ kg/m}^3)} = 4.75 \times 10^{12} \text{ m}^3$$

and taking the cube root

$$R = 1.68 \times 10^4 \text{ m} = 16.8 \text{ km}$$

Remarks: *By way of comparison, the mean diameter of the Sun is* 1.39×10^6 km.

FEUE WHE

Nuclear Shape With a few exceptions, nuclei are nearly spherical. Most of the exceptions occur in the rare earth elements (the transition region in the periodic table, $Z = 57$ to $Z = 71$), in which the shape is ellipsoidal, with the major axis differing from the minor axis by about 20 percent or less. In these heavy nuclides, the inner atomic electron wave functions penetrate the nucleus, and deviations from spherical shape, which correspond to deviations in the nuclear charge distributions, show up as small changes in the atomic energy levels. In direct analogy with the fact that the potential at points outside a static distribution of charges is determined by the dimensions of the distribution[7] and, conversely, that measuring the potential yields information about the distribution, measuring these small changes in the atomic energy levels yields information about the nuclear charge distribution, even though it can't be measured directly. If the nucleus is shaped like a watermelon (Figure 11-6*a*), with the extent of the distribution larger along the z axis than along the x and y axes, the average value of z^2 is larger than the average values of x^2 and y^2. In this case the *electric quadrupole moment* Q, which is proportional to $3(z^2)_{av} - (x^2 + y^2 + z^2)_{av}$, is positive. This is the most common case for nonspherical nuclei. Nuclei with negative quadrupole moments are shaped more like flattened pumpkins, with the two equal axes longer than the third axis, as in Figure 11-6*b*. The average value of the electric quadrupole moment is given by

$$\langle Q \rangle = Z \int \psi^* \left[3(z^2)_{av} - (x^2 + y^2 + z^2)_{av} \right] \psi \, dV \qquad \textbf{11-8}$$

> 0 for $z^2 > x^2, y^2$ (Figure 11-6*a*)

$= 0$ for $z^2 = x^2 = y^2$ (spherical)

< 0 for $z^2 < x^2, y^2$ (Figure 11-6*b*)

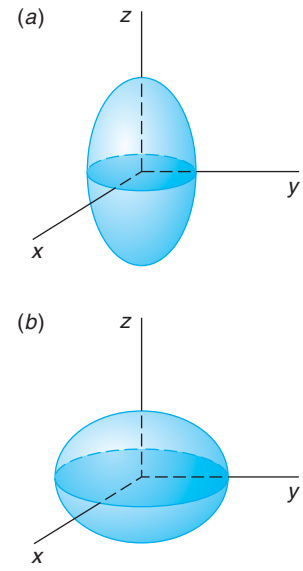

Figure 11-6 Nonspherical nuclear shapes. Nuclei with positive quadrupole moments have $(z^2)_{av}$ greater than $(x^2)_{av}$ or $(y^2)_{av}$ and are of watermelon shape, as in (*a*). Nuclei with negative quadrupole moments have $(z^2)_{av}$ less than $(x^2)_{av}$ or $(y^2)_{av}$ and are shaped like flattened pumpkins, as in (*b*).

Figure 11-7 shows the measured values of the electric quadrupole moment for the odd A nuclei, i.e., those for which either Z or N is odd. Equation 11-8 is evaluated for wave functions corresponding to the nuclear charge distributions of various theoretical models of the nucleus and compared with the values in Figure 11-7. As you might imagine, the calculations are formidable!

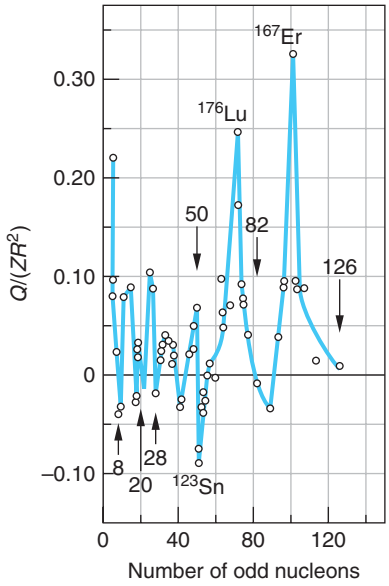

Figure 11-7 The electric quadrupole moment Q divided by Z and R^2, where R is the average nuclear radius, is plotted versus the number of nucleons of the odd type (Z or N). The arrows indicate the points where $Q/ZR^2 = 0$, corresponding to spherical shape.

Nuclear Stability

Among the more than 3000 known nuclides, there are only 266 whose ground states are stable. All of the rest have unstable ground states, which eventually undergo radioactive decay, that is, transition to some lower-energy state of a different element. Figure 11-8

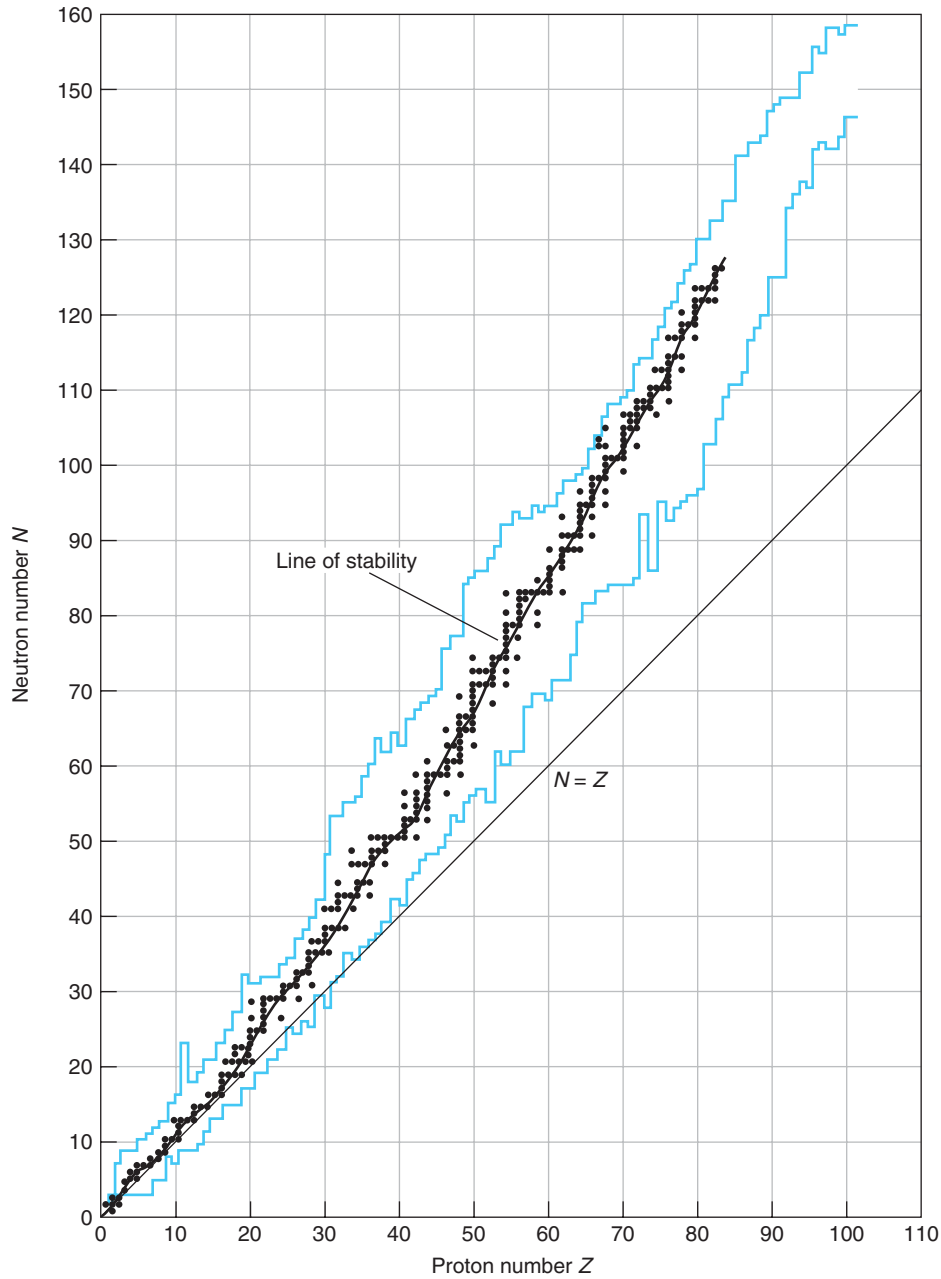

Figure 11-8 Plot of neutron number N versus proton number Z for the known nuclides. The 266 stable nuclides are indicated by the black dots. The area between the irregular colored lines represents the known unstable, or radioactive, nuclides whose lifetimes are longer than about a millisecond. The curved line through the stable nuclides is called the *line of stability*.

FÈUE WHE

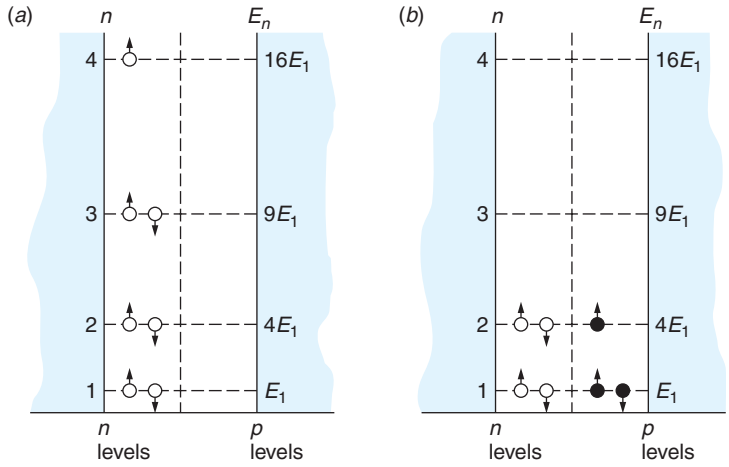

Figure 11-9 (*a*) Seven neutrons in an infinite square well. In accordance with the exclusion principle, only two neutrons can be in a given space state. The total energy is $16E_1 + (2 \times 9E_1) + (2 \times 4E_1) + (2 \times 1E_1) = 44E_1$. (*b*) Four neutrons and three protons in the same infinite square well. Because protons and neutrons are not identical, four particles (two neutrons and two protons) can be in the state $n = 1$. The total energy is $(3 \times 4E_1) + (4 \times 1E_1) = 16E_1$. This is much less than in (*a*). The integers on the left of each well are infinite square well principal quantum numbers.

shows a plot of the neutron number N versus the proton number Z for the stable nuclides and the known unstable ones whose lifetimes are longer than about a millisecond. The straight line is $N = Z$. The general shape of the *line of stability*, shown by the light curve tracing through the stable nuclides in Figure 11-8, can be understood in terms of the exclusion principle and the electrostatic energy of the protons. Consider the kinetic energy of A particles in a one-dimensional square well, which is an adequate model for demonstrating this point. The energy is smallest if $A/2$ are neutrons and $A/2$ are protons and greatest if all the particles are of one type (Figure 11-9). Hence there is a tendency, due to the exclusion principle, for N and Z to be equal. If we include the electrostatic energy of repulsion of the protons, the result is changed somewhat. This potential energy is proportional to Z^2. At large A, the energy is increased less by adding two neutrons than by adding one neutron and one proton, and so the difference $N - Z$ increases with increasing Z.

There is also a tendency for nucleons to pair with other identical nucleons. Of the 266 nuclides whose ground states are stable, 159 have even Z and even N, 50 have odd Z and even N, 53 have even Z and odd N, and only 4 have both odd N and Z. (See Table 11-2.)

Table 11-2 *N* versus *Z* for stable isotopes

	Z	
N	Even	Odd
Even	159	50
Odd	53	4

Since there are about 100 different elements and about 270 stable nuclides, there is an average of about 2.7 stable isotopes per element. There is a larger than the average number of stable isotopes for nuclei with Z equal to 20, 28, 50, and 82. For example, tin, with $Z = 50$, has 10 stable isotopes. Similarly, nuclides with these same numbers of neutrons have a larger than average number of isotones. These numbers, called *magic numbers*, are a manifestation of shell structure in very much the same way that the atomic "magic numbers" 2, 10, 18, and 36 correspond to closed-electron-shell structure. As we will discuss further in Section 11-6, the nuclear magic numbers, which also include 2, 8, and 126, represent configurations of particular stability. An *island of stability* is hypothesized to exist around $Z = 126$. In the search for it thus far, a few atoms with atomic numbers up to 118 have been created in that region. (Atoms with atomic number 117 have not yet been synthesized.)

Nuclides that fall between the irregular colored lines in Figure 11-8, except those marked by the black dots, are radioactive. We will discuss radioactivity in Section 11-3.

Masses and Binding Energies

The mass of an atom can be accurately measured in a mass spectrometer, which measures q/M for ions by bending them in a magnetic field.[8] The mass of an atom is slightly smaller than the mass of the nucleus plus the mass of the electrons because of the binding energy of the electrons. The binding energy of the electrons is defined by

$$B_{\text{atomic}} = M_N c^2 + Z m_e c^2 - M_A c^2 = \Delta m c^2 \qquad \textbf{11-9}$$

where M_N is the mass of the nucleus, M_A is the mass of the atom, m_e is the mass of an electron, and Δm is the mass equivalent of B_{atomic}. (See Section 2-3.) Because the binding energies of atoms are only of the order of keV, compared with nuclear binding energies of many MeV, atomic binding energies are usually neglected in nuclear physics. The binding energy of a nucleus with Z protons and N neutrons is defined as

$$B_{\text{nuclear}} = Z m_p c^2 + N m_n c^2 - M_A c^2 \qquad \textbf{11-10}$$

where m_p is the mass of a proton, m_n the mass of a neutron, and M_A the mass of the nucleus of mass number A. Since the mass of an atom is very nearly equal to the mass of the nucleus plus the mass of the electrons (neglecting the atomic binding energy), the nuclear binding energy can be accurately computed from

$$B_{\text{nuclear}} = Z M_{\text{H}} c^2 + N m_n c^2 - M_A c^2 \qquad \textbf{11-11}$$

where M_A is the atomic mass and M_{H} is the mass of a hydrogen atom. Note that the masses of the Z electrons cancel out. This expression is more convenient to use because it is the mass of the atom that is usually measured in mass spectrometers. The atomic masses of all stable nuclides and of many unstable ones are listed in Appendix A.

Once the mass of a nucleus or atom is determined, the binding energy can be computed from Equation 11-10 or 11-11. The binding energy per nucleon B/A is plotted against A for the most stable isotope of each element in Figure 11-10. The mean value is about 8.3 MeV/nucleon. The fact that this curve is approximately constant (for $A > 16$) indicates that the nuclear force is a *saturated* force. This is partially explained by the short range of the nuclear force (see Section 11-5). If each nucleon interacted with every other nucleon, there would be $A - 1$ interactions for each nucleon, and the binding energy per nucleon would be proportional to $A - 1$ rather than constant.

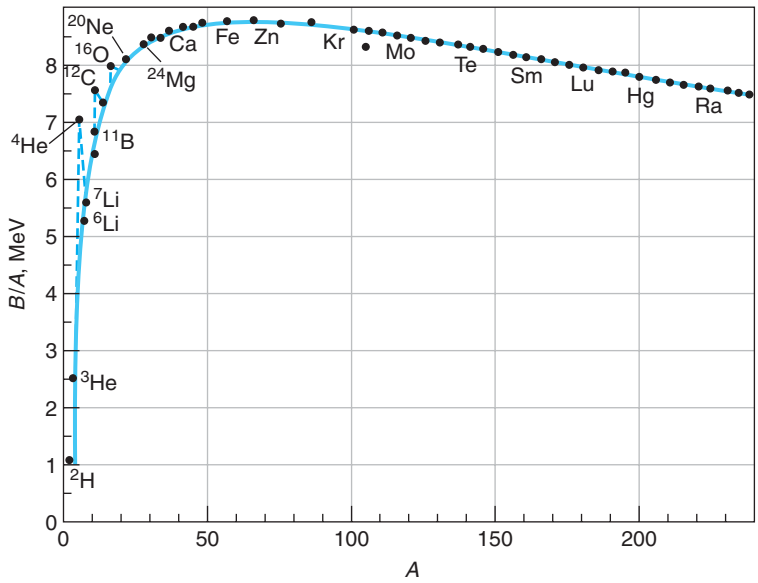

Figure 11-10 The binding energy per nucleon versus atomic mass number A. The solid curve represents the Weizsächer semiempirical binding-energy formula, Equation 11-12.

Figure 11-10 indicates that instead there is a fixed number of interactions per nucleon, as would be the case if each nucleon were attracted only to its nearest neighbors. Such a situation also leads to a constant nuclear density, consistent with the radius measurements. If the binding energy per nucleon were instead proportional to the number of nucleons, then the nuclear radius would be approximately constant, as is the case for the atomic radii.

More

Of the several models of the nucleus physicists have developed, the liquid-drop model has been one of the most useful. It has been successful in describing the fission process and nuclear reactions and, in particular, predicting the binding energies (i.e., masses) of isotopes and individual nucleons within the nucleus. These topics are discussed in *Liquid-Drop Model and the Semiempirical Mass Formula* on the home page: www.whfreeman.com/tiplermodernphysics5e. See also Equations 11-12 through 11-14 and Table 11-3 here, as well as Examples 11-4 through 11-6.

Nuclear Angular Momenta and Magnetic Moments

The spin quantum number of both the neutron and the proton is 1/2, which means that the nucleons are fermions. The angular momentum of the nucleus is a combination of the spin angular momenta of the nucleons plus any orbital angular momentum due to the motion of the nucleons. This resultant angular momentum is usually called *nuclear spin* and designated by the symbol **I**. The nucleons individually have magnetic moments, which also combine to produce the *nuclear magnetic moment*. Evidence for nuclear spin and magnetic moment was first found in atomic spectra. The nuclear spin adds to the angular momentum $\mathbf{J} = \mathbf{L} + \mathbf{S}$ of the electrons to form a total angular momentum **F**:

$$\mathbf{F} = \mathbf{I} + \mathbf{J} \qquad \textbf{11-15}$$

The possible quantum numbers for F are $(I + J), (I + J - 1), \ldots, |I - J|$, according to the usual rule for combining angular momenta. F obeys the selection rule $\Delta F = \pm 1, 0$, but no $F = 0 \rightarrow F = 0$. The number of possible values of F is $(2J + 1)$ or $(2I + 1)$, whichever is smaller. Because of the energy of the interaction between the electronic magnetic moment and the nuclear magnetic moment associated with I, each atomic spectral line is split into $(2J + 1)$ or $(2I + 1)$ components. This splitting is one of several effects that are the result of interactions of the nuclear spins and moments with the environment of the nucleus, including its own atomic electrons, collectively called *hyperfine structure*.[10] The hyperfine splitting of the spectral lines associated with the nuclear magnetic moment occurs for a reason that is exactly analogous to the spin-orbit coupling discussed in Section 7-5 that is the origin of the fine structure of the atomic spectral lines. The coupling between **I** and **J** expressed by Equation 11-15 results in a splitting of the *atomic* energy levels by an amount ΔE, in addition to the spin-orbit splitting of Equation 7-68, given by the analogous relation

$$\Delta E = g_N m_I \mu_N B_e \qquad \textbf{11-16}$$

where g_N is the nuclear Landé factor, m_I is the magnetic quantum number of the z component of **I**, $\mu_N = e\hbar/2m_p$ is the nuclear magneton, and B_e is the magnetic field at the nucleus produced by the electrons (Table 11-4). The product $g_N m_I \mu_N$ is the nuclear magnetic moment. Except for μ_N, the quantities on the right side of Equation 11-16 are all of the same order of magnitude as the corresponding ones in Equation 7-68; however, the ratio $\mu_N/\mu_B \approx 10^{-3}$. Thus, the hyperfine splitting for a given atom is very small, about 10^{-3} times the fine-structure splitting. Using as an example the sodium doublet levels $^2P_{1/2}$, $^2P_{3/2}$, and $^2S_{1/2}$ shown in Figure 7-30, which produce the yellow D lines, Figure 11-11 illustrates the hyperfine splitting of these levels resulting from $I - J$ coupling. It can be observed only with extremely high resolution. The use of tunable dye lasers and atomic beam fluorescence spectroscopy has made high precision measurements of these extremely small energy splittings possible in recent years.

For the case $I \leq J$, there are $(2I + 1)$ different F states; thus the nuclear spin can be determined by counting the number of lines in the hyperfine splitting. The spin of all even-even nuclides (those with even Z and even N) is zero in the ground state.

Table 11-4 Magnetic field B_e at the nucleus due to electron for selected alkali elements

Element	n	B_e, $^2S_{1/2}$(T)	B_e, $^2P_{1/2}$(T)	B_e, $^2P_{3/2}$(T)
H	1	17	—	—
Li	2	13	—	—
Na	3	44	4.2	2.5
K	4	63	7.9	4.6
Rb	5	130	16	8.6
Cs	6	210	28	13

Source: Data are from E. Segrè, *Nuclei and Particles*, 2d ed. (Menlo Park, CA: Benjamin/Cummings 1977), p. 259.

FEUE WHE

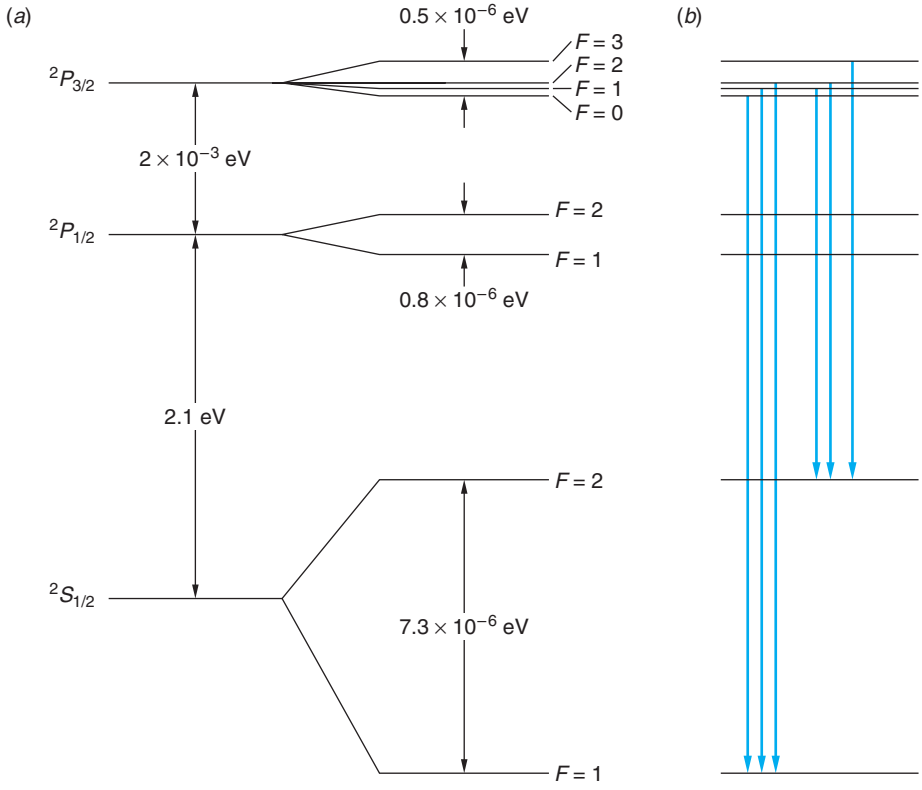

Figure 11-11 (*a*) Transitions between the sodium doublet levels produce the yellow *D* lines, $^2P_{1/2} \rightarrow {}^2S_{1/2}$ being D_1 and $^2P_{3/2} \rightarrow {}^2S_{1/2}$ being D_2. Coupling between the atomic angular momentum J and the nuclear spin $I = 3/2$ results in the hyperfine splitting, each level having total angular momentum $\mathbf{F} = \mathbf{I} + \mathbf{J}$. Note that the hyperfine splitting of each of the doublet levels is about 10^{-3} times that of the fine-structure splitting of the ^2P level. (*b*) The selection rule $\Delta F = \pm 1, 0$ leads to the D_2 line being split into six components. The D_1 line is correspondingly split into four components (not shown).

Evidently the nucleons couple together in such a way that their angular momenta add to zero in pairs, as is often the case for electrons in atoms. There is no such simple rule for other nuclides with either odd N or odd Z or both. Some of the successes of the shell model to be discussed in Section 11-6 are the correct prediction of nuclear spins for many nuclei.

The magnetic moment of the nucleus $g_N m_I \mu_N$ is of the order of the nuclear magneton, $\mu_N = e\hbar/2m_p$, since the magnitude of g_N is typically between 1 and 5 and the maximum value of $|m_I| = I$. The exact value is difficult to predict because it depends on the detailed motion of the nucleons. If the proton and neutron obeyed the Dirac relativistic wave equation, as does the electron, the magnetic moment due to spin would be 1 nuclear magneton for the proton because its charge is $+e$ and 0 for the neutron because it has no charge.[11] The experimentally determined moments of the nucleons are

$$(\mu_p)_z = +2.79285\ \mu_N$$
$$(\mu_n)_z = -1.91304\ \mu_N$$

As we will see in Chapter 12, the proton and neutron are more complex particles than the electron. It is interesting that the deviations of these moments from those predicted by the Dirac equation are about the same magnitude, 1.91 for the neutron and 1.79 for the proton. The reason that the magnetic moments of the nucleons have these particular values is not yet completely understood; the current theoretical predictions of μ_p and μ_n agree with high-precision, experimentally measured values only to within about 1 percent.

The degeneracy of the hyperfine levels in nuclei with nonzero spins, e.g., the proton in ^{1}H, is removed by an external **B** field, a nuclear analog of the Zeeman effect. Transitions between these levels, separated (in ^{1}H) by $2\mu_p B$, oscillate at the spin precession rate. Detection of the resulting absorption or emission of radiation allows "mapping" of the hydrogen-containing soft tissue, the basis for medical *magnetic resonance imaging* (MRI).

FEUE WHE

EXAMPLE 11-7 **Nuclear Spin of Thallium-205** High-resolution spectroscopic study of the spectrum of ^{205}Tl reveals that each component of the doublet $^2P_{1/2} \rightarrow {}^2S_{1/2}$ (377.7 nm), $^2P_{3/2} \rightarrow {}^2S_{1/2}$ (535.2 nm) consists of three hyperfine components. This requires that there be two hyperfine levels for each J. Determine the spin of the ^{205}Tl nucleus.

SOLUTION

If $I \leq J$, then there are $(2I + 1)$ different F levels, and if $I > J$, there are $(2J + 1)$ different F levels. Since the hyperfine spectrum indicates that there are two levels for each J, then for the $^2P_{3/2}$ level either

$$2I + 1 = 2 \quad \text{or} \quad 2J + 1 = 2$$

But we already know that $J = (3/2)$, so $(2J + 1)$ cannot equal 2; therefore $(2I + 1) = 2$ and the spin of the ^{205}Tl nucleus (in its ground state) must be $1/2$.

Note that for the $^2P_{1/2}$ and $^2S_{1/2}$ levels both of the equations above are satisfied since in these two cases $I = J$.

Questions

1. Why is N approximately equal to Z for stable nuclei? Why is N greater than Z for heavy nuclei?
2. Why are there no stable isotopes with $Z > 83$?
3. The mass of ^{12}C, which contains 6 protons and 6 neutrons, is exactly 12.000 u by the definition of the unified mass unit. Why isn't the mass of ^{16}O, which contains 8 protons and 8 neutrons, exactly 16.000 u?

11-3 Radioactivity

Of the more than 3000 nuclides known, only 266 are stable. All of the rest are radioactive; that is, they decay into other nuclides by emitting radiation. The term *radiation* here refers to particles as well as electromagnetic radiation. In 1900 Rutherford discovered that the rate of emission of radiation from a substance was not constant but decreased exponentially with time. This exponential time dependence is characteristic of all radioactivity and indicates that it is a statistical process. Because each nucleus is well shielded from others by the atomic electrons, pressure and temperature changes have no effect on nuclear properties.[12]

For a statistical decay (in which the decay of any individual nucleus is a random event), the number of nuclei decaying in a time interval dt is proportional to dt and to the number of nuclei present. If $N(t)$ is the number of radioactive nuclei at time t and $-dN$ is the number that decay in dt (the minus sign is necessary because N decreases), we have

$$-dN = \lambda N\, dt \qquad \textbf{11-17}$$

where the constant of proportionality, λ, is called the *decay constant*. λ is the probability per unit time of the decay of any given nucleus. The solution of this equation is

$$N(t) = N_0 e^{-\lambda t} \qquad \textbf{11-18}$$

where N_0 is the number of nuclei present at time $t = 0$. The decay rate is

$$R = -\frac{dN}{dt} = \lambda N_0 e^{-\lambda t} = R_0 e^{-\lambda t} \qquad \textbf{11-19}$$

Note that *both the number of nuclei and the rate of decay decrease exponentially with time*. It is the decrease in the rate of decay that is determined experimentally. Figure 11-12 shows N versus t. If we multiply the numbers on the N axis by λ, this becomes a graph of R versus t.

We can calculate the *mean lifetime* from Equation 11-18. The number of nuclei with lifetimes between t and $t + dt$ is the number that decay in dt, which is $\lambda N\, dt$; thus the fraction with lifetimes in dt is

$$f(t)\, dt = \frac{\lambda N\, dt}{N_0} = \lambda e^{-\lambda t}\, dt \qquad \textbf{11-20}$$

When we use this distribution function, the mean lifetime τ is

$$\tau = \int_0^\infty t f(t)\, dt = \int_0^\infty t\lambda e^{-\lambda t}\, dt = \frac{1}{\lambda} \qquad \textbf{11-21}$$

which is the reciprocal of the decay constant λ. The *half-life* $t_{1/2}$ is defined as the time after which the number of radioactive nuclei has decreased to half its original value. From Equation 11-18,

$$\frac{1}{2}N_0 = N_0 e^{-\lambda t_{1/2}} \quad \text{or} \quad e^{\lambda t_{1/2}} = 2$$

$$t_{1/2} = \frac{\ln 2}{\lambda} = (\ln 2)\tau = \frac{0.693}{\lambda} = 0.693\,\tau \qquad \textbf{11-22}$$

After each time interval of one half-life, the number of nuclei left in a given sample and the decay rate have both decreased to half of their previous values. For example, if the decay rate is R_0 initially, it will be $(1/2)R_0$ after one half-life, $(1/2)(1/2)R_0$ after two half-lives, and so forth. During one mean lifetime, the number of nuclei remaining in the sample and the decay rate have decreased to $1/e$ of their previous values. Thus, if the initial decay rate is R_0, it will be $(1/e)R_0$ after time τ has elapsed, $(1/e)(1/e)R_0$ after time 2τ, and so on. The SI unit of radioactivity is the *becquerel* (Bq), which is defined as one decay per second:

$$1\ \text{Bq} = 1\ \text{decay/s} \qquad \textbf{11-23}$$

A historical unit of activity, the *curie* (Ci), is also frequently used. The curie is defined as

$$1\ \text{Ci} = 3.7 \times 10^{10}\ \text{decay/s} = 3.7 \times 10^{10}\ \text{Bq} \qquad \textbf{11-24}$$

The curie is the disintegration rate of 1 g of radium. Since this is a very large unit, the millicurie (mCi), microcurie (μCi), and picocurie (pCi) are also often used.

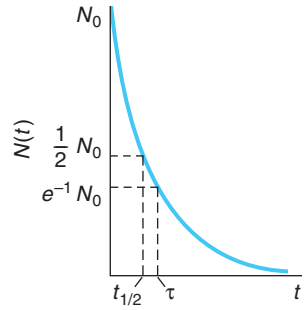

Figure 11-12 Exponential radioactive decay law. The number of nuclei remaining at time t decreases exponentially with time t. The half-life $t_{1/2}$ and the mean life $\tau = 1/\lambda$ are indicated. The decay rate $R(t) = \lambda N(t)$ has the same time dependence.

FEUE WHE

EXAMPLE 11-8 **Counting Rate of a Radioactive Sample** A radioactive source has a half-life of 1 minute. At time $t = 0$ it is placed near a detector and the counting rate (the number of decay particles detected per unit time) is observed to be 2000 counts/s. (*a*) Find the mean life and the decay constant. (*b*) Find the counting rate at times $t = 1$ min, 2 min, 3 min, and 10 min.

SOLUTION

1. For question (*a*), the mean life τ is related to the half-life $t_{1/2}$ by Equation 11-22:

$$t_{1/2} = (\ln 2)\tau$$

or

$$\tau = \frac{t_{1/2}}{\ln 2} = \frac{1 \text{ min}}{0.693} = 1.44 \text{ min} = 86.6 \text{ s}$$

2. From Equation 11-21, the decay constant is given by

$$\lambda = \frac{1}{\tau} = \frac{1}{86.6 \text{ s}} = 1.16 \times 10^{-2} \text{ s}^{-1}$$

3. *Method 1.* For question (*b*), the counting rate is proportional to the decay rate R in Equation 11-19. The counting rate at $t = 0$ has the same proportionality to R_0, so we can write the counting rate as R, substituting values for λ and for $t_{1/2}$:

$$R = 2000\, e^{-\lambda t} = 2000\, e^{-(1.16 \times 10^{-2})t}$$
$$= 2000\, e^{-(\ln 2)t/t_{1/2}}$$
$$= 2000\, e^{-(0.693)t}$$

where t is now expressed in minutes

4. The counting rate R can now be computed for each of the times $t = 1$ min, 2 min, 3 min, and 10 min as follows:

$$R(1 \text{ min}) = 2000\, e^{-(0.693)(1)} = 2000 \times 0.50 = 1000 \text{ counts/s}$$
$$R(2 \text{ min}) = 2000\, e^{-(0.693)(2)} = 500 \text{ counts/s}$$

and similarly

$$R(3 \text{ min}) = 250 \text{ counts/s}$$
$$R(10 \text{ min}) = 1.95 \text{ counts/s}$$

5. *Method 2.* Since the half-life is 1 min, the counting rate at $t = 1$ min will be half that at $t = 0$; at $t = 2$ min it will be half of that at $t = 1$ min, and so on. In general, at $t = n$ min the count rate will be

$$R = (1/2)^n R_0$$

and again

$$R(1 \text{ min}) = (1/2)^1 2000 = 1000 \text{ counts/s}$$

and

$$R(10 \text{ min}) = (1/2)^{10} 2000$$
$$= (0.0010)(2000) = 1.95 \text{ counts/s}$$

FEUE WHE

More

Very often the decay of a radioactive nucleus results in a new nucleus that is also radioactive and that, in general, has a different decay constant. In some cases such sequential decays may result in a dozen or more different radioactive isotopes. *Production and Sequential Decays*, on the home page (www.whfreeman.com/tiplermodernphysics5e), describes the way to calculate the total activity and the net rate at which new isotopes are produced. See Equations 11-25 through 11-29 and Figures 11-13 and 11-14 here, as well as Examples 11-9 and 11-10 and Questions 4 and 5.

11-4 Alpha, Beta, and Gamma Decay

From the time when Becquerel's discovery of radioactivity gave the first hint of the existence of the nucleus, much of what physicists have learned about nuclear structure has resulted from studies of radioactive nuclides, that is, by studying the transitions of nuclei from one quantum state to another of lower energy. As noted earlier, of the approximately 3000 known isotopes, all but 266 are radioactive. In addition, nearly all of a theoretically estimated 2000 more possible isotopes that have yet to be created are radioactive. The radioisotopes decay by one or another of at least nine different modes; however, most decays occur via one or sometimes two of the most common modes: alpha, beta, and gamma. Others occur by more unusual routes, such as emission of a proton or neutron or spontaneous fission. A few may decay by modes that are exceedingly rare, such as a double beta decay, which is the focus of considerable current theoretical and experimental interest. The fundamental purpose of the studies of radioactive nuclei is to obtain information about nuclear structure, the nature of the strong nuclear force, and the properties of elementary particles.

In the subsections that follow we will discuss the three most common types of decay in some detail, touching on certain of the others when pertinent. In these discussions it will be helpful to keep two points in mind. The first of these is that the line of stability in Figure 11-8 is the floor of an energy valley formed by plotting the binding energy for each isotope on an energy scale perpendicular to the N and Z axes, as illustrated in Figure 11-15*a*. In Figure 11-15*a* the energy is artificially truncated; however, there are theoretical limitations placed on the numbers of protons and neutrons that can be assembled into a nucleus, even a highly unstable one. These limits, given the whimsical name *driplines*, are shown in Figure 11-15*b* and define the N-Z boundaries within which lie the 5000 or so isotopes that may, in principle, exist. The limits are set by the energies at which the nuclei will spontaneously emit a proton or neutron.

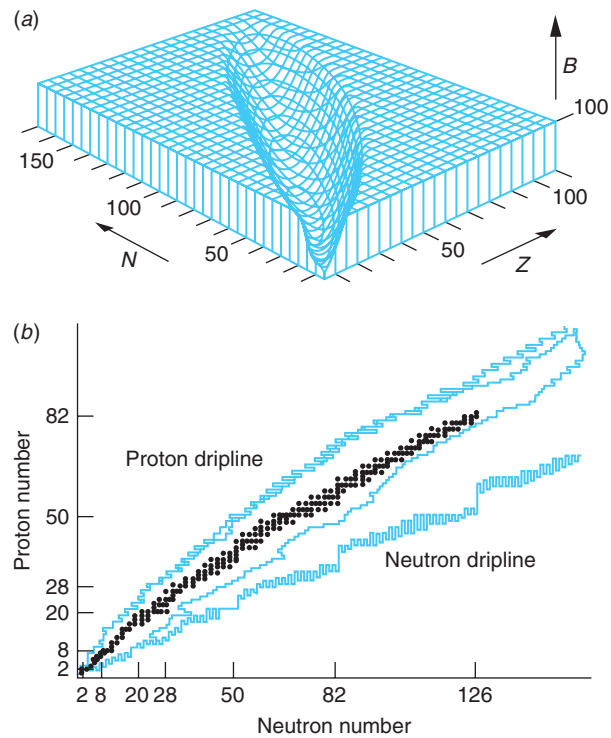

Figure 11-15 (*a*) The graph of Z versus N with the nuclear binding energy B (in MeV) plotted upward. The surface thus formed is truncated at 100 MeV to make the energy valley more clearly visible. (*b*) More than 5000 theoretically predicted nuclei lie between the proton and neutron driplines. Only about 3000 (those between the inner irregular colored lines) are found in nature or have been created in the laboratory, and only 266 of those are stable (black dots). The edges of the truncation in (*a*) are analogous to artificial driplines.

The second point to bear in mind is that radioactive-decay processes conform to the same conservation laws that are obeyed by all physical processes. In particular, (1) relativistic mass-energy, (2) electric charge, (3) linear momentum, (4) angular momentum, (5) nucleon number, and (6) lepton number[13] are all conserved quantities. The first four of these are already familiar to you from your previous study of physics. The last two relate specifically to the interactions and decays of fundamental particles and will be discussed in Chapter 12. As we discuss the three most common modes of radioactive decay, consequences of each of the conservation laws will be illustrated.

Alpha Decay

The α particles emitted by a tiny amount of ^{241}Am are used to ionize the air inside smoke detectors. When smoke is present, the ionized air molecules stick to the smoke particles, reducing a trickle current maintained in the ionized air, thereby triggering an alarm. Ionization-type smoke detectors are considerably more sensitive than those using photoelectric sensors.

In order for a radioactive substance to be found in nature, either it must have a half-life that is not much shorter than the age of Earth (about 4.5×10^9 years) or it must be continually produced by the decay of another radioactive substance or by a nuclear reaction. For a nucleus to be radioactive at all, its mass must be greater than the sum of the masses of the decay products. Many heavy nuclei are unstable to α decay. Because the Coulomb barrier inhibits the decay process (the α particle must "tunnel" through a region in which its energy is less than the potential energy, as shown in Figure 11-1*a*), the half-life for α decay can be very long if the decay energy is small, that is, if the width of the barrier to be tunneled through is large. Indeed, the relation between the half-life of an α emitter and the energy of the α particle is so striking that it was first noticed by two research assistants in Rutherford's laboratory, Geiger and Nuttall, in 1911, the same year that Rutherford discovered the nucleus. The general relation, called the Geiger-Nuttall rule, is illustrated in Figure 11-16 and given by Equation 11-30.

$$\log t_{1/2} = AE_\alpha^{-1/2} + B \qquad \textbf{11-30}$$

where E_α is the kinetic energy of the emitted α particle and A and B are experimentally determined constants.

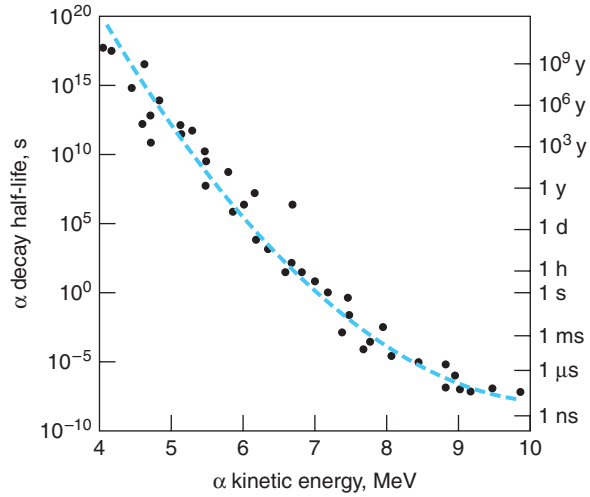

Figure 11-16 The Geiger-Nuttall relation is illustrated by the semilogarithmic graph of the α decay half-life versus the kinetic energy of the emitted α particle for the naturally occurring α emitters. The broken line represents the empirical Geiger-Nuttall rule given by Equation 11-30.

FEUE WHE

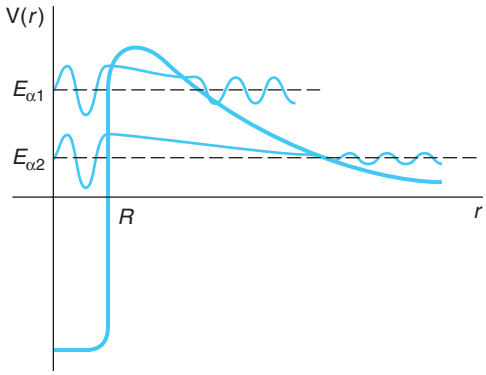

Figure 11-17 Schematic representations of the wave functions of two α particles with energies $E_{\alpha 1}$ and $E_{\alpha 2}$ within the nuclear potential well. The probability of α1 penetrating the barrier is larger than that for α2 since the barrier is narrower at $E_{\alpha 1}$. Thus, the amplitude of $\psi(\alpha 1)$ is larger outside the nucleus than that of $\psi(\alpha 2)$. Hence, $\lambda(\alpha 1) > \lambda(\alpha 2)$ and therefore $t_{1/2}(\alpha 1) < t_{1/2}(\alpha 2)$.

Subsequently, an expression for the half-life of an α emitter was derived from the Schrödinger equation treating α decay as a barrier penetration phenomenon. Its good agreement with experimental results was one of the earliest successful applications of wave mechanics. Briefly, the derivation considered an α particle confined within the nucleus with energy E_α as was shown in Figure 11-1. The wave functions for two such particles are illustrated in Figure 11-17. The potential for $r > R$ is taken to be the Coulomb function $V(r) = zZe^2/4\pi\epsilon_0 r$ where $z = 2$ for the α particle, with a smooth transition to the nuclear potential. The probability that the α particle will penetrate the barrier on any one approach is the transmission coefficient T that was derived in Section 6-6, Equations 6-75 and 6-76. The decay constant $\lambda = 1/\tau = 0.693/t_{1/2}$ is then given by the product of the transmission coefficient T and the frequency with which the nuclear α particle approaches the barrier. The latter, given by Equation 6-78, depends on the α particle's speed v, determined by its kinetic energy for $r < R$ in Figure 11-17 and the value of the nuclear radius. Thus,

$$\lambda = \frac{Tv}{2R} \qquad \textbf{11-31}$$

The result of the wave mechanical derivation, done by B. Taagepera and M. Nurmia, is

$$\log t_{1/2} = 1.61(ZE_\alpha^{-1/2} - Z^{2/3}) - 28.9 \qquad \textbf{11-32}$$

where $t_{1/2}$ is in years, E_α is in MeV, and Z refers to the daughter nucleus. Notice that the dependence of $t_{1/2}$ on the nuclear radius provides a method of measuring nuclear radii that is independent of the methods mentioned in Section 11-2.

Alpha-Decay Chains All very heavy nuclei ($Z > 83$) are theoretically unstable to α decay because the mass of the parent radioactive nucleus is greater than the sum of the masses of the decay products—the daughter nucleus and an α particle. When a nucleus emits an α particle, both N and Z decrease by 2, and A decreases by 4. There are four possible α-decay chains or sequences, depending on whether A equals $4n$, $(4n + 1)$, $(4n + 2)$, or $(4n + 3)$, where n is an integer. For the longest-lived nucleus in each sequence, $n = 58$ for the first and fourth and $n = 59$ for the second and third. All but one of these series are found in nature. The $(4n + 1)$ series is not, because its longest-lived member (other than the stable end product ^{209}Bi), ^{237}Np, has a half-life of only 2×10^6 years, which is much shorter than the age of Earth; hence ^{237}Np present when Earth was formed has long since decayed away.

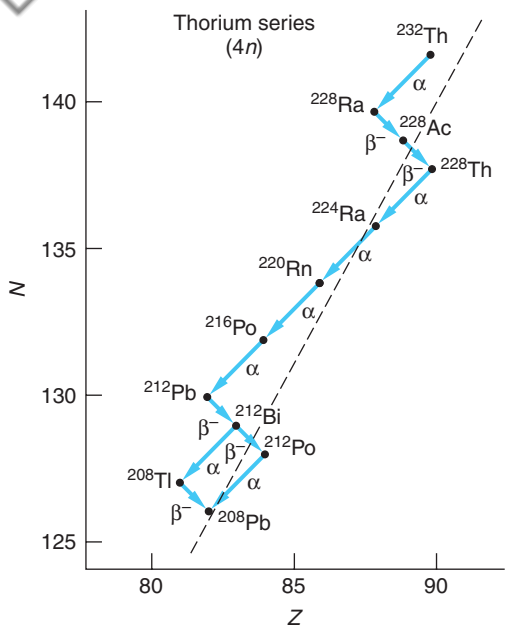

Figure 11-18 The thorium ($4n$) α-decay series. The broken line is the line of stability (floor of the energy valley) shown in Figures 11-8 and 11-15.

Figure 11-18 illustrates the thorium series, which has $A = 4n$ and begins with an α decay from ^{232}Th to ^{228}Ra. Decreasing n successively by 1 generates A for possible daughter nuclides until a stable one is reached. The daughter nuclide of an α decay is on the left, or neutron-rich, side of the stability curve (dashed line), so it often decays by β^- decay, in which one neutron changes to a proton by emitting an electron. In Figure 11-18 ^{228}Ra decays by β^- decay to ^{228}Ac, which in turn decays to ^{228}Th. There are then four α decays to ^{212}Pb, which β^- decays to ^{212}Bi. There is a branch point at ^{212}Bi, which decays either by α decay to ^{208}Tl or by β^- decay to ^{212}Po. The branches meet at the stable lead isotope ^{208}Pb. The $(4n + 2)$ series begins with ^{238}U and ends with ^{206}Pb. The $(4n + 3)$ series starts with ^{235}U and ends with ^{209}Pb. Figure 11-19 shows a typical α-decay spectrum.

More

The energy spectrum of the alpha particles emitted by a heavy nucleus such as ^{232}Th shows a number of sharp peaks with energies less than the decay energy Q. The highest energy of these corresponds to the transition from the parent's ground state to that of the daughter. The others are the result of alpha transitions to excited states of the daughter. In *Energetics of Alpha Decay*, on the home page (www.whfreeman.com/tiplermodernphysics5e), we describe how they can be used to construct the excited levels of the daughter nucleus. See also Figures 11-19 and 11-20, Equations 11-33 through 11-36, and Example 11-11 here.

Figure 11-19 Alpha-particle spectrum from ^{227}Th. The highest-energy α particles correspond to decay to the ground state of ^{223}Ra with a transition energy of $Q = 6.04$ MeV. The next highest energy particles, α_{30}, result from transitions to the first excited state of ^{223}Ra, 30 keV above the ground state. The energy levels of the daughter nucleus, ^{223}Ra, can be determined by measurement of the α-particle energies.

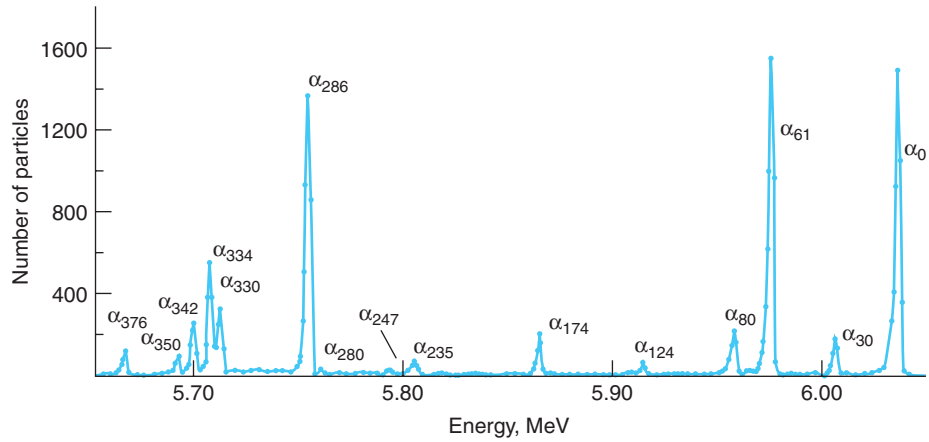

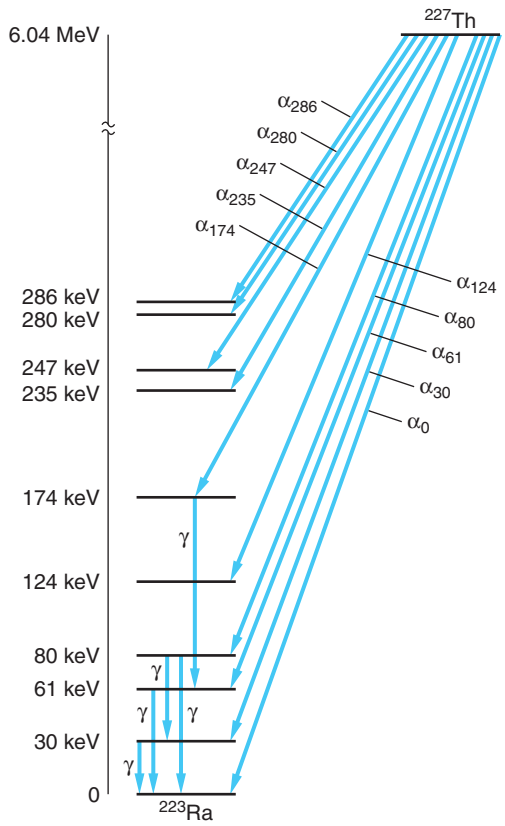

Figure 11-20 Energy levels of ^{223}Ra determined by measurement of α-particle energies from ^{227}Th, as shown in Figure 11-19. Only the lowest-lying levels and some of the γ-ray transitions are shown.

Beta Decay

There are three radioactive-decay processes in which the mass number A remains unchanged while Z and N change by ± 1. These are β^- decay, in which a neutron inside a nucleus changes into a proton with the emission of an electron; β^+ decay, in which a proton inside a nucleus changes into a neutron with the emission of a positron; and electron capture (EC), in which a proton in a nucleus changes to a neutron by capturing an atomic electron, usually a 1s electron from the K shell since these have the highest probability density in the vicinity of the nucleus. Those nuclei on the neutron-rich side of the energy valley in Figure 11-15 will tend to decay by β^- emission, while those on the proton-rich side will most probably decay by β^+ emission or electron capture. We will discuss each of these processes briefly.

β^- Decay The simplest example of β^- decay is that of the free neutron, which decays into a proton plus an electron with a half-life of about 10.8 minutes. The energy of decay is 0.78 MeV, which is the difference between the rest energy of the neutron (939.57 MeV) and that of the proton plus electron (938.28 + 0.511 MeV). More generally, in β^- decay, a nucleus of mass number A, atomic number Z, and neutron number N changes into one with mass number A, atomic number $Z' = Z + 1$, and neutron number $N' = N - 1$, conserving charge with the emission of an electron.

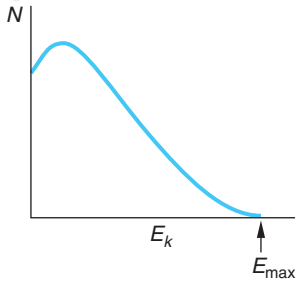

Figure 11-21 Energy spectrum of electrons emitted in β decay. The number of electrons per unit energy interval N is plotted versus kinetic energy. The fact that all the electrons do not have the same kinetic energy E_{max} suggests that there is another particle emitted that shares the energy available for decay.

The energy of decay Q is c^2 times the difference between the mass of the parent nucleus and that of the decay products. If we add the mass of Z electrons to both the parent nucleus and the decay products, we can write Q in terms of the *atomic* masses of the parent and daughter atoms:

$$\frac{Q}{c^2} = M_P - M_D \qquad \textbf{11-37}$$

Another way of understanding this result is to note that in β^- decay an electron of mass m_e leaves the atom, which is now a daughter *ion* of nuclear charge $(Z + 1)$ and Z atomic electrons. To obtain the mass of the *neutral* daughter atom, we must add the mass of an electron m_e so the total mass change is just the difference in mass between the parent and daughter *atoms*. If the decay energy Q were shared only by the daughter atom and the emitted electron, the energy of the electron would be uniquely determined by conservation of energy and momentum, just as in α decay. Experimentally, however, the energies of the electrons emitted in β decay are observed to vary from zero to the maximum energy available E_{max}. A typical energy spectrum is shown in Figure 11-21; compare this with the discrete spectrum of α-particle energies of Figure 11-19. Thus, in a particular decay event in which the electron carried away less than the energy E_{max}, it would appear that energy was not conserved since in that decay $Q/c^2 < M_P - M_D$. A moment of reflection will persuade you that linear momentum would not be conserved either and, recalling that the neutron, proton, and electron are all spin $1/2$ particles, neither would the angular momentum.

A solution to this apparent multiple failure of conservation laws was first suggested by Wolfgang Pauli in 1930. He proposed that a third particle was emitted in β decay that carried the energy, linear momentum, and angular momentum needed to conserve these quantities in each individual decay. It would carry no electric charge since charge was already conserved in β decay. Its mass would be much less than that of the electron since the maximum energy of electrons emitted in β decay is observed to be very nearly equal to the value of Q, the total energy available for the decay. In 1933 Enrico Fermi developed a highly successful quantum theory of β decay that incorporated Pauli's proposed particle, which Fermi called the *neutrino* ("little neutral one" in Italian) to distinguish it from the massive neutron that had been discovered by Chadwick earlier that same year. It was not until 1956, in an experiment performed by Clyde Cowan and Frederick Reines, that neutrinos were first observed in the laboratory. It is now known that there are six kinds of neutrinos, one (ν_e) associated with electrons, one (ν_μ) associated with muons, one (ν_τ) associated with the tau particle, and the *antiparticles* of each of those, written $\bar{\nu}_e$, $\bar{\nu}_\mu$, and $\bar{\nu}_\tau$. The electrons, muons, and taus together with the neutrinos constitute a family of particles called *leptons*, which will be discussed further in Chapter 12. The decay of the free neutron is then expressed by

$$n \longrightarrow p + \beta^- + \bar{\nu}_e \qquad \textbf{11-38}$$

and that of ^{198}Au, a more or less typical β^- emitter, by

$$^{198}\text{Au} \longrightarrow {}^{198}\text{Hg} + \beta^- + \bar{\nu}_e \qquad \textbf{11-39}$$

where the lepton conservation law (see Section 12-3) dictates the emission of an electron antineutrino to accompany a β^- decay. Presently the subject of intense experimental and theoretical research, current results place the upper limit of the electron neutrino's mass at about 2.2 eV/c^2, or no more than about 4×10^{-6} times the mass of the electron.

FÈUE WHE

β^+ Decay In β^+ decay, a proton changes into a neutron with the emission of a positron and a neutrino. A free proton cannot decay by positron emission because of conservation of energy (the rest energy of the neutron is greater than that of the proton), but because of binding energy effects, a proton inside a nucleus may emit a positron. A typical β^+ decay is

$$^{13}_{7}\mathrm{N} \longrightarrow {}^{13}_{6}\mathrm{C} + \beta^+ + \nu_e \qquad \textbf{11-40}$$

The only naturally occurring positron emitter known to exist is ^{40}K, which also may decay by β^- emission or electron capture! The β^+-decay equation is

$$^{40}_{19}\mathrm{K} \longrightarrow {}^{40}_{18}\mathrm{Ar} + \beta^+ + \nu_e \qquad \textbf{11-41}$$

As in all nuclear transformations, the decay energy Q is related to the difference in mass between the parent nucleus and the decay products. Note that if we add the mass of Z electrons to the nuclear masses ($Z = 7$ in the case of Equation 11-40 and $Z = 19$ in Equation 11-41), we obtain on the right side of each equation the mass of the daughter atom plus two extra electron masses (the positron and electron have identical mass). The decay energy for β^+ decay is thus related to the atomic mass of the parent and daughter atoms by

$$\frac{Q}{c^2} = M_P - (M_D + 2m_e) \qquad \textbf{11-42}$$

Again, we can understand this by noting that in β^+ decay, a positron of mass m_e leaves the system, which is now a negative daughter ion of nuclear charge $(Z - 1)$ and Z atomic electrons. To obtain the mass of the neutral daughter atom, we must subtract the mass of another electron, giving a net change of $2m_e$ in addition to the difference in mass of the parent and daughter atoms. Thus, β^+ decay cannot occur unless that energy difference is at least $2m_ec^2 = 1.022$ MeV.

As we have mentioned, neither electrons nor positrons exist inside the nucleus prior to the decay. They are created in the process of decay by the conversion of energy to mass, just as photons are created when an atom makes a transition from a higher to a lower energy state. In this regard β decay differs from α decay. There is, however, a fundamental difference between the emission of electrons (and neutrinos) that de-excite the bound states of nucleons that compose a nucleus and the emission of photons accompanying the de-excitation of the electrons bound to a nucleus. The latter bonding is due to the electromagnetic interaction, whereas the nucleons are bound by the strong nuclear force. However, electrons and neutrinos are not affected by the strong nuclear force and, since the neutron is uncharged, the electromagnetic interaction is not involved in its decay. Thus, in order to explain β decay, we must invoke a new interaction. Since β-decay lifetimes are typically quite long compared to the characteristic nuclear time scale ($\approx 10^{-23}$ s, the time for a particle moving at near the speed of light to cross the nucleus), the new interaction must act for a long (nuclear) time in order to generate the decay. In other words, it is weaker than the strong attractive force between the nucleons and is therefore called the *weak interaction* or the *weak force*. So we now have two nuclear forces, a strong one and a weak one. Like the strong nuclear force, the weak nuclear force also has a short range.

PET scanners used in medical diagnosis detect photons emitted in electron-positron annihilation following β^+ decay.

Electron Capture In electron capture, a proton inside a nucleus captures an atomic electron and changes into a neutron with the emission of a neutrino; thus the effect on the atomic number is the same as in β^+ decay. The energy available for this process is given by

$$\frac{Q}{c^2} = M_P - M_D \qquad \textbf{11-43}$$

Whenever the mass of an atom of atomic number Z is greater than that of the adjacent atom with atomic number $(Z - 1)$, electron capture is possible. If the mass difference is greater than $2m_e$, β^+ decay is also possible, and these two processes compete. The probability of electron capture is negligible unless the atomic electron is in the immediate vicinity of the nucleus. This probability is proportional to the square of the electron wave function integrated over the volume of the nucleus. It is significant only for the $1s$ electrons of the K shell or, with much lower probability, the $2s$ electrons of the L shell. A typical example of electron capture is

$$^{51}_{24}\text{Cr} \longrightarrow {}^{51}_{23}\text{V} + \nu_e \qquad \textbf{11-44}$$

which has $Q = 0.751$ MeV. Note that the emission of the neutrino conserves leptons since the captured electron has disappeared.

Further understanding of the β-decay processes can be gained by considering their relation to the energy valley of the N versus Z graphs shown in Figure 11-15, with the energy scale computed from the Weizsäcker formula (Equation 11-14). Cuts through Figure 11-15*a* at constant mass number A yield parabolas since Equation 11-14 is quadratic in Z, one parabola for $a_5 = 0$ (odd A) and two parabolas for $a_5 = \pm 12$ MeV/c^2 (even A). Figure 11-22 illustrates an example of each case. The β decays always proceed down the sides of the energy valley toward the lowest-energy, stable isotope on the valley floor. Notice in Figure 11-22*b* the possible double β decay from ^{60}Fe to ^{60}Ni.

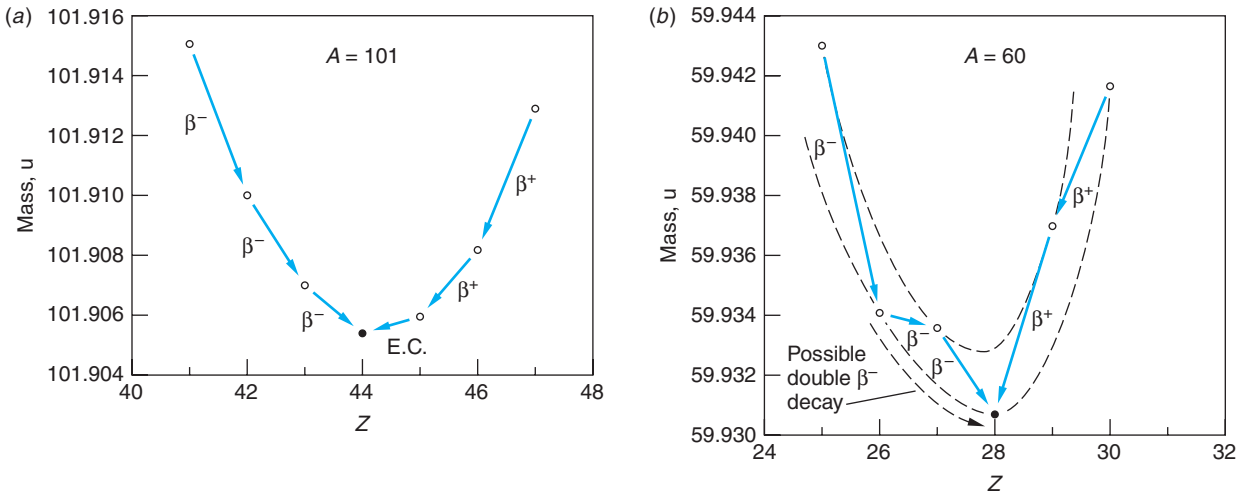

Figure 11-22 Profiles of constant atomic mass show the cross section of the energy valley of the N versus Z graph. The energy axes are expressed in mass units as computed from the Weizsächer mass formula. (*a*) Odd-A nuclei, such as $A = 101$ shown, have Z and N odd-even or even-odd and $a_5 = 0$. (*b*) Even-A nuclei are either even-even with $a_5 = 12$ MeV/c^2 or odd-odd with $a_5 = -12$ MeV/c^2. The even-even parabola lies below the odd-odd one.

Since β decay proceeds via the weak interaction, the probability of the weak force producing two β^- particles simultaneously is indeed small, as you might imagine. Prior to 1985 its existence had been inferred only indirectly by abundance measurements on decay products in geologic materials. In 1985 Steven Elliott and his co-workers made the first direct observation of double beta decay using ^{82}Se as the source. The decay equation is

$$^{82}_{34}\text{Se} \longrightarrow {}^{82}_{36}\text{Kr} + \beta^- + \beta^- + \bar{\nu}_e + \bar{\nu}_e \qquad \textbf{11-45}$$

The half-life for the double β decay measured by Elliott is 1.1×10^{20} years! Double beta decay has subsequently been observed in several other nuclides. Since recent experiments show that the neutrino has a very small mass, current theory (the Standard Model—see Chapter 12) would allow the decay in Equation 11-45 to proceed without the emission of neutrinos, albeit with an even lower probability. The implications of a neutrinoless double beta decay are profound for both particle physics and cosmology. Although active searches are currently under way, no such decays have yet been observed.

EXAMPLE 11-12 **Maximum β^+ Energy from ^{40}K** We noted earlier that one of the decay modes of ^{40}K is positron emission, shown in Equation 11-41. What is the maximum energy of the positrons?

SOLUTION

1. The maximum energy Q of the positrons is given by Equation 11-42, where ^{40}K is the parent and ^{40}Ar is the daughter:
$$\frac{Q}{c^2} = M_P - (M_D + 2m_e)$$

2. The atomic masses are given in Appendix A:
$$M(^{40}\text{K}) = 39.964000 \text{ u}$$
$$M(^{40}\text{Ar}) = 39.962384 \text{ u}$$
$$m_e = 5.4858 \times 10^{-4} \text{ u}$$

3. Substituting these into Equation 11-42 yields
$$\frac{Q}{c^2} = 39.964000 \text{ u} - [39.962384 + 2 \times 3.4858 \times 10^{-4}] \text{ u}$$
$$= 0.000519 \text{ u} \times 931.5 \text{ MeV}/c^2 \cdot u$$
$$= 0.483 \text{ MeV}/c^2$$

Remarks: *Neglecting the recoil of the Ar nucleus, the decay energy $Q = 0.483$ MeV is the maximum energy of the emitted positrons.*

EXAMPLE 11-13 **The Decay of $^{233}_{93}$Np** Determine which decay mode or modes among α decay and the three types of β decay are allowed for $^{233}_{93}$Np.

SOLUTION

The four decays whose possibility of occurrence we are to find are

α decay: $^{233}_{93}\text{Np} \longrightarrow {}^{229}_{91}\text{Pa} + \alpha$

β^- decay: $^{233}_{93}\text{Np} \longrightarrow {}^{233}_{94}\text{Pu} + \beta^- + \bar{\nu}_e$

β^+ decay: $^{233}_{93}\text{Np} \longrightarrow {}^{233}_{92}\text{U} + \beta^+ + \nu_e$

electron capture: $^{233}_{93}\text{Np} \longrightarrow {}^{233}_{92}\text{U} + \nu_e$

The decay energy Q for each of these is computed as follows:

α decay (Equation 11-34):

$$\frac{Q}{c^2} = 233.040805 - (229.032085 + 4.002603)$$
$$= 0.006117 \text{ u} = 5.70 \text{ MeV}/c^2$$

which is greater than zero; therefore, α decay is allowed.

β^- decay (Equation 11-37):

$$\frac{Q}{c^2} = 233.040805 - 233.042963$$
$$= -0.002158 \text{ u} = -2.01 \text{ MeV}/c^2$$

β^- decay is forbidden.

β^+ decay (Equation 11-42):

$$\frac{Q}{c^2} = 233.040805 - (233.039630 + 2 \times 5.4858 \times 10^{-4})$$
$$= 0.000078 \text{ u} = 0.073 \text{ MeV}/c^2$$

β^+ decay is allowed.

Electron capture (Equation 11-43):

$$\frac{Q}{c^2} = 233.040805 - 233.039630$$
$$= 0.001175 \text{ u} = 1.09 \text{ MeV}/c^2$$

Electron capture is allowed.

Thus, the available decay energy would allow α decay, β^+ decay, and electron capture, although the energy for β^+ decay is very small. β^- decay is forbidden. Experimentally, ^{233}Np decays more than 99 percent of the time by electron capture and about 0.3 percent of the time by α decay. β^+ decay has not been observed.

Gamma Decay

In γ decay, a nucleus in an excited state decays to a lower energy state of the same isotope by the emission of a photon. This decay is the nuclear analog of the emission of light by atoms. Since the spacing of the nuclear energy levels is of the order of MeV (as compared with eV in atoms), the wavelength of the emitted photons are of the order of

$$\lambda = \frac{hc}{E} \approx \frac{1240 \text{ eV} \cdot \text{nm}}{1 \text{ MeV}} = 1.24 \times 10^{-3} \text{ nm}$$

Gamma-ray emission usually follows beta decay or alpha decay. For example, if a radioactive parent nucleus decays by beta decay to an excited state of the daughter nucleus, the daughter nucleus often decays to its ground state by emission of one or more γ rays. The mean life for γ decay is usually very short. Direct measurements of mean lives as short as 10^{-11} s are possible. Measurements of lifetimes smaller than 10^{-11} s are difficult but can sometimes be accomplished by determining the natural line width Γ and using the uncertainty relation $\tau = \hbar/\Gamma$. A few γ emitters have very

long lifetimes, of the order of hours and even, in a few cases, years. Nuclear energy states with such long lifetimes are called *isomers* or *metastable states*. The differences in γ-ray lifetimes are a consequence of the quantum-mechanical selection rules that govern transitions between the energy levels of nuclei, just as they do between atomic energy levels. For example, large angular momentum (spin) changes are forbidden for γ transitions; that is, they have very low probability. This is the major reason that, for instance, the first excited state of ^{93}Nb, an isomer, decays to the ground state with a half-life of 13.6 years. The spin of the isomeric state is 1/2, while that of the ground state is 9/2. The decay requires the γ ray to carry away $4\hbar$ of angular momentum, a very unlikely occurrence that accounts for the long half-life.

The energy hf of a gamma-ray photon is the difference in energy of the states between which the transition occurs. That is,

$$hf = E_{\text{high}} - E_{\text{low}} \qquad \textbf{11-46}$$

where E_{high} is the energy of the upper level and E_{low} is that of the lower level. Several gamma decays are shown in Figure 11-20 between some of the excited states of ^{223}Ra that resulted from the α decay of ^{227}Th. For example, a γ ray is emitted from the 174-keV level of ^{223}Ra, reducing the excitation energy of that nucleus to 61 keV above the ground state. From Equation 11-46, the energy of that γ ray is equal to 174 keV − 61 keV = 113 keV. To be more precise, conservation of momentum requires that the ^{223}Ra nucleus carry a small part of this energy as it recoils from the emission of the photon. (See Figure 11-23.) The energy of the nuclear recoil E_r is given by

$$E_r = \frac{p^2}{2M} = \frac{(hf)^2}{2Mc^2} \qquad \textbf{11-47}$$

where M is the nuclear mass. All gamma-ray energies are small compared with atomic and nuclear rest energies; that is, $hf \ll Mc^2$ or $hf/Mc^2 \ll 1$; therefore, $E_r \ll hf$. Thus, Equation 11-46 is an excellent approximation of the gamma ray's energy.

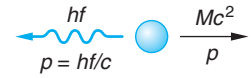

Figure 11-23 A nucleus of rest energy Mc^2 emits a photon of energy hf and momentum $p = hf/c$. Conservation of momentum requires that the nucleus also recoil with momentum p.

Internal Conversion An important alternative to gamma-ray emission for the de-excitation of an excited nuclear state, particularly low-lying states rather than being emitted as a photon, is the process of internal conversion. In this process the excitation energy of the state is transferred to an orbital electron, which is ejected from the atom. Those electrons with the highest probabilities of being close to the nucleus, the K and L electrons, are the ones most likely to be emitted. The ejected electron has kinetic energy equal to the nuclear transition energy minus the electron's binding energy. Since the latter are accurately known for nearly all elements, measuring the kinetic energies of the *conversion electrons* makes possible determination of many nuclear excited states. While internal conversion is quantum mechanically a one-step process, it was initially pictured as the emission of a photon followed by a photoelectric-effect interaction with an orbital electron of the same atom, hence the name *internal conversion*.

More

In 1958 Rudolf Mössbauer[14] observed a remarkable feature of gamma decay, the recoilless emission of gamma rays from ^{191}Ir. A discovery made while he was still a graduate student, it made possible high-precision-frequency measurements, leading to a host of applications. It is described in the section *The Mössbauer Effect* on the home page: www.whfreeman.com/tiplermodernphysics5e. See Figures 11-24 through 11-26 here.

The exceptional precision of frequency measurements made possible by the Mössbauer effect has applications in a broad range of areas, such as measurements of gravitational red shift, impurities and imperfections in crystalline solids, and the transverse Doppler effect (see Section 1-5), to name just three.

FEUE WHE

Questions

6. De-excitation of the first excited state of ^{93}Nb requires the gamma ray to carry away $4\hbar$ of angular momentum. Since the gamma ray's intrinsic angular momentum is $1\hbar$, how could it carry away $4\hbar$?
7. Why is the decay series $A = (4n + 1)$ not found in nature?
8. A decay by α emission is often followed by a β decay. When this occurs, it is usually a β^- decay. Why?
7. How can the application of very high pressure affect the lifetime of a sample that decays by electron capture? Why are other types of decay not affected?

11-5 The Nuclear Force

The study of nuclear physics is quite different from that of atomic physics. The simplest atom, the hydrogen atom, can be completely understood by solving the Schrödinger equation using the known potential energy of interaction between the electron and proton, $V(r) = -ke^2/r$ (though, as we have seen, the mathematics needed is fairly complicated). The simplest nucleus (other than a single proton) is the deuteron, consisting of a proton and a neutron. We cannot solve the Schrödinger equation for this problem and then compare with the experiment because, although many of its characteristics have been determined, the exact mathematical form of the potential energy of interaction V is not known. There is no macroscopic way to measure the force between a neutron and a proton. It is clear from the fact that many nuclei are stable that there are other forces much stronger than electromagnetic or gravitational forces between nucleons. Considering ^{4}He as an example, we see that the electrostatic potential energy of two protons separated by 1 fm is

$$V = \frac{ke^2}{r} = \frac{1.44 \text{ MeV} \cdot \text{fm}}{1 \text{ fm}} = 1.44 \text{ MeV}$$

and note that it is positive—i.e., the electrostatic force between the protons is, of course, repulsive. However, the energy needed to remove a proton or neutron from ^{4}He is about 20 MeV. The force responsible for such a large binding energy must be attractive and significantly stronger than the electrostatic force. This must certainly be the case since the neutrons are electrically neutral and hence do not feel the Coulomb force and the protons are all positively charged and thus feel a repulsive electrostatic force. Nor can we appeal to the gravitational attractive force between the protons to offset their Coulomb repulsion since, as Example 11-14 illustrates, the gravitational force between pairs of protons in the nucleus is insignificantly small compared to their Coulomb repulsion. Thus, the attractive force that holds the nucleons together must be strong, stronger even than the electromagnetic interaction. It is called the *nuclear* or *hadronic force* or often simply the *strong force*.

Determination of the characteristics of the nuclear force is one of the central problems of nuclear physics. Much information about this force can be and has been obtained from scattering experiments involving protons, neutrons, and other particles. Although the results of a scattering experiment can be predicted unambiguously from knowledge of the force law, the force law cannot be completely determined from the results of such experiments. The results of scattering experiments do indicate that

(1) the nuclear force has the same strength between any two nucleons—that is, *n*-*n*, *p*-*p*, or *n*-*p*; (2) the force is strong when the particles are close together and drops rapidly to zero when the particles are separated by a few fm; and (3) it is a saturated force. The potential energy of the nucleon-nucleus interaction can be roughly represented by a square well of about 40 MeV depth and a few fm width.

EXAMPLE 11-14 **Ratio of F_{grav}/F_{Coul} Between Protons** Compare the gravitational attractive force between two protons in an atomic nucleus (or anywhere else, for that matter) with the electrostatic repulsion between them.

SOLUTION

The electrostatic repulsion for two protons separated by a distance r is

$$F_{\text{Coul}} = \frac{1}{4\pi\epsilon_0}\frac{e^2}{r^2} = \frac{(1.60 \times 10^{-19}\ \text{C})^2}{4\pi\epsilon_0 r^2}$$

and the gravitational attraction between them is

$$F_{\text{Grav}} = G\frac{m_p^2}{r^2} = \frac{G(1.67 \times 10^{-27}\ \text{kg})^2}{r^2}$$

The ratio is independent of r and equal to

$$\frac{F_{\text{grav}}}{F_{\text{Coul}}} = \frac{Gm_p^2}{(1/4\pi\epsilon_0)e^2} = \frac{(6.67 \times 10^{-11}\ \text{N}\cdot\text{m}^2/\text{kg}^2)(1.67 \times 10^{-27}\ \text{kg})^2}{(8.99 \times 10^{9}\ \text{N}\cdot\text{m}^2/\text{C}^2)(1.60 \times 10^{-19})^2}$$

$$\frac{F_{\text{grav}}}{F_{\text{Coul}}} = 8.1 \times 10^{-37} \approx 10^{-36}$$

Solution of the nuclear-wave equation presents all of the mathematical complexities of our earlier studies of atomic and molecular systems plus some truly monumental new ones. Like the atomic and molecular systems, the nucleus (except for ^{1}H and ^{2}H) is a many-body system with all of the accompanying computational difficulties. In addition, the nuclear interaction is far more complex than the electromagnetic interaction and, even worse, it is not yet known how the nuclear interaction can be expressed in closed, analytic form; that is, we do not know the nuclear force law equivalent of Coulomb's law for the electrostatic force. This means that we cannot yet write down the exact form of the nuclear potential function that must be included in the wave equation in order to solve for the nuclear-wave functions and allowed energies.

Substantial progress has been made in recent years toward obtaining the analytic expression for the interaction. For instance, an estimate of the depth of the nuclear potential can be made by assuming its shape to be approximated by a square well and computing the ground-state energy of a nucleon, based on a reasonable assumption of the well width. Using 2 fm as a typical width for light nuclei (see Figure 11-5), the potential $-V$ for a nucleon is approximately

$$-V \approx E_1 \approx \frac{h^2}{8ma^2} = \frac{(6.63 \times 10^{-34}\ \text{J}\cdot\text{s})^2}{(8)(1.67 \times 10^{-27}\ \text{kg})(2 \times 10^{-15}\ \text{m})^2(1.60 \times 10^{-13}\ \text{J/MeV})}$$

$$V \approx -50\ \text{MeV}$$

Two protons separated by that same distance experience an electrostatic Coulomb repulsive potential given by

$$V_{\text{Coulomb}} = \frac{1}{4\pi\epsilon_0}\frac{e^2}{a} = \frac{(9 \times 10^9\ \text{N}\cdot\text{m}^2/\text{C}^2)(1.60 \times 10^{-19}\ \text{C})^2}{(2 \times 10^{-15}\ \text{m})(1.60 \times 10^{-13}\ \text{J/MeV})}$$

$$V_{\text{Coulomb}} = 0.72\ \text{MeV}$$

Thus, our square well approximation suggests that at 2 fm, the attractive nuclear potential exceeds the Coulomb repulsion experienced by a proton by nearly two orders of magnitude.[15]

More detailed understanding of the nature of the nuclear force and the shape and depth of the potential is provided by two types of experiments. First, just as atomic spectroscopy yielded information that made possible the determination of such things as the energies, spins, and magnetic moments of the electronic structure of the atoms, nuclear spectroscopy—i.e., the study of the emission and absorption of particles and radiation by the nuclei—yields valuable information concerning the ground and excited states of nuclei, including energies, magnetic moments, electric quadrupole moments, and spins. The second source of our detailed information comes from the analysis of scattering experiments. These are experiments in which particles that feel the nuclear force, such as protons or alpha particles, are used as projectiles "fired" at target nuclei. The de Broglie wavelength of projectile protons with kinetic energies of 20 MeV (or more) are of the order of nuclear dimensions:

$$\lambda = \frac{h}{p} = \frac{h}{\sqrt{2mE}} = \frac{6.63 \times 10^{-34}\ \text{J}\cdot\text{s}}{\sqrt{2 \times 1.67 \times 10^{-27}\ \text{kg} \times 20\ \text{MeV} \times 1.60 \times 10^{-13}\ \text{J/MeV}}}$$

$$\lambda = 6 \times 10^{-15}\ \text{m} = 6\ \text{fm}$$

Thus, such protons will experience considerable diffraction in collisions with the target nuclei. Analysis of the resulting diffraction pattern yields detailed information concerning the interaction between the particles. Many such experiments, particularly protons scattered from protons, called *p-p* scattering, and neutrons scattered from protons, or *n-p* scattering, reveal that the nuclear potential for proton-proton pairs and neutron-proton pairs are of the form sketched in Figure 11-27. Although the

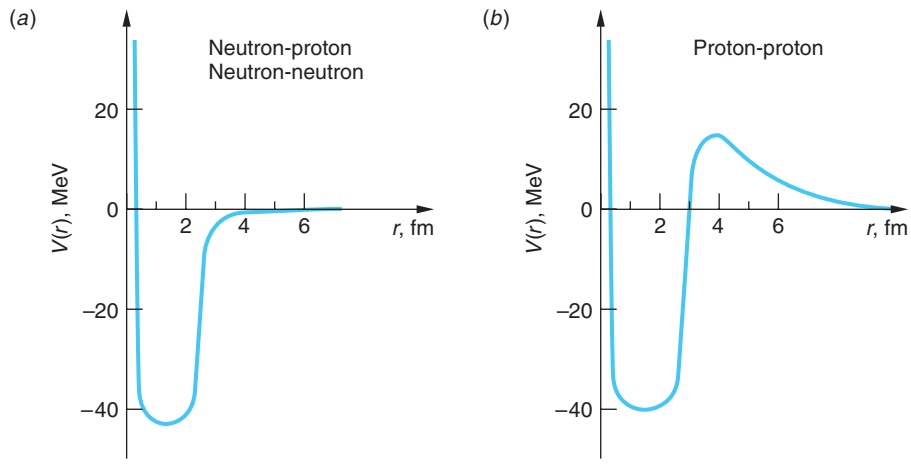

Figure 11-27 (*a*) The approximate shape of the potential between *n-p* and *n-n* pairs. The hard core suggested by the nearly constant central density of the nucleus has a radius of about 0.5 fm. (*b*) The *p-p* potential differs from those in (*a*) by the added Coulomb repulsion, which dominates beyond about 3 fm. Notice the *n-p* and *n-n* potential well is slightly deeper than the *p-p* potential due to the absence of the Coulomb repulsion.

shape of the potential for neutron-neutron pairs can only be determined indirectly since free neutrons are radioactive and we do not know how to make targets consisting only of neutrons (such as the matter of neutron stars), it appears to be identical to that of *n-p* pairs. In fact, when the Coulomb repulsion component of the *p-p* pair potential in Figure 11-27*b* is subtracted from the total potential $V(r)$, the remaining nuclear *p-p* potential is also the same as those for *n-p* and *n-n* pairs. This leads to the very important conclusion that *the nuclear force is independent of the charge of the nucleons*. This suggests that the proton and neutron can be considered as different charge states of the same particle, the nucleon. We will pursue this suggestion further in Chapter 12.

As described in Section 11-2, the charge radius of the proton is about 1 fm. The neutron is approximately the same size. As Figure 11-27 illustrates, two nucleons experience the attractive nuclear force as long as they are within about 2.5 fm of each other, but the force diminishes rapidly over the next 1/2 fm of separation and is essentially zero beyond 3 fm. Thus, we also conclude that *the nuclear force is a short-range force*. Nucleon pairs also experience an extremely strong repulsive component of the nuclear force when they approach within about 0.5 fm. This *hard core* is consistent with the observation that the central density is nearly the same for all nuclei (see Figure 11-27). That is, as more and more nucleons are added, the size of the nucleus increases in such a way that the density remains approximately constant, so something must prevent the nucleons from crowding too closely together. The short range of the nuclear force together with the repulsion of the hard core means that, as the size of the nucleus increases beyond the 2.5- to 3-fm range of the force, an individual nucleon will be able to interact with only a limited number of the other particles in the nucleus, namely its nearby neighbors that are within range of its force. This is analogous to the limited number of bonds associated with each atom in the covalent bonding of solids. For example, each carbon atom in diamond bonds with only four of its nearest neighbors, and we could describe the carbon covalent bond as being a saturated bond. Similarly, *the nuclear force is a saturated force*.

The Nuclear Exchange Force

Without knowing the analytic form of the nuclear potential function, we have been able to conclude that the nuclear force is a short-range, saturated, charge-independent, spin-dependent force with a hard core and a small noncentral component and is about two orders of magnitude stronger than the electrostatic force. What could be the origin or mechanism for such a force was first suggested by H. Yukawa[16] in 1935.

Yukawa proposed that the nuclear force resulted from an exchange of particles between the nucleons. He based his theory on an analogy with the quantum-mechanical explanation of the electrostatic interaction, one of two exchange mechanisms that you have previously studied, though perhaps not by that name. Classically, any distribution of charges produces an electric field $\mathscr{E}$ and the force felt by another charge q located in the field is the product $q\mathscr{E}$. Any change in the charge distribution changes $\mathscr{E}$; however, the information that a change has occurred does not appear instantaneously throughout the field but is propagated outward at the speed of light. Time-dependent changes in the charge distribution create time-dependent changes in $\mathscr{E}$, that is, electromagnetic radiation, or waves.[17] We have seen that the particle representation of the electromagnetic radiation is the photon. Quantum mechanically, every charge is continually emitting and absorbing photons, even when it is not moving. They are called *virtual photons*, meaning that they are not directly observable.

A charge can emit a virtual photon of energy hf without changing its energy or recoiling, i.e., without violating conservation of energy and momentum, provided that the photon exists for no longer than $\Delta t = \hbar/\Delta E$, where $\Delta E = hf$, as required by the uncertainty principle. The distance that the virtual photon can travel during the time Δt, called the range R, is given by

$$R = c\,\Delta t = c\hbar/\Delta E \qquad \textbf{11-48}$$

and substituting for ΔE,

$$R = c\hbar/hf = c/2\pi f = \lambda/2\pi \qquad \textbf{11-49}$$

A second charge located up to a distance R from the first can absorb the photon and a similar photon emitted by the second charge may be absorbed by the first, all without violating energy and momentum conservation. It is this exchange of virtual photons that results in the electrostatic Coulomb force between the two stationary charges in quantum mechanics. Note that there is no limit to the wavelength of the photon in Equation 11-49 since the energy of the photon may be arbitrarily small, the photon having no rest mass. Thus, the distance separating the two charges, the range R of the Coulomb force, may also be infinite, as you have already learned.

An exchange mechanism was also used in BCS theory to account for the attractive force between the electrons of the Cooper pairs. (See Section 10-8.) In that case, the exchange particles were the phonons and the range of the force was not infinite but determined by the fact that $\Delta E \approx$ the energy gap.

Yukawa proposed that the nuclear force could also be explained in terms of the exchange of virtual particles by the nucleons. These particles, which he called *mesons*, were pictured as the analogs of the virtual photons in the electromagnetic interaction and established the *meson field* in analogy with the electromagnetic field. The mechanism for the nuclear force was proposed to be an exchange of a meson between a pair of nucleons, as illustrated by Figure 11-28. Yukawa accounted for the observed short range of the nuclear force by assigning mass to the meson. Thus, the energy uncertainty ΔE in Equation 11-48 would be

$$\Delta E \geq mc^2$$

where m is the mass of the meson and mc^2 is its rest energy. The range R of the meson and therefore the nuclear force that it mediates cannot be larger than

$$R = c\,\Delta t = c\hbar/\Delta E = \hbar/mc \qquad \textbf{11-50}$$

since the speed of the meson must be less than the speed of light. Recall that h/mc is the Compton wavelength λ_c of the particle whose mass is m, so $R = \lambda_c/2\pi$. The range of the nuclear force was known to be about 1 fm, which allowed an approximation of the meson's expected mass from Equation 11-50:

$$m \approx 3.5 \times 10^{-28}\ \text{kg} \approx 380\, m_e \approx 200\ \text{MeV}/c^2$$

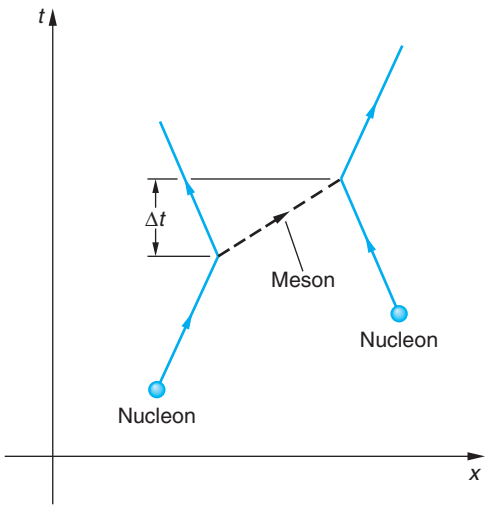

Figure 11-28 Schematic representation of the exchange of a meson by a pair of nucleons. The meson is emitted by the nucleon on the left, which recoils as a result and is absorbed after a time Δt by the nucleon on the right, which also recoils. The effect on the nucleons is as if they had interacted with each other. This kind of spacetime diagram of the interaction of fundamental particles is called a Feynman diagram (see Section 12-1). The x and t axes are normally omitted.

The observed charge independence of the nuclear force was incorporated by Yukawa into the theory by allowing the mesons to carry $+e$, 0, or $-e$ charge. Thus, the exchange of a neutral meson would leave both of the nucleons with their original charge, while the exchange of a charged meson would interchange their charges (see Figure 11-28). Note that $m = 0$ for photons in Equation 11-50 implies the infinite range of the electromagnetic force.

If the nucleon that emits the meson happens to interact with another particle (or nucleus) that has sufficient kinetic energy in the emitting nucleon's rest system to supply the meson's rest energy and also provide the recoil momentum to the emitting nucleon, thus conserving both energy and momentum, the virtual meson can become real and be observable in the laboratory. Such a situation is shown schematically in Figure 11-29. Note the analogy to the emission of photons (bremsstrahlung) by accelerated electrons in an x-ray tube (see Section 3-4). It was interactions such as shown in Figure 11-29 in which Yukawa's mesons, now called π *mesons* or *pions*, were first seen in cosmic rays in 1947, more than a decade after they were proposed.[18] The mass measured for the pions is 140 MeV/c^2, in quite good agreement with Yukawa's predicted approximate value of about 200 MeV/c^2, and all three charge versions were subsequently discovered, providing beautiful confirmation of Yukawa's theory. Since then additional mesons have been discovered and our understanding of the nuclear force has been modified to include the effect of their being exchanged by nucleons as well, but the pions remain as the dominant carrier of the force between nucleons and the cornerstone of our understanding of it. As we will discuss further in Chapter 12, the Standard Model of particle physics describes the nucleons and the mesons as composites of other, more fundamental particles, called *quarks*. The interaction between quarks to form these particles is mediated by a field particle, the *gluon*, carrying the strong force between quark pairs in analogy with our discussion above.

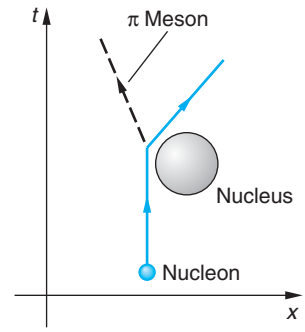

Figure 11-29 A Feynman-like diagram of a nucleon emitting a virtual pion in the vicinity of a nucleus. If the nucleus can provide at least the pion's rest energy and participate in the conservation of momentum, the pion may become real, i.e., visible in the laboratory.

EXAMPLE 11-15 **Range of the Nuclear Force** Using the experimentally measured mass of the pion, 140 MeV/c^2, estimate the range of the nuclear force.

SOLUTION

The range R cannot be larger than $\hbar c/mc^2$ according to Equation 11-50. We then have that

$$R = \frac{\hbar c}{mc^2} = \frac{(1.06 \times 10^{-34}\ \text{J} \cdot \text{s})(3.00 \times 10^{8}\ \text{m/s})}{(140\ \text{MeV}/c^2)(c^2)(1.60 \times 10^{-13}\ \text{J/MeV})}$$

$$R = 1.4 \times 10^{-15}\ \text{m} = 1.4\ \text{fm}$$

Questions

10. What property of the nuclear force is indicated by the fact that all nuclei have about the same density?
11. How does the nuclear force differ from the electromagnetic force?
12. Mesons that have been discovered in recent years are all more massive than the pion. What does that mean regarding the range of the force that they mediate?

FEUE WHE

EXPLORING
Probability Density of the Exchange Mesons

A nucleon continually emits and absorbs virtual mesons. The time Δt during which a virtual meson exists can be estimated from Equation 11-50:

$$\Delta t = \frac{\hbar}{mc^2} = \frac{(1.055 \times 10^{-34}\ \text{J} \cdot \text{s})}{(140\ \text{MeV}/c^2)(c^2)(1.60 \times 10^{-13}\ \text{J/MeV})}$$

$$\Delta t = 5 \times 10^{-24}\ \text{s}$$

This is not a very long time! Thus, a 10^{-20}-second time-exposure "snapshot" of a nucleon would show a cloud consisting of more than 10,000 mesons surrounding the nucleon! The probability density of the mesons can be determined using the results that we obtained from relativity and wave mechanics in Chapters 2 and 6, respectively. The relativistic expression connecting the total energy E and momentum p, the magnitude of the energy/momentum four-vector, is

$$(mc^2)^2 = E^2 - (pc)^2 \qquad \textbf{2-32}$$

With the appropriate operator substitutions from Table 6-1,

$$E \longrightarrow i\hbar\frac{\partial}{\partial t} \qquad p^2 \longrightarrow -\hbar^2\nabla^2 \qquad \textbf{11-51}$$

Equation 2-32 can be written as

$$\nabla^2\Phi(\mathbf{r}, t) - \frac{1}{c^2}\frac{\partial^2\Phi(\mathbf{r}, t)}{\partial t^2} = \left(\frac{mc}{\hbar}\right)^2\Phi(\mathbf{r},t) \qquad \textbf{11-52}$$

where $\Phi(\mathbf{r},t)$ is the wave function of the meson. Equation 11-52 is a relativistic wave equation. It was first obtained by Oskar Klein and Walter Gordon in 1926, the same year that Schrödinger developed his nonrelativistic wave equation.

That the extent of the meson field is related to the range of the nuclear force given by Equation 11-50 can be illustrated by computing the probability density of the meson $|\Phi|^2$ for a static, or time-independent, distribution. This is roughly analogous to the virtual photon distribution, or the electric field intensity, for a stationary charge. In this case, the time derivative of Φ vanishes and Equation 11-52 can be written as

$$\nabla^2\Phi(\mathbf{r}) = \left(\frac{mc}{\hbar}\right)^2\Phi(\mathbf{r}) = \frac{1}{R}\Phi(\mathbf{r}) \qquad \textbf{11-53}$$

whose solution is

$$\Phi(\mathbf{r}) = \frac{Ae^{-r/R}}{\mathbf{r}} \qquad \textbf{11-54}$$

where A is a factor determined by the normalization condition. The probability density is then

$$|\Phi(\mathbf{r})|^2 = \frac{|A|^2 e^{-2r/R}}{\mathbf{r}^2} \qquad \textbf{11-55}$$

and we see that the probability density of the mesons falls off exponentially at a rate determined by R. In other words, R determines the range of the exchange mesons as we had interpreted it in Equation 11-50. Figure 11-30 illustrates the probability distribution function $P(r) = |\Phi|^2 r^2$ for the virtual mesons. For values of r greater than about $0.5R$,

FEUE WHE

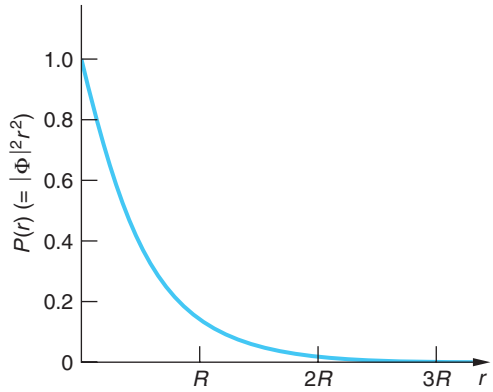

Figure 11-30 Probability $P(r)$, equal to $|\Phi|^2 r^2$, for the virtual mesons emitted by a nucleon, and the range $R = \hbar/mc$, the Compton wavelength of the mesons divided by 2π. There are essentially no mesons beyond about $3R$.

the curve agrees well with experimental results; however, for small values of r the measured meson density is much lower than Figure 11-30 would suggest. Indeed, if the predicted values at very small r values actually existed, they would lead to some quite unusual nuclear properties that are, in fact, not observed. Nuclear theorists conclude that the number of pions at very small r is somehow suppressed, likely as a result of the quark-gluon interaction mentioned above. This is an area of active current research.

11-6 The Shell Model

Existence of 126 as a magic number has prompted searches for unusually stable (but still radioactive) isotopes with Z in the vicinity of 126. Finding them will strengthen our understanding of nuclear structure. Thus far, the highest Z discovered is 118.

Although the general features of the binding energy of nuclei are well accounted for by the semiempirical mass formula that was based on modeling the nucleus as a liquid drop, the binding energy and other properties do not vary with perfect smoothness from nucleus to nucleus. It is not surprising that the smooth curve predicted by Equation 11-12 does not fit the data for very small A, for which the addition of a single proton or a neutron makes a drastic difference. However, even for medium and large A there are some substantial fluctuations of nuclear properties in neighboring nuclei. Consider the binding energy of the last neutron in a nucleus. (Note that this is not the same as the average binding energy per nucleon.) We can calculate this from the semiempirical mass formula by computing the difference in mass $M[(A-1), Z] + m_n - M(A, Z)$. Figure 11-31 shows a plot of the difference between the experimentally measured binding energy and that calculated from Equation 11-12 as a function of the neutron number N. There are large fluctuations near $N = 20$, 28, 50, 82, and 126. These are also the neutron numbers of the nuclei that have an unusually large number of isotones. Nuclei with these proton numbers (except that no element with $Z = 126$ has been observed) have an unusually large number of isotopes.

These numbers are the "magic numbers" that were referred to in Section 11-2. In the regions between these magic numbers, the binding energy of the last neutron is predicted quite accurately by the semiempirical mass

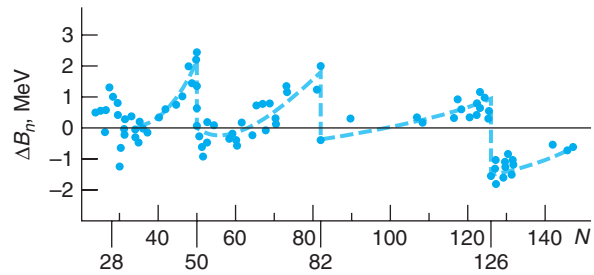

Figure 11-31 Difference in the measured binding energy of the last neutron and that calculated from mass formula versus neutron number. Note the similarity of this curve and the ionization energy of atoms versus Z (Figure 7-20). The neutron numbers 28, 50, 82, and 126 correspond to closed shells. These data show that the neutron with N = magic number $+1$ is much less tightly bound than that with N = magic number.

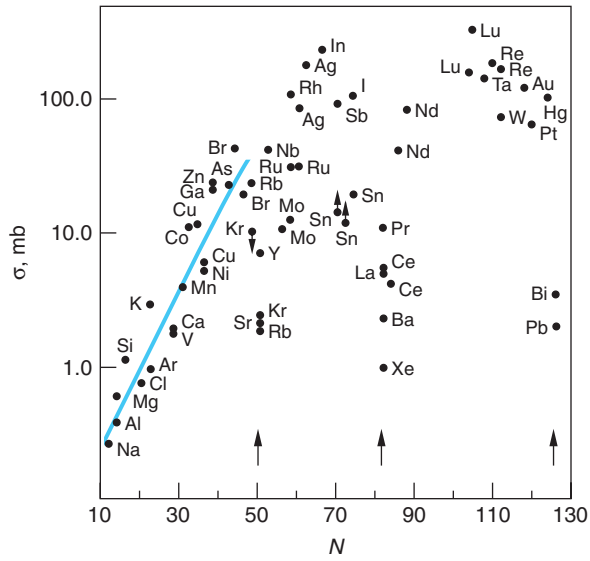

Figure 11-32 The capture cross section measures the probability that a neutron approaching a nucleus will be captured, or bound to the nucleus. The solid line traces the average value. Notice the sharp drop in capture probability of nearly two orders of magnitude at $N = 50$, 82, and 126.

formula. Figure 11-31 should be compared with Figure 7-20, which shows the binding energy of the last electron in an atom as a function of the atomic number Z. The similarity of these two figures suggests a shell structure of the nucleus analogous to the shell structure of atoms. There is considerable additional evidence for these magic numbers, such as the electric quadrupole moments (see Figure 11-7), the neutron capture cross sections illustrated in Figure 11-32, and the binding energies of the last neutron for isotopes of a given Z as shown in Figure 11-33. Additional evidence of nuclear shell structure is discussed in Mayer and Jensen (1955).

Although the unusual stability of the nuclei with N or Z equal to one of the magic numbers was noticed in the 1930s, there was no successful explanation in terms of shell structure until 1949. In the discussion of atoms in Chapter 7, we started with a fixed positive charge $+Ze$ and computed the energies of individual electrons, assuming first that each electron was independent of the others as long as the exclusion principle was not violated. The interaction of the outer electrons with the inner core could be taken care of by assuming an effective nuclear charge that is less than Z because of the screening of the nuclear charge by the inner electrons. This works quite well since the electrons are fairly far from each other in an atom. We could therefore use the individual electron quantum states of the hydrogen atom described by n, l, m_l, and m_s as a first approximation for the electrons in complex atoms. The atomic magic numbers come about naturally due to the large energy difference between one shell or subshell and the next. The actual calculations of atomic-wave functions and atomic energies require powerful approximation or numerical techniques, but they can be done reliably because the forces involved are well known.

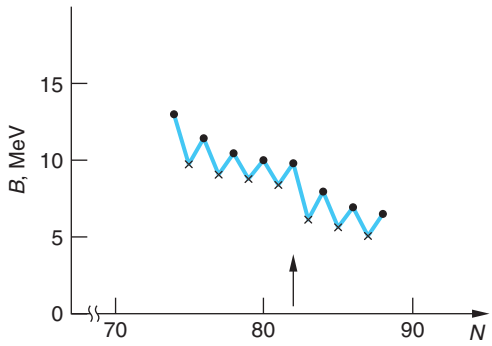

Figure 11-33 Binding energy B for the last neutron of the isotopes of Ce ($Z = 58$). These data are typical of nuclei with $Z > 20$. B decreases sharply (about 2 MeV) for $N = 82 + 1$. This graph also shows the pairing energy associated with a_s in the Weizsächer formula (see Section 11-2), where the last neutron is more tightly bound if N is even than if N is odd.

The situation is not the same for the nuclear-shell model. In the first place, there is no central potential analogous to the fixed positive charge of the atom. The interaction of the nucleons with one another is the only interaction present. In addition to being noncentral, the situation is further complicated by the fact that we know little about the strong force between nucleons beyond what we have

FEUE WHE

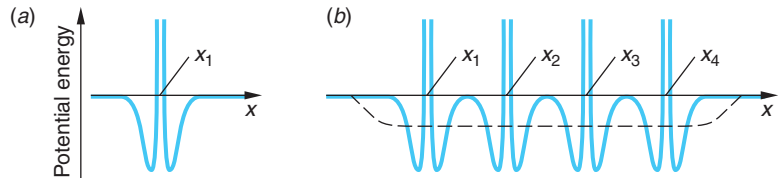

Figure 11-34 (*a*) A single nucleon moving in one dimension sees the potential due to a second nucleon located at x_1. (*b*) The potential seen by the single nucleon due to four other nucleons located along the x axis fluctuates rapidly; however, the average of the four potentials can be reasonably well approximated by the dashed curve, a finite well with sloping sides.

discussed: that it is saturated, has a short range, is charge independent, and is spin dependent. At first sight, it is difficult to imagine a neutron or proton moving almost freely in a well-defined orbit when there are $A - 1$ particles nearby exerting very strong forces on it. Despite these difficulties, the observed properties, such as are illustrated in Figures 11-7, 11-31, 11-32, and 11-33, give strong motivation to try a model in which each nucleon moves about more or less freely in an average potential field produced by the other nucleons. Figure 11-34 shows how such an average potential could be produced. The assumption that the nucleon can move in an orbit without making many collisions can be rationalized by using the exclusion principle. Consider N neutrons in some potential well. In the ground state, the N lowest energy levels will be filled. A collision between two neutrons that does not result in their merely exchanging states is forbidden by the exclusion principle if there are no accessible unfilled states. A collision involving the exchange of identical particles has no effect. Thus, only those nucleons in the highest filled levels, where there are empty states available nearby, can collide with one another. This is analogous to the result that most of the free electrons in a metal cannot absorb energy in random collisions with the lattice because all the nearby energy levels are full. Like the electrons, the nucleons also have a Fermi level.

The first shell-model calculations attempted to use a square well about 40 MeV deep to fit the nuclear energy levels, but they failed to produce the correct magic numbers. In 1949, M. Mayer and J. H. D. Jensen [19] independently showed that, with a modification in these calculations, the magic numbers do follow directly from a relatively simple shell model. Mayer and Jensen resolved the problem by proposing that the spin dependence of the nuclear force results in a very strong spin-orbit interaction, coupling the spin of each nucleon to its own orbital angular momentum. Thus, the nuclear spin-orbit effect depends on *j-j* coupling[20] rather than *L-S* coupling that characterizes the electron spin-orbit interaction (see Section 7-5). This strong spin-orbit interaction results in a decrease in the energy if the spin and the orbital angular momentum of the nucleon are parallel and an increase if they are antiparallel. Figure 11-35 illustrates the nuclear-shell model of Mayer and Jensen that yields the correct magic numbers. Depending on the details of the spin-orbit interaction in the superheavy elements, the island of stability may begin to

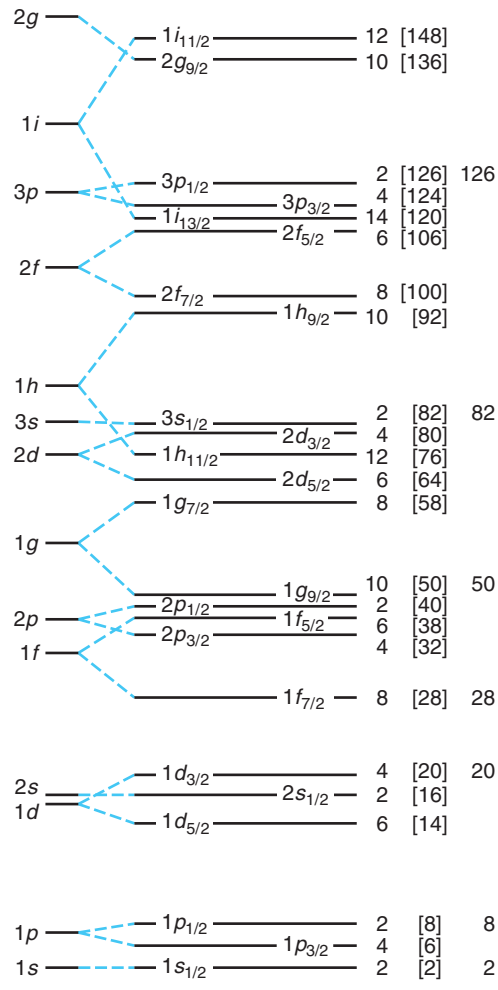

Figure 11-35 Energy levels for a single particle in a nuclear well, including spin-orbit splitting. The maximum number of particles in each level is given at the right, followed by the total number through that level in brackets. The total numbers just before the large energy gaps are the magic numbers. The spacing shown here is for protons; the spacing for neutrons is slightly different (lower).

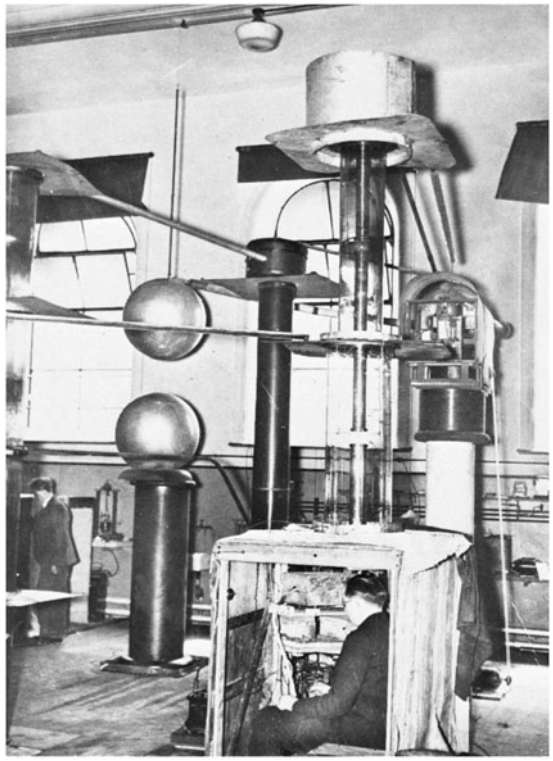

(*a*)

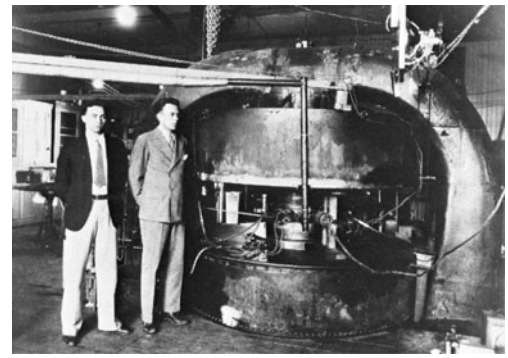

(*b*)

(*a*) The Cockcroft-Walton accelerator. Walton is sitting in the shielded enclosure in the foreground. J. D. Cockcroft and E. T. S. Walton produced the first transmutation of nuclei with artificially accelerated particles in 1932, for which they received the Nobel Prize (1951). (*b*) M. S. Livingston and E. O. Lawrence standing in front of their 27-in. cyclotron in 1934. Lawrence won the Nobel Prize (1939) for the invention of the cyclotron. [*(a) Courtesy of Cavendish Laboratory. (b) Courtesy of Lawrence Radiation Laboratory, University of California, Berkeley.*]

be evident at $Z = 114$ or 120 with metastable states whose lifetimes may be as long as hours or days. In the MORE section on the Web site we consider some of the more detailed qualitative aspects of the nuclear-shell model. Detailed calculations of energies and wave functions require many approximations, the understanding of which is a major area of continuing study in nuclear physics.

More

Finding the "Correct" Shell Model describes some of the qualitative aspects of the several approaches to developing the nuclear-shell model and its successes (and some failures) in predicting nuclear spins and magnetic moments. It is on the home page: www.whfreeman.com/tiplermodernphysics5e. See also Equations 11-56 and 11-57 and Figures 11-36 through 11-38.

11-7 Nuclear Reactions

When a particle is incident on a nucleus, any of several different things can happen. The particle may be scattered elastically or inelastically (in which case the nucleus is left in an excited state and decays by emitting photons or other particles) or the original particle may be absorbed and another particle or particles emitted.

Figure 11-39 illustrates schematically the several possible stages of a nuclear reaction. *Elastic scattering* refers to the reflection of the incident particle's wave at the edge of the nuclear potential well. This is the kind of scattering for α particles that

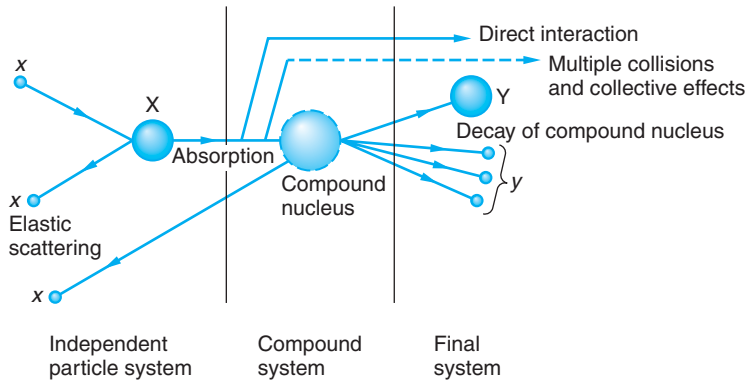

Figure 11-39 Schematic representation of the several possible stages of the nuclear reaction X (x, y) Y, according to the theory developed by V. Weisskopf and H. Feshbach.

was described by Rutherford's theory in Section 4-2. If the incident particle interacts with a single nucleon in the nucleus so that the nucleon leaves the nucleus, the reaction is called a *direct interaction*. Direct interactions are more probable at high energies since the incident particle can penetrate deeper into the nucleus. If the nucleon does not leave the nucleus but interacts with several other nucleons, complicated excited states can be formed in the nucleus. In such a case, when the energy carried by the incident particle is shared by many nucleons, the excited nucleus is called a *compound nucleus*. The compound nucleus can decay by emitting a particle identical to the incident particle and with the same kinetic energy (also elastic scattering) or by emission of one or more other particles (including photons). The decay of the compound nucleus can be treated as a statistical process independent of the detailed manner of formation, just as in the case of a radioactive nucleus.

In this section we will examine some of the systematics of nuclear reactions and some typical reactions produced by incident neutrons, protons, or deuterons. We will limit the discussion to energies of less than 140 MeV. At higher energies, mesons and other particles can be created. The study of higher-energy reactions is generally undertaken to reveal the properties of fundamental particles and of the nuclear force rather than the structure of the nucleus and will be discussed further in Chapter 12.

Energy Conservation

Consider a general reaction of particle x incident on nucleus X resulting in nucleus Y and particle y. The reaction may be written

$$x + \mathrm{X} \longrightarrow \mathrm{Y} + y + Q$$

or, as we will usually write it, X(x, y)Y. The quantity Q, defined by

$$Q = (m_x + m_{\mathrm{X}} - m_y - m_{\mathrm{Y}})c^2 \qquad \textbf{11-58}$$

is the energy released in the reaction and is called the Q *value* of the reaction.

When energy is released by a nuclear reaction, the reaction is said to be *exothermic*. In an exothermic reaction, the total mass of the initial particles is greater than that of the final particles and the Q value is positive. If the total mass of the initial particles is

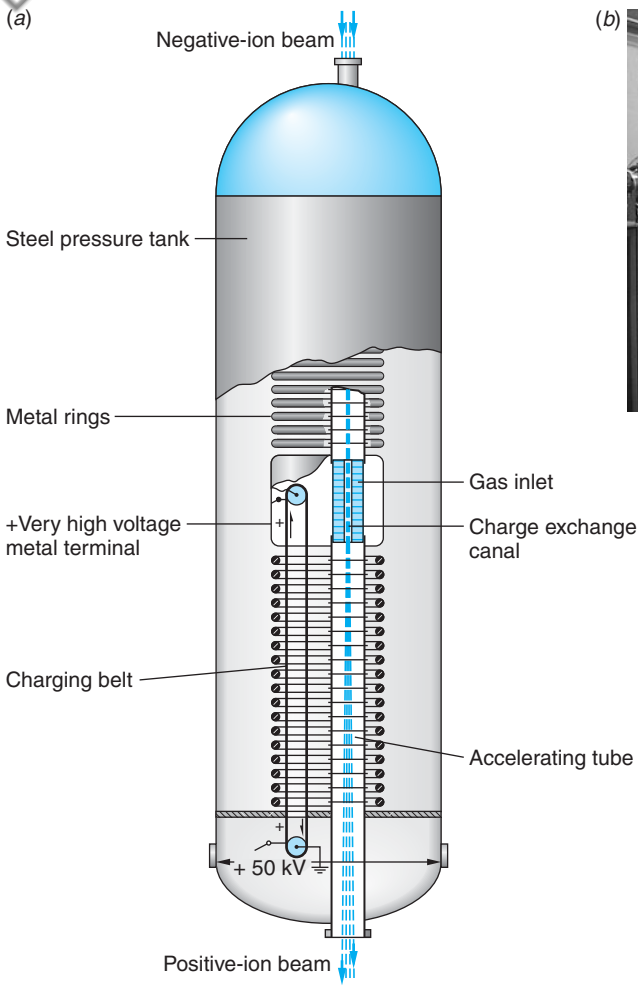

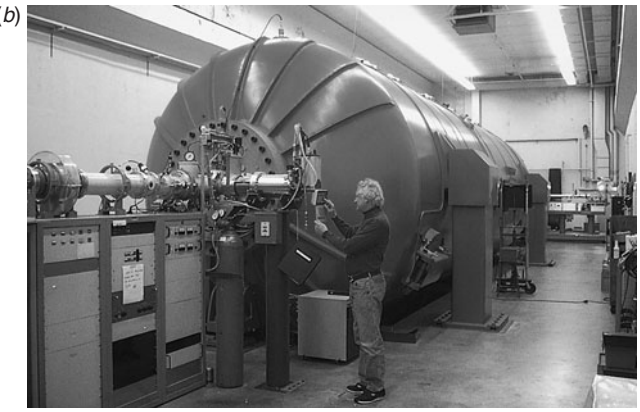

(*a*) Schematic diagram of a two-stage, or tandem, Van de Graaff accelerator. Negative ions at ground potential (atoms of a large fraction of the elements in the periodic table form stable negative ions) enter the beam tube at the top and are accelerated to the positive high-voltage terminal in the center, acquiring eV of kinetic energy. In the charge exchange canal, electrons are stripped from the negative ions in collisions with gas molecules, producing positive ions with charges up to $+Ze$. The positive ions are accelerated back to ground potential, acquiring an additional kinetic energy as large as ZeV. Large Van de Graaff accelerators have terminal voltages V over 16 million volts. Thus, for example, oxygen atoms stripped of all their electrons may be accelerated to energies of 100 MeV or more. (*b*) A portion of the tandem Van de Graaff laboratory at Purdue University. The high-voltage terminal is in the tank at the right rear, insulated from the surroundings by inert gas under high pressure. The beam travels in the tube and is deflected to experimental areas by the bending magnets. The Purdue accelerator is used extensively in accelerator mass spectrometry. [*Courtesy of David Elmore, Purdue University.*]

less than that of the final particles, the Q value is negative and energy is required for the reaction to take place. The reaction is then *endothermic*.

Examples are

$$n + {}^1\mathrm{H} \longrightarrow {}^2\mathrm{H} + \gamma + 2.22\ \mathrm{MeV} \quad \text{(exothermic)}$$

$$\gamma + {}^2\mathrm{H} \longrightarrow {}^1\mathrm{H} + n - 2.22\ \mathrm{MeV} \quad \text{(endothermic)}$$

Thus, an endothermic reaction cannot take place unless a certain threshold energy is supplied to the system. In the reference frame in which the total momentum is zero (the center-of-mass frame), the threshold energy is just $|Q|$. However, many reactions occur with nucleus X at rest relative to the laboratory. In this frame, called the *laboratory frame*, the incident particle x must have energy greater than $|Q|$ because, by conservation of momentum, the kinetic energy of y and Y cannot be zero. Consider the nonrelativistic case of x, of mass m, incident on X, of mass M (Figure 11-40).

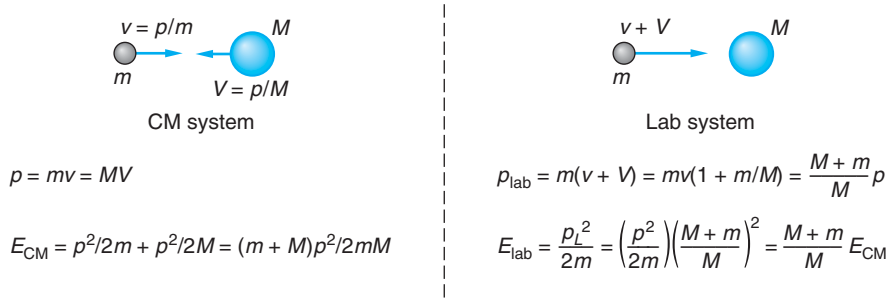

Figure 11-40 Energetics of nuclear reaction in center-of-mass system and laboratory system. The energies are related by $E_{lab} = [(M + m)/M]E_{CM}$.

In the center-of-mass frame, both particles have momenta of equal magnitude and the total kinetic energy is

$$E_{CM} = \frac{p^2}{2m} + \frac{p^2}{2M} = \frac{1}{2}p^2\left(\frac{m + M}{mM}\right) \qquad \textbf{11-59}$$

where $p = mv = MV$. We transform to the lab frame by adding V to each velocity so that M is at rest and m has velocity $v + V$. The momentum of m in the lab frame is then

$$p_{lab} = m(v + V) = mv\left(1 + \frac{m}{M}\right) = p\left(\frac{m + M}{M}\right)$$

and its energy is

$$E_{lab} = \frac{p_{lab}^2}{2m} = \frac{p^2}{2m}\left(\frac{m + M}{M}\right)^2 = \frac{m + M}{M}E_{CM} \qquad \textbf{11-60}$$

The threshold for an endothermic reaction in the lab frame is thus

$$E_{th} = \frac{m + M}{M}|Q| \qquad \textbf{11-61}$$

(If the incident particle is a photon, the Lorentz transformation must be used. For low energies, the momentum of a photon is small and approximate methods can be used. For a photon, $pc = E$, whereas for a proton or neutron, $pc = (2mc^2E)^{1/2} \gg E$ for $E \ll 140$ MeV.)

EXAMPLE 11-16 Q Value of a Nuclear Reaction Find the Q value of the reaction

$$p + {}^7\text{Li} \longrightarrow {}^4\text{He} + {}^4\text{He}$$

and state whether the reaction is exothermic or endothermic. The atomic mass of ^{7}Li is 7.016003 u.

FEUE WHE

SOLUTION

Using 1.007825 u for the mass of ^{1}H and 4.002602 u for the mass of ^{4}He from Appendix A, we have for the total mass of the initial particles

$$m_i = 1.007825 \text{ u} + 7.016003 \text{ u} = 8.023828 \text{ u}$$

and for the total mass of the final particles

$$m_f = 2(4.002602 \text{ u}) = 8.005204 \text{ u}$$

Since the initial mass is greater than the final mass by

$$\Delta m = m_i - m_f = 8.023828 \text{ u} - 8.005204 \text{ u} = 0.018624 \text{ u}$$

mass is converted into energy and the reaction is exothermic. The Q value is positive and given by

$$Q = (\Delta m)c^2 = (0.018624 \text{ u})c^2(931.5 \text{ MeV/u} \cdot c^2) = 17.35 \text{ MeV}$$

Note that we used the mass of atomic hydrogen rather than that of the proton and the atomic masses of the ^{7}Li and ^{4}He atoms rather than the masses of the individual nuclei so that the masses of the four electrons on each side of the reaction cancel.

EXAMPLE 11-17 Threshold Energy in Lab Frame Compute the minimum kinetic energy of protons incident on ^{13}C nuclei at rest in the laboratory that will produce the endothermic reaction $^{13}\text{C}(p, n)^{13}\text{N}$.

SOLUTION

1. The minimum, or threshold, energy of the incident protons in the lab frame is given by Equation 11-61:

$$E_{\text{th}} = \frac{m + M}{M}|Q|$$

2. The magnitude of the Q value of the reaction is

$$\frac{|Q|}{c^2} = m_{\text{final}} - m_{\text{initial}}$$
$$= [M(^{13}\text{N}) + m_n] - [M(^{13}\text{C}) + M(^1\text{H})]$$

3. The masses of the particles involved are tabulated in Appendix A:

$$M(^{13}\text{C}) = 13.003355 \text{ u} \quad M(^1\text{H}) = 1.007825 \text{ u}$$
$$M(^{13}\text{N}) = 13.005738 \text{ u} \quad m_n = 1.008665 \text{ u}$$

4. Substituting these into the expression for $|Q|$ gives

$$|Q| = (14.014403 - 14.011180) \text{ u} \cdot c^2$$
$$= 0.003223 \text{ u} \cdot c^2 \times 931.5 \text{ MeV/u} \cdot c^2$$
$$= 3.00 \text{ MeV}$$

5. Substituting this value, $m = M(^1\text{H})$, and $M = M(^{13}\text{C})$ into Equation 11-61 gives

$$E_{\text{th}} = \frac{1.007825 + 13.003355}{13.003355} \times 3.00$$
$$= 3.23 \text{ MeV}$$

Cross Section

The probability that a particle incident on a nucleus will scatter or induce a reaction depends on the particle's energy and what particular particle and nucleus are involved. It is as if different kinds of particles approaching a given nucleus "see" targets of different sizes. Similarly, identical particles with different energies "see" the same target nucleus larger or smaller than actual size. This effect is a consequence of the detailed arrangement of the allowed energy states of the target nucleus. A useful measure of the effective size of a nucleus for a particular scattering or nuclear reaction is the *cross section* σ. If I is the number of particles incident per unit time per unit area (the incident intensity) and R is the number of reactions per unit time per nucleus, the cross section is defined as

$$\sigma = \frac{R}{I} \qquad \textbf{11-62}$$

Consider, for example, the bombardment of ^{13}C by protons. A number of reactions might occur. Elastic scattering is written $^{13}C(p, p)^{13}C$; the first p indicates an incident proton, the second indicates that the particle that leaves is also a proton. If the scattering is inelastic, the outgoing proton is indicated by p' and the nucleus in the resulting excited state by $^{13}C^*$ and one writes $^{13}C(p, p')^{13}C^*$. Some other possible reactions are

(p, n)	$^{13}C(p, n)^{13}N$
capture	$^{13}C(p, \gamma)^{14}N$
(p, α)	$^{13}C(p, \alpha)^{10}B$

Each possible scattering or reaction has its own cross section, called the *partial cross section*. The partial cross section is also defined by Equation 11-62 with R equal to the number of events of the specific kind per unit time per nucleus. The total cross section is the sum of the partial cross sections:

$$\sigma = \sigma_{p,p} + \sigma_{p,p'} + \sigma_{p,n} + \sigma_{p,\gamma} + \sigma_{p,\alpha} + \ldots$$

Cross sections have the dimensions of area. Since nuclear cross sections are of the order of the square of the nuclear radius, that is, $(10^{-14}\ \text{m})^2$, a convenient unit for them is the *barn*, defined by

$$1\ \text{barn} = 10^{-24}\ \text{cm}^2 = 10^{-28}\ \text{m}^2 \qquad \textbf{11-63}$$

The cross section for a particular reaction is a function of energy. For an endothermic reaction, it is zero for energies below the threshold.

Compound Nucleus

In 1936, Niels Bohr pointed out that many low-energy reactions could be described as two-stage processes—the formation of a compound nucleus and its subsequent decay. In this description, the incident particle is absorbed by the target nucleus and the energy is shared by all the nucleons of the compound nucleus. After a time that is long compared with the time necessary for the incident particle to cross the nucleus, enough of the excitation energy of the compound nucleus becomes concentrated in one particle for it to escape. The emission of a particle is a statistical process that depends only on the state of the compound nucleus and not on how it was produced.

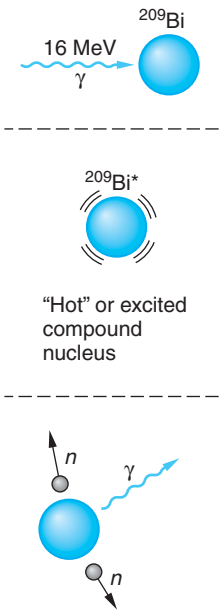

Figure 11-41 Nuclear reaction via formation of compound nucleus. The 16-MeV photon is absorbed by the ^{209}Bi nucleus, producing an excited nucleus that lives so long that excitation energy is shared by many nucleons. The excited nucleus then decays by emitting neutrons and photons, each with energy of the order of a few MeV.

An incident 1-MeV proton has a speed of about 10^7 m/s, so that it takes time $R/v \approx 10^{-14}/10^7 = 10^{-21}$ s to cross a nucleus. The lifetime of a compound nucleus can be inferred to be about 10^{-16} s. This is too short to be measured directly, but it is so long compared with 10^{-21} s that it is reasonable to assume that the decay is independent of how it was formed.

The compound nucleus for the reactions on ^{13}C shown above is ^{14}N*. This nucleus can be formed by many other reactions, such as

$$\begin{aligned} {}^{10}\text{B} + \alpha &\longrightarrow {}^{14}\text{N}^* \longrightarrow {}^{12}\text{C} + d \\ {}^{13}\text{N} + n &\longrightarrow {}^{14}\text{N}^* \longrightarrow {}^{10}\text{B} + \alpha \\ {}^{14}\text{N} + \gamma &\longrightarrow {}^{14}\text{N}^* \longrightarrow {}^{14}\text{N} + \gamma \\ {}^{12}\text{C} + d &\longrightarrow {}^{14}\text{N}^* \longrightarrow {}^{13}\text{N} + n \end{aligned} \qquad \textbf{11-64}$$

The reactions on the left are called the *entrance channels* and the decays on the right are called the *exit channels*.

Since the decay of ^{14}N* is independent of the formation, we can write the cross section for a particular reaction such as $^{13}\text{C}(p, n)^{13}\text{N}$ as the product of the cross section for the formation of the compound nucleus, σ_c, and the relative probability of decay by neutron emission, P_n:

$$\sigma_{p,n} = \sigma_c P_n \qquad \textbf{11-65}$$

An illustration of the statistical decay of the compound nucleus is afforded by the energy distribution of neutrons from reactions such as (Figure 11-41)

$$\gamma + {}^{209}\text{Bi} \longrightarrow {}^{208}\text{Bi} + n$$

where σ shows a broad peak at 14 to 20 MeV and neutrons "evaporate" as ^{209}Bi decays to the ground state.

Excited States of Nuclei from Nuclear Reactions

The excited states of a nucleus can be determined in two ways from nuclear reactions. A peak in the cross section $\sigma(E)$ as a function of energy indicates an excited state of the compound nucleus, corresponding to the relatively large probability of the incident particle giving up all its energy in the single event of exciting an allowed energy level. (Think of the Franck-Hertz experiment as an analogy.) Information about the lifetimes τ of the excited states of the compound nucleus is obtained by measuring the energy width Γ of these peaks, or *resonances*, and using the uncertainty principle $\tau\Gamma \approx \hbar$. Figure 11-42 shows the cross section for formation of ^{14}N by the reaction $^{10}\text{B} + \alpha \rightarrow {}^{14}\text{N}^*$ as a function of the α-particle energy. The peaks in this curve indicate energy levels in the ^{14}N nucleus. The Q value for this reaction is $M(^{10}\text{B})c^2 + M(\alpha)c^2 - M(^{14}\text{N})c^2 = 11.61$ MeV. The Q value is the binding energy of the incident particle in the compound nucleus, which is always of the order of 6 to 10 MeV; thus levels with energy less than 6 MeV cannot be reached in the compound nucleus.

The kinetic energy in the center-of-mass frame is related to the lab energy of the α particle by

$$E_{\text{CM}} = \frac{M}{M+m}E_{\text{lab}} = \frac{10}{14}E_{\text{lab}}$$

FÈUE WHE

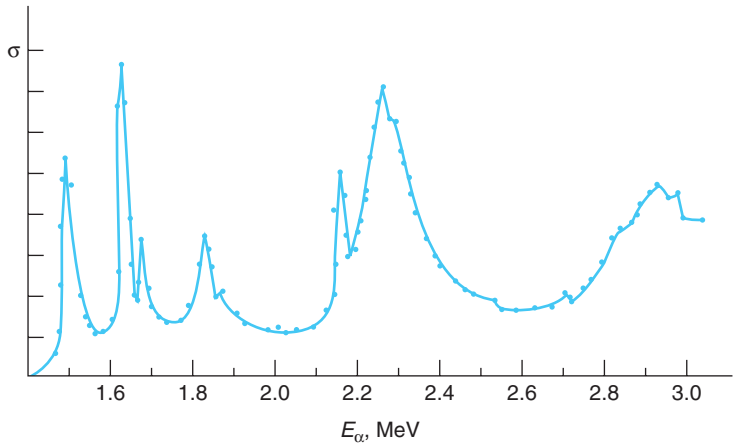

Figure 11-42 Cross section for the reaction $^{10}B + \alpha \rightarrow {}^{14}N^*$ versus energy. The resonances indicate energy levels in the compound nucleus $^{14}N^*$.

The peak in Figure 11-42 at $E_{lab} = 1.63$ MeV corresponds to an excited state in ^{14}N of energy $E = 11.61 + (10/14)(1.63) = 12.77$ MeV. The same level can be excited by the reaction $^{12}C + {}^2H \rightarrow {}^{14}N^*$. For this case, the Q value is 10.26 MeV. Thus, the deuteron energy in the lab must be

$$E_d = \left(\frac{14}{12}\right)(12.77 - 10.26) = 2.93 \text{ MeV}$$

A second way to determine the energy levels in a nucleus is to observe the energies of particles scattered inelastically. In this case, the energy levels of the target nucleus are determined. Figure 11-43 shows the energy spectrum of protons from the reaction $p + {}^{14}N \rightarrow {}^{14}N^* + p'$ using 6.92-MeV protons. (The horizontal scale in this figure is proportional to the momentum of the protons since this is what is measured experimentally.) The two peaks in the curve correspond to energy losses of 2.31 and 3.75 MeV, which indicated energy levels in ^{14}N of 2.31 and 3.75 MeV. The excited product nucleus decays from these states by γ emission. The method of inelastic scattering can determine energy levels of the target nucleus lying relatively close to the ground state, whereas the levels excited in the compound nucleus must be much higher because of the Q values for formation of the compound nucleus.

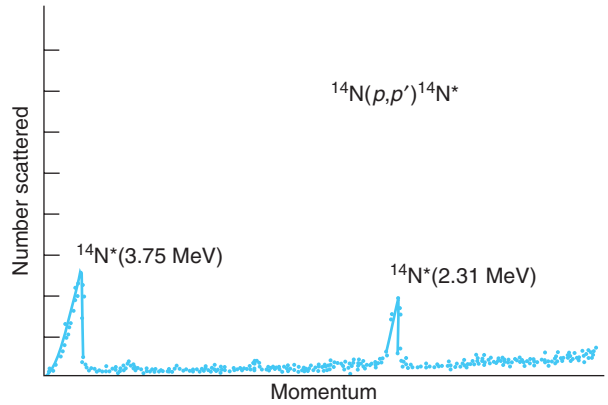

Figure 11-43 Spectrum of protons scattered from ^{14}N, indicating energy levels in ^{14}N.

Reactions with Neutrons

Neutrons are used to dope silicon with phosphorus more uniformly than the conventional diffusion method. Irradiating Si with neutrons produces the P dopant via the reaction and subsequent decay $n + {}^{30}\text{Si} \rightarrow {}^{31}\text{Si} \rightarrow {}^{31}\text{P} + \beta^- + \bar{\nu}$. Silicon doped with P this way can operate at higher power levels in rectifier applications than diffusion-doped silicon.

Nuclear reactions involving neutrons are important for understanding the elemental analytical technique of neutron activation analysis and the operation of nuclear reactors. The most likely reaction with a nucleus for a neutron of more than about 1 MeV is scattering. However, even if the scattering is elastic, the neutron loses some energy to the nucleus because conservation of momentum requires that the nucleus recoil. If a neutron is scattered many times in a material, its energy decreases until it is of the order of the energy of thermal motion kT, where k is the Boltzmann constant and T is the absolute temperature. (At ordinary room temperatures, kT is about 0.025 eV.) The neutron is then equally likely to gain or lose energy from a nucleus when it is elastically scattered. A neutron with energy of the order of kT is called a *thermal neutron*.

At low energies, a neutron is more likely to be captured, with the emission of a γ ray from the excited nucleus:

$$n + {}^{A}_{Z}\text{M} \longrightarrow {}^{A+1}_{Z}\text{M} + \gamma$$

For example,

$$n + {}^{107}_{47}\text{Ag} \longrightarrow {}^{108}_{47}\text{Ag} + \gamma$$

Since the binding energy of a neutron is of the order of 6 to 10 MeV and the kinetic energy of the neutron is negligible by comparison, the excitation energy of the compound nucleus is from 6 to 10 MeV, and γ rays of this energy are emitted. Figure 11-44 shows the neutron capture cross section for silver as a function of the energy of the neutron. Except for the resonances, the cross section $\sigma(n, \gamma)$ varies smoothly with energy, decreasing with increasing energy approximately as $1/v$, where v is the speed of the neutron. This energy dependence can be understood as follows. Consider a neutron moving with speed v near a nucleus of diameter $2R$. The time it takes the neutron to pass the nucleus is $2R/v$. Thus, the neutron capture cross section is proportional to the time spent by the neutron in the vicinity of the nucleus. The dashed line in Figure 11-44 indicates this $1/v$ dependence.[21] At the maximum of the large resonance, the value of the cross section is very large ($\sigma > 5000$ barns) compared with a value of only about 10 barns just past the resonance. Many elements show similar resonances in the neutron capture cross sections. For example, the maximum cross section for ^{113}Cd is about 57,000 barns. Thus, ^{113}Cd is a strong absorber, which makes it very useful as a shield against low-energy neutrons.[22]

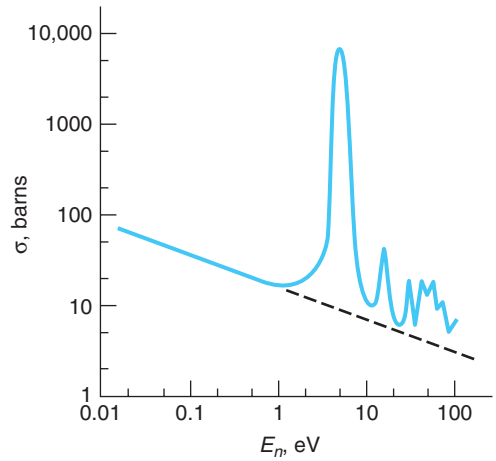

Figure 11-44 Neutron capture cross section for Ag versus energy. The dashed-line extension would be expected if there were no resonances and the cross section were merely proportional to the time spent near the nucleus, i.e., proportional to $1/v$. The resonance widths of a few eV indicate states with lifetimes of the order of $h/\Gamma \approx 10^{-16}$ s.

FEUE WHE

Questions

13. What is meant by the cross section for a nuclear reaction? Why is that term used to describe it?
14. Why is the neutron capture cross section (excluding resonances) proportional to $1/v$?
15. What is meant by the Q value of a reaction? Why is the reaction threshold not equal to Q?
16. Why can't low-lying energy levels (1 to 2 MeV above the ground state) be studied using neutron capture?

EXAMPLE 11-18 Determination of Reaction Rates The cross section for the reaction $^{91}Zr(n,\gamma)^{92}Zr$ is 900 millibarns for thermal neutrons. This reaction is produced in the so-called thermal column of a reactor where the *flux* of thermal neutrons is 6.5×10^{12} neutrons/cm$^2 \cdot s$. The sample of natural Zr is a circular foil 1.0 cm in diameter and 20.0 μm thick. The density of Zr is 6.506 g/cm^3, and ^{91}Zr makes up 11.27 percent of natural Zr. Compute the rate of this reaction.

SOLUTION

First we need to compute the number of ^{91}Zr atoms in the sample. This number is given by

$$N(^{91}\text{Zr}) = \frac{N_A V \rho_{\text{Zr}}}{M_{\text{Zr}}} \times 0.1127$$

where the volume of the sample $V = 2.00 \times 10^{-3} \times (\pi/4)\text{cm}^3$ and the molecular weight of Zr, $M_{\text{Zr}} = 91.22$ g/mol. Thus,

$$N(^{91}\text{Zr}) = \frac{(6.02 \times 10^{23} \text{ atoms/mol})\left(2.00 \times 10^{-3} \times \frac{\pi}{4} \text{ cm}^3\right) \times 6.506 \text{ g/cm}^3}{91.22 \text{ gm/mol}}$$

$$N(^{91}\text{Zr}) = 1.04 \times 10^{19} \text{ atoms}$$

From the definition of the cross section given by Equation 11-62, the number of (n, γ) reactions per unit time per ^{91}Zr nucleus is

$$R = \sigma I = (900 \times 10^{-3} \text{ barns} \times 10^{-24} \text{ cm}^2/\text{barn}) \times 6.5 \times 10^{12} \text{ neutrons/cm}^2 \cdot \text{s}$$

$$R = 5.85 \times 10^{-12} \text{ s}^{-1} \text{ per } ^{91}\text{Zr nucleus}$$

The rate $\mathcal{R}$ at which the reaction $^{91}Zr(n, \gamma)^{92}Zr$ proceeds is then

$$\mathcal{R} = N(^{91}\text{Zr})R = (1.04 \times 10^{19} \, ^{91}\text{Zr nuclei})(5.85 \times 10^{-12} \text{ s}^{-1} \text{ per } ^{91}\text{Zr nucleus})$$

$$\mathcal{R} = 6.08 \times 10^{7} \text{ s}^{-1}$$

Remarks: *This is a low reaction rate, given the high neutron flux. It is the result of the low neutron capture cross section of ^{91}Zr and the other naturally occurring Zr isotopes. This is the principal reason why zirconium is used to enclose nuclear reactor fuel elements.*

11-8 Fission and Fusion

Two nuclear reactions, fission and fusion, are of particular importance. In the fission of ^{235}U, for example, the uranium nucleus is excited by the capture of a neutron and splits into two nuclei, each with very roughly half of the original total mass. A typical fission reaction is

$$^{235}U + n \longrightarrow {}^{92}Kr + {}^{142}Ba + 2n + 179.4\ \text{MeV} \qquad \textbf{11-66}$$

The Coulomb force of repulsion drives the fission fragments apart, giving them very large kinetic energies. As a result of collisions with other atoms, this energy eventually shows up as thermal energy. In fusion, two light nuclei such as those of deuterium and tritium (^2H and ^3H) fuse together to form a heavier nucleus (in this case ^4He plus a neutron). A typical reaction is

$$^2H + {}^3H \longrightarrow {}^4He + n + 17.6\ \text{MeV} \qquad \textbf{11-67}$$

Figure 11-45 shows a plot of the mass difference per nucleon $(M - Zm_p - Nm_n)/A$ versus A in units of MeV/c^2. This curve is just the negative of the binding energy curve of Figure 11-10. From Figure 11-45 we see that the rest energy per particle for both very heavy nuclides ($A \approx 200$) and very light nuclides ($A \leq 20$) is more than that for nuclides of intermediate mass. Thus, in both fission and fusion the total mass decreases and energy is released. Since for $A = 200$ the rest energy is about 1 MeV per nucleon greater than for $A = 100$, about 200 MeV is released in the fission of a heavy nucleus. The energy release in fusion depends on the particular reaction. For the $^2H + {}^3H$ reaction in Equation 11-67, 17.6 MeV is released. Although this is less than the energy released in a single fission, it is a greater amount of energy per unit mass, as Example 11-19 illustrates. In this section, we will look at some of the features of fission and fusion that are important for their application in reactors to generate electricity.

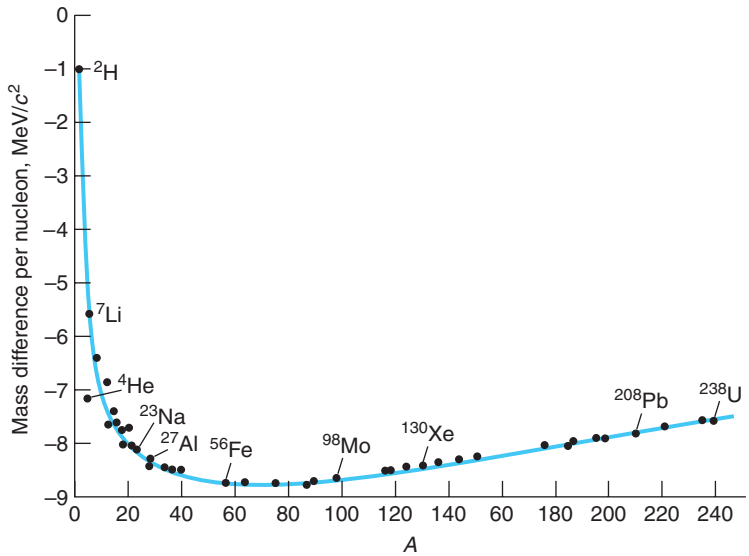

Figure 11-45 Plot of mass difference per nucleon $(M - Zm_p - Nm_n)/A$ in units of MeV/c^2 versus A. The rest energy per nucleon is smaller for intermediate-mass nuclei than for either very light or very heavy nuclei.

EXAMPLE 11-19 **Energy Release in Fission and Fusion** Compare the energy release per unit mass in the fusion of deuterium and tritium (Equation 11-67) with that of a typical fission reaction, such as that of ^{235}U given by Equation 11-66.

SOLUTION

(*a*) A quick approximate comparison can be made by noting that the energy difference per nucleon between ^{235}U and its fission products is about 1.0 MeV. In the fusion of $^{2}H + {}^{3}H$, it is 17.6 MeV/5 nucleons = 3.5, or about 3.5 times larger. Thus, the energy released per kilogram will also be about 3.5 times larger in the fusion reaction.

(*b*) The mass differences per nucleon for ^{235}U and the two fission products in Equation 11-66 can be estimated from Figure 11-45. A more accurate calculation of the total binding energy can be made with the aid of Equation 11-12 and used to compute the total mass differences as follows:

$$^{235}U: \quad -7.6\ \text{MeV}/c^2 \text{ per nucleon} \longrightarrow -1797.1\ \text{MeV}/c^2 \text{ per nucleus}$$

$$^{92}Kr: \quad -8.7\ \text{MeV}/c^2 \text{ per nucleon} \longrightarrow -800.9\ \text{MeV}/c^2 \text{ per nucleus}$$

$$^{142}Ba: \quad -8.4\ \text{MeV}/c^2 \text{ per nucleon} \longrightarrow -1189.5\ \text{MeV}/c^2 \text{ per nucleus}$$

The difference between the mass of ^{235}U and the sum of masses for the fission products is 193.3 MeV/c^2. Thus, the energy release per fission event (with these particular products) is 193.3 MeV. The mass of ^{235}U (see Appendix A) is 235.043924 u = 3.9030×10^{-25} kg. Therefore, the energy release per kilogram in the fission of ^{235}U is

$$\frac{\left(\dfrac{193.3\ \text{MeV}}{^{235}\text{U}}\right)}{\left(\dfrac{3.903 \times 10^{-25}\ \text{kg}}{^{235}\text{U}}\right)} = 4.95 \times 10^{26}\ \text{MeV/kg}$$

The energy release in the deuterium/tritium fusion reaction is

$$\frac{17.6\ \text{MeV}}{M_d + M_t} = \frac{17.6\ \text{MeV}}{8.353 \times 10^{-27}\ \text{kg}} = 2.11 \times 10^{27}\ \text{MeV/kg}$$

Thus, the fusion reaction releases about 4.3 times the energy/kg released by the fission reaction.

Fission

The fission of uranium was discovered in 1938 by O. Hahn and F. Strassmann,[23] who found, by careful chemical analysis, that medium-mass elements (in particular, barium) were produced in the bombardment of uranium with neutrons. The discovery that several neutrons are emitted in the fission process led to speculation concerning the possibility of using these neutrons to cause further fissions, thereby producing a chain reaction. When ^{235}U captures a thermal neutron, the resulting ^{236}U nucleus undergoes fission about 85 percent of the time and emits gamma rays as it de-excites to the ground state about 15 percent of the time. The fission process is somewhat analogous to the oscillation of a liquid drop, as shown in Figure 11-46. If the oscillations are violent enough, the drop splits in two. Using the liquid-drop model, A. Bohr and J. Wheeler calculated the critical energy E_c needed by the ^{236}U nucleus to undergo fission. (^{236}U is the compound nucleus formed by the capture of a neutron by ^{235}U.)

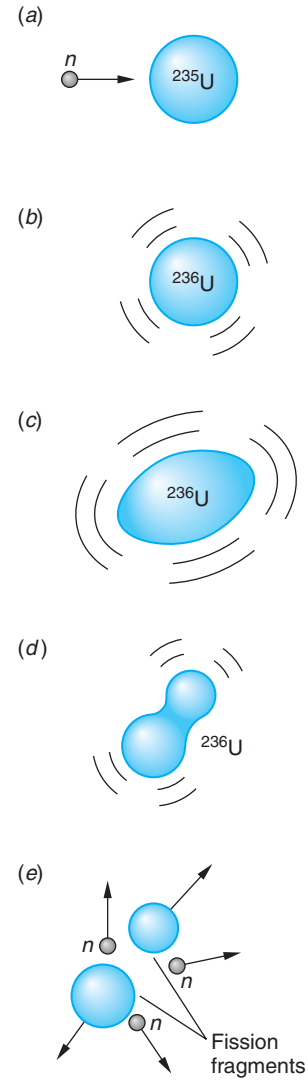

Figure 11-46 Schematic illustration of nuclear fission. (*a*) The absorption of a neutron by ^{235}U leads to (*b*) ^{236}U in an excited state. (*c*) Oscillation deforms the excited ^{236}U nucleus. (*d*) The oscillation of ^{236}U has become unstable. (*e*) The nucleus splits apart into two nuclei of medium mass and emits several neutrons that can produce fission in other nuclei.

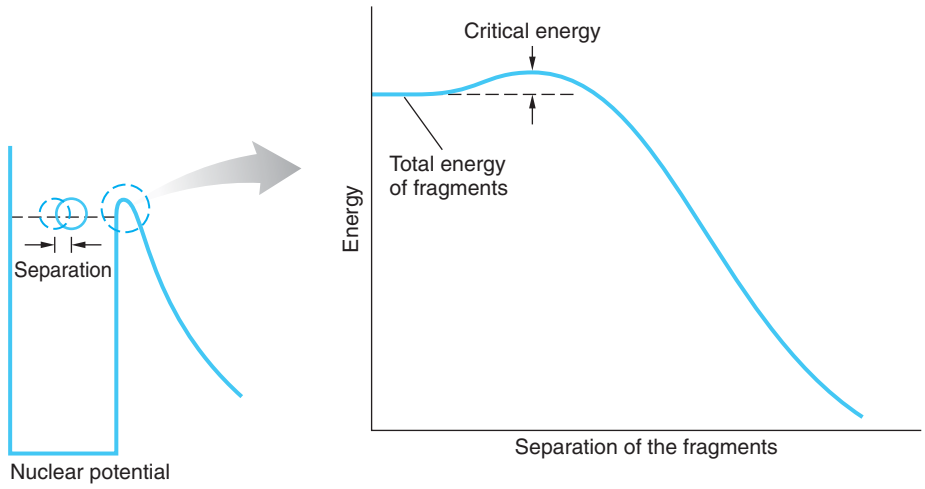

Figure 11-47 The nucleus may exist instantaneously as two fragments as shown on the left; however, the Coulomb potential barrier prevents their fission. To overcome the barrier, energy equal to the critical energy must be provided.

The critical energy is the magnitude of the Coulomb barrier seen by the fragments, as illustrated in Figure 11-47. For this nucleus, the critical energy is about 6.2 MeV, which is less than the 6.5 MeV of excitation energy produced when ^{235}U captures a neutron. The capture of a neutron by ^{235}U therefore produces an excited state of the ^{236}U nucleus that has more than enough energy to break apart. On the other hand, the critical energy for the fission of the ^{239}U nucleus is 5.9 MeV. The capture of a neutron by a ^{238}U nucleus produces an excitation energy of only 5.2 MeV. Therefore, when a thermal neutron is captured by ^{238}U to form ^{239}U, the excitation energy is not great enough for fission to occur. In this case the excited ^{239}U nucleus de-excites by γ or α emission. Nuclides that may fission upon capturing a slow neutron are called *fissile*.

We noted earlier that all nuclei with $Z > 83$ are radioactive. Among the possible decay modes of the very heavy nuclei ($Z > 90$) is that of spontaneous fission. These nuclei may break apart into two nuclei even if left to themselves without absorbing a neutron. We can also understand spontaneous fission using the analogy of a liquid drop of positive charges. If the drop is not too large, surface tension can overcome the repulsive forces of the charges and hold the drop together. There is, however, a certain maximum size beyond which the drop will be unstable and will spontaneously break apart since the repulsive force is proportional to the number of protons, which is proportional to the volume, hence to R^3, whereas the surface tension is proportional to the surface area and so increases only as R^2. (See Section 11-2.) Spontaneous fission puts an upper limit on the size of a nucleus and therefore on the number of elements that are possible. It should be noted that the probability for spontaneous fission in naturally occurring nuclides is quite low compared with the other possible decay modes. For example, the half-life of ^{238}U for α decay is 4.5×10^9 years, while that for spontaneous fission is about 10^{16} years. The reason is that fission, like α decay, is inhibited by the Coulomb barrier. Even though the process is energetically possible, the large positively charged fission fragments have a very low probability of tunneling through the Coulomb barrier part of the nuclear potential.

A fissioning nucleus can break into two medium-mass fragments in many different ways, as shown in Figure 11-48. Depending on the particular reaction, one, two, or three neutrons may be emitted. The average number of neutrons emitted in the thermal-neutron-induced fission of ^{235}U is about 2.4. Equation 11-66 is a typical fission reaction. The reason that several neutrons are emitted is that the fission fragments are typically neutron rich and far off the line of stability, as shown in Figure 11-49.

FÈUE WHE

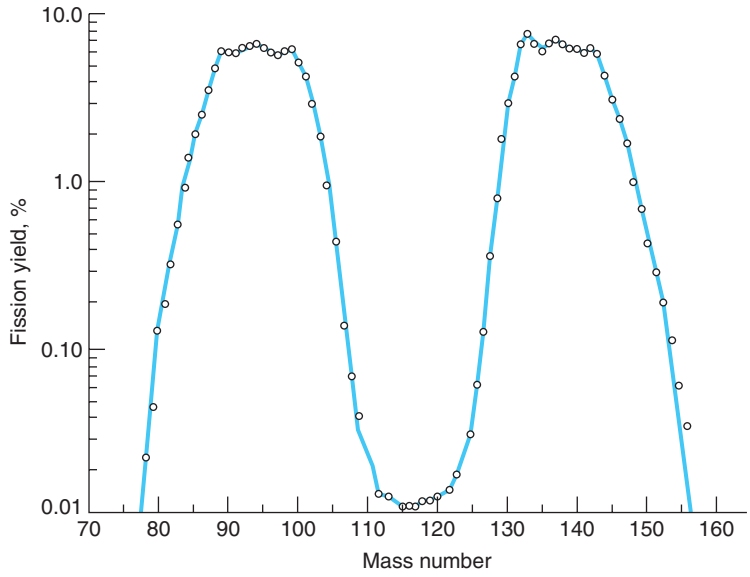

Figure 11-48 Distribution of fission fragments from the thermal-neutron-induced fission of ^{235}U. Symmetric fission, in which the uranium nucleus splits into two nuclei of nearly equal mass, is much less probable than asymmetric fission, in which the fragments have unequal masses. Note the symmetry of the light and heavy lobes of the distribution, including the small variations in the tops of the peaks and the convex outer edges. [*Data from G. J. Dilorio, Direct Physical Measurement of Mass Yields in Thermal Fission of Uranium-235, Garland, New York, 1979.*]

As a result, neutrons are spontaneously emitted during fission and the fragments β^- decay toward stability. The Coulomb force of repulsion drives the fission fragments apart with very large kinetic energies. This energy is transferred to other nearby atoms via collisions, eventually showing up as thermal energy of the surroundings. We have seen that about 200 MeV per nucleus is released in such a fission, a large amount of energy. By contrast, in the chemical combustion reaction, only about 4 eV is released per molecule of oxygen consumed.

The fission fragments and their decay products that build up in reactors are the source of many radioisotopes used in medical diagnosis, treatment, and research. Important among these is ^{99}Mo, the source of ^{99}Tc, the most widely used radioisotope in nuclear medicine.

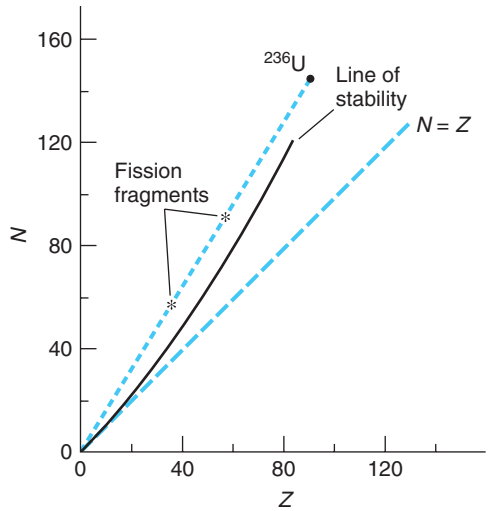

Figure 11-49 Fission of ^{236}U ($^{235}U + n$) produces fragments that are neutron-rich and well to the left of the line of stability. As a result, the fission is accompanied by the prompt emission of one or more of the excess neutrons followed by β^- decay of the fission fragments to further reduce their neutron numbers.

EXAMPLE 11-20 Kilowatt-hours from ^{235}U Calculate the total energy in kilowatt-hours released in the fission of 1 g of ^{235}U, assuming that 200 MeV is released per fission.

SOLUTION

Since 1 mol of ^{235}U has a mass of 235 g and contains $N_A = 6.02 \times 10^{23}$ nuclei, the number of ^{235}U nuclei in 1 g is

$$N = \frac{6.02 \times 10^{23} \text{ nuclei/mol}}{235 \text{ g/mol}} = 2.56 \times 10^{21} \text{ nuclei/g}$$

The energy released per gram is then

$$\frac{200 \text{ MeV}}{\text{nucleus}} \times \frac{2.56 \times 10^{21} \text{ nuclei}}{1 \text{ g}} \times \frac{1.6 \times 10^{-19} \text{ J}}{1 \text{ eV}} \times \frac{1 \text{ h}}{3600 \text{ s}} \times \frac{1 \text{ kW}}{1000 \text{ J/s}} = 2.28 \times 10^4 \text{ kW} \cdot \text{h/g}$$

Remark: *This is approximately equal to the amount of electrical energy used by a typical U.S. household in 15 months.*

The discovery that several neutrons were emitted in the fission process led to speculation concerning the possibility of using these neutrons to initiate other fissions, thereby producing a *chain reaction*. On December 2, 1942, less than four years after Hahn and Strassmann's discovery of fission, a group led by Enrico Fermi produced the first self-sustaining chain reaction in a nuclear reactor that they had constructed at the University of Chicago.[24]

The application of both fission and fusion to the development of nuclear weapons has had a profound effect on our lives for more than 60 years. The peaceful application of these reactions to the development of energy resources may well have an even greater effect in the future, provided that satisfactory solutions are found to problems concerning safety, environmental protection, and the spread of nuclear weapons technology. Indeed, as world demand for energy increases, the diminishing finite reserves of fossil fuels will undoubtedly result in increasing use of nuclear reactors to provide the primary energy for the generation of electricity. The MORE section *Nuclear Power* is a comprehensive primer on fission reactors and closely related issues.

More

Nuclear fission reactors provided 6.0 percent of the energy consumed worldwide in 2005. *Nuclear Power*, on the home page at www.whfreeman.com/tiplermodernphysics5e, is a thorough review of existing and possible future types of fission reactors, the nuclear fuel cycle, reactor control, and safety issues. See also Equations 11-68 through 11-70 here, as well as Tables 11-5 and 11-6, Figures 11-50 through 11-54, and Examples 11-21 through 11-23.

FÈUE WHE

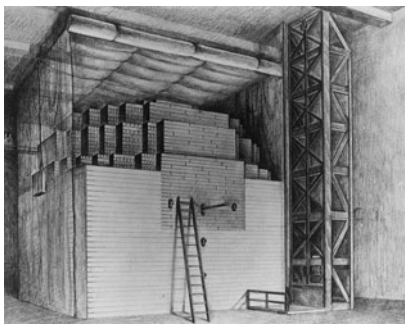

(*a*)

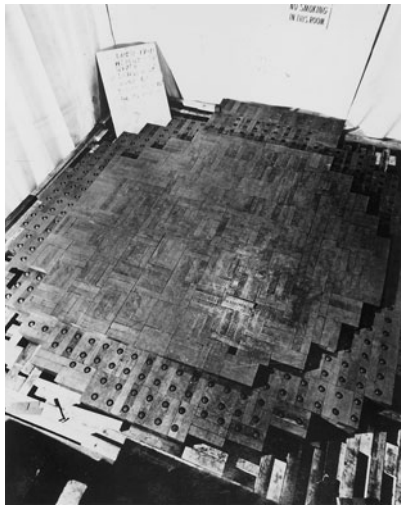

(*b*)

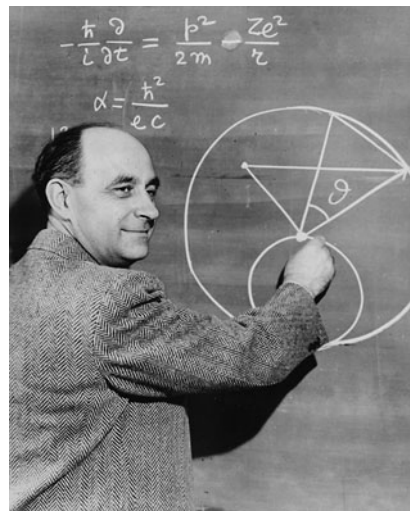

(*c*)

(*a*) A sketch of the world's first nuclear reactor, the CP-1 (for Chicago Pile number 1). Projecting from the near face next to the top of the ladder is one of the cadmium-plated rods used to control the chain reaction by absorbing neutrons. The cubical balloon surrounding the reactor, open on the near side, was to contain neutron-activated radioactive air. News of the reactor's successful test was transmitted by A. H. Compton, one of those present, to President Franklin Delano Roosevelt's adviser (and Harvard University president) J. B. Conant in a phone call thus: "The Italian navigator [i.e., Fermi] has landed in the New World," said Compton. "How were the natives?" asked Conant. "Very friendly," was Compton's reply. (*b*) The only photograph of CP-1 known to exist, taken during addition of the 19th layer of graphite. Alternate layers of graphite, containing uranium metal and/or uranium oxide, were separated by layers of solid-graphite blocks. Layer 18, almost covered, contained uranium oxide. (*c*) Enrico Fermi, leader of the group of scientists who succeeded in initiating the first man-made nuclear chain reaction, on December 2, 1942. [*(a) and (b) American Institute of Physics, Emilio Segrè Visual Archives; courtesy of Argonne National Laboratory, University of Chicago. (c) Courtesy of Argonne National Laboratory.*]

Fusion

The production of power from the fusion of light nuclei has the potential for future use because of the relative abundance of the fuel and the absence of some of the hazards presented by fission reactors. In fusion, two light nuclei such as deuterium (^{2}H) and tritium (^{3}H) fuse together to form a heavier nucleus. A typical fusion reaction is

$$^2\text{H} + {}^3\text{H} \longrightarrow {}^4\text{He} + n + 17.6\ \text{MeV} \qquad \textbf{11-71}$$

As was shown in Example 11-19, the energy released in this fusion reaction is (17.6 MeV)/(5 nucleons) = 3.52 MeV per nucleon, or about 3.5 times as great as the 1 MeV per nucleon released in fission. The technology necessary to make fusion a practical source of energy has not yet been developed. We will consider the fusion reaction of Equation 11-71; other reactions present similar problems.

Because of the Coulomb repulsion between the ^{2}H and ^{3}H nuclei, very large kinetic energies, of the order of 1 MeV, are needed to get the nuclei close enough together for the attractive nuclear forces to become effective and cause fusion. Such energies can be obtained in an accelerator, but since the scattering of one nucleus by the other is much more probable than fusion, the bombardment of one nucleus by the other in an accelerator requires the input of more energy than is recovered. Therefore, to obtain energy from fusion, the particles must be heated to a temperature great enough for the fusion reaction to occur as the result of random thermal collisions. Because a significant number of particles have kinetic energies greater than the mean kinetic energy $(3/2)kT$ and because some particles can tunnel through the Coulomb barrier, a temperature T corresponding to $kT \approx 10$ keV is adequate to ensure that a reasonable number of fusion reactions will occur if the density of particles is sufficiently high. The temperature corresponding to $kT = 10$ keV is of the order of 10^8 K. Such temperatures occur in the interiors of stars, where such reactions are common. At these temperatures, a gas consists of positive ions and negative electrons called a *plasma* (see Chapter 10). One of the problems arising in attempts to produce controlled fusion reactions is that of confining the plasma long enough for the reactions to take place. In the interior of the Sun the plasma is confined by the enormous gravitational field of the Sun. In a laboratory on Earth, confinement is a difficult problem.

The energy required to heat a plasma is proportional to the density of its ions n, whereas the fusion rate is proportional to n^2, the square of the density (since the rate is the product of the Maxwell energy distribution and the fusion cross section, both of which are proportional to n). If τ is the confinement time, the output energy is thus proportional to $n^2\tau$. If the output energy is to exceed the input energy, we must have

$$C_1 n^2 \tau > C_2 n$$

where C_1 and C_2 are constants. In 1957, the British physicist J. D. Lawson evaluated these constants from estimates of the efficiencies of various hypothetical fusion reactors and derived the following relation between density and confinement time, known as *Lawson's criterion*:

$$n\tau > 10^{20}\ \text{s} \cdot \text{particles/m}^3 \qquad \textbf{11-72}$$

If Lawson's criterion is met and the thermal energy of the ions is great enough ($kT \approx 10$ keV), the energy released by a fusion reactor will just equal the energy input; that is, the reactor will just break even. For the reactor to be practical, much more energy must be released.

Two schemes for achieving Lawson's criterion are currently under investigation. In one scheme, *magnetic confinement*, a magnetic field is used to confine the plasma.[25] In the most common arrangement, first developed in Russia and called the *tokamak*, the plasma is confined in a large toroid. The magnetic field is a combination of the doughnut-shaped magnetic field due to the current in the windings of the toroid and the self-field due to the current of the circulating plasma. An international consortium of nations is currently constructing the International Thermonuclear Experimental Reactor (ITER) tokamak in France. Production of the first plasma is scheduled for 2016. The Chinese Experimental Advanced Superconducting Tokamak (EAST) which uses superconducting windings recognized as essential for continuous energy production, began operation late in 2006. The break-even point using magnetic confinement was achieved a few years ago, but we are still a long way from building a practical fusion reactor.

FÈUE WHE

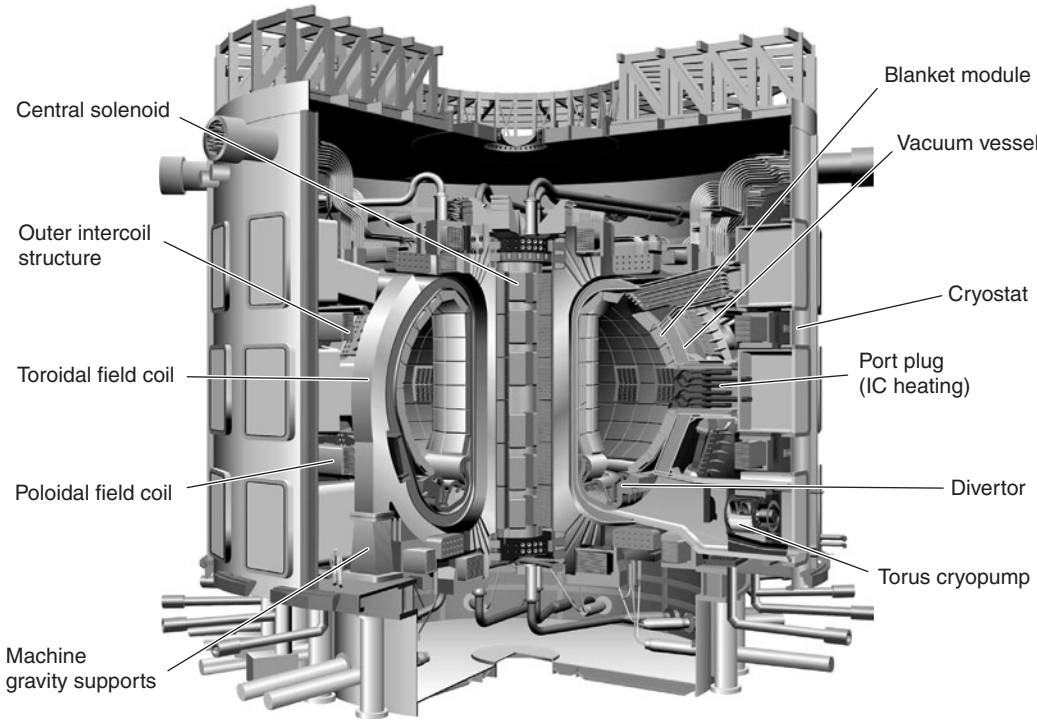

Schematic of the ITER tokamak experimental fusion reactor. The toroidal field coils, encircling the 6.2-m maximum diameter doughnut-shaped tritium-deuterium plasma contained in the vacuum vessel, are designed to conduct current for 300 s up to, eventually, steady state. The design plasma current is 15×10^6 A, producing a magnetic field of 5.3 T. This field is the principal means of confining the deuterium-tritium plasma that circulates within the vacuum vessel. Sets of poloidal field coils, perpendicular to the toroidal coils, carry an oscillating current that generates a current through the confined plasma itself, heating it ohmically. Additional poloidal fields help stabilize the confined plasma. Design total fusion power is 15 MW. ITER's first plasma is expected to be produced in 2016. Follow the development of ITER at *www.iter.org*. [*ITER Organization.*]

In a second scheme, called *inertial confinement*, a pellet of frozen-solid deuterium and tritium is bombarded from all sides by intense pulsed laser beams of energies of the order of 10^6 J lasting about 10^{-8} s. (Intense ion and electron beams are also used.) Computer simulation studies indicate the momentum absorbed by the hydrogen nuclei from the beams should compress the pellet to about 10^4 times its normal density and heat it to a temperature greater than 10^8 K. This should produce about 10^6 J of fusion energy in 10^{-10} s, which is so brief that confinement is achieved by inertia alone. (See Figure 11-55*a* and *b*.) In theory, after this burst of fusion energy is radiated away from the site to be absorbed by a heat-transfer fluid, such as liquid lithium, another pellet is injected at the confluence of the beams and the process repeats.

Because the break-even point has barely been achieved in magnetic confinement fusion and because the building of a fusion reactor involves many practical problems that have not yet been solved, for example, activation of the reactor walls, the availability of fusion to meet world energy needs is not expected for several decades.

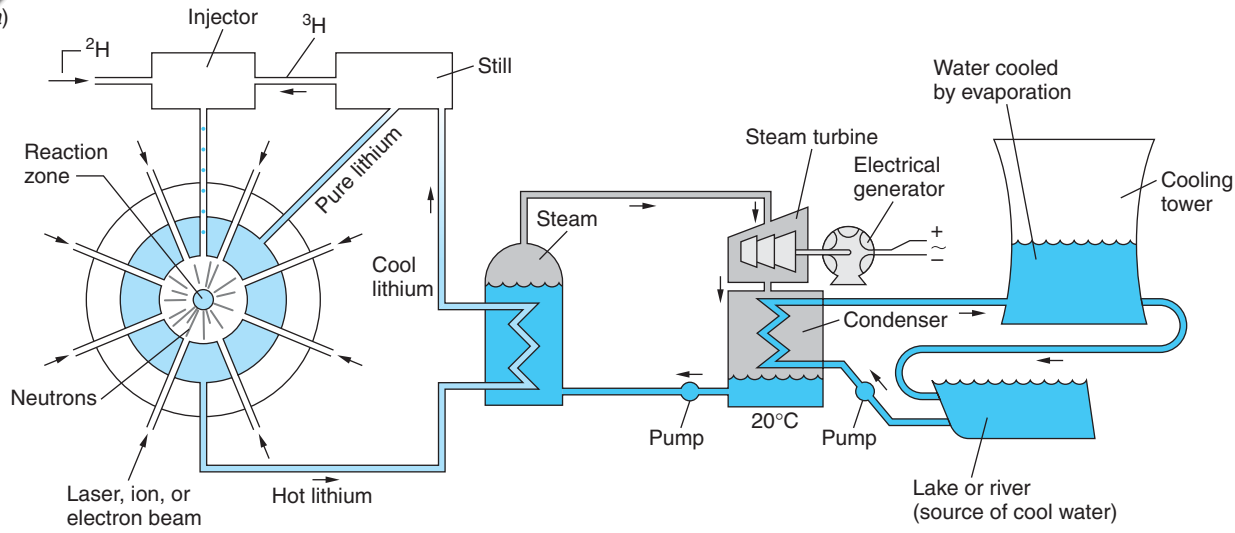

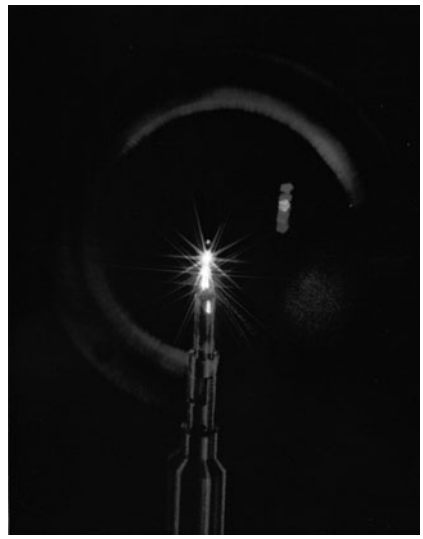

(b)

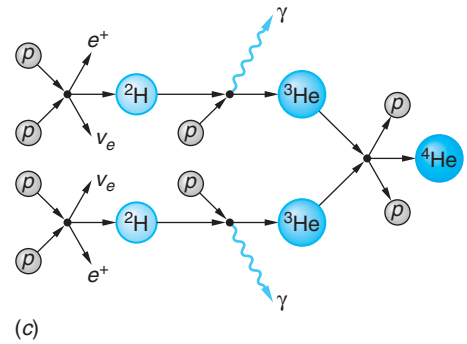

Figure 11-55 (*a*) Schematic diagram of a possible fusion reactor using inertial confinement and the $^2\text{H} + {}^3\text{H} \rightarrow {}^4\text{He} + n$ reaction. This reaction produces 17.6 MeV per fusion, and the neutron produced reacts with either ^{6}Li (slow neutron) or ^{7}Li (fast neutron) to produce the ^{3}H needed for the reaction. The latter reaction produces an additional slow neutron; thus, every two neutrons produced by fusion have the potential for generating three ^{3}H nuclei; that is, this system may also be a tritium breeder. (*b*) The Nova inertial confinement fusion reactor uses 10 powerful laser beams focused on a hydrogen-containing pellet 0.5 mm in diameter. The resulting fusion reaction, visible here as a tiny bright star, lasts 10^{-10} s and releases 10^{13} neutrons. (*c*) The proton-proton reaction is the primary source of the Sun's energy. The neutrino produced in the initial reaction escapes from the core. The net energy produced per cycle is about 26.7 MeV. [*(b) Courtesy of Lawrence Livermore National Laboratory, U.S. Department of Energy.*]

EXAMPLE 11-24 **Fusion Temperature for $^1H + {}^1H \rightarrow {}^2H + e^+ + \nu$** The fusion of two protons requires that two particles be separated by no more than about 10^{-14} m in order for the attractive force of the nuclear potential to overcome the repulsive force of the Coulomb potential. Compute (*a*) the minimum temperature of a hydrogen plasma that will enable a proton with the average energy of those in the plasma to overcome the Coulomb barrier and (*b*) the energy released in the fusion.

SOLUTION

(*a*) The height of the potential energy barrier seen by the protons is given by

$$U = \frac{1}{4\pi\epsilon_0}\frac{e^2}{r} = \frac{(9 \times 10^9\ \text{N}\cdot\text{m}^2/\text{C}^2)(1.60 \times 10^{-19}\ \text{C})^2}{3.0 \times 10^{-15}\ \text{m}}$$

$$U = 7.68 \times 10^{-14}\ \text{J} = 0.48\ \text{MeV}$$

In order to overcome this barrier, the average energy of the protons in the plasma, $(3/2)kT$, must equal at least half this amount; that is, each of the two fusing protons must have 3.84×10^{-14} J.

$$(3/2)kT = 3.84 \times 10^{-14}\ \text{J}$$

where k is Boltzmann's constant. Thus,

$$T = \frac{2 \times 3.84 \times 10^{-14}\ \text{J}}{3 \times 1.38 \times 10^{-23}\ \text{J/K}} = 1.9 \times 10^9\ \text{K}$$

(*b*) The energy released, equal to the Q value of the fusion reaction, is

$$\begin{aligned} Q &= [2m(^1\text{H}) - m(^2\text{H}) - 2m_e]c^2 \\ &= [2 \times 1.007825\ \text{u} - 2.014102\ \text{u} - 0.001097\ \text{u}]c^2 \\ &= 0.000451\ \text{u}\cdot c^2 \times 931.5\ \text{MeV/u}\cdot c^2 = 0.42\ \text{MeV} \end{aligned}$$

where the atomic mass values are given in Appendix A. Thus, the energy release per $^1H + {}^1H$ fusion is 0.42 MeV. That of the $^2H + {}^3H$ fusion illustrated in Figure 11-55*a* is 17.6 MeV, which explains why the latter reaction is used in controlled fusion experiments.

The Source of the Sun's Energy The present energy content of the Sun as calculated from thermodynamics would be radiated away in about 3×10^7 years. Since life has existed on Earth for approximately 100 times that long, we can conclude that the Sun has been radiating at close to its present rate for at least 3×10^9 years. Therefore, the Sun must have a supply of energy far larger than that represented by the hot plasma and the observed radiation field. The source of the Sun's energy is nuclear fusion. Current theory proposes that, as the young Sun contracted, its temperature rose. Eventually the temperature of the core reached about 1.5×10^7 K, which is high enough for the hydrogen nuclei (protons) in the plasma to have sufficient energy on the average (about 1 keV) to fuse into helium nuclei. This reaction, actually a chain of reactions, was first proposed by H. A. Bethe and is referred to as the *proton-proton cycle*. The first reaction in the chain is (see Example 11-24)

$$^1\text{H} + {}^1\text{H} \longrightarrow {}^2\text{H} + e^+ + \nu_e + 0.42\ \text{MeV}$$

The probability for this reaction is very low except for those protons in the high-energy tail of the Maxwell-Boltzmann distribution. This sets a limit on the rate at which the Sun can produce energy and thus ensures a long lifetime for the Sun and similar stars. This limit is sometimes called the "bottleneck" of the solar fusion cycle. Once ^{2}H (deuterium) is formed, the following reaction becomes very probable:

$$^2\text{H} + {}^1\text{H} \longrightarrow {}^3\text{He} + \gamma + 5.49\ \text{MeV}$$

It is followed by:

$$^3\text{He} + {}^3\text{He} \longrightarrow {}^4\text{He} + 2\ {}^1\text{H} + \gamma + 12.86\ \text{MeV}$$

This process by which hydrogen nuclei are "burned" to helium nuclei is shown schematically in Figure 11-55*c*. There are other possible reactions for converting ^{3}He to ^{4}He, all of which have the same net Q value. Their rates, however, differ depending on the composition and temperature of the interior.

The neutrinos produced in the proton-proton cycle escape from the core, providing our only means for direct observation of the Sun's interior. The measured value of the total power radiated by the Sun and the known total Q value of the proton-proton cycle allow a calculation of the total reaction rate. In addition, the alternative reactions for ^{4}He have different neutrino energy spectra, thus providing a way of determining the relative contributions of each reaction and gaining information about the composition and temperature of the core. However, the measured rate at which solar neutrinos arrive at Earth is less than half that predicted by theoretical calculations based on the standard solar model. This discrepancy is referred to as the *solar-neutrino problem*. Solving this problem was the focus of a recent major international research effort. Results from the Sudbury (Canada) and Super-Kamiokande (Japan) neutrino observatories show that neutrinos have a small mass and may transform from one type to another, leading to the observed discrepancy. (See Section 12-5.)

Questions

17. Explain why water is more effective than lead in slowing down fast neutrons.
18. What happens to the neutrons produced in fission that do not produce another fission?
19. Why does fusion occur spontaneously in the Sun but not on Earth?

More

The *Interaction of Particles and Matter* is of central importance in understanding the biological effects of ionizing radiation, in the development and use of nuclear radiation detectors, and in protecting the environment from potential radiation hazards. This topic is discussed for charged particles, neutrons, and photons on the home page: www.whfreeman.com/tiplermodernphysics5e. See also Equations 11-73 through 11-83 here, as well as Figures 11-56 through 11-61 and Example 11-25.

FEUE WHE

11-9 Applications

Certainly among the most important of the applications of nuclear reactions and interactions have been those developed in the field of nuclear medicine, particularly in the area of diagnosis, but also including the treatment of cancer and certain other diseases. State-of-the-art detectors and computer-based data analysis have made critical contributions to these developments. Also important to a broad spectrum of disciplines ranging from art through chemistry and geology to zoology are the precision isotope-specific analytical techniques of *accelerator mass spectrometry* and *neutron activation analysis*. Anthropologists, archeologists, and geologists routinely rely on the decay properties of a number of radioisotopes to determine the age of artifacts and samples. Examples of these applications will be discussed briefly in this concluding section of the chapter.

Potential oil- and gas-bearing regions in exploratory oil wells are identified by lowering an intense source of neutrons (usually a mixture of ^{239}Pu and ^{9}Be or ^{241}Am and ^{9}Be) into the well along with a gamma-ray detector. The neutrons produce gamma rays via $X(n, \gamma)Y$ reactions in the surrounding rock. Analysis of the gamma-ray spectra identifies elements in the rock that are typical indicators of the presence of oil and natural gas.

Neutron Activation Analysis

This isotope-specific analytical method for elements is capable of very high sensitivity and accuracy. While some elements are more readily analyzed by activation analysis than others, it is particularly useful for the many elements that cannot be conveniently assayed by the more standard chemical methods of trace analysis. It has a wide range of applications from identifying trace pollutants in the environment through semiconductor processing and materials science to the analysis and authentication of works of art.

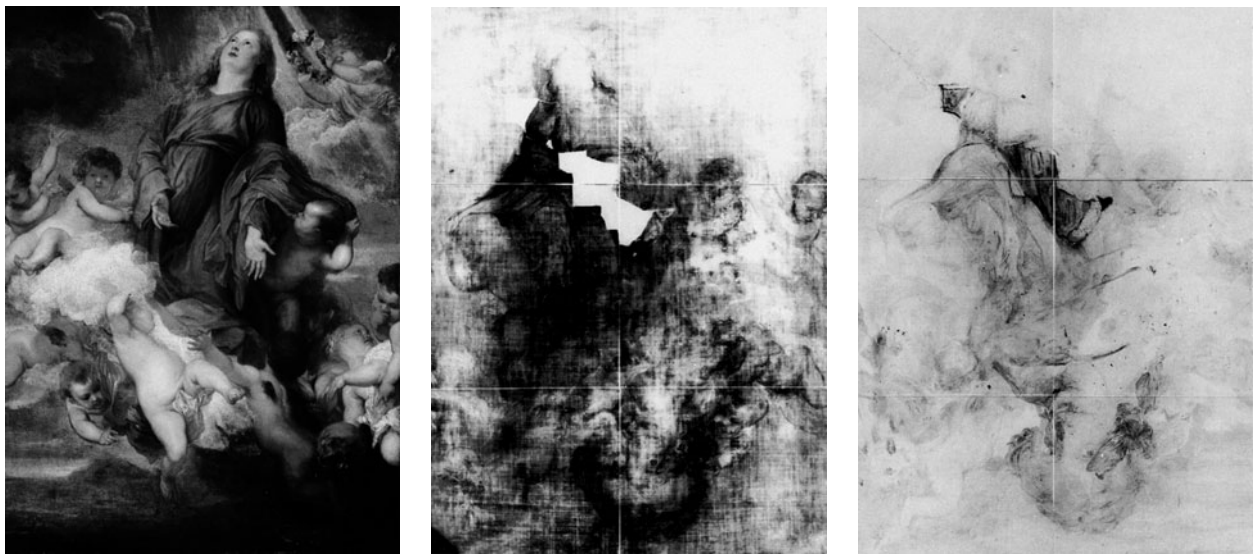

(*a*) (*b*) (*c*)

An application of neutron activation analysis. Hidden layers in paintings are analyzed by bombarding the painting with neutrons and observing the radiative emissions from nuclei that have captured a neutron. Different elements used in the painting have different half-lives. (*a*) Van Dyck's painting *Saint Rosalie Interceding for the Plague-Stricken of Palermo*. The black-and-white images in (*b*) and (*c*) were formed using a special film sensitive to electrons emitted by the radioactively decaying elements. Image (*b*), taken a few hours after the neutron irradiation, reveals the presence of manganese, found in umber, a dark earth pigment used for the painting's base layer. (Blank areas show where modern repairs, free of manganese, have been made.) The image in (*c*) was taken four days later, after the umber emissions had died away and when phosphorus, found in charcoal and boneblack, was the main radiating element. Upside down is revealed a sketch of Van Dyck himself. The self-portrait, executed in charcoal, had been overpainted by the artist. (See Problem 11-83.) [*(a) Courtesy of Metropolitan Museum of Art, New York City. (b) and (c) Courtesy of Paintings Conservation Department, Metropolitan Museum of Art, New York City.*]

The method consists of exposing the sample to be analyzed to a high flux of slow neutrons. Isotope ${}^{A}_{Z}\mathrm{M}$ of the element of interest undergoes the reaction ${}^{A}_{Z}\mathrm{M}(n, \gamma){}^{A+1}_{Z}\mathrm{M}$, as described in Section 11-7, where ${}^{A+1}_{Z}\mathrm{M}$ is radioactive. ${}^{A+1}_{Z}\mathrm{M}$ can be identified by its half-life and the energy of its beta- and gamma-ray emissions. The activity $R(t)$ after the beginning of the neutron irradiation is given by

$$R(t) = \lambda N(t) = R_0(1 - e^{-\lambda t}) \qquad \textbf{11-84}$$

where λ is the decay constant of ${}^{A+1}_{Z}\mathrm{M}$ and R_0 is the constant production rate of that isotope. $R(t)$ is measured and R_0 is computed from Equation 11-62 since $R_0 = N_0 R$, where N_0 is the number of ${}^{A}_{Z}\mathrm{M}$ nuclei in the sample. Thus,

$$R_0 = N_0 R = N_0 \sigma I \qquad \textbf{11-85}$$

where σ is the cross section for the reaction ${}^{A}_{Z}\mathrm{M}(n, \gamma)\ {}^{A+1}_{Z}\mathrm{M}$ in cm^2 and I is the neutron flux in neutrons/$\mathrm{s} \cdot \mathrm{cm}^2$. Equation 11-84 can then be written

$$R(t) = N_0 \sigma I(1 - e^{-\lambda t}) \qquad \textbf{11-86}$$

When the half-life is short enough, irradiation is usually continued to saturation, that is, until $R(t) = R(\infty) = N_0 \sigma I$. Table 11-7 gives saturation activities per μg for a few isotopes. The number of atoms of ${}^{A}_{Z}\mathrm{M}$ in the sample is, at the saturation activity,

$$N_0 = \frac{R(\infty)}{\sigma I}$$

and the mass of ${}^{A}_{Z}\mathrm{M}$ in the sample is

$$m({}^{A}_{Z}\mathrm{M}) = \frac{N_0 W}{N_A} = \frac{R(\infty) W}{N_A \sigma I} \qquad \textbf{11-87}$$

where W is the atomic weight of the element and N_A is Avogadro's number.

Table 11-7 Selected saturation activities ($I = 10^{12}$ neutrons/$\mathrm{min} \cdot \mathrm{cm}^2$)

${}^{A}_{Z}\mathrm{M}$	${}^{A+1}_{Z}\mathrm{M}$	Saturation activity $R(\infty)$ decays/$\mathrm{m} \cdot \mu\mathrm{g}$
${}^{55}\mathrm{Mn}$	${}^{56}\mathrm{Mn}$	8.8×10^6
${}^{63}\mathrm{Cu}$	${}^{64}\mathrm{Cu}$	1.7×10^6
${}^{127}\mathrm{I}$	${}^{128}\mathrm{I}$	1.6×10^6
${}^{197}\mathrm{Au}$	${}^{198}\mathrm{Au}$	1.7×10^7

EXAMPLE 11-26 **The "Gold" Chain** After buying a chain advertised as 10 percent pure gold, the suspicious purchaser irradiates one 25-mg link in a constant neutron flux of 10^{10} neutrons/s · cm^2 for a time long enough for any gold activity to saturate. She then measures the activity of the link to be 7.5×10^4 decays/s with a detector whose efficiency is 12 percent. What is the percent by weight of gold in the link? (σ for ^{197}Au is 98.8 barns.)

SOLUTION

Since the detector efficiency is 12 percent, the actual value of $R(\infty)$ is

$$R(\infty) = \frac{7.5 \times 10^4 \text{ decays/s}}{0.12} = 6.3 \times 10^5 \text{ decays/s}$$

From Equation 11-87 we can then compute

$$m(^{197}\text{Au}) = \frac{(6.3 \times 10^5 \text{ decays/s})(197 \text{ g/mol})}{(6.02 \times 10^{23} \text{ atoms/mol})(98.8 \times 10^{-24} \text{ cm}^2)(10^{10} \text{ neutrons/s/cm}^2)}$$

$$m(^{197}\text{Au}) = 2.1 \times 10^{-4} \text{ g}$$

The weight percent of gold in the link is then

$$\%\text{Au} = \left(\frac{2.1 \times 10^{-4} \text{ g}}{25 \times 10^{-3} \text{ g}}\right) \times 100 = 0.8\%$$

or less than 1/10 of the advertised amount.

Nuclear Magnetic Resonance

In Section 7-7, we saw that the energy levels of the atom were split in the presence of an external magnetic field (the Zeeman effect) because of the interaction of the atomic magnetic moment and the field. Since nuclei also have magnetic moments, the energy levels of a nucleus is also split in the presence of a magnetic field. We can readily understand this by considering the simplest case, the hydrogen atom, for which the nucleus is a single proton.

The potential energy of a magnetic moment μ in an external magnetic field **B** is given by

$$U = -\mu \cdot \mathbf{B} \qquad \textbf{11-88}$$

The potential energy is lowest when the magnetic moment is aligned with the field and highest when it is in the opposite direction. Since the spin quantum number of the proton is 1/2, the proton's magnetic moment has two possible orientations in an external magnetic field: parallel to the field (spin up) or antiparallel to the field (spin down). The difference in energy of these two orientations (Figure 11-62) is

$$\Delta E = 2(\mu_z)_p B \qquad \textbf{11-89}$$

When hydrogen atoms are irradiated with photons of energy ΔE, some of the nuclei are induced to make transitions from the lower state to the upper state by resonance absorption. These nuclei then decay back to the lower state, emitting photons of energy ΔE. The frequency of the photons absorbed and emitted is found from

$$hf = \Delta E = 2(\mu_z)_p B$$

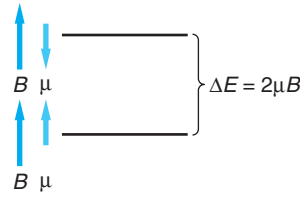

Figure 11-62 A proton has two energy states in the presence of a magnetic field, corresponding to whether the magnetic moment of the proton is aligned parallel or antiparallel to the field.

In a magnetic field of 1 T, this energy is

$$\begin{aligned}\Delta E &= 2(\mu_z)_p B \\ &= 2(2.79\mu_N)\left(\frac{3.15 \times 10^{-8}\ \text{eV/T}}{1\ \mu_N}\right)(1\ \text{T}) \\ &= 1.76 \times 10^{-7}\ \text{eV}\end{aligned}$$

and the frequency of the photons is

$$\begin{aligned}f &= \frac{\Delta E}{\hbar} = \frac{1.76 \times 10^{-7}\ \text{eV}}{4.14 \times 10^{-15}\ \text{eV} \cdot \text{s}} \\ &= 4.25 \times 10^{7}\ \text{Hz} = 42.5\ \text{MHz}\end{aligned}$$

This frequency is in the radio band of the electromagnetic spectrum; hence the radiation is called *RF* (radio-frequency) *radiation*. The measurement of this resonance frequency for free protons can be used to determine the magnetic moment of the proton.

When a hydrogen atom is in a molecule, the magnetic field at the proton is the sum of the external magnetic field and the local magnetic field due to the electrons and nuclei of the surrounding material. Since the resonance frequency is proportional to the total magnetic field seen by the proton, a measurement of this frequency can give information about the internal magnetic field seen in the molecule. This is called *nuclear magnetic resonance*. It is a sensitive tool for probing the internal magnetic structure of materials.

Nuclear magnetic resonance is also used as an alternative to x rays or ultrasound for medical imaging, in which case it is called *m*agnetic *r*esonance *i*maging (MRI). A patient can be placed in a magnetic field (provided by superconducting magnets) that is constant in time but not in space. When the patient is irradiated by a broadband RF source, the resonance frequency of the absorbed and emitted RF photons is then dependent on the value of the magnetic field, which can be related to specific positions in the body of the patient. Since the energy of the photons is much less than the energy of molecular bonds and the intensity used is low enough so that it produces negligible heating, the RF photons produce little, if any, biological damage. Diagnosis with MRI requires no surgical procedure and is more sensitive than other methods in detecting tumors in soft tissue.

Computer-Assisted Tomography

Wilhelm Roentgen received the first physics Nobel Prize in 1901 for his discovery of x rays in 1895, an event that also marked the beginning of *radiography*, the use of radiation and particle beams to produce images that are otherwise inaccessible. For half a century x rays were the probing beam of medical imaging. Then in the late 1940s the introduction of radioisotopes into a patient's body made it possible for physicians to target particular organs and produce images that recorded their behavior, a technique now a part of the specialty of nuclear medicine. The isotopes used are typically relatively short-lived gamma emitters since α and β particles have ranges in biological tissue that are too short to be useful. The detector normally employed is a collimated (to provide directional information) scintillation crystal viewed by a photomultiplier. (See Figure 11-63.) The image is then constructed by a computer from the output of the photomultiplier.